THE
PHYSICAL REVIEW
A Journal of Experimental and Theoretical Physics
VOL. 46, NO. 12 DECEMBER 15, 1934 SECOND SERIES

Counter Calibration and Cosmic-Ray Intensity

J. C. STREET AND R. H. WOODWARD, *Harvard University*
(Received October 1, 1934)

An absolute calibration of a set of counters has been obtained by determining their efficiencies and effective volumes. From observations recorded with this calibrated set, the number of ionizing cosmic rays is 0.80 ± 0.028 per cm^2 per minute from unit solid angle at the vertical at sea level. The number of such rays from all directions as obtained by integration over an angular distribution curve is 1.48 ± 0.055 cm^{-2} $min.^{-1}$. This combined with Millikan's ionization chamber measurements gives an average specific ionization of 100 ± 3.7 ion pairs per cm path of a ray. Comparison with previous measurements is made.

INTRODUCTION

THE study of cosmic radiation with ionization chambers gives a measure of the ionization produced in a closed vessel under the conditions of the experiment. Millikan[1] has made a careful study of his apparatus and as a result has been able to give an absolute measurement of the number of ions produced in air under standard conditions at sea level. Many observers have used Geiger-Müller counters to obtain relative values for the number of ionizing rays passing through a region defined by their particular arrangements of counters. To relate the two methods it is desirable to determine the absolute intensity of ionizing rays; i.e., the number per cm^2 per min. per unit solid angle. Johnson[2] has expressed his results on the angular distribution in this way but has pointed out that they are not strictly equal to the absolute intensities because of uncertainties in the efficiencies and end corrections of his counters. In the following paragraphs we discuss briefly our procedure for the experimental determination of the efficiencies and sensitive volumes of a set of counters. Accidental coincidences and the effects of showers are also considered. With the aid of these results we obtain a value for the vertical ray intensity which in conjunction with the angular distribution curve of Johnson and Stevenson[3] and Millikan's ionization data leads to a determination of the average ionizing power of the corpuscles.

ACCIDENTAL COUNTS

In a coincidence counting circuit it is important to reduce the number of accidental coincidences as far as possible. We have used a circuit similar to that described by Johnson and Street.[4] It was shown there that the resolving time τ could be determined approximately from the circuit constants, and the double and triple accidental counting rates determined from the

[1] R. A. Millikan, Phys. Rev. **39**, 397 (1932).
[2] T. H. Johnson, Phys. Rev. **43**, 307 (1933).
[3] T. H. Johnson and E. C. Stevenson, Phys. Rev. **43**, 583 (1933).
[4] T. H. Johnson and J. C. Street, J. Frank. Inst. **215**, 239 (1933).

approximate[5] relations

$$A_{12}=2N_1N_2\tau, \quad (1a)$$

$$A_{123}=2(N_{23}N_1+N_{13}N_2+N_{12}N_3)\tau, \quad (1b)$$

where the N's with single subscripts are the individual counting rates of the designated counters and those with double subscripts the coincidence counting rates of two counters. We have made a more precise measurement of the accidental counts by direct measurement with the arrangement of counters shown in Fig. 1. The

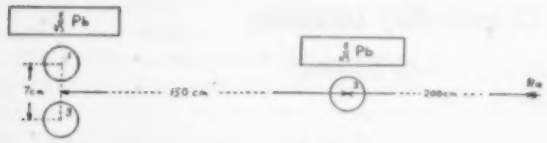

FIG. 1. Arrangement of counters for the measurement of accidental counts.

lead shields greatly reduce the true coincidence rate due to showers. The various observed rates for the normal case and when stimulated by a radium capsule are given in the first part of Table I. To a first approximation the rates N_{12}

TABLE I. *Counter rates, normal and when stimulated by radium capsule.*

	Normal	Stimulated		Normal	Stimulated
N_1	148 min.$^{-1}$	333 min.$^{-1}$	A_{12}	0.028 min.$^{-1}$	0.133 min.$^{-1}$
N_2	138	551	A_{23}	.027	.219
N_3	142	306	A_{123}	.0014	.0050
N_{12}	0.046	0.258	R_{12}*	.017	.013
N_{13}	7.69	6.58	R_{13}	7.66	6.45
N_{23}	.047	.234	R_{23}	.020	.015
N_{123}	.003	.006	R_{123}	.001	.001
A_{13}	.029	.245	τ_{12}	6.7×10^{-7} min.	
			τ_{23}	6.5×10^{-7} min.	

and N_{23} for the stimulated case are accidental coincidences because of the relatively small normal rates. With this assumption approximate determinations of τ_{12} and τ_{23} were obtained by use of (1a). These τ's were used to find the accidental rates A_{12} and A_{23} for the normal case and from these the real rates $[R_{12}=N_{12}-A_{12}$ and $R_{23}=N_{23}-A_{23}]$ due to showers and to horizontal rays were obtained. R_{12} and R_{23} are reduced by radium stimulation on account of the lower counter efficiency for that condition. This has been determined (see section of this paper on efficiency) to give the real rates for the stimulated case. The accidental rates for the stimulated case were then found by subtracting the real from the observed rates and these in turn were used to obtain more accurate values of the resolving times. The accidental and real rates and the resolving times are tabulated in the latter part of the table. The circuits are symmetrical and we have taken the average of τ_{13} and τ_{23} as the value to be used in subsequent calculations.

EFFICIENCIES

For three counters placed in line in a vertical plane as shown in Fig. 2, a triple coincidence may represent the passage of a single ray through

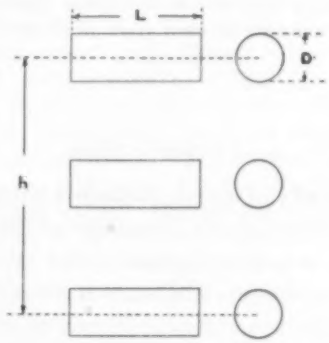

FIG. 2. Arrangement of counters for the measurement of the efficiency of the central counter.

the train of counters or the simultaneous excitation of the three counters by several rays from a shower. Likewise a double coincidence between the two extreme counters may be due to a single ray passing through them (and the central counter) or it may be due to shower particles passing through the extreme counters. If the observed triple and double coincidence rates are corrected for accidental counts and the latter rate for those showers with no ray through the central counter, the resulting rates will represent occurrences of simultaneous excitation in all three counters. The two rates should be equal provided the central counter produces a discharge whenever a ray passes through it. Since the

[5] *Note:* The expressions are applicable if the double rates are small in comparison with the individual rates in (1a) and if the triple rate is small in comparison with the double rates in Eq. (1b). When these conditions are not fulfilled the following relations are more accurate

$A_{12}=2(N_1-R_{12})(N_2-R_{12})\tau$

$A_{123}=2[N_{23}N_1+N_{13}N_2+N_{12}N_3-R_{123}(N_1+N_2+N_3)]\tau$,

where R_{12} and R_{123} are the real double and triple rates.

counters are not perfectly efficient in producing discharges the corrected rates are not equal and the efficiency of the central counter is given by the ratio of the triple rate to double. The results of a series of efficiency measurements are given in Table II.

TABLE II. *Efficiency (E) of counters.*

Central counter	h	c_t/T	c_d/T	N_t	N_d	N_t/N_d	E
1	20	2.43	2.66 ±0.018	2.43	2.64	0.922	0.938 ±0.0096
2	20	2.38	2.58 ± .016	2.38	2.56	.930	.948 ± .0088
3	20	2.48	2.70 ± .023	2.48	2.68	.926	.943 ± .0120
3	40	0.631	0.743 ± .011	0.628	0.719	.873	.943 ± .0209

The first column gives the number of the central counter the efficiency of which is being measured and the second the distance in cm between extreme counters. The numbers of counts per min. c_t/T and c_d/T have been corrected for barometric fluctuations[6] and reduced to a pressure of 76 cm of mercury. The probable errors have been estimated from the residuals. From these rates the accidental counts have been subtracted to give N_t and N_d. Showers were reduced to a minimum by carrying out the experiment under a light roof (one inch of wood about two meters above the counter set). To determine the correction due to the remaining showers we have made use of the data for the two separations of the end counters as given in the lower two lines of the table. Here it is apparent that the counting rate decreases rapidly with increasing separation whereas it is reasonable to assume that the shower coincidences do not vary appreciably. The apparent efficiency N_t/N_d with no correction for showers is considerably less for the greater spacing. The true efficiency must be independent of the spacing and this condition is realized if we subtract from all the double rates a constant 0.052 count per min. which we attribute to showers. The final corrected efficiencies are given in the last column.

The efficiencies have also been determined by a second method from an independent set of data. The counters were placed in line and the individual counting rates controlled by means of a radium capsule. It is assumed that immediately following a discharge of a counter there is an interval of time σ during which it is insensitive, probably due to the fact that the potential difference between the two electrodes is insufficient to produce another discharge. This period of inactivity together with the individual counting rate limits the efficiency of the counter.

$$E_1 = 1 - N_1\sigma_1 \quad (2a); \qquad E_1' = 1 - N_1'\sigma_1 \quad (2b)$$

where the primed symbols refer to values obtained when the counters were stimulated by a radioactive source. The observed double counting rates are

$$N_{12} = E_1E_2n_{12}, \quad (3a)$$

$$N_{12}' = (E_1 - \Delta E_1)(E_2 - \Delta E_2)n_{12} \quad (3b)$$

and similar expressions for the other pairs, where ΔE is the difference between efficiencies for the normal and stimulated condition and n_{12} is the actual number of ionizing rays passing through the two counters. The difference between normal and stimulated double counting rates is obtained from Eq. (3).

$$\Delta N_{12}/N_{12} = \Delta E_1/E_1 + \Delta E_2/E_2 - \Delta E_1\Delta E_2/E_1E_2, \quad (4)$$

$$\Delta N_{12}/N_{12} = \Delta N_1\sigma_1/(1 - N_1\sigma_1) + \Delta N_2\sigma_2/(1 - N_2\sigma_2) - \sigma_1\sigma_2\Delta N_1\Delta N_2/(1 - N_1\sigma_1)(1 - N_2\sigma_2). \quad (5)$$

In this and two similar equations for $\Delta N_{13}/N_{13}$ and $\Delta N_{23}/N_{23}$ all quantities but the three σ's are observed experimentally. The observed rates (corrected for barometric fluctuations and for accidental counts) for the three counters in line are tabulated in Table III together with the σ's

TABLE III.

	Normal		Stimulated	
N_1	145	min.$^{-1}$	572	min.$^{-1}$
N_2	133		621	
N_3	132		568	
N_{12}	3.70		2.59	
N_{13}	10.59		7.17	
N_{23}	10.77		6.58	
σ_1	2.7	$\times 10^{-4}$ min.		
σ_2	4.0	$\times 10^{-4}$ min.		
σ_3	5.0	$\times 10^{-4}$ min.		
E_1	0.960			
E_2	.947			
E_3	.934			

[6] E. C. Stevenson and T. H. Johnson, Washington Meeting of Am. Phys. Soc., April, 1934; Phys. Rev. **45**, 758A (1934).

and E's found from the solution of the equation. The conditions of this test were exactly similar to the arrangement which gave the data in Table II. The agreement between the two independent determinations of the efficiencies is good evidence that the assumptions employed are valid.

Effective Dimensions of a Counter

In order to determine the effective diameter of a counter, the three counters were arranged as shown in Fig. 3 and the ratios of the triple to double counting rates were measured for various displacements of the central counter. Assuming that the counters behave as uniformly sensitive rectangular areas, it is possible to derive approximate expressions for the ratio as a function of the displacement s and the diameter D.

$$\text{For } s<D/2, \quad N_t/N_d=K[1-2(s/D)^2], \quad (6a)$$

$$\text{For } s>D/2, \quad N_t/N_d=2K(1-s/D)^2. \quad (6b)$$

The theoretical curve is shown in Fig. 3 with the experimental points. The values of K and D were determined from the maximum and half values of N_t/N_d and a constant triple counting rate 0.066 per min. due to showers was subtracted from the experimental observation. The curve is in good agreement with the experimental points, indicating that the counter is uniformly sensitive over its diameter. The effective diameter is found to be the same as the internal geometric diameter, 3.82 cm.

The effective length L was measured by turning the central counter through 90° as shown in Fig. 4. The theoretical curve was obtained from formulas (6) and has been plotted in the figure. Under the conditions of operation, the effective length was found to be 10.5 cm as compared with the geometric length of 13 cm. This difference is probably dependent on the threshold and operating potentials as well as on the geometry. The threshold and operating potentials were in all our measurements 1200 and 1500 volts, respectively. The central wire in the counters was three mil tungsten.

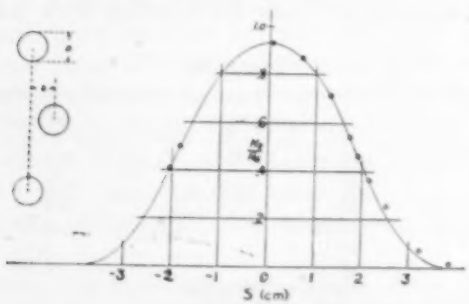

Fig. 3. Arrangement of counters for the determination of the effective diameter of a counter. The ratio of the triple to double counting rate is plotted as a function of the displacement of the central counter. Observations are shown as points on the theoretical curve.

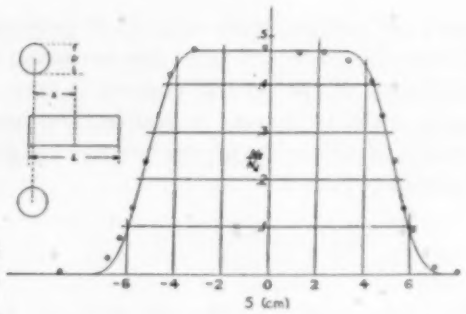

Fig. 4. Arrangement of counters for the determination of the effective length of a counter. Observed values of N_t/N_d are shown as points on the theoretical curve.

The effective diameter and length have been measured for only a single counter, but the relative cross-sectional areas have been computed from the counting rates of the three arrangements in Table II.

Integration over Counters

With these values for the lengths, diameters and efficiencies, $j(0)$ the intensity in rays per unit area from unit solid angle at the vertical can be obtained by integration over the counters. Employing the approximations used by Johnson[2] that for the small angles along the counter lengths the intensity varies as the square of the cosine of the angle from the vertical and that the variation over the diameter is negligible, the vertical triple counting rate is given by

$$N_t=E_1E_2E_3j(0)D^2h^4\int_0^L\int_0^L\frac{dl_1dl_2}{[h^2+(l_1-l_2)^2]^3}, \quad (7a)$$

$$N_t=\tfrac{1}{4}E_1E_2E_3j(0)D^2\left[\frac{L^2}{L^2+h^2}+\frac{3L}{h}\tan^{-1}\frac{L}{h}\right]. \quad (7b)$$

Since the computation was made for plane surfaces rather than for cylinders, there is an additive correction for the circular ends. The upper counter as seen from the lower is a rectangle with half ellipses on the ends. The number of rays passing through one counter and a half ellipse of the other is

$$N=\tfrac{1}{8}j(0)\frac{\pi}{h}\frac{D^3}{4}\left[1-\frac{h^4}{(h^2+L^2)^2}\right]. \quad (8)$$

The total correction is four times this amount which combined with Eq. (7b) gives

$$N_t=\tfrac{1}{4}j(0)E_1E_2E_3D^2\left\{\frac{\pi D}{2h}\left[1-\frac{h^4}{(h^2+L^2)^2}\right]+\frac{L^2}{L^2+h^2}+\frac{3L}{h}\tan^{-1}\frac{L}{h}\right\}. \quad (9)$$

It is also necessary to take account of the fact that the width as well as the length needs correction due to the cylindrical form of the counters. This correction is a 0.7 percent increase in diameter for each counter for the 20 cm spacing and is a fourth as much for the 40 cm spacing.

Substitution of the values of Table II gives 0.750 for $j(0)$ for the 20 cm spacing and 0.732 for 40 cm. The agreement between the two values tends to verify Eq. (9). The three counters which were used in this work were selected because of their remarkable constancy. In over two years of continuous operation no detectable change in their sensitivity in a coincidence counting unit has been observed. The counter walls, however, are fairly thick, approximately 2.5 mm nonex glass plus 0.3 mm copper. On this account, the value of $j(0)$ cited above includes only those rays with sufficient energy to penetrate four counter walls; i.e., 1 cm glass plus 1.2 mm copper. We have not counted the upper wall of the top counter for we have reason to believe from Schindler's[7] curves that as many rays are produced as are absorbed in this wall. To obtain $j(0)$ for rays of lesser penetrating power we arranged a double coincidence set of thin walled Pyrex glass counters (0.7 mm glass plus 0.13 mm copper per single wall) and measured the fractional decrease in counting rate when two of the heavy-walled counters were introduced as absorber between the Pyrex counters. This decrease was found to be 7 percent of the total. Thus $j(0)$ becomes 0.80 ± 0.028 ionizing ray per cm^2 per unit solid angle per minute.

The total intensity from all directions of ionizing rays per cm^2 considering the unit of area always perpendicular to the ray is

$$J=2\pi\int_0^{\pi/2} j(\theta)\sin\theta d\theta. \quad (10)$$

The integration has been performed graphically by using the experimental curve of Johnson and Stevenson[3] and gives the result of 1.48 ± 0.055 rays per cm^2 per min.

If we assume that all rays have the same ionizing power, the volume ionization Q in ion pairs per cm^3 per minute is related to J by the expression

$$Q=JI, \quad (11)$$

where I represents the average number of ion pairs along one cm of path of a ray under the conditions for which Q is determined. Putting $Q=2.48$ ions cm^{-3} sec.$^{-1}$ in air under standard conditions as given by Millikan[1] we obtain 100 ± 3.7 ions cm^{-1} for I.

Previous results are 135 ± 13 ion pairs per cm by Köhlhorster and Tuwin[8] with a counter method, 60 cm^{-1} from W. F. G. Swann's[9] direct measurement with a linear amplifier, an upper limit of 70 cm^{-1} by Evans and Neher[10] from fluctuation measurements and an estimate of 122 cm^{-1} by Anderson[11] from energy loss measurements with a cloud chamber. We are confident of the accuracy of our ray intensity measurement but it is possible that a fraction of the residual ionization in a closed vessel is due to some form of radiation which does not contribute to the coincidence rates. This may occur in three ways none of which have definitely been shown to be inconsistent with other experiments. These are (1) shower groups of particles which pass together through the train of counters and there-

[7] H. Schindler, Zeits. f. Physik **72**, 625 (1931).

[8] Köhlhorster and Tuwin, Zeits. f. Physik **73**, 130 (1931).
[9] W. F. G. Swann, Phys. Rev. **44**, 961 (1933).
[10] Evans and Neher, Phys. Rev. **45**, 144 (1934).
[11] C. Anderson, Phys. Rev. **44**, 406 (1933).

fore register as one particle, (2) recoil nuclei[12] from neutron collisions, and (3) low energy (less than 10^6 volt) electrons in equilibrium with the primary radiation which contribute to the ionization because of the equilibrium condition but not to the coincidence rate because they do not penetrate the intermediate counter walls. Since our measurements were taken under conditions which would be expected to give few if any showers from nearby material it seems unlikely that (1) is an important contribution. If we adopt the *extreme* view that we have as many shower groups passing through the very small solid angle subtended by our counters as are observed by Anderson[13] in his cloud chamber which is practically surrounded by dense material we find that our value of J is increased to 1.87 rays cm^{-2} $min.^{-1}$ and I therefore reduced to 79 ion pairs per cm. There is no existing evidence which permits an estimate of the importance of (2) and (3). Should it be found that they are important our value for I would be lowered to approach the results of Swann and Evans and Neher but no correction will raise our value unless there is a considerable error in the volume ionization.

[12] G. L. Locher, Phys. Rev. **44**, 779 (1933).

[13] Anderson, Millikan, Neddermeyer and Pickering, Phys. Rev. **45**, 352 (1934).

DECEMBER 15, 1934 PHYSICAL REVIEW VOLUME 46

Self-Consistent Field and Some X-Ray Terms of the Sodium Atom*

E. H. KENNARD AND E. RAMBERG, *Department of Physics, Cornell University*

(Received October 5, 1934)

Self-consistent field functions were found for neutral sodium, for which they are tabulated, and for the six internally ionized states $1s$, $2p$, $1s2s$, $2p2s$, $1s2p$, $(2p)^2$, these figures denoting in each case the quantum symbols of the missing electrons. With these functions the corresponding atomic energies were computed by the method of Fock and Slater. Applying a first-order correction for relativity and spin-orbit interaction, a close check is obtained between the observed and calculated frequency of Na $K\alpha$, the deviation being of the order of 0.1 percent. Finally the energy parameters of the Fock equations were computed to the first order in the exchange for the $2s$ and $2p$ electrons in the singly ionized states and are compared with the corresponding ionization energies, which they exceed by about 10 percent.

INCIDENTAL to an inquiry into the origin of the $K\alpha$-satellites[1] it became necessary to compute energies by the self-consistent field method[2] for the states belonging to the configurations $1s$, $2p$, $1s2s$, $2p2s$, $1s2p$, $(2p)^2$, denoting configurations in every case by the quantum symbols of the electrons missing from the neutral atom. The results of this work including the computation for the normal sodium atom, are reported in this note.

The equations employed in calculating the electron wave functions differed from those used by Hartree in the manner suggested by Fock,[3] i.e., in retaining higher order Coulomb terms and exchange terms for electrons in the same subshell. They differ from Fock's equations by the omission of the non-diagonal (exchange) terms, and their solutions may be regarded as a first approximation to the solutions of Fock's equations. Averaging the potential over the sphere by using as weight function the angular distribution function, $|Y_l^m(\vartheta, \varphi)|^2$, for the electronic state (n, l, m, μ) whose wave function we wish to find, the equation for the normalized radial part of this wave function, $f(n, l, m, \mu; r)/r$, becomes:

* This research was supported by a grant from the Heckscher Foundation established at Cornell University by August Heckscher.

[1] See succeeding paper in this issue.

[2] D. R. Hartree, Proc. Cam. Phil. Soc. **24**, 89, 111 (1928).

[3] V. Fock, Zeits. f. Physik **61**, 126 (1930).

$$\left[-\frac{1}{2}\frac{d^2}{dr^2}-\frac{Z_p(n,l,m,\mu;r)}{r}+\frac{l(l+1)}{2r^2}-E(n,l,m,\mu)\right]f(n,l,m,\mu;r)=0, \quad (1)$$

where

$$\frac{Z_p(n,l,m,\mu;r)}{r}=\frac{N}{r}-\sum_{n',\,l',\,m',\,\mu';\,k}\{a^k(lm;l'm')-\delta(nl\mu;n'l'\mu')b^k(lm;l'm')\}G^k(n',l',m',\mu';r)$$

and

$$G^k(n',l',m',\mu';r)=\int_0^\infty \frac{r^k(a)}{r^{k+1}(b)}|f(n',l',m',\mu';r')|^2dr'; \quad \begin{matrix} r(a)=r';\ r(b)=r \text{ for } r>r'. \\ r(a)=r;\ r(b)=r' \text{ for } r<r'. \end{matrix}$$

Here n, l, m, μ, are total, orbital, orbital magnetic, and spin magnetic quantum numbers, respectively. $Y_l^m(\vartheta, \varphi)$ is a normalized tesseral harmonic, $E(n, l, m, \mu)$ the energy parameter of the electron, Z_p the effective nuclear charge for potential, N the true nuclear charge or atomic number. The sum over the primed quantum numbers is to be extended over all occupied electron states of the atom. The coefficients a^k and b^k have been given by Slater.[4] The factor $\delta(n, l, \mu; n', l', \mu')$ is equal to unity if $n=n'$, $l=l'$ and $\mu=\mu'$ and vanishes otherwise. Atomic units[5] are used throughout.

Apart from the normal atom the specific "magnetic" states of the atom for which the self-consistent field was computed were (100–½); (21–1–½); (100–½) (200–½); (21–1½) (200–½); (100–½) (21–1–½); (210–½) (210½); these quantum numbers ($n\,l\,m\,\mu$) referring to the vacant states in the following array for the normal atom:

(100 ½) (200 ½) (21–1 ½) (210 ½) (211 ½) (300½)
(100–½) (200–½) (21–1–½) (210–½) (211–½).

The approximations to the self-consistent field were carried out until the maximum differences in the effective nuclear charge for initial and final field amounted to −0.006, 0.008, 0.008, −0.020, −0.011, −0.005 for the six ionized states in this order and 0.012 for the normal state. The energy parameters of the individual electronic wave functions are given in Table I. The individual $2p$ electrons have differing radial functions and energy parameters in the atomic states involving a single vacancy in the $2p$ subshell, as indicated in the table.

In Table II are given, as an example, the normalized radial functions $f(r)$ for the electronic states $1s$, $2s$, $2p$ and $3s$ of normal sodium, together with the effective nuclear charge for potential Z_p.[6] The number of significant figures to which the wave functions are given in the table is that obtained in the self-consistent field calculations and applied afterwards in the calculation of the energies. It must be expected that these figures deviate from the best self-consistent field functions obtainable not only in

TABLE I. *Energy parameters in Rydbergs* of electronic wave functions of sodium.*

Atomic state: / Electron state:	Normal	(100–½)	(21–1–½)	(100–½) (200–½)	(21–1–½) (20 0–½)	(10 0–½) (21–1–½)	(210–½) (210 ½)
$1s$	81.07	90.60	82.94	92.87	85.12	93.13	85.30
$2s$	4.173	6.102	5.785	8.029	7.630	8.104	7.693
$2p$ (21–1½), (211½)			4.502		6.425	7.078	
$2p$ (210½)	2.756	4.893	4.368	6.881	6.281	6.926	6.133
$2p$ (210–½), (211–½)			4.234		6.137	6.774	
$3s$	0.323	0.963	0.940	1.779	1.741	1.790	1.747

* 1 Rydberg (or 1 Ry) = ½ atomic unit is the ionization energy of hydrogen with fixed nucleus. As frequency measure it is, correspondingly, the minimum frequency which will ionize hydrogen photoelectrically.

[4] J. C. Slater, Phys. Rev. **34**, 1293 (1929).
[5] Reference 2, p. 91.

[6] The writers will be glad to supply tables of the wave functions and atomic fields for the six remaining atomic states to other workers to whom they might be of use.

TABLE II. *Atomic field and wave functions for normal sodium.*

r	Z_p	$1s$	$2s$	$2p$	$3s$	r	Z_p	$1s$	$2s$	$2p$	$3s$
0.01	10.651	0.63061	0.14704	0.00351	0.02527	1.2	0.967	0.00044	−0.6832	0.65106	−0.01891
.02	10.310	1.1304	0.26272	0.01331	0.04514	1.4	0.790	0.00008	−0.5145	0.51682	0.05412
.03	9.983	1.5202	0.35128	0.02840	0.06035	1.6	0.675	0.00001	−0.3788	0.40395	0.12464
.04	9.671	1.8179	0.41645	0.04791	0.07154	1.8	0.593		−0.2744	0.31219	0.19024
.05	9.377	2.0387	0.46148	0.07111	0.07924	2.0	0.529		−0.1965	0.23918	0.24964
.06	9.101	2.1955	0.48921	0.09733	0.08399	2.2	0.476		−0.13936	0.18194	0.30212
.07	8.841	2.2994	0.50211	0.12600	0.08617	2.4	0.428		−0.09803	0.13759	0.34747
.08	8.598	2.3598	0.50234	0.15663	0.08616	2.6	0.385		−0.06866	0.10353	0.38573
.09	8.368	2.3846	0.49179	0.18878	0.08430	2.8	0.345		−0.04780	0.07759	0.41712
.10	8.153	2.3806	0.47213	0.22209	0.08087	3.0	0.308		−0.03313	0.05793	0.44199
.12	7.757	2.3078	0.4110	0.29081	0.07026	3.5	0.228		−0.01306	0.02754	0.4788
.14	7.399	2.1771	0.3287	0.36062	0.05598	4.0	0.166		−0.00506	0.01292	0.4860
.16	7.071	2.0134	0.2324	0.42983	0.03930	4.5	0.118		−0.00194	0.00600	0.4718
.18	6.767	1.8343	0.1280	0.49716	0.02120	5.0	0.082		−0.00074	0.00276	0.4432
.20	6.481	1.6515	0.0197	0.56168	0.00246	5.5	0.056		−0.00028	0.00126	0.4058
						6.0	0.038		−0.00010	0.00058	0.3643
.24	5.949	1.3037	−0.1960	0.67982	−0.03481						
.28	5.462	1.0026	−0.3974	0.78109	−0.06945	6.5	0.026		−0.00004	0.00026	0.3218
.32	5.009	0.75677	−0.5754	0.86456	−0.09982	7.0	0.017		−0.00001	0.00012	0.2807
.36	4.588	0.56326	−0.7262	0.93066	−0.12523	7.5	0.011		−0.00001	0.00005	0.2419
.40	4.198	0.41475	−0.8489	0.98063	−0.14550	8.0	0.007			0.00002	0.2063
						8.5	0.005			0.00001	0.1746
.5	3.354	0.18669	−1.0435	1.0460	−0.17528	9.0	0.003				0.1468
.6	2.688	0.08145	−1.1173	1.0484	−0.18183	9.5	0.002				0.1224
.7	2.172	0.03486	−1.1102	1.0110	−0.17181	10.0	0.001				0.1016
.8	1.781	0.01474	−1.0535	0.9506	−0.15069						
.9	1.486	0.00618	−0.9703	0.8784	−0.12249	11.0	0.000				0.0689
1.0	1.264	0.00258	−0.8752	0.8016	−0.08997	12.0	0.000				0.0460

the last, but also in the fourth and even the third significant figure. Nevertheless the use of five places in the wave functions is justified, and the normalization integrals were calculated to six significant figures; for in calculating the mean value of any quantity such as the energy, the error depends on the first power of the error in the normalization of the wave functions but only on the second power of their deviation from the correct normalized self-consistent field functions, so that it is reasonable to carry the normalization to a higher accuracy than can be claimed for the wave functions themselves.

To obtain the energies of the several atomic states correct to the first order in the exchange between electrons of different subshells but neglecting spin and relativity effects, a wave function for the atom was constructed by forming a normalized antisymmetric combination, Ψ, of products of the individual electronic wave functions. With this wave function Ψ the diagonal matrix element of the Hamiltonian H,

$$H=\sum_{j=1}^{z}\left(-\frac{1}{2}\nabla_j^2-\frac{N}{r_j}\right)+\sum_{j>k}^{z}\frac{1}{r_{kj}} \qquad (2)$$

was computed. Here z is the number of electrons of the atom or ion ($=11$, 10 or 9 in our case), the summations being carried out over all electrons and electron pairs, respectively. To facilitate the evaluation of the matrix element it is advisable to orthogonalize the one-electron functions, i.e., to subject the radial functions having different n but similar angular quantum numbers (in our case only the s-functions, with $l=0$, are affected) to an orthogonalizing transformation:

$$g(n, l, m, \mu; r)=\sum_p c_{np} f(p, l, m, \mu; r) \qquad (3)$$

such that

$$\int g(n, l, m, \mu; r) g(n', l, m, \mu; r) dr=\delta(n, n').$$

Replacing the f's by the g's leaves the atomic wave function unaltered if we, at the same time, replace the normalizing factor of the previously formed antisymmetric linear combination by $1/(z!)^{\frac{1}{2}}$. Any such orthogonalizing transformation will do; the procedure suggested by Slater,[7] that is to leave the function of lowest n unaltered and, successively, to make the functions of higher n orthogonal to those of lower n by adding suitable fractions of the latter, which have already been made mutually orthogonal, to the former, is probably the most convenient.

In terms of the radial factors $g(n, l, m, \mu; r)/r$ of the normalized orthogonal functions the ex-

[7] J. C. Slater, Phys. Rev. **42**, 39 (1932).

pression for the diagonal matrix element of the Hamiltonian (2) becomes:

$$E=\sum_{i=1}^{s}\int_0^\infty\left[\frac{1}{2}\left(\frac{dg_i}{dr}\right)^2+\frac{l_i(l_i+1)}{2}\frac{g_i^2}{r^2}-\frac{Ng_i^2}{r}\right]dr$$

$$+\sum_{i>j}^{s}\sum_k\{a^k(l_im_i;\,l_jm_j)F_{ij}^k-\delta(\mu_i;\,\mu_j)b^k(l_im_i;\,l_jm_j)G_{ij}^k\}. \quad (4)$$

Here the subscript i is an abbreviation for the ensemble of quantum numbers $(n_i,\ l_i,\ m_i,\ \mu_i)$ and

$$F_{ij}^k=\int_0^\infty\frac{r^k(a)}{r^{k+1}(b)}|g_i(r)|^2|g_j(r')|^2drdr',$$
$$G_{ij}^k=\int_0^\infty\frac{r^k(a)}{r^{k+1}(b)}g_i(r)g_j(r)g_i(r')g_j(r')drdr' \quad (4a)$$

are Slater's electrostatic-interaction-energy parameters.

The quadratures involved were carefully checked and repeated.[8] They were carried out in identical fashion for the several states so as to minimize the effect of systematic errors on the differences between the energies. The individual terms in the energy integral (4) were calculated to four decimal places. The results of a preliminary calculation of the atomic energies in Rydbergs are compared in Table III with those of the final calculations in order to give an idea of the check obtained.

Both the orthogonalization of the wave functions and the quadratures were carried out separately for the two sets of calculations. The final set is to be preferred, as some slight errors in the calculations leading to the preliminary set have not been compensated and the experience gained in the previous work made possible a more advantageous arrangement of the calculations. Table III does not, of course, set an upper limit to the errors in the calculated energies in case the wave functions employed were themselves insufficiently good approximations to the self-consistent field functions (see discussion in connection with Table II). To increase the accuracy of the functions, however, which in itself might have been desirable for the present purpose, would have necessitated carrying more figures in the self-consistent field calculations and using narrower intervals in r at the same time and this would have greatly increased the labor involved. The calculations as performed represent a compromise between desirable accuracy and permissible extensiveness.

Having found the energy for one magnetic state pertaining to each configuration, we can find the set of terms belonging to the latter either by applying Slater's method of diagonal sums or by solving the secular equation for the

TABLE III. *Atomic energies in Rydbergs obtained in preliminary and final calculation.*

Atomic state:	(100-½) (200-½)	(21-1-½)	(100-½) (200-½)	(21-1-½) (20 0-½)	(10 0-½) (21-1-½)	(210-½) (210 ½)
Prel. calc.	−244.36	−320.76	−237.18	−314.28	−239.51 −239.53	−316.01
Final calc.	−244.33	−320.79	−237.18	−314.28	−239.54	−316.01

TABLE IV. *Atomic energies in Rydbergs for sodium.*

Term	*Energy*	*Term*		*Energy*
Normal	*−323.40*			
1s ^2S (^2S)	*−244.33*	*2p* ^2P (^2P)		*−320.79*
^1S (^2S)	$-244.33+2G_{14}^0=-244.30$	^1P (^2P)	$-320.79+\frac{1}{3}G_{14}^1$	$=-320.76$
1s2s ^4S (^3S)	*−237.18*	*2p2s* ^4P (^3P)		*−314.28*
^2S (^2S)	$-237.18+M_{124}^-=-237.06$	^2P (^3P)	$-314.28+M_{234}^-$	$=-314.16$
^2S (^1S)	$-237.18+M_{124}^+=-236.62$	^2P (^1P)	$-314.28+M_{234}^+$	$=-313.26$
1s2p ^4P (^3P)	*−239.54*	$(2p)^2$ ^4P (^3P)	$-316.01-\frac{9}{25}F_{22}^2-\frac{1}{3}G_{24}^1$	$=-316.46$
^2P (^3P)	$-239.54+M_{134}^-=-239.47$	^2P (^3P)	$-316.01-\frac{9}{25}F_{22}^2+\frac{1}{3}G_{24}^1$	$=-316.39$
^2P (^1P)	$-239.54+M_{134}^+=-239.15$	^2D (^1D)	$-316.01-\frac{3}{25}F_{22}^2$	$=-316.15$
		^2S (^1S)	$-316.01+\frac{9}{25}F_{22}^2$	$=-315.73$

[8] Except in the case of normal sodium.

electrostatic interaction.[9] Calculating the electrostatic-interaction parameters for this purpose with the orthogonalized one-electron functions used in calculating the expression (4) we obtain the atomic energies in Rydbergs (without relativity and spin effects) given in Table IV. The term symbol in parenthesis indicates the term of the ion from which, through the addition of the valence electron, the atomic term is derived. The M's are defined as follows:

$$M^{\pm}_{124}=G_{12}{}^{0}+G_{24}{}^{0}+G_{14}{}^{0}\pm(G_{12}{}^{0^2}+G_{24}{}^{0^2}+G_{14}{}^{0^2}-G_{12}{}^{0}G_{24}{}^{0}-G_{24}{}^{0}G_{14}{}^{0}-G_{14}{}^{0}G_{12}{}^{0})^{\frac{1}{2}},$$

$$M^{\pm}_{234}=\frac{1}{3}G_{23}{}^{1}+\frac{1}{3}G_{34}{}^{1}+G_{24}{}^{0}\pm\left(\frac{1}{9}G_{23}{}^{1^2}+\frac{1}{9}G_{34}{}^{1^2}+G_{24}{}^{0^2}-\frac{1}{9}G_{23}{}^{1}G_{34}{}^{1}-\frac{1}{3}G_{34}{}^{1}G_{24}{}^{0}-\frac{1}{3}G_{24}{}^{0}G_{23}{}^{1}\right)^{\frac{1}{2}},$$

$$M^{\pm}_{134}=\frac{1}{3}G_{13}{}^{1}+\frac{1}{3}G_{34}{}^{1}+G_{14}{}^{0}\pm\left(\frac{1}{9}G_{13}{}^{1^2}+\frac{1}{9}G_{34}{}^{1^2}+G_{14}{}^{0^2}-\frac{1}{9}G_{13}{}^{1}G_{34}{}^{1}-\frac{1}{3}G_{34}{}^{1}G_{14}{}^{0}-\frac{1}{3}G_{14}{}^{0}G_{13}{}^{1}\right)^{\frac{1}{2}}.$$

In order to obtain a check on the accuracy of the method by comparison with observation, and at the same time to find the order of magnitude of the neglected relativity correction and spin-orbit interaction energies, the latter quantities were calculated as a first-order correction to the energy in the case of the two singly ionized states—the initial and final states of the unresolved doublet $K\alpha_{1,2}$. The total correction ΔE for the energy of the atom is the sum of the individual corrections for every electron considered separately; it can be written (cf. Darwin[10]):

$$\Delta E=\frac{\alpha^2}{4}\sum_{k=1}^{s}\int_0^\infty f_k(r)\left\{-2\left(\frac{Z_{pk}(r)}{r}+E_k\right)^2-\frac{Z_k(r)}{r^2}\frac{d}{dr}-\left(\frac{l}{-l-1}\right)\frac{Z_k(r)}{r^3}\right\}f_k(r)dr. \tag{5}$$

Here $-Z_{pk}/r$ is the potential energy of an electron in a spectroscopic state k with quantum numbers n, l, j, m_j, E_k its energy parameter, $Z_k/r^2=d/dr\,(-Z_{pk}/r)$ the field in which it moves, and f_k/r the radial factor of its wave function (unaltered in this approximation by the spin); α is the fine-structure constant. The last term in the integrand vanishes for s-electrons and otherwise gives the doublet splitting; the upper coefficient, l, must be used for $j=l+\frac{1}{2}$ and the lower, $-l-1$, for $j=l-\frac{1}{2}$. The calculation leads to -0.305 Ry as correction for the $1s$ state and -0.432 Ry for the $2p$ state. The doublet splitting comes out as 0.0132 Ry (2.0 X. U.). We thus obtain for the corrected terms, disregarding the spin splitting,

$1s\ ^3S(^2S)$	*244.64* Ry	$2p\ ^3P(^2P)$	*321.22* Ry,
$\ \ ^1S(^2S)$	*244.61* Ry	$\ \ ^1P(^2P)$	*321.19* Ry.

This makes possible a comparison of the calculated mean frequency (in Rydbergs) of $K\alpha_{1,2}$ with the measured frequency of the unresolved doublet:

$$K\alpha_{1,2}\colon \nu/R=\begin{matrix}76.58\text{ (calc.)}\\76.67\text{ (obs.)}.\end{matrix}$$

The agreement is sufficiently close to give some confidence in the accuracy of the methods employed. The relativity and spin-orbit corrections were not calculated for the doubly ionized states because the total correction for the line $K\alpha_{1,2}$ is sufficiently small (0.13 Ry) so that it can be assumed to be the same for analogous transitions between doubly ionized states.

To obtain a check on the values of the differences between the energies of the singly and doubly ionized states, which were of primary

[9] Strictly speaking this is true only when the g's for the magnetic states pertaining to the same configuration are the same, as they would be if they did not depend on the magnetic quantum numbers. Actually the g-functions for the several magnetic states are so nearly alike that the error introduced by using the same g's throughout in calculating the separation parameters is small—the error in the term separations due to this cause probably does not exceed a few hundreds of a Rydberg in any case.

[10] C. G. Darwin, Proc. Roy. Soc. **A118**, 654 (1928); see Eqs. (4.2) and (4.3).

interest in the application of the results of the present work, a simpler method of calculation can be applied; though not capable of giving as nearly correct results as the procedure so far discussed, this method has the additional advantage of putting a lesser claim on the accuracy of the wave functions employed. As V. Fock[11] and T. Koopmans[12] have shown, the energy parameters E_i of that particular set of solutions ψ_i of the Hartree equations with exchange,[13] for which

$$a_{ij} \equiv H_{ij} + \sum_{k=1}^{x} \{(ikGjk) - (ikGkj)\} = E_i \delta_{ij}, \quad (6)$$

where $$H_{ij} = \delta(l_i, m_i, \mu_i; l_j, m_j, \mu_j) \cdot \int_0^\infty \left[\frac{1}{2} \frac{dg_i}{dr} \frac{dg_j}{dr} + \frac{l_j(l_j+1)}{2} \frac{g_i g_j}{r^2} - \frac{N g_i g_j}{r} \right] dr$$

and $$(ikGjs) = \int \psi_i^*(1) \psi_k^*(2) \frac{1}{r_{12}} \psi_j(1) \psi_s(2) d\tau_1 d\tau_2, \qquad \psi(1) = S_\mu(1) \cdot Y_l^m(\vartheta_1, \varphi_1) \cdot g(r_1)/r_1,^{14}$$

i.e., for which the matrix **a** with elements a_{ij} is diagonal, will represent the ionization potentials of the atom provided we may disregard the alteration in the charge distribution of the remaining electrons which results from the removal of an electron with energy parameter E_i. As we shall see, the latter effect, while negligible for valence electrons, is not immaterial in determining the ionization potentials of inner (in our case $2s$ and $2p$) electrons. Here, however, we are primarily interested in the differences of these ionization potentials for two states, $1s$ and $2p$; in obtaining these differences we may expect the errors in question largely to cancel out, so that this method might provide a valuable check for the same differences as computed directly from the atomic energies in Table IV.

From any orthogonal set of solutions of the Fock equations, or a first approximation thereto, we may obtain the energy parameters of the set of solutions diagonalizing **a** to an equal approximation by solving the secular equation for this matrix. The latter process is greatly simplified by the fact that the non-diagonal elements of **a** vanish unless the spin- and magnetic quantum numbers of the two states involved are the same and the azimuthal quantum numbers are either both odd or both even. As Koopmans points out, the coordination of definite energy parameters to each electron and their interpretation as ionization potentials has meaning only when the atomic wave function has the form of a single

TABLE V. *Energy differences between doubly ionized and singly ionized states of sodium.*

$\mu = +\frac{1}{2}$:	(100)(200)(21−1)(210)(211)(300)	(100)(200)(21−1)(210)(211)(300)	
$\mu = -\frac{1}{2}$:	(**200**)(21−1)(210)(211)	(100)(**200**) (210)(211)	
$1s2s$	^4S (^3S) 7.65 (7.15) Ry	$2p2s$	^4P (^3P) 7.02 (6.51) Ry
	^2S (^3S) 7.77 (7.27)		^2P (^3P) 7.14 (6.63)
	^2S (^1S) 8.21 (7.71)		^2P (^1P) 8.04 (7.53)
$\mu = +\frac{1}{2}$:	(100)(200)(21−1)(210)(211)(300)	(100)(200)(21−1)(**210**)(211)(300)	
$\mu = -\frac{1}{2}$:	(200)(**21−1**)(210)(211)	(100)(200) (210)(211)	
$1s2p$	^4P (^3P) 5.44 (4.80) Ry	$(2p)^2$	5.00 Ry
	^2P (^3P) 5.51 (4.87)		^4P (^3P) 4.85 (4.32)
	^2P (^1P) 5.83 (5.18)		^2P (^3P) 4.92 (4.39)
			^2D (^1D) 5.16 (4.63)
			^2S (^1S) 5.58 (5.06)

[11] V. Fock, Zeits. f. Physik **81**, 195 (1933).
[12] T. Koopmans, Physica **1**, 104 (1933).
[13] A unitary transformation of a set of solutions ψ_i of these equations yields a new set of solutions of the same equations, as hereby neither the atomic (antisymmetric) wave function nor the orthogonal character of the set of solutions are affected. It is therefore always possible to find a set of solutions which diagonalizes the matrix on the left of Eq. (6).
[14] The factor $S_\mu(1)$ indicates the spin character of the function ψ and obeys the relation $S_\mu^*(1) \cdot S_{\mu'}(1) = \delta(\mu; \mu')$.

Slater determinant. In the more general case that the real wave functions must be represented by linear combinations of determinants, however, it is still possible to calculate the electronic energy parameters in the above fashion for single determinant wave functions and then to find the required energy differences by applying Slater's rule of diagonal sums.

In Table V are given the numerical results of these calculations. Above each column of figures the configuration of the $1s$ or $2p$ state is indicated with that electronic state printed in heavy type whose energy parameter was computed. The first figure in each column represents this energy parameter (with sign reversed, measured in Rydbergs); in all cases the figures labeled by terms symbols are the energy differences between the indicated doubly ionized states and the $1s$ ^3S (^2S) and the $2p$ ^3P (^2P) states, respectively, either equal to the energy parameter values or derived from them by the method of diagonal sums. On the right of them (in parenthesis) are given the same energy differences obtained directly from Table IV.

It is seen that the ionization potentials as computed from the energy parameters of the electrons are too high by about 10 percent. The application of these results is discussed further in a subsequent paper on the *Origin of the Kα-satellites*.

DECEMBER 15, 1934 PHYSICAL REVIEW VOLUME 46

Origin of $K\alpha$-Satellites*

E. H. KENNARD AND E. RAMBERG, *Department of Physics, Cornell University*

(Received October 5, 1934)

The hypothesis, proposed by Druyvesteyn and others, that the $K\alpha$-satellites arise from transitions of a $2p$ ($L_{II, III}$) electron into the $1s$ (K) shell in the presence of one or two further vacancies in the L shell is tested (1) by comparing in the case of sodium the separations from the parent line for the lines due to transitions of the first type calculated by self-consistent field methods with the observed separations of the satellites and (2) by effecting a similar comparison between observation and theory for a number of other elements, the separations being obtained in this case by a simplified method previously used by H. C. Wolfe but extended to include the effects of spin-orbit interaction. It is found that the results can be accounted for if the lines α', α_3 and α_4 are attributed to transitions in atoms lacking one additional electron in the L shell, probably of the type $1s2p \rightarrow (2p)^3$, and the lines α_5, α_6, α_7 and α_8 to transitions in atoms lacking two additional electrons in the L shell. A consideration of the effect of chemical combination supports these conclusions.

WENTZEL[1] in 1921 first suggested that the satellites on the short wave-length side of $K\alpha_{1,2}$ of the light elements were due to transitions taking place in atoms with more than one vacancy in their inner shells. While his original coordinations have, to a large extent, not stood the test of time, the idea was elaborated by other authors, especially Druyvesteyn,[2] with satisfactory results in the case of a number of other satellites. Following another lead given by Wentzel,[3] Ray[4] and Langer[5] made coordinations between observed lines and transitions taking account of the term multiplicities predicted by the theory of complex spectra. These were not, however, supported by quantitative data and cannot be brought into agreement with our present results. An actual calculation of the satellite-parent line separations without the use of empirical data was first made by H. C. Wolfe,[6] who was able to show that in potassium the line

* This research was supported by a grant from the Heckscher Foundation established at Cornell University by August Heckscher.

[1] G. Wentzel, Ann. d. Physik **66**, 437 (1921).

[2] M. J. Druyvesteyn, Zeits. f. Physik **43**, 707 (1927); *Het Röntgenspectrum van de tweede Soort*, Dissertation Groningen (1928).

[3] G. Wentzel, Zeits. f. Physik **31**, 445 (1925).

[4] B. B. Ray, Phil. Mag. **8**, 772 (1929).

[5] R. M. Langer, Phys. Rev. **37**, 457 (1931).

[6] H. C. Wolfe, Phys. Rev. **43**, 221 (1933).

structure to be expected as the result of transitions between the L and the K shell with an additional vacancy in the L shell ($2s$ or $2p$ shell) agreed in order of magnitude with the observed satellite structure.[7]

Wolfe's calculations were carried out by applying Slater's theory of complex spectra[8] to the initial and final states of the doubly and singly ionized atom, with the Hartree functions of the neutral atom throughout in place of Slater's orthogonal functions. This method neglects the readjustment of the residual electron cloud which results from the removal or displacement of any one electron and hence cannot be expected to give very accurate results in the case of the lighter atoms, where the contribution of any one inner electron is considerable. It was the aim of the present work to gain further insight into the probable origin of the $K\alpha$-satellites by applying more accurate methods in at least one case and to extend the range of elements studied.

For detailed study sodium was selected for the following reasons: All of its five principal satellites have been observed; in view of its position at the extreme left of the periodic table, the effects of chemical combination and of binding in the crystal lattice may be expected to be negligible; finally, the number of its electrons is small enough to make the work of computation not unduly extensive. An additional advantage is that we can safely assume Russell-Saunders coupling.

Two methods of calculating absolute and relative positions of energy levels for sodium have been outlined and applied in a preceding paper.[9] In Table I the results of the calculations for the frequency differences (in Rydbergs) between the parent line $K\alpha_{1,2}$ ($K\rightarrow L_{II,\,III}$ or $1s\rightarrow 2p$) and lines arising from analogous transitions in atoms which have an additional vacancy in the L shell are given.[10] The first column in Table I indicates

TABLE I. *Separations from Na $K\alpha$ calculated for transitions in atoms with an additional vacancy in the L shell.*

Transition	(1) $\Delta\nu/R$	(2) $\Delta\nu/R$	Intensity
$1s2s\,{}^1S\rightarrow 2p2s\,{}^1P$	0.18	0.17	(1)
$1s2s\,{}^3S\rightarrow 2p2s\,{}^3P$	0.64	0.63	(3)
$1s2p\,{}^1P\rightarrow (2p)^2\,{}^1S$	0.12	0.25	1
$1s2p\,{}^3P\rightarrow (2p)^2\,{}^3P$	0.48	0.59	9
$1s2p\,{}^1P\rightarrow (2p)^2\,{}^1D$	0.55	0.67	5

the transitions for which the separations from the parent line have been computed: the configuration symbol indicates in what shells vacancies occur; thus $1s2s$ stands for two vacancies, one in the $1s$ or K shell and one in the $2s$ or L_I shell, $(2p)^2$ for two vacancies in the $2p$ or the $L_{II,\,III}$ shell. The term symbols in the table, following the usual x-ray practice, are determined by the vacancies in the inner shells alone. This is justified by the slightness of the interaction between the electrons of the valence shell with the incomplete inner shells. In S.S. these term symbols have been indicated throughout in parenthesis. The second column, labeled (1), gives the separations for the transitions as calculated directly from the computed atomic energies, the third, labeled (2), those calculated from the energy parameters of the wave equations for the missing electrons. The differences between the results obtained by the two methods are large but not unreasonable in view of the differences between the ionization potentials computed by the two methods (see S.S., Table V). From a theoretical point of view the first method is so much superior to the second that, given perfectly accurate wave functions and energy calculations, the whole divergence would have to be attributed to the inadequacy of the second method. S.S., Table III, shows furthermore that errors in the energy calculations by the first method are unlikely to account for a large share of the difference. On the other hand, the first method depends much more on the accuracy of the self-consistent field functions; and errors in these may, as discussed in S.S., lead to errors in the energy differences of the same

[7] Check calculations performed with wave functions kindly furnished by Dr. Wolfe indicated numerical errors in the calculation of some of the screening and exchange integrals and hence in the separations as published by him. This accounts for the great differences between his results and those given in Tables III and IV, below.

[8] J. C. Slater, Phys. Rev. **34**, 1293 (1929).

[9] E. H. Kennard and E. Ramberg, Phys. Rev. **46**, 1034 (1934); this paper will be referred to as S.S.

[10] The data obtained by taking differences in S.S., Table V, differ from those presented at the Washington meeting of the American Physical Society, April 26, 1934 and published in Phys. Rev. **45**, 754 (1934) owing to subsequent application of corrections for imperfect normalization of the wave functions.

order as those inherent in the second method. The results in column (1) may thus well be in error by amounts of the order of 0.1 Rydberg. In the last column relative probabilities of the transitions are given, calculated from the angular parts of the coordinate matrix elements; those in parenthesis are not comparable with those without parenthesis, as they refer to different sets of configurations.

In Table II are given for comparison the separations of the observed satellites from their parent line $K\alpha_{1,2}$. The measurements are due to Wetterblad[11] and are given in Siegbahn's[12] tables.

TABLE II. *Observed parent-line-satellite separations for Na Kα.*

Line	$\Delta\nu/R$	Line	$\Delta\nu/R$
$K\alpha'$	0.31	$K\alpha_5$	1.09
$K\alpha_3$	0.52	$K\alpha_6$	1.29
$K\alpha_4$	0.64		

It is seen that all the transitions considered, i.e., all possible transitions with an additional vacancy in the L shell,[13] definitely fall into the range of the satellites α', α_3 and α_4 and cannot possibly be made to account for the group lying further out, α_5 and α_6. However, it is evident that the results obtained are not sufficiently exact to prescribe uniquely a coordination between transitions and observed lines. Such a coordination must rest on additional information concerning, e.g., the change of the satellite structure with atomic number.

In order to obtain such information the simple method used by Wolfe[6] to calculate the separations for potassium was extended to include the effects of spin-orbit interaction and applied to a series of elements which extended over most of the range over which the $K\alpha$-satellites have been observed. Houston,[14] Goudsmit[15] and Laporte and Inglis[16] have shown how, in the cases arising in the present work, from a knowledge of the exchange integrals for the wave functions pertaining to valence electrons or to vacancies in closed shells as well as the spin-orbit interaction energies, it is possible to find the separations of the terms of any given configuration for any intermediate type of coupling. In our case the exchange integrals were calculated for Cl(17), K(19) and Cu(29) with wave functions for the respective negative and positive ions published by Hartree[17] and for Na(11) with functions calculated for neutral Na by the writers (S.S.). The spin-orbit interaction parameters could be taken directly from the observed doublet separation of $K\alpha_{1,2}$. We can then calculate the relative positions of the lines due to transitions between two given doubly ionized configurations. To find, also, the positions of these lines relative to $K\alpha_{1,2}$, it is simplest to consider those states which have a j-value realized only once for their configurations, as the wave functions for these states are independent of coupling strengths. The differences in energy between these states and the singly ionized ones which give rise to the parent line are expressible in terms of certain screening integrals in addition to exchange integrals and spin-orbit interaction parameters; both types of integrals were computed with the Hartree functions.

The several separations are given by the following formulas:

Separation of the lines $1s2s\ {}^3S_1 \rightarrow 2p2s\ {}^3P_2$ and $K\alpha_2$ $(1s\ {}^2S_{\frac{1}{2}} \rightarrow 2p\ {}^2P_{\frac{1}{2}})$:

$$F^0(10,20) - F^0(20,21) - G^0(10,20) + 1/3\,G^1(20,21) + 3A.$$

Separation of the lines $1s2p\ {}^3P_2 \rightarrow (2p)^2\ {}^3P_1$ and $K\alpha_2$:

$$F^0(10,21) - F^0(21,21) - 1/3\,G^1(10,21) + 1/25\,F^2(21,21).$$

[11] T. Wetterblad, Zeits. f. Physik **42**, 611 (1927).

[12] M. Siegbahn, *Spektroskopie der Röntgenstrahlen*, 2nd Ed., Springer (1931).

[13] It may be mentioned that we can estimate the separation corresponding to an additional vacancy in any one subshell by taking the difference of the energy parameters for that subshell in the $1s$ and $2p$ states. Thus we find from S.S., Table I, that an additional vacancy in the $1s$ or K shell would give rise to a separation of about 8 Ry, one is the $3s$ or M_{I} shell to a separation of about 0.02 Ry. This leaves us with the transitions in Table I, above, as the only transitions in *doubly* ionized atoms which may account for the $K\alpha$-satellites and which, at the same time, both obey the selection rules for Russell-Saunders coupling and involve the jump of one electron only.

[14] W. V. Houston, Phys. Rev. **33**, 297 (1929).

[15] S. Goudsmit, Phys. Rev. **35**, 1325 (1930).

[16] O. Laporte and D. R. Inglis, Phys. Rev. **35**, 1337 (1930).

[17] D. R. Hartree, Proc. Roy. Soc. **A141**, 282 (1933); **A143**, 506 (1934).

Separation from $1s2s\ ^3S_1$ of

$1s2s\ ^1S_0$: X; $X=2G^0(10, 20)$.

Separation from $2p2s\ ^3P_2$ of

$2p2s\ ^3P_1$: $1/2(X+3A)-1/2((X-A)^2+8A^2)^{\frac{1}{2}}$;

$X=2/3\ G^1(20, 21)$.

$^3P_0$: $3A$.

$^1P_1$: $1/2(X+3A)+1/2((X-A)^2+8A^2)^{\frac{1}{2}}$.

Separation from $1s2p\ ^3P_2$ of

$1s2p\ ^3P_1$: $1/2(X+3A)-1/2((X-A)^2+8A^2)^{\frac{1}{2}}$;

$X=2/3\ G^1(10, 21)$.

$^3P_0$: $3A$.

$^1P_1$: $1/2(X+3A)+1/2((X-A)^2+8A^2)^{\frac{1}{2}}$.

Separation from $(2p)^2\ ^3P_1$ of

$(2p)^2\ ^3P_2$: $X-3/2\ A-((X-3/2\ A)^2+4XA)^{\frac{1}{2}}$;

$X=1/25\ F^2(21, 21)$.

$^3P_0$: $5/2\ X-(25/4\ X^2-5XA+9A^2)^{\frac{1}{2}}$.

$^1D_2$: $X-3/2\ A+((X-3/2\ A)^2+4XA)^{\frac{1}{2}}$.

$^1S_0$: $5/2\ X+(25/4\ X^2-5XA+9A^2)^{\frac{1}{2}}$.

The spin-orbit interaction parameter A is, throughout, one-third of the separation of $K\alpha_2$ and $K\alpha_1$ ($2p\ ^2P_{\frac{1}{2}}-2p\ ^2P_{1\frac{1}{2}}$); the F's and G's are the screening and exchanging integrals introduced by Wolfe[6] and are of the same form as the F_{ij}^k and G_{ij}^k defined in S.S., Eq. (4a).

The numerical results are tabulated in Tables III and IV and represented graphically in Fig. 1. The intensities in the second column of Table IV, relative to the strongest line in each group as 100, are calculated for Russell-Saunders coupling, those in the last column for the case of intermediate coupling found in Cu(29). It is seen that even in the case deviating furthest from Russell-Saunders coupling, Cu(29), the energy which is radiated in the form of singlet-triplet intercombination lines is less than 8 percent of the total energy radiated. For K(19), furthermore, the relative intensity of the strongest intercombination line is less than 1/5 of that for Cu(29). This justifies the disregard of the effect on the intensities of the deviation from Russell-Saunders coupling in the case of the lighter elements.

In Fig. 1 the heights of the "calculated" lines are proportional to their predicted intensities, whereas the relative lengths of the "observed" lines at most indicate the order of decreasing intensity, e.g., in Na α_3, α_4, α', α_5, α_6. The positions of the observed lines are taken from the work of Wetterblad[11] (for Na), Ford[18] and Richtmyer and Taylor[19] (for Cu). Intensities of lines due to the transitions $1s2s\rightarrow 2p2s$ (light lines) and those of lines due to the transitions $1s2p\rightarrow(2p)^2$ (heavy lines) are not comparable, the relative probabilities of excitation of the initial states being unknown. The horizontal distances are throughout proportional to $\Delta\lambda/\lambda$, $\Delta\lambda$ being measured from $K\alpha_2$, so that, as both $\Delta\lambda$ and λ are approximately proportional to the square of the atomic number,[20] corresponding observed satellites for different elements almost fall on the same vertical line. In this manner it becomes clearly evident how the strongest lines due to the transitions $1s2s\rightarrow 2p2s$ and $1s2p\rightarrow(2p)^2$ approach the principal satellites, $K\alpha_3$ and $K\alpha_4$, more and more closely as, with increasing atomic number, the approximations involved in the method of calculation becomes more nearly justified. It is also seen that the effect of the spin-orbit interaction on the predicted line structure is by no means negligible for elements heavier than Cl(17). Here the spread of the multiplets near the extreme right of the figure, always of the same order of magnitude as the doublet separation of the parent line, becomes comparable with the separation of the observed satellites α_3 and α_4.

With the results of Table I and Fig. 1 before us, the following coordination is tentatively suggested:

$K\alpha'$	$1s2p\ ^1P\rightarrow(2p)^2\ ^1S$ $1s2s\ ^1S\rightarrow 2p2s\ ^1P$	1 (1)	a
$K\alpha_3$	$1s2p\ ^3P\rightarrow(2p)^2\ ^3P$	9	b
$K\alpha_3'$	$1s2s\ ^3S\rightarrow 2p2s\ ^3P$	(3)	b'
$K\alpha_4$	$1s2p\ ^1P\rightarrow(2p)^2\ ^1D$	5	c

The letters a, b, b', c in the last column mark the corresponding lines or groups of lines in Fig. 1; the

[18] O. R. Ford, Phys. Rev. **41**, 577 (1932).
[19] F. K. Richtmyer and L. S. Taylor, Phys. Rev. **36**, 1044 (1930).
[20] F. K. Richtmyer, Phil. Mag. **6**, 64 (1928).

TABLE III. *Separations of energy levels in Rydbergs.*

		Na(11)	Cl(17)	K(19)	Cr(24)*	Cu(29)
	A	0.004	0.040	0.073	0.227	0.492
$1s2s$	X	.488	.984	1.138	1.524	1.972
	$^1S_0$	.488	.984	1.138	1.524	1.972
	$^3S_1$	0	0	0	0	0
$2p2s$	X	.878	1.625	1.865	2.453	3.052
	$^1P_1$	.882	1.667	1.944	2.725	3.721
	$^3P_0$	.013	.12	.22	.68	1.475
	$^3P_1$	.009	.078	.140	.408	.807
	$^3P_2$	0	0	0	0	0
$1s2p$	X	0.236	0.579	0.705	1.025	1.342
	$^1P_1$	.241	.625	.795	1.365	2.224
	$^3P_0$	.013	.12	.22	.68	1.475
	$^3P_1$	.009	.074	.130	.340	.594
	$^3P_2$	0	0	0	0	0
$(2p)^2$	X	.122	.246	.288	.396	.505
	$^1S_0$	.605	1.201	1.398	1.987	2.851
	$^1D_2$	.239	.458	.518	.658	.790
	$^3P_0$	.004	.029	.041	−.007	−.329
	$^3P_1$	0	0	0	0	0
	$^3P_2$	−.009	−.086	−.163	−.546	−1.257

* Screening and exchange integrals for Cr(24) were obtained by interpolation.

TABLE IV. *Separations of lines from $K\alpha_2$ in Rydbergs.*

Transition	Intensity (L, S)	Na (11)	Cl (17)	K (19)	Cr (24)	Cu (29)	Intensity (Cu)
$1s\rightarrow 2p$							
$^2S_{\frac{1}{2}}\rightarrow{}^2P_{1\frac{1}{2}}$	—	0.013	0.12	0.22	0.68	1.475	—
$1s2s\rightarrow 2p2s$							
$^1S_0\rightarrow{}^1P_1$	60	.738	1.216	1.417	2.054	2.840	57.9
$^3S_1\rightarrow{}^3P_0$	20	1.121	1.779	2.003	2.575	3.114	20
$^3S_1\rightarrow{}^3P_1$	60	1.125	1.821	2.083	2.847	3.782	57.9
$^3S_1\rightarrow{}^3P_2$	100	1.134	1.899	2.223	3.255	4.589	100
$^3S_1\rightarrow{}^1P_1$	0	—	—	—	—	.868	2.1
$^1S_0\rightarrow{}^3P_1$	0	—	—	—	—	5.754	2.1
$1s2p\rightarrow(2p)^2$							
$^1P_1\rightarrow{}^1S_0$	20	0.734	1.389	1.569	2.166	2.776	20
$^3P_2\rightarrow{}^3P_1$	25	1.098	1.965	2.172	2.788	3.403	25
$^3P_1\rightarrow{}^3P_0$	20	1.103	2.010	2.261	3.135	4.326	20
$^3P_1\rightarrow{}^3P_1$	15	1.107	2.039	2.302	3.128	3.997	11.4
$^3P_2\rightarrow{}^3P_2$	75	1.107	2.051	2.335	3.334	4.660	65.0
$^3P_0\rightarrow{}^3P_1$	20	1.111	2.085	2.392	3.468	4.879	20
$^1P_1\rightarrow{}^1D_2$	100	1.100	2.132	2.449	3.495	4.837	81.1
$^3P_1\rightarrow{}^3P_2$	25	1.116	2.125	2.465	3.674	5.254	34.1
$^1P_1\rightarrow{}^3P_1$	0	—	—	—	—	5.627	3.6
$^1P_1\rightarrow{}^3P_2$	0	—	—	—	—	6.884	.8
$^3P_1\rightarrow{}^1D_2$	0	—	—	—	—	3.207	8.8
$^3P_2\rightarrow{}^1D_2$	0	—	—	—	—	2.613	10.0

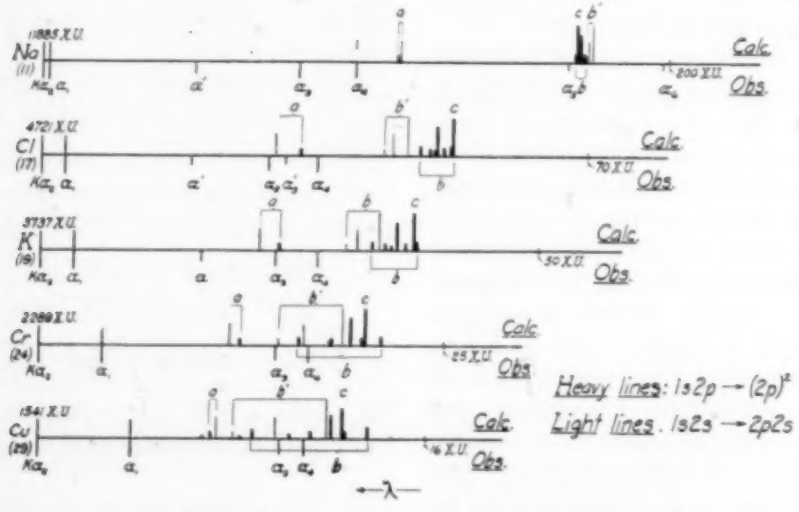

FIG. 1. Comparison of the calculated line structure corresponding to an additional vacancy in the L shell with the observed $K\alpha$-satellites.

preceding column repeats the relative intensities given in Table I. This coordination assigns only secondary importance to the transition $1s2s \rightarrow 2p2s$; it is assumed that the singlet line approximately coincides with $1s2p\ ^1P \rightarrow (2p)^2\ ^1S$, the triplet (coordinated to $K\alpha_3'$) with $1s2p\ ^3P \rightarrow (2p)^2\ ^3P$. Finally we suppose that a more rapid decrease in relative intensity with atomic number occurs for the transition $1s2s \rightarrow 2p2s$ than for $1s2p \rightarrow (2p)^2$,[21] so that the lines due to the former transition would play no rôle in the case of the heavier elements.

With these assumptions, which would require for theoretical verification especially a calculation of relative probabilities of excitation, the principal features of the observed satellite structure can readily be explained. Even without introducing the transition $1s2s \rightarrow 2p2s$, we find that there must be a reversal in intensity between $K\alpha_3$ and $K\alpha_4$ in the neighborhood of $P(15)$, as observed by Ford,[18] for the following reason: whereas for the lighter elements the complete unresolved triplet multiplet must be coordinated to $K\alpha_3$, giving an intensity ratio 9 : 5 for $K\alpha_3/K\alpha_4$, for the heavier elements the weaker components of this multiplet move away from the center leaving the diagonal line $^3P_2 \rightarrow {}^3P_2$ alone to be coordinated to $K\alpha_3$ and giving an intensity ratio 3.75 : 5 for $K\alpha_3/K\alpha_4$. The coordination of $K\alpha_4$ to a singlet transition agrees well with the absence of structure usually reported for this line.[22] The separation of the lines $1s2p\ ^3P_2 \rightarrow (2p)^2\ ^3P_2$ and $1s2p\ ^1P \rightarrow (2p)^2\ ^1D$ is, for small spin-orbit interaction, given by a simple difference of exchange integrals, which increases linearly with atomic number; this can be shown to be in accord with the observed parallelism of the "Moseleygrams" for α_3 and α_4.[20] Furthermore, the approximate calculations must give too small values for this separation, the error decreasing with increasing atomic number, so that a more exact treatment would be expected to improve the agreement with observation.

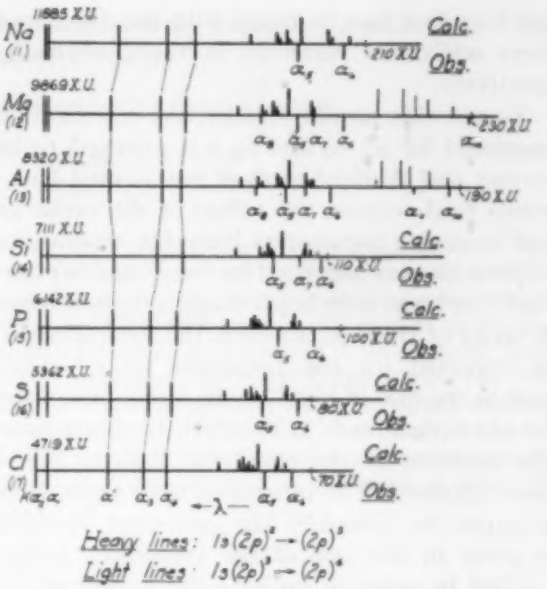

FIG. 2. Comparison of the calculated line structure corresponding to two and three additional vacancies in the $L_{II,\ III}$ shell with the observed outlying groups of $K\alpha$-satellites.

As to the further outlying satellites, it has already been stated that, in the case of sodium, the lines α_5 and α_6 certainly cannot be accounted for by one-electron transitions in *doubly* ionized atoms. In addition to α_5 and α_6, which have been observed in the range from Na(11) to Cl(17) by Wetterblad,[11] Ford,[18] Deodhar[22] and others, fainter satellites in their immediate neighborhood, α_7 and α_8, have recently been found for Mg(12) and Al(13) by Carlsson[23] and Karlsson and Siegbahn.[24] Karlsson and Siegbahn also found, for the same elements, a group of two extremely faint and diffuse lines, α_{10} and α_{11}, of still shorter wave-length. These observed lines are plotted to scale in Fig. 2. All of these satellites, besides being much fainter, are found to fade out more rapidly with increasing atomic number than does the principal group, α', α_3 and α_4. This, together with the fact that the parent line and the three groups α'–α_4, α_5–α_8 and α_{10}–α_{11} are separated by approximately equal distances, suggests that these groups might be

[21] This is suggested by the decrease with increasing atomic number in the probability of the photo-effect of the L_I ($2s$) shell compared with that of the $L_{II,\ III}$ ($2p$) shell, using the same primary radiation. See H. R. Robinson and A. M. Cassie, Proc. Roy. Soc. **A113**, 282 (1927).

[22] G. B. Deodhar, Proc. Roy. Soc. **A131**, 635 (1931) has observed a doubling of both α' and α_4 in the case of Si(14), but this is not in agreement with the findings of Ford[18] and, furthermore, was not found by Deodhar on a plate taken by Bäcklin.

[23] E. Carlsson, Zeits. f. Physik **76**, 741 (1932).

[24] H. Karlsson and M. Siegbahn, Zeits. f. Physik **88**, 76 (1934).

due to transitions in atoms with one, two, and three additional vacancies in the L shell, respectively.

To test this surmise further, the coordination suggested for α', α_3 and α_4 was assumed to be correct and Wolfe's[6] method was worked backwards to determine the values of the exchange and screening parameters from the separations of these lines as measured by Ford[18] and Wetterblad[11] and was then applied again to determine, in terms of these parameters, the separations to be expected for the transition $1s(2p)^2 \rightarrow (2p)^3$ and, in the case of Mg(12) and Al(13), also those for the transition $1s(2p)^3 \rightarrow (2p)^4$. In this manner the positions of the calculated lines in Fig. 2 were obtained. The intensities were taken from a paper by Ufford.[25] The spin-orbit splitting is given in the case of the transitions $1s(2p)^2 \rightarrow (2p)^3$ in order to indicate the spread of the multiplets. Intensities of lines belonging to the transitions $1s(2p)^2 \rightarrow (2p)^3$ and $1s(2p)^3 \rightarrow (2p)^4$ are of course plotted to different scales, since the former require triple and the latter quadruple ionization. The agreement between the calculated and observed line structure is quite satisfactory. The deviation is greatest for α_{10} and α_{11}, the lines coordinated to transitions in quadruply ionized atoms (in the case of Mg(12) α_{11} is masked by a β-line and is therefore not observable); this is to be expected as here the extrapolation involved in the calculation is greatest.

As a final point the question of chemical combination may be considered. Bäcklin[26] and Richtmyer[27] have both shown that, compared with metallic silicon, the satellites $K\alpha_{3,4}$ for silicon oxide are shifted relative to the parent line toward shorter wave-lengths by amounts comparable to the absolute shift of the parent line itself. The spectrograms for Mg, Al and their oxides published by Karlsson and Siegbahn[24] show the same effect and show furthermore that the shift for the $\alpha_{5,6}$ group is considerably larger still. This effect is to be expected on the present theory. As a limiting case of the effect of chemical combination we can compare the shift of the parent line and of the satellites $K\alpha_{3,4}$ (assuming the latter to be due to the transition $1s2p \rightarrow (2p)^2$) in the case of sodium when the valence electron is removed completely. Either shift is just equal to the difference in the ionization energies of the valence electron in the final and initial states for the transition in question. Identifying again ionization energies with energy parameters for the Hartree equations we obtain for the shift of the parent line (see S.S., Table I) $0.963-0.940=0.023$ Ry (3.6 X. U.), for that of the satellite $1.790-1.747=0.043$ Ry (6.7 X. U.). For higher stages of internal ionization the $3s$ electron will clearly be drawn still closer in toward the nucleus, resulting in a still larger shift when it is removed or displaced; hence the increased shift of the $\alpha_{5,6}$ group with chemical combination can be regarded as evidence in favor of the coordination of the lines of this group to transitions in triply ionized atoms.

The group $\alpha_{10,11}$ is unfortunately too faint and diffuse to make such a check possible. On the other hand, the slightness of the effect which chemical combination has on the character of these lines, as on all of the α satellites, is sharply contrasted in the spectrograms of Karlsson and Siegbahn with the behavior of the β-lines. This indicates clearly that the valence shell is not involved in the origin of any of the α satellites.

It is quite possible, in the opinion of the writers, that the specific coordinations suggested for α', α_3 and α_4 may have to be modified somewhat when further knowledge becomes available. To attempt a similarly detailed explanation of the further outlying satellites, α_5, α_6, α_7 and α_8, and particularly, α_{10} and α_{11}, would be premature in the light of the meager observational data extant at present. On the other hand, the writers believe that the present work definitely leads to the following conclusion: The satellite group $\alpha'-\alpha_4$ arises from jumps of a $2p$ electron into the $1s$ shell in the presence of one additional vacancy in the L shell, whereas the group $\alpha_5-\alpha_8$ is due to similar transitions in the presence of two additional vacancies in the L shell.

After making the coordinations for the satellites $\alpha'-\alpha_6$ we were interested to note that they were almost the same as those which Druyvesteyn[3] had suggested in his dissertation in 1928.

[25] C. W. Ufford, Phys. Rev. **40**, 974 (1932).
[26] E. Bäcklin, Zeits. f. Physik **38**, 215 (1926).
[27] F. K. Richtmyer, Phys. Rev. **37**, 457 (1931).

Measurement of Absolute X-Ray Intensities and Absolute Sensitivity of X-Ray Film with a Geiger-Müller Counter*

GORDON L. LOCHER,† *Bartol Research Foundation of the Franklin Institute*
AND
DONALD P. LEGALLEY, *The Pennsylvania State College*

(Received July 7, 1934)

A special Geiger-Müller counter for measuring absolute intensities of x-rays of known wave-lengths is described. The rays pass through the counter in such a way that only electrons set free in the gas of the counter are counted. The absorbing gas column is krypton at 6.31 cm pressure, 1.08 cm thick, and 0.0062 cm^2 in cross section. For fluorescent Zr K-rays, the absorption in the counter is 3.75 percent, as computed on the basis of the energy distribution of the radiation: $K\alpha : K\beta : K\gamma = 0.829 : 0.154 : 0.017$, and absorption coefficients computed from Richtmyer and Warburton's formulae. A "standard beam" of fluorescent Zr-rays from a specially constructed x-ray tube has been calibrated with the counter. With this beam, the minimum exposure of x-ray film for detectable blackening is found to be about 0.72×10^6 quanta cm^{-2}, incident on the film, or 4.1×10^4 quanta cm^{-2} absorbed in the emulsions (Eastman Ultra-Speed Duplitized X-Ray Film). The total absorption coefficients of the film, celluloid, and emulsion, for the Zr-rays, are found to be, respectively, 8.63 cm^{-1}, 1.66 cm^{-1} and 13.0 cm^{-1}. Time-blackening curves are given. These show discontinuities at exposures of about 10^7 quanta cm^{-2}.

I. INTRODUCTION

THE great sensitivity of Geiger-Müller counters for counting charged particles is well known. Besides their applications to problems of cosmic rays and radioactivity, in which the electrified particles penetrate the counting tubes from outside, they have been adapted for counting photoelectrons liberated internally by light, γ-rays and x-rays. The work reported here concerns the use of a counter for measurements of feeble x-ray intensities, by means of the photoelectric action of the x-rays on the gas of the counter. By this method it is possible to make absolute measurements of the flux of x-radiation with as good accuracy as that with which the energy-distribution of the incident radiation and its absorption coefficients in the gas are known.

Huppertsburg[1] has employed a counter with solid metal walls for comparison of the intensities of heterogeneous x-rays, and deduced the absolute sensitivity of the counter by measuring the corresponding ionization produced in an ionization chamber whose sensitivity he calculated. He showed that the counting rate was proportional to the area exposed, for a given x-ray beam, and that the photoelectrons came almost exclusively from the walls of his counter; the absorption in the gas was negligible.

In the experiments described here, almost monochromatic fluorescent x-rays are used. Absolute intensities are measured by means of the photoelectric action of the rays on the *gas* of the counter, by measuring the counting rates, using the efficiency of the counter as computed from the energy-distribution of the incident rays, the absorption coefficients of the gas, and the thickness and pressure of the gas. The counter thus forms a small ionization chamber in which the number of individual photoelectrons is counted, instead of measuring the amount of ionization in the customary manner.

II. THE COUNTER

Figs. 1, (a) and (b), are respectively, an x-ray photograph of the counter and a photograph of its cylinder-electrode (cathode). The x-rays enter and leave the counter through "bubble" windows of very thin glass, concave inwards. A narrow pencil of rays passes through the counter along a transverse diameter of the cylinder, in such a way as to miss the wire electrode, which is slightly off center. The cathode is a heavy gold-plated brass cylinder, 1.0 cm in diameter and 1.8 cm long, slightly flared at the edges. Two small lead blocks inserted in its walls collimate a beam of rays 0.0062

* Presented at the Physical Society meeting, Boston, Mass., Dec. 28–30, 1933; Phys. Rev. **45**, 292 (1934).
† National Research Fellow.
[1] A. Huppertsburg, Zeits. f. Physik **75**, 231 (1932).

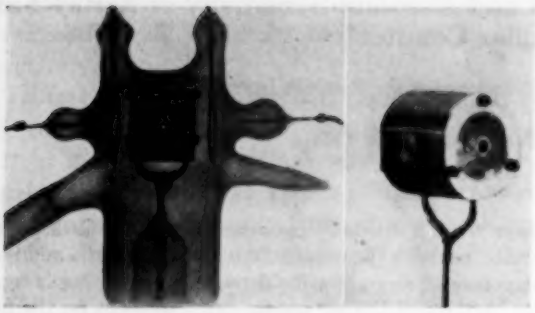

a b

FIG. 1. X-ray photographs of apparatus.

cm² in cross section by means of holes, respectively, 0.089 cm and 0.225 cm in diameter, for the entrance and exit of the rays. The inner surfaces of the windows are covered with cellophane disks, 0.0025 cm thick; these are sufficient to exclude the entrance of electrons liberated elsewhere than inside the cylinder, but their total absorption is so small that the scattering and photoelectron emission from the cellophane itself may be neglected. The ends of the cylinder are covered with disks of thick mica, to prevent stray ions from diffusing into the sensitive region.[2] The wire electrode is of bare tungsten, 0.0076 cm in diameter. The gas consists of approximately 98.5 percent krypton and 1.5 percent xenon at 6.31 cm of mercury, at 27.35°C.

Externally, the counter is shielded from stray radiation by sheets of lead so arranged that the number of accidental impulses due to stray radiation is reduced to a (measured) minimum. A series of thick lead blocks with holes of suitable diameters, mounted between the x-ray source and the counting tube, restrict the incident beam of x-rays to a size only a little greater than that allowed to pass through the counter.

The counter must be very accurately aligned with the source of x-rays, in order that the area of the beam passing through it shall be the same as that of the front collimating hole of its cathode, and in order that none of the radiation passing through the cathode shall strike the metal surface. This is accomplished by sighting through the small holes of the counter on the source of x-rays, which is illuminated with a bright light, with a telescope placed several meters beyond the apparatus.

Apart from the loss of impulses due to plurality of discharges falling within intervals less than the resolving-time of the apparatus, and the spurious discharges due to radiations of various kinds, there is assumed to be a one-to-one correspondence between the number of photoelectric absorption events in the counter and the number of impulses recorded; i.e., the efficiency of the counter for counting the photoelectrons liberated in it is taken as $1-\epsilon$, where ϵ is the loss due to multiple discharges occurring within the resolving-time of the apparatus. This seems reasonable, since each photoelectron produces some 700 pairs of ions, any pair of which would suffice to discharge the counter.

III. AMPLIFYING AND RECORDING APPARATUS

The circuit used for amplifying and recording the counter impulses has been described elsewhere.[3] It consists of a two-stage resistance-coupled amplifier with high-gain tubes (RCA 257), driving a pair of grid-controlled gaseous-discharge tubes (W.E. 256–A), arranged in a Wynn-Williams thyratron circuit. The significant time constants of the apparatus were found by oscillograph measurements to be approximately as follows: (a) recovery time of the counter and its attendant circuit, 0.0038 sec.; (b) resolving time of the circuit with the pair of relay tubes, <0.0007 sec.; (c) resolving time of the electromechanical impulse counter (a watch driven by a light relay), with one pair of relay tubes, ~ 0.008 sec., or 0.004 sec., with two pairs, and so on. The high-voltage supply is obtained from a rectifier of the type designed by Street and Johnson,[4] and is constant to <0.1 percent.

The counter wire is coupled to the amplifier through a $25\mu\mu$f condenser, and to ground through a resistance of 3.3×10^8 ohms.

Correction for loss of impulses, due to the arrival of more than one impulse within the resolving time of the apparatus, may be made by

[2] The two loop electrodes, shown in Fig. 1a, were inserted for collecting stray electrons, but were not used.

[3] G. L. Locher, J. Frank. Inst. **216**, 553 (1933). Telephones are inserted at *J* (Fig. 1).

[4] J. C. Street and T. H. Johnson, J. Frank. Inst. **214**, 155 (1932). The "first type" of voltage control is used. The tube for regulating the voltage is of type 57; this gives better regulation than a 24-A tube.

means of the formula $N_{true}=N_{observed}(x/1-e^{-x})$, where x is the average number of impulses arriving within the longest resolving time of the apparatus.[3] This correction is precise if the resolving time is precisely known. In this experiment, however, the rates of counting have mostly been kept sufficiently low that the loss due to this effect may be neglected. By using a low counting rate, one also avoids the danger of error due to change of apparent sensitivity of the counter with high speeds of operation.[5]

IV. Source of X-Rays

Fig. 2 shows the x-ray tube, which has a molybdenum anode and a zirconium metal fluorescer, F, arranged inside the tube in a region of intense radiation density. The fluorescent radiation emerges through a very thin window, W, of Pyrex glass. X-rays from about 1.06 cm² area of the fluorescer pass through holes in a series of lead baffles into the counting tube.

The incident radiation is assumed to be purely fluorescent Zr K-radiation, with wave-lengths and energy distribution as given in Table I.

V. Quantum Efficiency of the Counter

The fraction of the x-rays absorbed in the gas is calculated on the basis of the wave-lengths and energy-distribution given above, the pressure and constitution of the gas, and the length of path in the counter. In krypton and xenon, the scattering may be neglected, as compared with the fluorescent absorption. The atomic fluorescent absorption coefficients, τ_a, of the gas are calculated from the formula of Richtmyer and Warburton,[6] in Table II.

The number of atoms per cc in the gas (98.5 percent Kr+1.5 percent Xe at 6.312 cm mercury, at 27.35°C) is 2.043×10^{18}. The absorbing path in the counter is 1.079 cm.

From the data given above, we get the fractions $f_{K\alpha}$, $f_{K\beta}$, and $f_{K\gamma}$, of the $K\alpha$, $K\beta$, and $K\gamma$ radiation absorbed in the counter, namely,

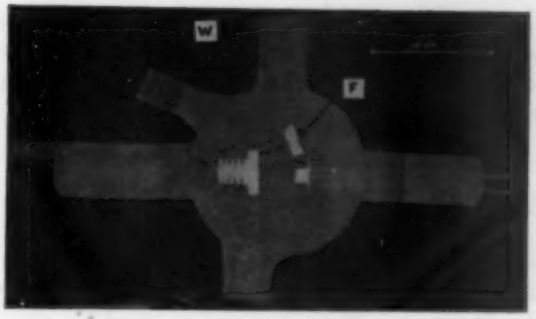

Fig. 2. Photograph of x-ray tube.

Table I. *Energy-distribution of Zr K-radiation.*

Wave-lengths[7]	
$K\alpha_1=0.7843$A	$K\beta=0.7005$A
$K\alpha_2=0.7885$A	$K\gamma=0.6883$A
Weighted mean $K\alpha=(2K\alpha_1+K\alpha_2)/3=0.7857$A	
Energy-distribution	
$K\alpha/K\beta=5.38$;[8]	$K\beta/K\gamma=9.0$;[9]
or $K\alpha:K\beta:K\gamma=48.42:9:1$	
Relative numbers of quanta	
$N_{K\alpha}:N_{K\beta}:N_{K\gamma}=0.845:0.140:0.015$	

Table II. *Atomic fluorescent absorption coefficients* $\times 10^{20}$.

	Krypton	Xenon	98.5% Kr+1.5% Xe
$K\alpha_{1,2}$	1.857	1.362	1.818
$K\beta$	1.294	0.965	1.289
$K\gamma$	1.225	0.913	1.220

$f_{K\alpha}=1-e\exp[-\tau_{K\alpha}x]=0.0393$ or 3.93 percent
$f_{K\beta}=1-e\exp[-\tau_{K\beta}x]=0.0280$ or 2.80 percent
$f_{K\gamma}=1-e\exp[-\tau_{K\gamma}x]=0.0265$ or 2.65 percent.

For the mixture of radiation in the beam, we have the total fraction, f, absorbed: $f=0.0375$ or 3.75 percent.

If every photoelectron discharges the counter, the total efficiency is, accordingly, 3.75 percent; and the multiplication factor between the number of quanta passing through the counter and the number of discharges is 26.67. We here assume that the radiation is pure fluorescent Zr

[5] A spurious increase of sensitivity after rapid operation is especially found in some counters containing photosensitive materials (G. L. Locher, Phys. Rev. **42**, 525 (1932); it usually becomes more conspicuous as the voltage applied to the counter is raised.

[6] F. K. Richtmyer and F. W. Warburton, Phys. Rev. **22**, 539 (1923).

[7] A. H. Compton, *X-Rays and Electrons*, p. 396.

[8] Interpolated from data of E. C. Unnewehr, Phys. Rev. **22**, 529 (1923). We assume that the ratio of the areas under the Zr $K\alpha$ and Zr $K\beta$-lines is the same for fluorescent as for characteristic radiation. A. H. Compton found this to be true for silver (Proc. Nat. Acad. Sci. **14**, 549 (1928)).

[9] Interpolated from data of A. E. Lindh; *Hand. der Exp. Physik*, Vol. 24, Part 2.

K-radiation, also that its energy-distribution is not appreciably altered by selective absorption in materials between the fluorescer and the counting chamber.

VI. Calibration of the X-Ray Beam

A "standard" x-ray beam has been calibrated for use in measurements of the sensitivity and blackening of films. Table III gives the data on this beam and illustrates the method by which the counter was used to calibrate it.

TABLE III. *"Standard" beam of fluorescent Zr x-rays.*

Voltage applied to counter: 680±0.1%
Area of beam traversing counter: 0.0062 cm²
Distance between fluorescer and counter: 58.8 cm
Potential applied to x-ray tube: 29,400 volts, peak, ± about 5%; constant to about 1%
Current through x-ray tube: 0.003 ampere ±about 1%
R_D = "accidental" counting rate: front aperture of counter covered, x-ray tube running, = 61.8 min.$^{-1}$ ±1.26% (6300 impulses)
R_L = correction for light from tube filament[10] = 6.5 min.$^{-1}$ ±7.1% (196 impulses)
R_T = total rate of counter, with apertures open, = 281 min.$^{-1}$ ±0.58% (29,600 impulses)
R_X = rate due to x-rays, only, = 213.6 min.$^{-1}$ ±about 1%
N_C = No. quanta passing through counter per minute = 26.67×213.6 = 5696.7
N_0 = No. quanta cm^{-2} min.$^{-1}$ = 5696/0.0062 = 9.03×10^5, approx.
N_0' = No. quanta cm^{-2} sec.$^{-1}$ = 1.50×10^4, approx.

VII. Measurements on X-Ray Film

Eastman Ultra-Speed Duplitized X-Ray Film[11] was used in the experiments described below. The exposed films were all developed for 5 min. at 18°C in Eastman D–19 developer; films exposed simultaneously were developed simultaneously. In all exposures, the x-rays were incident on the side of the film which has the heavy emulsion.

The energy flux at the film (57.3 cm from the fluorescer) was approximately 9.57×10^5 quanta cm^{-2} min.$^{-1}$, or 1.60×10^4 cm^{-2} sec.$^{-1}$. The samples of film were held between sheets of opaque paper in a heavy brass cassette which was perforated on both sides for the entrance and exit of the x-rays. The blackening effect of the softer fluorescent rays from the brass appears to have been small. Three kinds of experiments were performed..

(1) Minimum number of quanta for detectable blackening

Films were exposed to the standard beam for a series of short intervals and developed under identical conditions. An exposure of about 45 seconds gave visible blackening; this corresponds to 7.2×10^5 quanta per cm². The sensitivity of this film seems surprisingly high; if the quanta were spread uniformly over the surface, only 85 per mm are required to give visible blackening.

(2) Absorption coefficients of film, emulsion and celluloid

These were determined by measuring the counting rates with the standard beam, filtered, respectively, through 10 thicknesses of film (0.250 cm) and 10 thicknesses of celluloid from which the emulsions had been dissolved away (0.204 cm). The total absorption coefficients found in this manner are: $\mu_{film} = 8.63$ cm^{-1}; $\mu_{celluloid} = 1.66$ cm^{-1}; $\mu_{emulsion} = 13.0$ cm^{-1}. These values are subject to any error arising from modification of the wave-lengths and energy-distribution while passing through the absorbing material. Such error is probably small, since the incident x-rays are almost monochromatic. The results are believed to be reliable to within 10 percent.

Using the coefficients given above, we may calculate the number of quanta absorbed in the emulsion, for detectable blackening. This is approximately 4.1×10^4 cm^{-2}, or 20 quanta per mm, if spaced on a uniform lattice.

(3) Time-blackening experiments

Fig. 3 shows the time-blackening curve for the film, which was exposed to the standard beam for intervals of 2.5 to 60 minutes. The "blackening," as measured with a densitometer, is defined as the difference between the amounts of light transmitted through the background of the film and the exposed spot, respectively, called L_0 and L. These data are also shown in curve C, Fig. 4, in which the "density of blackening," D, is plotted against time. D is defined thus: $D = \log_{10} L_0/L$.

[10] The counter responds to far-violet and ultraviolet light, in spite of the gold plating on its cathode, and the fact that its windows are of Pyrex glass. The transmission of the light through the windows results from their thinness (about 0.002 cm each).

[11] The film was very kindly supplied by the Eastman Kodak Co. for the purpose.

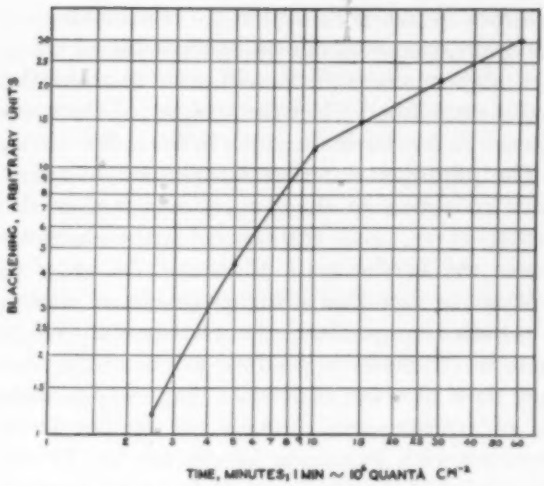

FIG. 3. Blackening of film exposed to x-rays.

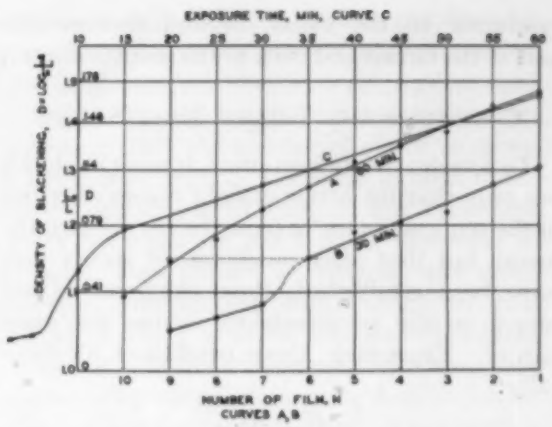

FIG. 4. Blackening of films through which the x-ray beam passed successively.

In another series of exposures, the beam of x-rays passed successively through 10 thicknesses of film, in the manner used by Brindley and Spiers.[12] The blackening of successive films was then measured with a densitometer. Curves *A* and *B*, Fig. 4, show the results for exposures of 60 and 30 minutes. The densities of blackening shown on these curves are very much smaller than those given by Brindley and Spiers; the two sets of data may accordingly be regarded as complementary, within the limits of the equivalence of the wave-lengths of the incident x-rays and the unknown equivalence of characteristics of the films used.

The authors wish to express their appreciation to Dr. W. F. G. Swann for his discussions of the problem and his interest in the investigation.

[12] G. W. Brindley and F. W. Spiers, Phil. Mag. **16**, 686 (1933).

DECEMBER 15, 1934 PHYSICAL REVIEW VOLUME 46

A Contribution to the Theory of Barrier Layer Cells

RUSSELL H. VARIAN, *Stanford University*

(Received October 19, 1934)

It is shown that the theory of the photovoltaic effect developed by Frenkel and Joffe is incomplete because it contains no adequate explanation of the direction of flow of the current. The proper direction of current flow follows as a natural consequence if the great difference in rate of energy loss by photoelectrons in the semiconductor and the metal is taken into account. In the metal collisions between photoelectrons and conduction electrons are frequent, and transfer of energy is rapid, whereas in the semiconductor such collisions are infrequent, and transfer of energy by elastic collisions of a photoelectron with atoms is slow. Hence rapidly moving photoelectrons tend to migrate into the metal and there lose their energy and become trapped.

INTRODUCTION

A BARRIER layer photo-cell such as the Cu_2O or Se cell consists of a closed conducting circuit which comprises a semiconductor forming a link in a metallic circuit, and a very thin barrier to the passage of electrons between the metal and semiconductor at one junction. In order for the cell to function, ionization must be produced in the semiconductor close to the barrier layer. This causes a continuous flow of electrons across the barrier layer from the semi-

conductor to the metal, around the metallic part of the circuit and back to the semiconductor.

Conditions the Theory Must Satisfy

To account for such an effect, it must be shown not only that the action of light causes electrons in the semiconductor to cross the barrier into the metal, but that after conditions of steady flow have been established, these electrons do not return to the semiconductor across the same barrier. Expressing these conditions algebraically:

$$N_1 > N_3, \tag{1}$$

where N_1 = number of electrons crossing the barrier from semiconductor to conductor; N_2 = number of electrons crossing the other boundary from semiconductor to conductor; N_3 = number of electrons crossing the barrier from conductor to semiconductor and N_4 = number of electrons crossing the other boundary from conductor to semiconductor.

After a steady current flow has been established, there must be no net gain or loss of electrons by the semiconductor. Hence

$$N_1 + N_2 = N_3 + N_4. \tag{2}$$

Therefore if N_1/N_3 is increased by the action of light, N_2/N_4 is decreased, and

$$N_1/N_3 > N_2/N_4. \tag{3}$$

The necessary conditions for a steady current having now been formulated, it remains to establish a mechanism which will meet these conditions.

Discussion of the Theory of Frenkel and Joffe

Frenkel and Joffe[1] have published a theory of the photovoltaic effect utilizing the same concept which they employed so effectively to explain the Cu_2O rectifier. This theory seems incomplete in certain respects, but by introduction of a neglected factor it may be made adequate to explain the facts.

In their treatment there is a marked difference in the potential energy levels of the conduction electrons in the metal and in the semiconductor, the conduction levels in the semiconductor being at a higher potential. Equilibrium between the two is established when the transfer of electrons across the barrier is the same in both directions.

The photovoltaic effect is assumed to result from ionization of the semiconductor near the barrier layer, and transfer of photoelectrons across the barrier into the metal. In order to explain the fact that a higher quantum energy is required to produce the photovoltaic effect than is required to produce photoconduction, they show by wave mechanics that the probability of transmission through the barrier layer increases with increasing kinetic energy. Hence the barrier is a smaller obstacle to photoelectrons of high kinetic energy than to those of low kinetic energy, and photoelectrons of high kinetic energy will therefore dominate in the resultant photocurrent.

The deficiency of the theory of Frenkel and Joffe lies in the fact that no good reason is given for the direction of electron flow. In fact, one would expect the flow to be opposite to that found by experiment, because of the following considerations. First, the energy to extract an electron from a bound state in the semiconductor, and give it sufficient energy to penetrate the barrier, is certainly as high as and probably somewhat higher than the energy necessary to extract an electron from the metal and give it the same kinetic energy with which to penetrate the barrier. Second, the optical absorption coefficient of the metal is much higher than that of the semiconductor, and one would therefore expect a greater concentration of photoelectrons close to the barrier in the metal, than in the semiconductor. One would therefore expect more electrons to enter the semiconductor than to enter the metal.

The contribution to the steady current of electrons which have lost their photoelectric velocities is zero. This conclusion may be reached either from theoretical or experimental considerations. It has previously been mentioned that more energetic quanta are required to produce the photovoltaic effect than to produce photoconduction, from which we can conclude that slow photoelectrons do not enter into the

[1] J. Frenkel and A. Joffe, Phys. Zeits. d. Sow. **1**, 1 (1932).

photovoltaic effect. When a steady state has been reached in the dark there are as many electrons entering as leaving the semiconductor. Under these conditions the probability of a thermally freed electron leaving the semiconductor by a particular route must be equal to the probability of its replacement by an electron entering by the same route. If it were otherwise a continuous current could flow under conditions of thermodynamic equilibrium. Since an electron which has lost its photoelectric velocity is indistinguishable from one thermally freed, it cannot contribute to the photovoltaic current.

Modified Theory

The theory becomes adequate if the great difference in the rate of loss of velocity of a photoelectron in the semiconductor and the metal is taken into account.

According to present views, the concentration of free electrons in semiconductors is very much lower than it is in conductors, and therefore collisions between free electrons in the semiconductor are very rare. The photoelectrons, unless they have enough energy to excite electrons in bound states will have to lose their kinetic energy by collisions with whole atoms. Because of the great difference in mass between electrons and atoms, electrons will lose their energy very slowly. In fact, if we assume the space lattice of Cu_2O to be composed of free elastic spheres having the masses of Cu and O atoms, an electron will still possess about half its initial kinetic energy after 15,000 collisions. This figure is given for order of magnitude only. Because of this slow energy loss an electron is able to migrate distances many free paths in length through the semiconductor before it loses its photoelectric energy, and may collide with the barrier layer many times before its energy is lost; hence both the chance of an electron crossing the barrier and the volume of the semiconductor effective in supplying electrons is increased by the slow loss of energy.

Under equilibrium conditions equipartition of energy between atoms and electrons necessarily holds, but the deviation of electron velocities from the mean in the semiconductor is much less than that of the atoms, or of the electrons in the metal, because the individual gains and losses of energy by collision are a much smaller proportion of the total energy of the electrons. At first sight this might appear to violate the equilibrium requirement that the number of electrons crossing the barrier must be the same in both directions for electrons of all energies. But while high velocity electrons are much more numerous in the metal, their chance of entering the semiconductor, and staying long enough to gain equilibrium with it is small, because of the great number of collisions required and the high probability of return across the barrier before the energy loss has been achieved. It is therefore obvious that a photoelectron possessing considerably more than the mean thermal energy will have a relatively high probability of crossing the barrier and quickly losing its excess energy in the dense electron atmosphere of the metal, whereas a similar photoelectron originating in the metal will have a very low probability of accomplishing the reverse process. Hence $N_1/N_3 > 1$ in the presence of light and by Eq. (2) $N_1/N_3 > N_2/N_4$.

The time during which a photoelectron will maintain a high kinetic energy in the conductor is very short as it can rapidly lose its energy in the dense electron atmosphere because the energy of a photoelectron is above the top of the fermi distribution. Therefore photoelectrons entering the metal from the semiconductor will have a low probability of return, whereas the photoelectrons which escape from the metal into the semiconductor have a very high probability of return. Therefore N_1 is markedly increased by the presence of photoelectrons whereas N_3 is not. From Eq. (2) it follows that an increase in N_1/N_2 results in a decrease in N_3/N_4 therefore expression (3) holds, and a current will flow.

Experimental Support of the Modified Theory

This theory accounts easily for the results obtained by Schottky[2] which lead him to surmise that photoelectrons freed in the semiconductor are able to make a great many collisions and still succeed in crossing the barrier layer. It will

[2] W. Schottky, Phys. Zeits. **32**, 833 (1931).

also explain the failure of Nasledow and Nemenow[3] to produce a barrier layer cell in which electrons would flow from the metal to the semiconductor, for even though a copious emission of electrons were obtained from the metal, most of the electrons would return to the metal before they lost their kinetic energy.

The author wishes to thank Dr. Felix Bloch and Dr. Robert Oppenheimer for valuable help and criticism.

[3] D. N. Nasledow and L. M. Nemenow, Phys. Zeits. d. Sow. **3**, 1 (1933).

DECEMBER 15, 1934 PHYSICAL REVIEW VOLUME 46

Sparking Potentials at Low Pressures

STEPHEN S. CERWIN, *Ryerson Physical Laboratory, University of Chicago*

(Received October 22, 1934)

Sparking potentials were observed between outgassed nickel electrodes in air at low pressures. The spark length d was varied from 2–10 mm and the pressure p reduced from 1 mm of mercury to 0.06 mm. Sparking potentials as high as 80,000 volts were observed, and agreed approximately with Paschen's law. The sparking potential V for $p \cdot d < 0.95$ is given by $p \cdot d \cdot e^{V/136,500} = 1$.

IT is well known that as the pressure of a gas diminishes, the potential difference necessary to produce a spark discharge between flat electrodes, separated by a fixed distance, also diminishes, until at a critical pressure the sparking potential reaches a minimum value. Below this critical pressure the potential required to produce a discharge, rapidly increases as the pressure is lowered.

Many experiments were made by Peace,[1] Paschen[2] and Carr[3] to check Paschen's law, which stated that at a given potential difference, the field being uniform, the product of the pressure at which the discharge occurs and the distance between the electrodes is constant. This law seems to be fairly established experimentally thus far.

Carr[3] who carried the investigation below the critical pressure found that the sparking potential rose extremely fast as the pressure was lowered but he was only able to reach a voltage of 1800 volts due to the restrictions in the design of his apparatus. The portion of the curve beyond this voltage has not as yet been investigated. Many experiments involve the use of electrodes close together, with gas pressures and potentials bordering on those at which a spark takes place; thus it is of interest to know just when such a discharge may occur. This investigation was carried out with this point in view. The experiments described in this paper deal with sparking potentials in air with nickel electrodes. Carr[4] has shown that the sparking potentials of almost all the common gases with the exception of hydrogen are grouped very closely around that of air in the low range of pressures.

Apparatus

A high voltage transformer and a kenotron supplied the rectified high voltage. A microammeter in series with Shallcross high resistances and a Kelvin electrostatic voltmeter served as a means of measuring the potential difference across the discharge tube, that is, between the electrodes. Since no condenser was used in the rectified high voltage, the microammeter resistance method with half wave rectification gave average values of the voltages read, which were multiplied by π in order to give the peak voltages that were interpreted as the sparking potentials.

[1] L. R. Peace, Roy. Soc. Proc. **A62**, 111 (1889).
[2] E. T. Paschen, Ann. d. Physik **37**, 69 (1889).
[3] W. R. Carr, Phil. Trans. Roy. Soc. **201**, 403 (1903).
[4] W. R. Carr, Phil. Trans. **A201**, 410 (1903).

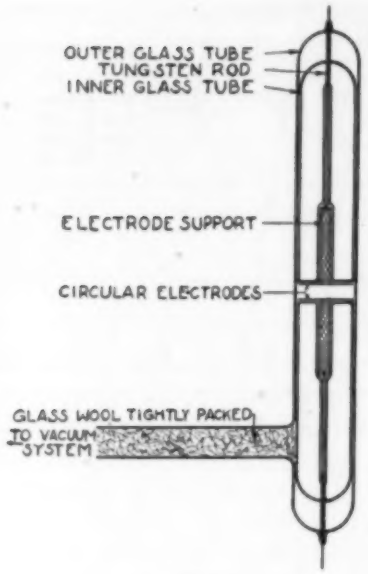

FIG. 1.

A mercury diffusion pump backed by an oil pump was used to lower the pressure to the desired point, a McLeod gauge was used to measure the pressure. The discharge tube was isolated from the rest of the high vacuum system by a trap, thus eliminating mercury or any other vapors that may be in the system. Fractional amounts of dry air were allowed to pass into the discharge tube by a system of stopcocks connected to a reservoir, which could be evacuated to any pressure. This method allowed very small changes to be made.

The design of the discharge tube was the most difficult part of these experiments. Since at the lower pressures the resistance to a discharge is greater for close electrodes than for more distant ones, the discharge will take the easiest, which in this case is the longest, path. In the early stages of this work, this phenomenon was often seen; the discharge going through very small cracks seeking a much easier path, sometimes doubling back to the ground electrode. This was prevented by finally designing the tube as shown in Fig. 1, where the glass tube holding the electrode was tightly telescoped into an outer tube. The tube connecting the discharge tube to the vacuum system was tightly packed with glass wool for several inches thus effectively stopping the discharge from passing to the McLeod gauge or pump.

It was found that the discharge would occur between the sides of the electrodes rather than between the flat faces as desired in this case. To prevent this they were made very thin and pressed very tightly to the glass tube holding them. It would probably have been much better if they could have been imbedded into the glass itself. The corners were rounded off to prevent concentration of the field at the edge of the electrode. The faces were flat, smooth and parallel. The electrodes were thoroughly out-gassed by heating in vacuum to a red heat with an inductance furnace to prevent any spurious gases from being liberated while the field was being applied, which by increasing the pressure between the electrodes would cause a premature discharge.

In the operation of this discharge tube the electrode which came out of the closed end A was connected to the high potential, while the other electrode connection B was grounded. The voltage was applied to the terminals of the discharge tube and if after a few minutes no discharge started, the voltage was raised and applied again and again in a similar manner until a discharge was formed. After making at least two more such observations, this potential was recorded as the sparking potential for that particular pressure. One-half hour was allowed to elapse between readings at different pressures.

The time delay of the discharge, first observed by Warburg,[5] was especially pronounced in the vicinity of the critical pressure, but seemed to diminish as the voltage was increased. It was rather difficult at first to determine the exact sparking potential, for the longer the application of the potential, the lower the spark occurred. However this was controlled by having a constant maximum time delay. Also this tendency diminished rapidly as the voltage was increased, in fact it was replaced at the high voltages by small premature electrical breakdown sparks. These were attributed to very small impurities in the electrodes themselves and were disregarded since a self-sustaining spark discharge did not form. The data in this range were slightly irregular presumably for that reason, although the irregu-

[5] Warburg, Ann. d. Physik **62**, 385 (1897).

larity also might be caused by a small error in the pressure which would make a very large error in the potential difference.

Results

The data are plotted in Fig. 2. The pressure in mm of mercury is plotted on a logarithmic scale in order to cover the range and illustrate all the curves together. The points for the lower portions of the curve are averages for two or three readings while those for the higher voltages are single readings. This was due to the fact that at the higher voltages when the discharge occurred, it did so with a hot, bright flash that finally burned the electrodes and sputtered the inner walls of the glass tube between them, thus ruining the discharge tube. Some of the curves are shortened for this reason, and because tubes with exactly the same characteristics could not be built. The life of the tubes was prolonged by taking readings with spark discharges of very short duration after the point had been approximately determined.

The points for the higher pressures and low sparking potentials agree with those of Carr[6] as far as he went, while the points of the upper end of the curve, i.e., for $p \cdot d < 0.95$ fall approximately on a straight line. The equation of this line is $V = 18 - 314{,}000 \log_{10} (p \cdot d)$, where V is the sparking potential in volts, p is the pressure in millimeters of mercury and d is the spark gap in millimeters. As $V \gg 18$ for all cases to which the formula may be applied, we may neglect the constant term on the right and say that for $p \cdot d < 0.95$; the sparking potential is connected

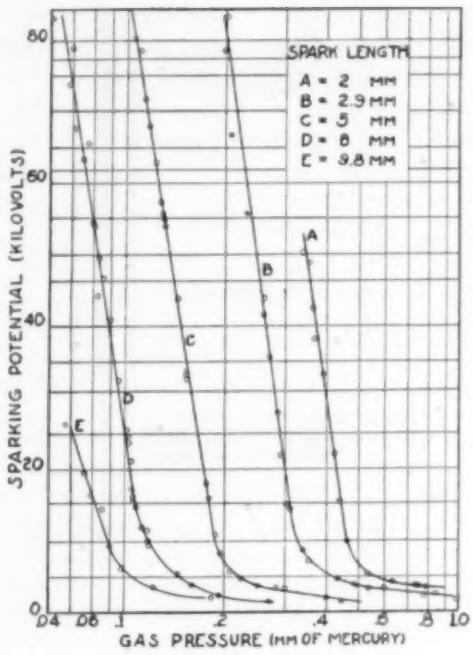

Fig. 2.

with the pressure and spark gap approximately by the formula $p \cdot d \cdot e^{V/136.500} = 1$.

According to Paschen's law the sparking potential is a function of the product of the pressure and the spark length. To the extent that the observations agree with the above formula, it is seen that the law holds. The sparking potentials were plotted against the products of pressure and spark length and were found to fall approximately on one curve. The points showing disagreement were those for the highest voltages where the irregularities in Fig. 2 are greatest.

The author wishes to acknowledge the many essential suggestions and constant helpful advice, which Professor A. J. Dempster, who suggested this problem, has given in the course of this work.

[6] W. R. Carr, Phil. Trans. **A201**, 414 (1903).

Polarization and Intensity Measurements in the Raman Spectrum of Carbon Dioxide

A. LANGSETH, *University of Copenhagen* and J. RUD NIELSEN, *University of Oklahoma*

(Received October 26, 1934)

The relative intensities and the depolarizations (for unpolarized incident light) of the two principal Raman bands of carbon dioxide have been measured. The following results were obtained:

$$\rho_{1286}=0.18, \quad \rho_{1389}=0.14, \quad I_{1286}/I_{1389}=0.61.$$

THE relative intensities of the two principal Raman bands of carbon dioxide were estimated visually by Dickinson, Dillon and Rasetti[1] and by Bhagavantam.[2] The latter also determined the depolarizations of the two bands. Recently, Isabel Hanson[3] has measured photometrically (at two different temperatures, 50°C and 200°C) the intensities of the 1286 cm^{-1}, the 1389 cm^{-1} and the 1410 cm^{-1} bands, excited by the 2537A mercury line.

The present work was carried out with an experimental arrangement previously employed to measure the depolarizations of the Raman bands of carbon disulphide.[4] The CO_2 gas was contained in a glass tube at a pressure of 20 atmospheres and a temperature of 25°C. The slit of the liquid-prism spectrograph was 0.1 mm wide, and the position of the Wollaston prism in the collimator tube was so adjusted that the "perpendicular" component of the 1286 cm^{-1} band, excited by the 4358A mercury line, fell nearly midway between the "parallel" components of the 1286 cm^{-1} and 1389 cm^{-1} bands. Two exposures were made lasting 48 hours and 144 hours, respectively, the density marks, produced by a step-weakener, being exposed one-third as long as the Raman spectrum.

Fig. 1 shows the intensity distribution, evaluated from a record taken with a Moll microphotometer of the plate exposed 48 hours. The correction for the continuous background, which varied somewhat from one band to the other, was very large, averaging 50 percent of the maximum intensity. The intensity distribution curve is analyzed into component bands as indicated by the dotted curves. It will be seen that whereas the ratio between the intensities of the parallel components of the principal bands as well as the depolarization of the 1389 cm^{-1} band can be determined with considerable accuracy, there is some difficulty in determining accurately the perpendicular component and, hence, the depolarization of the 1286 cm^{-1} band. This is due almost entirely to the broadening of the strong parallel components rather than to the presence of the weak satellites or to Raman bands excited by other mercury lines than 4358A. The dispersion was not large enough to separate the satellites from the principal bands. In Fig. 1, the arrows marked *a* and *d* indicate where the parallel components of the satellites, 1265 cm^{-1} and 1410 cm^{-1}, should appear. The observed intensity distribution curve shows no evidence of the presence of the 1265 cm^{-1} band but rather definite evidence, as indicated by the dotted curve, of the 1410 cm^{-1} band. The satellites are too weak and too far from the maxima of the principal bands to influence perceptibly the observed values for these maxima. Moreover, their presence would be a source of error only if they had depolarizations differing greatly from those of the principal bands.

The arrows marked *b* and *c* show where the parallel components of 1389 cm^{-1} excited by the 4339A and 4347A mercury lines should fall. There is evidence of the band excited by 4347A, although the maximum of the dotted curve seems shifted a little to one side. The low intensity of this band indicates that, for the light emitted by a quartz mercury arc, the value given

[1] R. G. Dickinson, R. T. Dillon and F. Rasetti, Phys. Rev. **34**, 582 (1929).
[2] S. Bhagavantam, Nature **127**, 817 (1931); Ind. J. Phys. **6**, 319 (1931).
[3] Isabel Hanson, Phys. Rev. **46**, 122 (1934).
[4] A. Langseth, J. Utoft Sørensen and J. Rud Nielsen, J. Chem. Phys. **2**, 402 (1934).

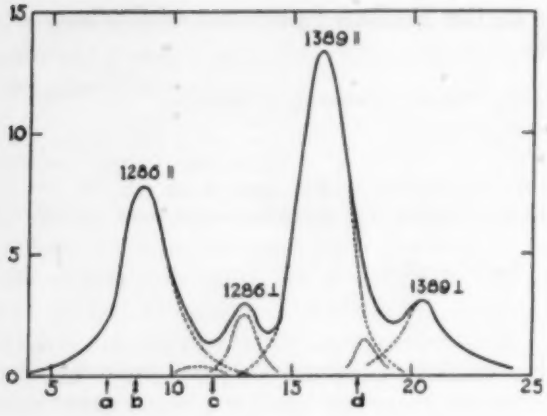

FIG. 1. Energy distribution curve.

in most spectral tables for the ratio between the intensities of the 4347A and the 4358A lines is not even of the right order of magnitude. As shown by the position of the arrow *b*, the parallel component of 1389 cm^{-1}, excited by the 4339A mercury line, lies rather close to the parallel component of 1286 cm^{-1} excited by 4358A. This will tend to make the observed intensity of the latter band too high. However, although no data are available to permit a quantitative estimate, it is evident from the low intensity of the band at *c*, together with the fact that the line 4339A is much weaker than 4347A, that this error is very small.

The results obtained are listed in Table I.

TABLE I. *Depolarizations and intensity ratio.*

Exposure time	ρ_{1286}	ρ_{1389}	I_{1286}/I_{1389}
48 hours	0.20	0.14	0.60
144 hours	0.16	0.14	0.63
Average:	0.18	0.14	0.61

The depolarizations are for unpolarized incident light. Because of the greater broadening of the parallel components, the data derived from the 144 hour exposure are somewhat less accurate than those obtained from the shorter exposure. The error in the average value of ρ_{1286} may be as high as 15 percent. The depolarization of the 1389 cm^{-1} band is probably correct to within 8 percent, and the intensity ratio to 5 percent.

The observed depolarizations are lower than the value 0.2 obtained by Bhagavantam[2] for both bands by a visual method. As in the case of carbon disulphide, for which similar values were found for the depolarizations,[4] the stronger band is more highly polarized than the weaker band. However, in view of the aforementioned errors, which influence the measurement of the perpendicular component of 1286 cm^{-1}, it is possible that the difference in the depolarizations of the two bands is less than observed.

A calculation of the depolarization of the Raman band associated with the totally symmetrical vibration of CO_2, based upon previous work of Ramanathan[5] and others, has been made by Bhagavantam.[6] He obtained a value 0.3 that is roughly twice as high as the observed depolarizations. Also for other molecules, this method of calculation leads to too high values for the depolarization.[7]

The observed intensity ratio confirms remarkably the value 10 : 15 estimated visually by Dickinson, Dillon and Rasetti but differs considerably from the values 1 : 3 and 1 : 2 obtained by Bhagavantam by a more elaborate method. The average value 0.61 for the intensity ratio is in exact agreement with that found by Hanson at 200°C but is somewhat higher than the supposedly more accurate value 0.57 found by her at 50°C. The values for the intensity ratio listed in Table I have been evaluated by multiplying the ratio between the intensities of the parallel components of the 1286 cm^{-1} and 1389 cm^{-1} bands by $1.18/1.14=(1+\rho_{1286})/(1+\rho_{1389})$. Even if it be assumed that the observed difference between the depolarizations of the two bands is due entirely to experimental errors, we find a value 0.59 for the intensity ratio which is higher than the lower of the two values obtained by Hanson.

[5] K. R. Ramanathan, Proc. Roy. Soc. **A107**, 684 (1925).
[6] S. Bhagavantam, Ind. J. Phys. **6**, 557 (1932).
[7] Cf. G. Placzek, *Rayleigh-Streuung und Raman-Effekt*, Marx: *Handbuch der Radiologie*, p. 365, 2nd Ed., Vol. 6, Part II, Braunschweig, 1934.

The Absorption Spectrum of Arsenic

G. E. GIBSON AND ANGUS MACFARLANE,* *Department of Chemistry, University of California, Berkeley*

(Received August 27, 1934)

A new band-system has been found when ultraviolet light is absorbed by arsenic vapor, heated to 1100°C. Some eighty band-heads have been detected between the wave-lengths of 2200 and 2750A. An analysis of the vibrational levels has been made, which shows that the spectrum can be ascribed to the diatomic molecule. The value of ω_e is 432 cm^{-1} for the lower and 271 cm^{-1} for the upper state. The vibrational levels of the excited molecule are greatly perturbed, as is shown by irregularities in the plot of $\Delta G(v')$ against v'. The continuous absorption of arsenic in the ultraviolet is considerable in extent. It is therefore probable that its potential energy curve is cut by another, due to a third state of the molecule, which causes predissociation. Energies of dissociation have been calculated and, by analogy with phosphorous, suggestions have been made as to the states of the atoms produced by dissociation. A doubling of the band-heads in a restricted region of the system has been observed. A critical survey of previous work on the fluorescence spectrum of arsenic is included and an attempt has been made to allot, as far as is possible, vibrational quantum numbers to the bands there observed.

INTRODUCTION

IN a note in the *Philosophical Magazine* for 1875, Norman Lockyer gave an account of his researches on the spectra emitted by elements heated in a furnace. To arsenic he ascribed a "channelled" spectrum in the green. He was doubtful of this observation, however, and announced that he intended to examine it again, but he does not appear to have published any further investigations he may have made.

Rosen[1] illuminated arsenic vapor with mercury light of wave-length 2537A, and obtained in fluorescence five weak lines which were tentatively ascribed to the As_2 molecule. On account of their faintness, he was not able to measure the lines with any great accuracy, as indeed is apparent from the inconsistency of the first differences of his wave numbers (Table VI).

Swings and Migeotte[2] have extended the number of lines in the fluorescence spectrum, using for excitation the following mercury lines: (2536.7, 2534.9); (2483.87, 2482.76, 2482.07); (2655.3, 2653.9, 2652.2); (2806.84, 2805.42, 2804.52, 2803.53A). The correlation of the fluorescence lines with our absorption bands is delayed until a later section.

Kimball and Bates[3] photographed a carbon arc, the negative electrode of which had been drilled and filled with arsenic, run in an atmosphere of hydrogen and at a potential difference of 110 volts. Three bands were found, two of which, with origins at 32,380.2 cm^{-1} and 31,636.9 cm^{-1}, were ascribed to AsH, while the third whose head was 31,802.6 cm^{-1} was considered to be due to As_2. Rydberg,[4] however, showed that these bands were probably identical with the CH bands at λ3143A, already investigated by Fortrat and by Hori.

Winand[5] has published an account of his researches in the spectroscopy of arsenic. Despite intense excitation and prolonged exposure, he was unable to reproduce the fluorescence spectrum recorded by Rosen. His results consist of two series of measurements, the first of the absorption coefficients of the vapor between λ3100 and λ3900, the second of the wave-lengths of the bands emitted on excitation by an external ring-electrode discharge. These latter compose, besides two systems of bands around 2200A which were too faint to be measured, a spectrum extending from λ2800A to λ5000A, which Winand considers probably arises from the diatomic molecule. Their wave-lengths are given in Table I, together with a classification that he adopts, dividing the bands into two categories, according as they are to be observed in the discharge in the central portion of the tubes or in the parts around the electrodes. All these bands are degraded to the ultraviolet.

The first three members of the "central"

* Commonwealth Fund Fellow.

[1] Rosen, Zeits. f. Physik **43**, 69 (1927).

[2] Swings and Migeotte, Comptes rendus **197**, 836 (1933).

[3] Kimball and Bates, Nature **128**, 969 (1931).

[4] Rydberg, Nature **129**, 167 (1933).

[5] Winand, Bulletin de la Classe des Sciences, Academie royale de Belgique, (5) **18**, 422 (1932).

TABLE I. *Band-heads of emission spectrum of arsenic (Winand).*

	System		System
2810	A Central	3543	IV_2 Electrodes
2816		3584	IV_1 Electrodes
2869		3657	
2882		3688	F Central
2966	B Central	3720	V_3 Electrodes
2972			
2978	I Electrodes	3769	V_2 Electrodes
3127	C Central	3820	V_1 Electrodes
3135		3909	G Central
3163	II Electrodes	3932	VI_4 Electrodes
3306	D Central	3958	VI_3 Electrodes
3318		4018	VI_2 Electrodes
3389	III Electrodes	4081	VI_1 Electrodes
3483	E Central	4144	H Central
3501			

system are single; the remaining five consist each of two closely spaced band-heads. Taking the mean of the frequencies of these latter, Winand expresses the system by the formula:

$$\tilde{\nu} = \tilde{\nu}_0 - bn + cn^2$$

$$= 37459 - 1945n + 35n^2, \quad n = 1 \cdots 8,$$

it being assumed that a similar band at λ2670A is the first number of the series. The spacing of these bands is thus considerably greater than that in the fluorescence spectrum of Rosen (420 cm^{-1}). No analysis of the "electrode" system has been attempted.

EXPERIMENTAL

The impurities with which elementary arsenic is most likely to be contaminated are antimony, arsenic oxide, which is formed on exposure of the element to air at room temperature and possibly arsenic sulphide. Although the two latter sublime at a lower temperature than arsenic itself, it is in practice difficult to ensure their complete removal by fractional sublimation, while, according to Orloff[6] it is impossible to free arsenic from antimony by this method.

In the mode of preparation finally employed this difficulty was overcome by forming arsenic *in situ* under conditions where such impurities are unlikely to occur. Recrystallized sodium arsenate was freed from antimonate by fractional precipitation with magnesia mixture. The middle portion was digested with hydrochloric acid and again fractionally precipitated. From the final fraction arsine was developed by the action of zinc on a solution in hydrochloric acid. The gas was dried by passage through a trap cooled to −20°C with an alcohol-carbon dioxide freezing mixture and then over phosphorous pentoxide. This portion of the apparatus was freed from air by displacement by a current of pure hydrogen, which was also used to carry the arsine forward through the system.

The pure dry arsine then passed through a tap into a wide Pyrex tube connected by means of a graded seal to the quartz absorption cell and also to the pumps. This system had been previously thoroughly evacuated and outgassed, finally being filled with hydrogen prior to the generation of arsine. Then, on heating the walls of the Pyrex tube, arsenic was deposited as a metallic mirror. After sufficient of the element had accumulated, it was sublimed up and down the tube in the hydrogen stream to remove any possible traces of the oxide. The gas generating train was then removed and the pumps were started. When evacuation was complete, the arsenic was sublimed into the absorption cell and this was sealed off.

Vandevelde[7] and Reckleben and Scheiber[8] have disproved Retgers's[9] statement that a solid hydride, AsH, is formed when arsenic is heated in an atmosphere of hydrogen. The element sublimes without chemical change; the yellow-brown product is an allotropic modification which soon reverts to the metallic form.

The earlier measurements were made with a quartz absorption cell 20 cm in length. There is, however, so much general absorption of ultraviolet light by arsenic vapor that very long exposures were necessary. The extent of the absorption increases rapidly with pressure as well as with temperature. Therefore a longer cell, 72 cm in length, was substituted to permit the use of lower pressures, thus also increasing the proportion of diatomic molecules. In this

[6] Orloff, Chem. Zeits. **26**, 290 (1901).

[7] Vandevelde, Bull. Acad. Belg. (3), **30**, 78 (1895).

[8] Reckleben and Scheiber, Zeits. f. anorg. Chemie **70**, 255 (1911).

[9] Retgers, Zeits. f. anorg. Chemie **4**, 429 (1893).

way, the time of exposure was reduced and the number of bands observed was considerably extended. Even so, so greatly does the continuous absorption vary with frequency, that it was necessary to find the best conditions of pressure afresh for each short wave-length range.

The furnace in which the absorption cell was heated was an alundum tube, $5\frac{1}{2}$ cm in internal diameter. It was well lagged with silocel packing, and the windings of stout chromel wire were spaced more closely at the ends than in the center, to assist in the production of even temperatures along its length. The ends were blocked with plane quartz windows. With 6 amperes at 220 volts, temperatures of 1100°C were attained as recorded by chromel-alumel thermocouples.

The side-arm of the cell protruded from the furnace and, to control the pressure of arsenic within, was separately heated through coils wound on the quartz tube and on a quartz cap that fitted over the end. Results were obtained with temperatures of the side-arm furnace, as registered by thermocouples placed inside the heating coils, of from 380° to 500°C. The measurements of the vapor pressure of arsenic are somewhat scattered, but these temperatures would appear to correspond to pressures of from 2 mm to 50 mm. Preuner and Brockmöller[10] have made vapor density determination from which it may be deduced that at 1000°C, the partial pressure due to the diatomic molecules will be 2.4 mm when the total pressure is 5 mm and about 20 mm when it is 50 mm. The dissociation of arsenic involves two equilibria, $As_4 \rightleftharpoons 2As_2$ and $As_2 \rightleftharpoons 2As$, and the second stage is appreciable at 1000°C.

The source of continuous ultraviolet light was a hydrogen discharge tube made according to the specifications of Bay and Steiner.[11] The tube was water-cooled and was operated with a current of 0.5–1 ampere at 6000 volts. A series of diaphragms cut out stray light which might have been reflected from the walls of the absorption tube. The spectrum of the source was continuous throughout the ultraviolet with the exception of six lines around 2500A.

A Hilger E3 quartz spectrograph was used to analyze the light. Photographs were made on Eastman 50 and on Imperial Eclipse 850 plates, the latter appearing to be the more efficient. On account of the falling off of the sensitivity of photographic plates beyond 2500A, attempts were made by preillumination to bring out the images with the greatest intensity. The contrast of the plates in the further ultraviolet is so low, however, that this procedure made little noticeable improvement.

The wave numbers of the band-heads were measured by comparison with the iron arc spectrum. A linear interpolation over short ranges of the spectrum was made of the comparator readings of the known frequencies and a correction curve of the differences, $\tilde{\nu}$ vac. $-\tilde{\nu}$ linear, was drawn and applied to the calculated band-head wave numbers.

Results

The bands observed lie between 2200A and 2750A; the wave numbers of the band-heads that have been measured are recorded in Table II. As has already been mentioned, the continuous absorption by arsenic vapor in this region has made it exceedingly difficult to obtain intense and well-contrasted pictures of this spectrum. The overlapping of band-heads that is to be expected in the middle of the system is, for reasons later to be discussed, abnormally great in this case, and in certain regions the bands possess diffuse instead of sharply-defined heads. For these reasons no high order of accuracy is claimed for these frequency determinations. Repeated measurements of the more intense bands agree to about one wave number; in other cases the concordance is less.

The bands of highest frequency possess sharply-defined heads and can be assigned to

Table II. *Frequencies of band-heads in* cm^{-1} *(absorption).*

44820	42839	41734	40885	39715	39182	38662	37994
44601	42669	41654	40802	39674	39139	38611	37892
44349	42582	41543	40722	39599	39087	38567	37731
44106	42481	41476	40639	39559	39034	38556	37581
43856	42414	41406	40557	39506	38971	38460	37485
43604	42331	41306	40447	39457	38920	38409	37321
43432	42221	41229	40300	39384	38880	38304	37176
43352	42150	41148	40020	39301	38828	38252	36913
43098	41985	41046	39877	39256	38768	38144	36770
42924	41895	40980	39808	39228	38721	38053	36509

[10] Preuner and Brockmöller, Zeits. f. physik. Chemie **81**, 129 (1912).
[11] Bay and Steiner, Zeits. f. Physik **59**, 48 (1929); **45**, 337 (1927).

TABLE III. *Deslandres diagram of the band-heads of arsenic.*

$\Delta G(v'')$			428	426	423	421	419	414	411	407	405		
$\Delta G(v')$	v' / v''	0	1	2	3	4	5	6	7	8	9	10	11
262	0					(38567)	38144	37731	37321	36913	36509	—	—
258	1			—	(39256)	38828	38409	37994	37581	37176	36770		
249	2				39506	39087	38662	38252					
(262)	3				—	—	38920d	—					
(277)	4			40447dd	40020d	39599d	39182d	38768d					
258	5		(41148)	40722	40300	39877	39457						
247	6		41406	40980	40557	—	39715						
243	7		41654	41229	40802	—							
258	8	(42331)	41895d	41476d	41046dd	(40639)dd							
257	9	42582d	42150d	41734dd	41306	40885d	—						
257	10	42839	42414	41985	(41543)								
255	11	43098	42669	(42221)									
253	12	43352	42924	(42481)									
252	13	43604	43178										
250	14	43856	43432										
	15	44106											
	16	(44349)											
	17	(44601)											
	18	—											
	19	—											
	20	—											
	21	—											

Notes: Figures in brackets are uncertain.

— indicates bands observed but not measured, by reason of faintness or of overlapping.

d indicates a diffuse, dd a very diffuse band-head.

relatively short v' progressions that converge but slowly. Because of the falling-off of the sensitivity of the photographic plate as well as their intrinsic low intensity, the four bands of shortest wave-length could not be measured under the travelling-microscope. Visually, however, it is readily seen that they are a continuation of the first measurable progression (see Fig. 1) and there have been no signs on any of the spectrograms of bands arising from a lower vibrational level of the lower state than this. It may be tentatively assumed therefore, that the bands of highest wave number arise from transitions from the ground level of the unexcited molecule.

The first discernible band of the next v' progression, arising on this assignment of quantum numbers from the vibrational level $v''=1$, appears only after five measurable bands of the first, of higher frequency, have been recorded. The value of v' corresponding to the most probable transition thus varies rapidly with v'' in this portion of the spectrum, and there are therefore but few adjacent bands of the two progressions that are both of sufficient intensity to permit the accurate measurement of the spacing of the two lowest levels of the ground state of the molecule, $\Delta G(v'')_1$. Careful redetermination of the frequencies of the heads of the four most suitable bands gave a value of 428 cm^{-1} for this difference. This figure is in accordance with the interval between successive bands of the series on the long-wave side of the spectrum, which are to be expected to form v'' progressions to the lower v' levels, and thus confirms the relative placing of the v' progressions in the Deslandres diagram (Table III).

Anticipating the allocation of vibrational quantum numbers to the observed levels of the upper state, which is based on the assumption that the bands farthest towards the visible represent transition to the lowest of them, a change of character in the band-system is to be observed when the levels $v'=8$ and 9 are reached. Instead of possessing sharply-defined

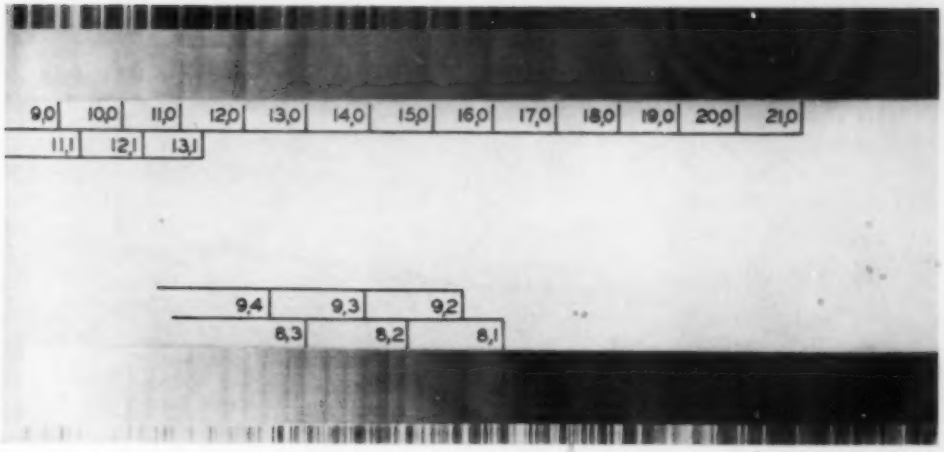

FIG. 1. (a) The bands of the $(v', 0)$ progression. (b) The appearance of diffuse band-heads in the lower v' levels.

heads, the bands present a diffuse appearance, while the values of $\Delta G(v')$, making all allowance for the lesser accuracy of frequency measurement, represent a discontinuity in the curve of its plot against v'. The sharply-defined heads reappear in the bands that can be placed above these in the vertical columns of the Deslandres diagram, corresponding to values of v' from 5 to 7, but there is a further alternation of appearance beyond this, the bands corresponding to the levels $v'=3$ and 4 being diffuse in appearance and in the three lowest levels observed resuming the original sharpness. (See Fig. 1.)

Such marked changes in character of the bands show that the upper state is considerably perturbed, suggesting that its potential energy curve is crossed by a second due to another state of the molecule. Until a detailed analysis of the spectrum has been made under higher dispersion no definite conclusions can be drawn. However, some general inferences may be made, confidence in which is strengthened by consideration of the spectrum of diatomic phosphorus, the behavior of which might be expected to be analogous. Herzberg[12] has made a complete study of the phenomenon of predissociation of this molecule.

The analysis of the band-system of phosphorus shows that the transition is $^1\Sigma_u^+ \rightarrow {}^1\Sigma_g^+$, the lower state dissociating into two normal ^4S atoms and the upper into two excited atoms, one in a ^2D and the other in a ^2P state. In emission, although bands corresponding to transitions from the level $v'=11$ are observed with high intensity, none that can be attributed to a higher vibrational level is to be found. Further, in the $v'=10$ and 11 bands, the rotational structure of both P and R branches breaks off abruptly, the last lines observed possessing a normal intensity. The differences in energy of the vibrational levels show that at $v'=11$ the molecule is far from normal dissociation. Predissociation must, therefore, be due to another electronic state possessing a much lower energy of dissociation, whose potential energy curve cuts that of the $^1\Sigma_u^+$ state. To this third state an electronic structure $^3\Sigma_u^+$ or $^3\Pi$ is assigned, dissociating into one normal (^4S) and one excited (^2D) atom.

The remaining vibrational levels are considerably perturbed by this crossing of potential energy curves, as is shown by the differences in the $G(v', 0)$ terms given in Table IV. The frequencies of these band-heads are accurately represented by the equation $\tilde{\nu}=46{,}790.1+472.62v'-2.600v'^2+0.0217v'^3$ for the v' levels from 6 to 11. The energies of the lower levels, however, diverge markedly from those calculated from this equation, the maximum deviation being 7 cm^{-1}, which is far outside the experimental error. To account for this perturbation, Herzberg draws the potential energy curve of the $^3\Sigma_u^+$ or $^3\Pi$ state causing predissociation with a shallow minimum above that of the other upper

[12] Herzberg, Ann. d. Physik (5) **15**, 677 (1932).

TABLE IV. *The vibrational levels of P_2 and As_2.*

v	Phosphorus $\Delta G(v', 0)$ cm^{-1}	Arsenic $\Delta G(v')$ cm^{-1}	Arsenic $\Delta G(v'')$ cm^{-1}
0			
	471.7	262	428
1			
	470.4	258	426
2			
	454.1	249	423
3			
	453.4	(262)	421
4			
	448.0	(277)	419
5			
	449.1	258	414
6			
	441.0	247	411
7			
	437.9	243	407
8			
	433.2	258	405
9			
	429.2	257	
10			
	425.1	257	
11			
		255	
12			
		253	
13			
		252	
14			
		250	
15			
		(243)	
16			
		(252)	
17			

Note: The differences in brackets are the more doubtful.

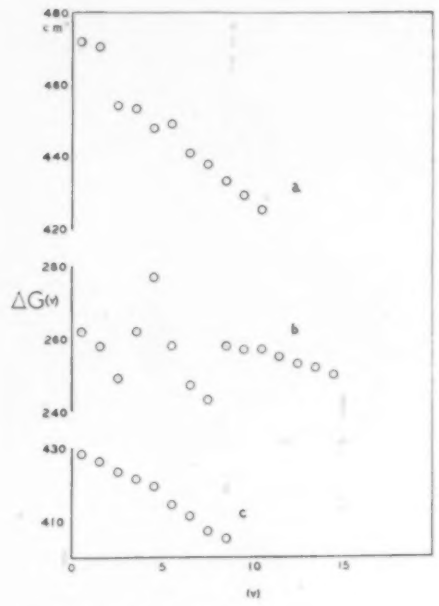

FIG. 2. The plot of $G(v)$ against v for (a) the upper state of phosphorus, (b) the upper and (c) the lower state of arsenic.

state. Except for the fact that no abrupt termination of the band system of arsenic at a certain value of v' occurs, its character is similar to that of phosphorus. This difference is accounted for by the fact that, while the present measurements were made in absorption, Herzberg used an emission method. The probability of radiationless transfer to the dissociating state of molecules excited to levels of higher energy than the predissociation level will be much greater than that of return to the lower state. The absence of bands of higher v' levels in the absorption measurements of phosphorus by Jakowlewa[13] may be attributed to a natural fading of intensity. The last band measured in the $(1, v'')$ progression is that for which $v'=7$, and in the $(v''=0)$ that for which $v'=10$. Otherwise, the prevalence of continuous absorption and the substitution of diffuse for sharp-headed bands in two separate ranges of v' levels clearly argue that predissociation occurs in the arsenic molecule also. Fig. 2, where $\Delta G(v')$ is plotted against v' for both phosphorus and arsenic, shows that the perturbation of the upper levels is even more pronounced with the latter. From the points of discontinuity in the curve, it may be deduced that the potential energy curves of the two upper states cut near the vibrational level for which $v'=8$ and again at $v'=3$.

PRODUCTS AND ENERGIES OF DISSOCIATION

Accurate estimation of the energies of dissociation of the electronic states is not possible, since the levels observed are far from the convergence. An estimate has been made in both cases by linear extrapolation of the plot of $\Delta G(v)$ against v. For the upper state the extrapolation depends only on the seven levels above the predissociation point. Energies of dissociation so determined will in all probability be much higher than the true values. This procedure gives 23,750 cm^{-1} as the figure for D' and 30,100 cm^{-1} as that for D''. The latter is equivalent to 85.6 calories; the thermochemical value

[13] Jakowlewa, Zeits. f. Physik **69**, 548 (1931).

of Pruener and Brockmöller,[10] based on vapor density determinations between 900°C, and 1100°C, is 30 calories.

The energy difference between the products of dissociation of the lower and upper states may now be estimated from the equation:

$$E_{\text{atoms}} + D'' = D' + \tilde{\nu}(0, 0),$$

where $\tilde{\nu}(0, 0)$ is the difference in energy between the ground vibrational levels of the molecule in the normal and excited states, 40,230 cm^{-1}. Substitution of these figures gives for the excitation energy of the atoms forming the upper state, 33,880 cm^{-1}, an inaccurate value of course, since it depends on the uncertain energies of dissociation. However, we may hazard on this basis the guess that, as with phosphorus, the upper electronic state dissociates into a ^2P and a ^2D atom, which requires an energy excess over two ^4S atoms of 10,591+18,185 cm^{-1} = 28,776 cm^{-1}.

If the predissociating state is formed, as by analogy with phosphorus is probable, from one normal ^4S and one excited ^2D atom, the energy difference of the two pairs of atoms will be 10,951 cm^{-1}. Adding to this the value, of D'', 30,100 cm^{-1}, will give the height of the limit of the predissociating curve above the zero vibrational level of the lower state, 41,050 cm^{-1}. This is but slightly greater than the (0, 0) interval, 40,230 cm^{-1} and corresponds almost exactly to the appearance of the first predissociation of the vibrational level $v' = 3$, whose height above the ground level of the lower state 41,040 cm^{-1}. So long and uncertain is the extrapolation on which the value of D'' depends, however, that one hesitates to consider this agreement as more than coincidence.

The Bands at the Low Frequency End of the Spectrum

The bands farthest towards the visible are found to be v'' progressions. As at the high frequency end of the system, the last heads are too faint to be measurable under the comparator. It seems clear that they do not represent a fresh progression and consequently this first series has been assumed to be the progression terminating in the zero level of the upper state. The $\Delta G(v'')$ values exhibit no such irregularities as are found in the $\Delta G(v')$; their plot against v'', which has been used as described above to estimate the heat of dissociation, is given in Fig. 2c. The figures are the mean of those differences that can be most accurately determined. From them the equation representing the heads of the (0, v'') progression is found to be:

$$\tilde{\nu} = 40{,}447.0 - 432.1(v'' + \tfrac{1}{2}) + 1.5(v'' + \tfrac{1}{2})^2.$$

Thus ω_e'' is 432.1 cm^{-1} and $x_e\omega_e''$ 1.5 cm^{-1}. The $G(v')$ figures cannot be similarly treated but backward extrapolation of the plot of the unperturbed upper levels against v' gives a value of ω_e' of 271 cm^{-1}. The ΔG figures are included with Herzberg's date in Table IV. He found that ω_e for the ground state of phosphorus was 777.62 and $x_e\omega_e$ 2.8118 cm^{-1}; the corresponding figures for the upper state were 472.62 and 2.60 cm^{-1}. As might be expected from its higher atomic weight, the arsenic figures are lower than those for phosphorus. The similarity between the two sets of data strengthens the belief that this band-system is that of the diatomic arsenic molecule.

A somewhat remarkable doubling of the heads occurs in this region of the spectrum. At first sight these appeared to be separate progressions, but it has been found impossible to place them as such in the Deslandres diagram. Their frequencies would require that they should fall below and to the right of the v'' progressions. So placed they lie slightly above the 45° line and constitute a separate branch of the Condon parabola; such an arrangement is inconsistent. Further the $\Delta G''$ values are altogether too high for such a position and those of $\Delta G'$ are out of agreement with the general trend of the main system. By virtue of those differences they must occupy a position overlapping the main v'' progressions; there is then excellent agreement of the ΔG values of the two subsystems. The heads of the interloping bands lie some 55 cm^{-1} further towards the ultraviolet than the corresponding bands of the main branch. These facts are shown in the reproduction of the appropriate part of the Deslandres diagram (Table V). The band-heads that fit with the rest of the scheme are lettered A, the subsidiary heads B.

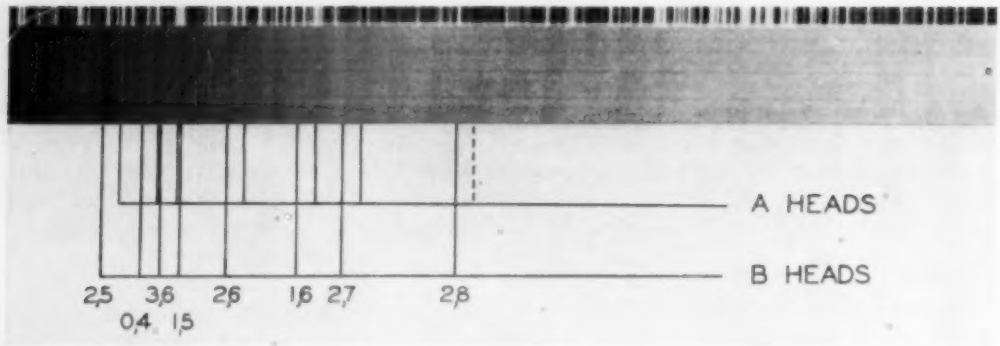

FIG. 3. The low frequency end of the system showing the main (A) and subsidiary (B) band-heads.

The rows of figures designated $\Delta\tilde{\nu}$ are the differences in frequency of the two heads.

Head for head correspondence does not exist between the figures for the two series, partly because of the excessive overlapping that this complication causes and the diffuseness that is due to predissociation in the higher v' levels. In overexposed positives, it is possible to see the composite nature of the band-heads that are not separately measurable under the microscope (Fig. 3). The second system may well extend therefore to higher v' levels than is recorded, but there is no trace of it on the pictures at the high frequency end of the spectrum.

The lack of correspondence among the heads of lowest frequency is due, however, to a rapid variation in their relative intensity. This is well shown in the photograph (Fig. 3). The B heads in the $(0, v'')$ progression are not discernible beyond a value of $v''=4$, nor in the $(1, v'')$ progression beyond $v''=6$, although the A heads can be traced up to $v''=11$ in the first and $v''=9$ in the second. In the progression of next highest number of v', however, the B heads are consistently stronger than the A, the (2, 7) and (2, 8) members of the latter series being marked at this dispersion by little more than the greater intensity of the absorption. The same is true in the $(3, v'')$ progression, save that the A heads are unfortunately concealed by overlapping. With higher vibrational levels of the upper state that is possibly the fate of the B heads; no band can be definitely ascribed to this series with a value of v' greater than four. Since the agreement between the ΔG figures of the A and B heads is good when both series have been observed, it seems justifiable to use the latter in estimating $\Delta G'$ (2, 5). In the A series only one band-head of the $v'=3$ level can be found that is free from overlapping, and its frequency is not accurately measurable by reason of its faintness.

TABLE V. *Doubling of heads of bands of the v'' progressions.*

v' \ v''	2	3	4	5	6	7	8	9
	A		(38567)	38144	37731	37321	36913	36509
0	*B*	39034	38611					
$\Delta\nu$			(44)					
	A	(39256)	38828	38409	37994	37581	37176	36770
1	*B*	39301	38880	38460	38053			
$\Delta\nu$		(45)	52	51	59			
	A	39506	39087	38662	38252			
2	*B*	39559	39139	38721	38304	37892	37485	
$\Delta\nu$		53	52	59	52			
	A	x	x	d 38920				
3	*B*	39808	39384	38971	38556			
$\Delta\nu$				51				
	40447 *A*	40020	39599	d 39182	d 38768			
4	*B*			? 39228				
$\Delta\nu$				? 46				

At present it is difficult to account for this doubling of the band-heads in a restricted region of the Deslandres diagram. The spectrum of sulphur, which is generally similar in its predissociation phenomena, presents an analogous case, which, however, is confined to the v'' progression of the lowest v' level. At a distance of 20 cm^{-1} beyond the main band-heads subsidiary ones are found, but these are always considerably the lower in intensity. Henri and Teves[14] had suggested that they were due to the

[14] Henri and Teves, Nature **114**, 894 (1924).

R branches, but Christy and Naudé[15] have shown that these form the main band-heads and that no Q branches exist, the electronic transition being $^3\Sigma_u^- \rightarrow {}^3\Sigma_g^-$. The latter authors attribute the weaker bands to a different electronic state.

However, such an explanation would appear to be precluded as far as arsenic is concerned by the agreement between the ΔG values and the absence of B heads at the higher frequency end of the spectrum. No isotopes of arsenic have as yet been recorded and indeed it is difficult to see how the facts could be accounted for as an isotopic displacement. There remains the possibility, confirmation of which must await analysis of the rotational structure, that the A and B heads are formed by different branches of the same bands. Even if this is the explanation, the rapid variation in the relative intensities of the sub-heads is somewhat remarkable. This is to be expected when the B_v values of the upper and lower states are nearly equal, so that their variation with v' and v'' may cause a large change in $(B_v' - B_v'')$. In arsenic they may be expected to differ greatly in magnitude, since ω'' is much larger than ω'; and for most molecules B/ω is a constant in all its electronic states.

The Fluorescence Spectrum

The lines observed in fluorescence by Rosen cannot be easily identified, since they were too weak to be accurately measurable. In all probability they represent the $(0, v'')$ progression from $v''=1$ to $v''=5$. Of these, only the A heads of the $v''=4$ and 5 and the B heads of the $v''=3$ and 4 bands have been found. Rosen's figure for the line corresponding to the (0, 4) band-head lies between the frequencies of the two sub-heads and, correspondingly, his value for the (0, 3) band is lower than, and for the (0, 5) band is higher than the new measurements of the B and A head, respectively. Since his spectrograph appears to have had a dispersion of 300 cm^{-1} per mm, more than twice as small as that of the Hilger instrument, it is not unlikely that in a weak photograph the two lines might be measured as one.

There is, however, another possible allocation of vibrational quantum numbers to these fluorescence lines. They may represent the $(v'=3)$ progression from $v''=3$ to 7. On this assignment, Rosen's frequencies are consistently higher by some 30 cm^{-1} than those of the strong B heads, recorded in absorption from $v''=3$ to $v''=6$. Since the A heads of this level are very much the weaker and lie at frequencies 50 cm^{-1} lower still, there is no possibility of attributing the discrepancy to confusion of the two. The former allotment may therefore be considered the more likely.

This conclusion is strengthened by consideration of Swings and Migeotte's redetermination of the fluorescence frequencies. A comparison of the resonance and absorption measurements is made in Table VI. Section (a) of this records

Table VI. *The fluorescence spectrum of As*.

Order	Rosen		Swings and Migeotte		Absorption		$(v'=0)$
	(a) Bands excited by Hg lines 2536.7 and 2534.9A.						
					A heads	B heads	v''
−1	39850		39844				1
		441		435			
0	39409		39409†				2
		404		394			
1	39005		39015			39034	3
		425		405			
2	38580		38610		38567	38611	4
		410		414			
3	38170		38196		38144	38197*	5

Order	Swings and Migeotte		Absorption	$(v'=5)$
	(b) Bands excited by Hg lines, 2483.87, 2483.76, 2482.07A.			
				v''
−2	41,084		41,148	1
		402		
−1	40,682		40,722	2
		419		
0	40,263†		40,300	3
		395		
1	39,868		39,877	4

Order	Swings and Migeotte	
	(c) Bands excited by Hg lines 2655.3, 2653.9, 2652.2A.	
−1	38091	
		424
0	37667†	
		367
1	37300	
		380
2	36920	
		370
3	36550	
		377
4	36173	

* Calculated.
† Swings and Migeotte do not include the frequencies of the 0 order band; for purposes of comparison, selection from the wave numbers of the exciting lines has been made in the same way that they have done. (see text).

the results of excitation with mercury light of wave-length 2536.7 and 2534.9A. Column I gives the order of the resonance lines; II and IV their frequencies as measured by Rosen and by Swings and Migeotte, respectively; III and V the values of $\Delta\nu$ in the two series; VI the frequencies of the A and B heads of the $(0, v'')$

[15] Christy and Naudé, Phys. Rev. **37**, 902 (1931).

progression obtained from absorption measurements and column VII and vibrational quantum numbers of the lower state, v''. Swings and Migeotte's figures for the (0, 3), (0, 4) and (0, 5) bands are considerably higher than Rosen's and in good accordance with the absorption measurements of the B bands. There is however nothing to correspond to the simultaneous appearance of double heads observed in the absorption bands.

The fluorescence measurements made by the latter authors but not by Rosen are included in the same table. Section (b) contains the measurements of the fluorescence lines excited by the mercury lines, $\lambda = 2655.3, 2653.9, 2652.2$A, corresponding to which three fluorescent lines of each band are found. The frequencies given are those of the "center of gravity" of each "triplet," by which presumably the mean is meant. In all probability, the molecules excited by the three frequencies of incident light are in different rotational states of the same vibrational level. The band-head will lie therefore to one side or other of the resonance triplet, in this case towards the farther ultraviolet since the bands are degraded to the red. The separation of the two extreme mercury lines is about 30 cm^{-1}. It is to be expected, therefore, that the band-heads measured in absorption will have higher frequencies than the corresponding results of Swings and Migeotte. The closest correspondence is found in the (5, v'') progression, the comparative figures being given in columns I and III of Table VIb, and the values of v'' in column IV. It is interesting to note that this level lies above that at which predissociation, marked by the diffuseness of the band-heads, first appears. Molecules excited to this level of the upper state have therefore a long enough life period to make their return to the lower with emission of radiation probable, in accordance with the observation that in absorption these band-heads regain their sharpness of outline.

The series excited by the λ2804A lines consists of two positive terms. They were, however, too feeble for the measurement of their frequencies to be possible.

Column I of Table VI (c) contains the wave numbers of the centers of gravity of the "triplets" excited by the mercury lines 2655.3, 2653.9 and 2652.2A, an overall separation of 45 cm^{-1}; the band-heads must therefore lie at least 22 cm^{-1} higher. The differences, $\Delta G(v'')$, in column II are much smaller than any of those found by us in absorption. It is presumed therefore that these fluorescence lines represent transitions to a higher v'' level, and, since the frequency of the fluorescence "triplet," 36,920 cm^{-1}, is very near to that of the (0, 8) band-head, 36,913 cm^{-1} they must represent transitions to a higher v' state as well. This series cannot be assigned to the (0, v'') progression, for its last member would then compete with the first of the 2537 fluorescence "doublets" for the same, (0, 5), place in the Deslandres diagram, and the $\Delta G(v'')$ values are too small for this to be possible. This fluorescence spectrum represents, therefore, a progression not observed in absorption. It is satisfactory to find that none of these fluorescence series indicate the existence of v'' levels lower than those found in the absorption measurements and do not, therefore, disturb the present assignment of vibrational quantum numbers.

The Influence of the Stark Effect on the Fine Structure of the Balmer Lines of Hydrogen

N. P. HEYDENBURG,* *University of Wisconsin*

(Received October 22, 1934)

In view of the discrepancies reported between the observed and theoretical doublet splitting of the Balmer lines of hydrogen, a detailed study of the Stark effect of the H_α and H_β lines has been made to determine whether small electric fields, which might be present in the discharge tube, could account for the observed results. Calculations have been made for several field strengths using the standard theory of the Stark effect. Doppler curves were plotted for each component and superimposed to give resultant curves. For the H_β line, fields up to 100 volts/cm did not produce a sufficient asymmetry in the doublet components to account for the results of Houston and Hsieh. For a field of 500 volts/cm, H_α has a doublet separation which agrees with that observed by Gibbs and Williams. However, the general shape of the H_β line has changed completely at a field of 400 volts/cm, so that the same field will not account for the doublet separations of all the Balmer lines.

INTRODUCTION AND THEORY

SEVERAL papers have recently appeared on the fine structure of the Balmer lines of both ordinary and heavy hydrogen. Houston and Hsieh[1] have found that the observed doublet separation of the Balmer lines H_β through H_ϵ is about 4 percent smaller than that given by the Dirac theory. The validity of their method for determining this separation depends on the doublet components being symmetrical about their centers. Gibbs and Williams[2] have made measurements on the H_α line of H^1 and H^2 and find a decrease in the doublet separation for H^1 of about 6 percent while for H^2 the separation is very nearly in agreement with the theoretical value. Kopfermann[3] has been able to resolve the H_α line of H^2 into three components with separations less than 2 percent smaller than those predicted.

Since one cannot be sure of the conditions existing in the discharge tubes used for exciting these lines it seems important that the effect of an electric field on the shape of the resultant components should be investigated. It was thought that a Stark effect might perhaps change the position of the components so as to produce an asymmetry in the resultant doublets, which would introduce a correction to the results of Houston and Hsieh. The position of the components might also shift in such a way as to change the separation of the resultant doublet peaks. The calculations were made using the standard theory of the Stark effect[4] for hydrogen with spin. Only the matrix elements between terms with the same principle quantum number n are taken into account, the effect of matrix elements between terms with different n being negligible. A convenient reference system for labeling the rows and columns of the energy matrix is obtained by using symmetric and antisymmetry combinations of wave functions with the same inner quantum number j, the same magnetic quantum number m, and different azimuthal quantum numbers l. The part of the energy matrix referring to any one j is diagonal in this system and the only nondiagonal elements are those for which the j for the rows is different from the j for the columns. Letting the electronic charge be $-e$, and the axis of the electric field E be z, the nonvanishing matrix elements of the perturbing energy eEz can be brought by a canonical transformation to the form:

$$(j,(-1)^\beta|eEz|j+1,(-1)^\alpha)=-3/8\,a_H eE[(j+1)^2-m^2]n\{[n^2-(j+1/2)^2]^{1/2}+(-)^{\alpha+\beta}[n^2-(j+3/2)^2]^{1/2}\}/(j+1),$$

* National Research Fellow.

[1] Houston and Hsieh, Phys. Rev. **45**, 263 (1934).

[2] Gibbs and Williams, Phys. Rev. **45**, 475 (1934).

[3] Kopfermann, Naturwiss. **22**, 218 (1934).

[4] Schlapp, Proc. Roy. Soc. **A119**, 313 (1928); Rojansky, Phys. Rev. **33**, 1 (1929); Bethe, *Handbuch d. Physik*, Vol. 24, 416.

$$(j,(-)^\beta|eEz|j,(-)^\alpha)=-3/8\,a_H eEmn[(-)^\alpha+(-)^\beta][n^2-(j+1/2)^2]^{1/2}/j(j+1),$$

$$(j,(-)^\beta|eEz|(j+1)_{\max},m)=-(3/4\sqrt{2})a_H eE[(j+1)^2-m^2]^{1/2}n[n^2-(j+1/2)^2]^{1/2}/(j+1);\ (j=n-3/2).$$

Here even or odd values of α or β correspond, respectively, to symmetric or antisymmetric states and a_H stands for the Bohr radius. The wave functions which correspond to this form of the matrix are:

$$(j,(-)^\alpha)=2^{-1/2}[(l=j-1/2,j,m)+(-)^\alpha(l=j+1/2,j,m)],$$

where

$$(l=j-1/2,j,m)=R_{n,\,j-1/2}\{(j+m)^{1/2}Y_{j-1/2}^{m-1/2}S_{1/2}+(j-m)^{1/2}Y_{j-1/2}^{m+1/2}S_{-1/2}\}(2j)^{-1/2},$$

$$(l=j+1/2,j,m)=R_{n,\,j+1/2}\{(j-m+1)^{1/2}Y_{j+1/2}^{m-1/2}S_{1/2}-(j+m+1)^{1/2}Y_{j+1/2}^{m+1/2}S_{-1/2}\}(2j+2)^{-1/2}.$$

Here the normalizing angular factors of the orbital spin functions are:

$$Y_l^m=(-)^m[(2l+1)/4\pi]^{1/2}[(l-m)!/(l+m)!]^{1/2}e^{im\varphi}(\sin\theta)^m(d/d\cos\theta)^{l+m}[(\cos^2\theta-1)^l/2^l l!]$$

and $S_{1/2}$, $S_{-1/2}$ are spin functions satisfying $(S_x+iS_y)S_{-1/2}=2^{1/2}S_{1/2}$. The sign of the radial factor $R_{n,\,l}$ is the same as that in Sommerfeld's *Ergänzungsband*.

The roots of the secular determinates corresponding to these matrices were then obtained. Fields are to be considered weak when the elements having different j's are small compared to the diagonal elements with the same j's. When these elements are of the same order of magnitude the fields will be called intermediate.

The matrix elements for z, $x+iy$, $x-iy$ which must be multiplied by the appropriate coefficients of the new wave functions in calculating the intensities of the various components are given by the following equations:

$$(1/\sqrt{2}[(n,l=j+1/2,j,m)+(-)^\alpha(n,l=j-1/2,j,m)]|z|1/\sqrt{2}[(n',l=j+1/2,j,m)$$
$$+(-)^\beta(n',l=j-1/2,j,m)])=\frac{m}{4j(j+1)}[(-)^\beta R_{n',\,j-1/2}^{n,\,j+1/2}+(-)^\alpha R_{n',\,j+1/2}^{n,\,j-1/2}],$$

$$(1/\sqrt{2}[(n,j+1/2,j+1,m)+(-)^\alpha(n,j+3/2,j+1,m)]|z|1/\sqrt{2}[(n',j-1/2,j,m)$$
$$+(-)^\beta(n',j+1/2,j,m)])=\frac{[(j+m+1)(j-m+1)]^{1/2}}{2(j+1)}\cdot 1/2[R_{n',\,j-1/2}^{n,\,j+1/2}+(-)^{\alpha+\beta}R_{n',\,j+1/2}^{n,\,j+3/2}],$$

$$(1/\sqrt{2}[(n,j-1/2,j-1,m)+(-)^\alpha(n,j-3/2,j-1,m)]|z|1/\sqrt{2}[(n',j-1/2,j,m)$$
$$+(-)^\beta(n',j+1/2,j,m)])=\frac{[(j+m)(j-m)]^{1/2}}{2j}\cdot 1/2[(-)^\beta R_{n',\,j+1/2}^{n,\,j-1/2}+(-)^\alpha R_{n',\,j-1/2}^{n,\,j-3/2}],$$

$$(1/\sqrt{2}[(n,j+1/2,j+1,m\pm1)+(-)^\alpha(n,j+3/2,j+1,m\pm1)]|x\pm iy|1/\sqrt{2}[(n',j-1/2,j,m)$$
$$+(-)^\beta(n',j+1/2,j,m)])=\mp\frac{[(j\pm m+2)(j\pm m+1)]^{1/2}}{2(j+1)}\cdot 1/2[R_{n',\,j-1/2}^{n,\,j+1/2}+(-)^{\alpha+\beta}R_{n',\,j+1/2}^{n,\,j+3/2}],$$

$$(1/\sqrt{2}[(n,j+1/2,j,m\pm1)+(-)^\alpha(n,j-1/2,j,m\pm1)]|x\pm iy|1/\sqrt{2}[(n',j-1/2,j,m)$$
$$+(-)^\beta(n',j+1/2,j,m)])=\frac{[(j\pm m+1)(j\mp m)]^{1/2}}{2j(j+1)}\cdot 1/2[R_{n',\,j-1/2}^{n,\,j+1/2}+(-)^{\alpha+\beta}R_{n',\,j+1/2}^{n,\,j-1/2}],$$

$$(1/\sqrt{2}[(n,j-1/2,j-1,m\pm1)+(-)^\alpha(n,j-3/2,j-1,m\pm1)]|x\pm iy|1/\sqrt{2}[(n',j+1/2,j,m)$$
$$+(-)^\beta(n',j-1/2,j,m)])=\pm\frac{[(j\mp m)(j\mp m-1)]^{1/2}}{2j}\cdot 1/2[R_{n',\,j+1/2}^{n,\,j-1/2}+(-)^{\alpha+\beta}R_{n',\,j-1/2}^{n,\,j-3/2}],$$

where $$R^{n,\ l}_{n',\ l'}=\int_0^\infty R_{n,\ l}R_{n',\ l'}r^3dr.$$

Only ratios of these integrals are needed in the present calculations, the ratios necessary in the present calculations are given by:

$$R^{n,\ s}_{2,\ p}/R^{n,\ p}_{2,\ s}=n/2\sqrt{3}(n_2-1)^{1/2},\qquad R^{n,\ d}_{2,\ p}/R^{n,\ p}_{2,\ s}=2n/\sqrt{3}(n^2-4)^{1/2}.$$

TABLE I. *Intensity and position of the fine structure components of the Balmer lines at 100 and 400 volts/cm.*

Initial level n; $W(m)$	Final level n; j; m; $\pm$	$E=100$ volts/cm Intensity	$E=100$ volts/cm Position	400 volts/cm Intensity	400 volts/cm Position
4, W_1 (3/2)	2, 3/2, 3/2,	17.47	−0.0666	17.86	+0.0864
" W_2 "	" "	0.44	− .0940	0.03	− .0173
" W_3 "	" "	1.25	− .1179	0.09	− .1183
" W_4 "	" "	0.13	− .1462	0.01	− .2231
" W_5 "	" "	16.35	− .1730	17.58	− .3266
4, W_1 (1/2)	2, 3/2, 1/2,	22.00	− .0555	16.20	+ .1600
" W_2 "	" "	0.38	− .0790	3.90	+ .0680
" W_3 "	" "	0	− .1032	2.60	− .0340
" W_4 "	" "	1.22	− .1320	0.15	− .1365
" W_5 "	" "	8.70	− .1557	6.20	− .2387
" W_6 "	" "	5.45	− .1888	6.38	− .3437
" W_7 "	" "	4.43	− .2321	10.16	− .4585
4, W_1 (1/2)	2, 1/2, 1/2, +	8.91	+ .3011	17.60	+ .5024
" W_2 "	" "	13.94	+ .2776	8.95	+ .4104
" W_3 "	" "	3.29	+ .2534	0.28	+ .3084
" W_4 "	" "	5.30	+ .2246	0.25	+ .2059
" W_5 "	" "	0.51	+ .2009	3.06	+ .1037
" W_6 "	" "	4.28	+ .1678	5.61	− .0013
" W_7 "	" "	0.73	+ .1245	0.81	− .1161
4, W_1 (1/2)	2, 1/2, 1/2, −	1.41	+ .3159	1.12	+ .5598
" W_2 "	" "	5.03	+ .2924	5.69	+ .4678
" W_3 "	" "	4.62	+ .2682	4.34	+ .3658
" W_4 "	" "	0.96	+ .2394	0.10	+ .2633
" W_5 "	" "	3.75	+ .2157	0.45	+ .1611
" W_6 "	" "	1.94	+ .1826	4.50	+ .0561
" W_7 "	" "	18.00	+ .1393	21.50	− .0587
4, W_1 (5/2)	2, 3/2, 3/2,	15.50	− .0854	17.40	− .0078
" W_2 "	" "	0.37	− .1139	0	− .1142
" W_3 "	" "	19.80	− .1381	18.26	− .2163
4, W_1 (3/2)	2, 3/2, 1/2,	7.99	− .0666	6.53	+ .0817
" W_2 "	" "	2.74	− .0940	5.07	− .0220
" W_3 "	" "	1.04	− .1179	0.06	− .1230
" W_4 "	" "	8.60	− .1462	6.69	− .2278
" W_5 "	" "	3.60	− .1730	5.37	− .3313
4, W_1 (3/2)	2, 1/2, 1/2, +	4.19	+ .2900	6.75	+ .4241
" W_2 "	" "	6.62	+ .2626	6.27	+ .3204
4, W_2 (3/2)	2, 1/2, 1/2, +	2.91	+0.2387	3.36	+0.2194
" W_4 "	" "	9.17	+ .2104	6.64	+ .1146
" W_5 "	" "	0.04	+ .1836	0.11	+ .0111
4, W_1 (3/2)	2, 1/2, 1/2, −	0.22	+ .3048	0.16	+ .4815
" W_2 "	" "	3.49	+ .2774	5.14	+ .3778
" W_3 "	" "	3.27	+ .2535	3.37	+ .2768
" W_4 "	" "	4.73	+ .2252	5.71	+ .1720
" W_5 "	" "	11.60	+ .1984	8.70	+ .0685
4, W_1 (1/2)	2, 3/2, −1/2,	2.72	− .0555	0.61	+ .1600
" W_2 "	" "	3.67	− .0790	5.73	+ .0680
" W_3 "	" "	0.14	− .1032	0.90	− .0340
" W_4 "	" "	2.58	− .1320	0.22	− .1365
" W_5 "	" "	2.42	− .1557	1.41	− .2387
" W_6 "	" "	2.80	− .1888	5.40	− .3437
" W_7 "	" "	0.21	− .2321	0	− .4585
4, W_1 (1/2)	2, 1/2, −1/2, +	0.63	+ .3159	0.39	+ .5598
" W_2 "	" "	0.37	+ .2924	0	+ .4678
" W_3 "	" "	0	+ .2682	0.59	+ .3658
" W_4 "	" "	0.55	+ .2394	2.74	+ .2633
" W_5 "	" "	0.50	+ .2157	1.07	+ .1611
" W_6 "	" "	10.75	+ .1826	8.76	+ .0561
" W_7 "	" "	0.85	+ .1393	0.26	− .0587
4, W_1 (1/2)	2, 1/2, −1/2, −	0.19	+ .3011	0	+ .5024
" W_2 "	" "	4.62	+ .2776	7.04	+ .4104
" W_3 "	" "	1.13	+ .2534	1.11	+ .3084
" W_4 "	" "	4.02	+ .2246	3.65	+ .2059
" W_5 "	" "	2.50	+ .2009	1.54	+ .1037
" W_6 "	" "	0.80	+ .1678	0.37	− .0013
" W_7 "	" "	0.30	+ .1245	0.05	− .1161
4, W_1 (1/2)	2, 3/2, 3/2,	1.35	− .0555	0.71	+ .1647
" W_2 "	" "	0.24	− .0790	0	+ .0727
" W_3 "	" "	0.61	− .1032	2.55	− .0293
" W_4 "	" "	0.06	− .1320	0	− .1318
" W_5 "	" "	4.93	− .1557	3.98	− .2340
" W_6 "	" "	0.17	− .1888	0	− .3390
" W_7 "	" "	0	− .2321	0.23	− .4538

TABLE II. *Intensity and position of the fine structure components of the Balmer lines at 200, 500 and 1800 volts/cm.*

Initial level n; $W(m)$	Final level n; j; m; $\pm$	$E=200$ volts/cm Intensity	$E=200$ volts/cm Position	500 volts/cm Intensity	500 volts/cm Position	1800 volts/cm Intensity	1800 volts/cm Position
3, W_1 (3/2)	2, 3/2, 3/2,	31.60	−0.0631	25.65	−0.0086	24.60	+0.2398
" W_2 "	" "	0.64	− .1149	0	− .1143	0	− .1141
" W_3 "	" "	13.50	− .1500	19.25	− .2051	22.70	− .4536
3, W_2 (1/2)	2, 3/2, 1/2,	40.20	− .0531	30.50	+ .0347	30.90	+ .4407
" W_2 "	" "	0.51	− .1065	3.03	− .0606	3.24	+ .1107
" W_3 "	" "	17.05	− .1345	18.56	− .1482	17.91	− .2288
" W_4 "	" "	2.48	− .2168	5.30	− .2600	4.24	− .5832
" W_5 "	" "	2.33	− .2812	3.13	− .3889	2.12	− .9555
3, W_1 (1/2)	2, 1/2, 1/2, +	5.98	+ .2979	10.80	+ .3734	6.69	+ .8067
" W_2 "	" "	35.00	+ .2445	25.80	+ .2781	21.27	+ .4767
" W_3 "	" "	0.87	+ .2165	0.13	+ .1905	0.51	+ .1372
" W_4 "	" "	0.34	+ .1342	6.22	+ .0777	15.44	− .2172
" W_5 "	" "	0.89	+ .0698	0.82	− .0502	1.10	− .5895
3, W_1 (1/2)	2, 1/2, 1/2, −	1.94	+ .3275	1.51	+ .4464	0.40	+1.0605
" W_2 "	" "	11.72	+ .2741	7.30	+ .3511	2.28	+ .7305
" W_3 "	" "	14.68	+ .2461	11.45	+ .2635	12.00	+ .3910
" W_4 "	" "	2.58	+ .1638	2.10	+ .1507	1.52	+ .0366
" W_5 "	" "	14.00	+ .0994	21.10	+ .0228	29.30	− .3357
3, W (5/2)	2, 3/2, 3/2,	48.00	− .0854	48.00	− .0854	48.00	− .0854
" W_1 (3/2)	2, 3/2, 1/2,	18.45	− .0643	14.50	− .0161	16.88	+ .1538
" W_2 "	" "	12.10	− .1161	13.76	− .1218	8.17	− .2000
" W_3 "	" "	1.25	− .1512	1.68	− .2126	2.08	− .5938
3, W_1 (3/2)	2, 1/2, 1/2, +	4.24	+ .2876	0.45	+ .3226	3.64	+ .5197
" W_2 "	" "	25.30	+ .2349	25.10	+ .2169	35.25	+ .1659
3, W_2 (3/2)	2, 1/2, 1/2, +	0.06	+0.1998	0.17	+0.1261	0.48	−0.1737
3, W_1 (3/2)	2, 1/2, 1/2, −	0.49	+ .3163	0.34	+ .3956	0	+ .7736
" W_2 "	" "	7.80	+ .2645	9.05	+ .2809	4.89	+ .4197
" W_3 "	" "	16.46	+ .2294	16.28	+ .1901	17.75	+ .0801
3, W_1 (1/2)	2, 3/2, −1/2,	8.09	− .0531	2.53	+ .0347	0.37	+ .4407
" W_2 "	" "	8.65	− .1065	11.70	− .0606	17.98	+ .1107
" W_3 "	" "	3.08	− .1345	3.10	− .1482	1.49	− .2288
" W_4 "	" "	0.26	− .2168	1.95	− .2600	1.63	− .5832
" W_5 "	" "	0.37	− .2812	0.10	− .3889	0	− .9555
3, W_1 (1/2)	2, 1/2, −1/2, +	0.75	+ .3275	0.55	+ .4464	0	+1.0605
" W_2 "	" "	3.10	+ .2741	0.24	+ .3511	0	+ .7305
" W_3 "	" "	0	+ .2461	0.60	+ .2635	0.76	+ .3910
" W_4 "	" "	13.24	+ .1638	14.52	+ .1507	17.22	+ .0366
" W_5 "	" "	1.07	+ .0994	0.71	+ .0228	0	+ .3357
3, W_1 (1/2)	2, 1/2, −1/2, −	0.56	+ .2979	0.06	+ .3734	0.06	+ .8067
" W_2 "	" "	7.00	+ .2445	8.00	+ .2781	3.81	+ .4767
" W_3 "	" "	5.11	+ .2163	5.03	+ .1905	6.93	+ .1372
" W_4 "	" "	1.61	+ .1342	0.93	+ .0777	0.76	− .2172
" W_5 "	" "	1.45	+ .0698	0.27	− .0502	0	− .5895
3, W_1 (1/2)	2, 3/2, 3/2,	1.08	− .0519	1.16	+ .0422	0.39	+ .5267
" W_2 "	" "	0.73	− .1053	0.05	− .0531	0	+ .1967
" W_3 "	" "	5.20	− .1333	8.14	− .1407	9.13	− .1428
" W_4 "	" "	1.12	− .2156	0.20	− .2535	0	− .4972
" W_5 "	" "	0.09	− .2800	0	− .3814	0.08	− .8695

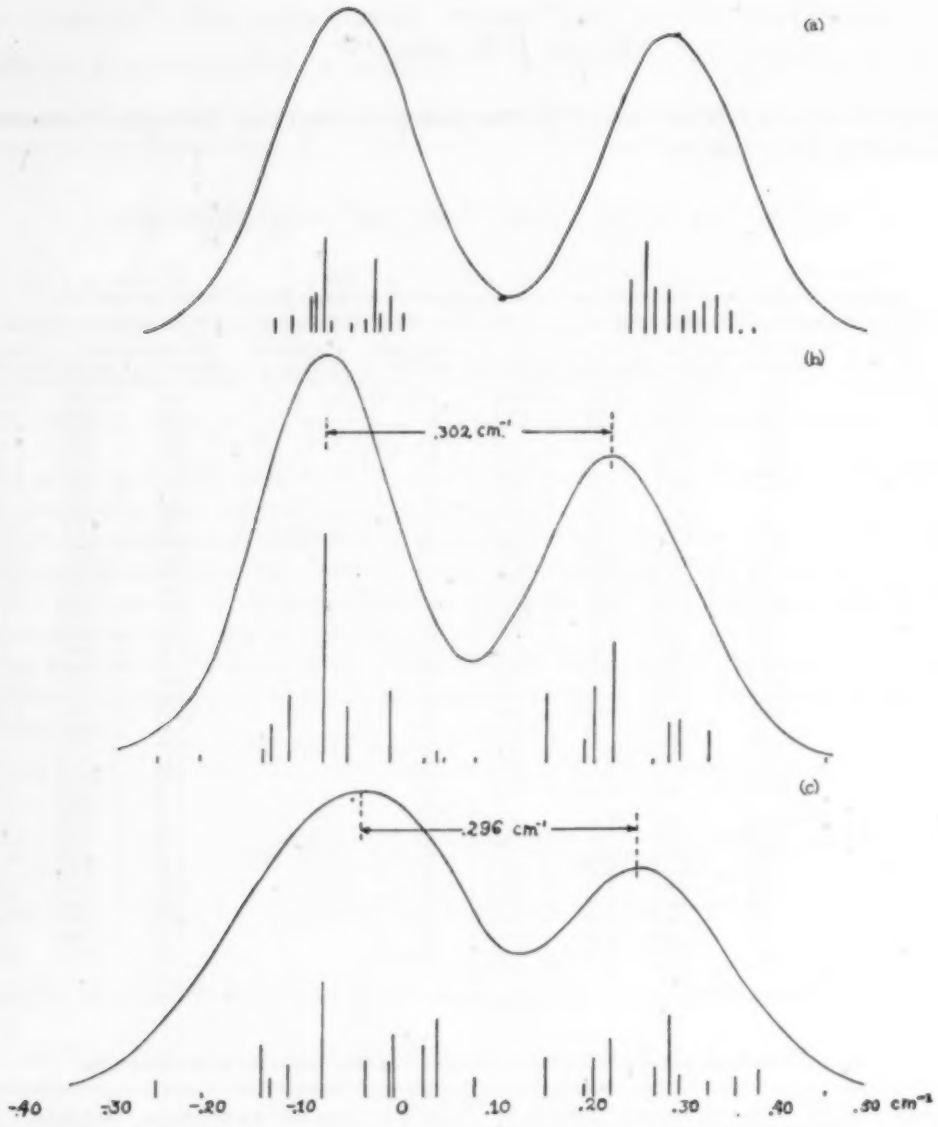

FIG. 1. (a). Resultant curve for H_β line, 100 volts/cm, longitudinal case. Temperature for Doppler curves 108°K. (b) and (c). Intensity curves for H_α, longitudinal and transverse cases, respectively; $E=500$ volts/cm. Temperature for Doppler curves 167°K.

DISCUSSION

The intensity and position of the components for several fields are given in Tables I and II for the H_α and H_β lines, respectively. The initial levels have been identified by their energies and the quantum number m, as j is no longer quantized in intermediate fields. Since the fields used are essentially weak for the lower levels with the exception of the 1800 volt case, j, m and the symmetry of the state are used for identification. This designation may also be used for the 1800 volt case with the understanding that these states are no longer pure states but are mixtures with the state given as the predominant one. The values of the energies referred to as $W_r(m)$ in these tables are given in Table III for $n=2$, 3 and 4.

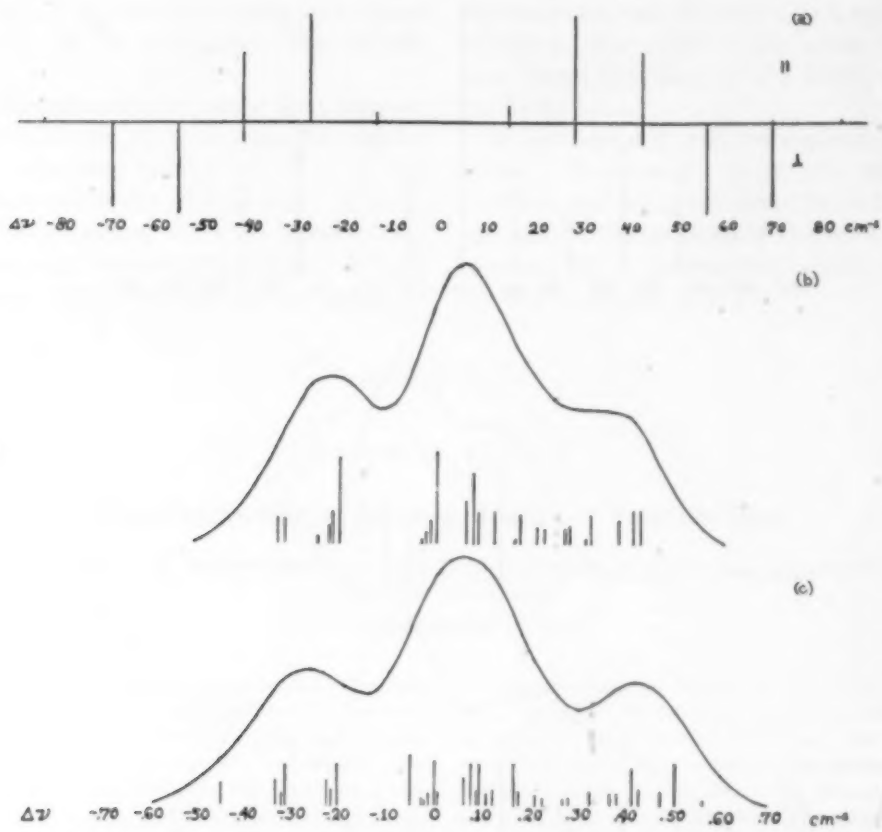

FIG. 2. (a). Components for $H\beta$ at 110,000 volts/cm. (b) and (c). Intensity curves for $H\beta$, $E=400$ volts/cm, longitudinal and transverse cases, respectively. Temperature for Doppler curves 167°K.

Doppler curves were drawn for each component and superimposed to give the resultant curves in Figs. 1, 2 and 3. The temperatures used for these curves were such as to give the observed half-breadth of the resultant lines. The components are shown as straight lines with lengths proportional to their intensities. In Fig. 1(a) is plotted the resultant curve for $H\beta$ at 100 volts/cm for the longitudinal case (observation in the direction of the field). The transverse case (observation perpendicular to field) was not plotted here as it was found to differ very little from the above

TABLE III. *Values of the energies referred to as $W_r(m)$ in Tables I and II for $n=2$, 3 and 4.*

Level $W(m)$, $n=4$	100 volts	400 volts
W_1 (5/2)	0.0356 cm^{-1}	0.1135 cm^{-1}
W_2 "	.0071	.0071
W_3 "	− .0171	− .0950
W_1 (3/2)	.0544	.2077
W_2 "	.0270	.1040
W_3 "	.0031	.0030
W_4 "	− .0252	− .1018
W_5 "	− .0520	− .2053
W_1 (1/2)	.0655	.2860
W_2 "	.0420	.1940
W_3 "	.0178	.0920
W_4 "	− .0110	− .0105
W_5 "	− .0347	− .1127
W_6 "	− .0678	− .2177
W_7 "	− .1111	− .3325

Level $W(m)$, $n=3$	200 volts	500 volts	1800 volts
W (5/2)	0.0359 cm^{-1}	0.0359 cm^{-1}	0.0359 cm^{-1}
W_1 (3/2)	.0582	.1127	.3611
W_2 "	.0064	.0070	.0072
W_3 "	− .0287	− .0838	− .3324
W_1 (1/2)	.0694	.1635	.6480
W_2 "	.0160	.0682	.3180
W_3 "	− .0120	− .0194	− .0215
W_4 "	− .0943	− .1322	− .3759
W_5 "	− .1587	− .2601	− .7482

$n=2$ $W(m)$	200 volts	400 volts	500 volts	1800 volts
W_1 (1/2)	0.1225 cm^{-1}	0.1260 cm^{-1}	0.1288 cm^{-1}	0.2073 cm^{-1}
W_2 "	− .2285	− .2164	− .2099	− .1587
W_3 "	− .2581	− .2738	− .2829	− .4125

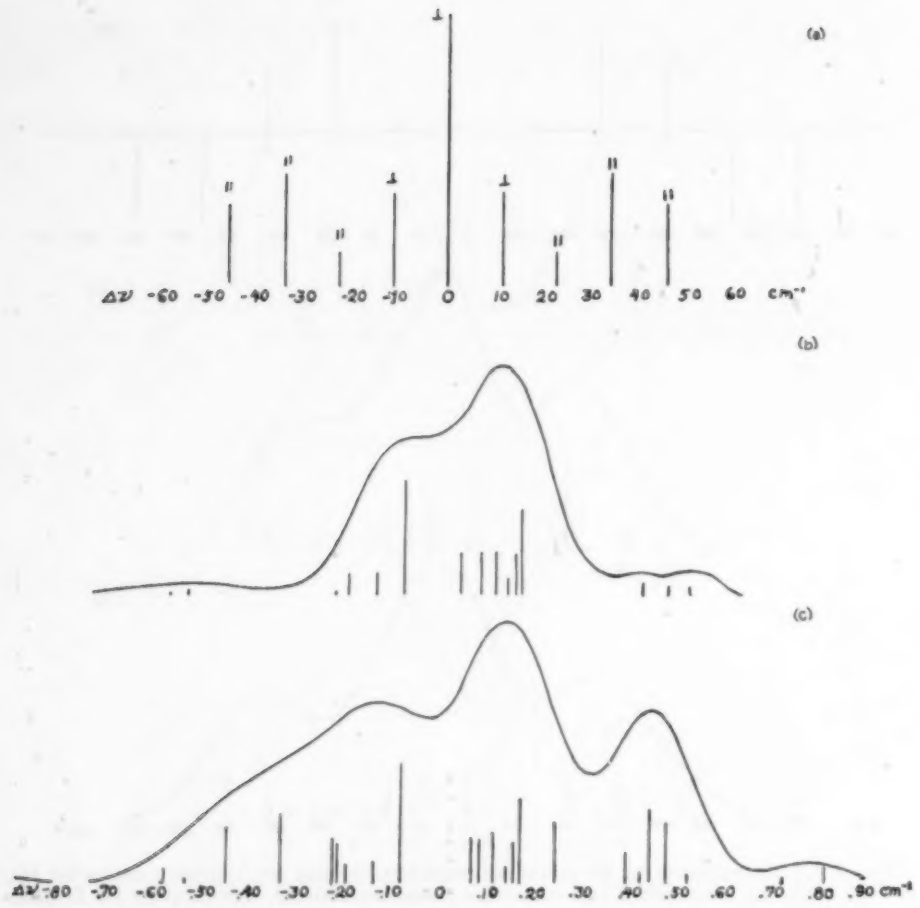

FIG. 3. (a). Components for H_α at 180,000 volts/cm. (b) and (c). Intensity curves for H_α, longitudinal and transverse cases, respectively, $E = 1800$ volts/cm. Temperature for Doppler curves 275°K.

curve. The lower extremities of the doublet components show very little assymmetry, not sufficient to account for more than 1 percent of the discrepancy observed by Houston and Hsieh. This is contrary to the results reported previously.[5] However, the earlier results were based on calculations in which only diagonal elements (having same j's) in the energy matrix were taken into account. It was found later that the non-diagonal terms were of some importance for the upper levels even at fields of 100 volts/cm.

The resultant curves for H_α at 500 volts/cm for the longitudinal and transverse cases are plotted in Figs. 1(a) and 1(b), respectively. The separation of the two peaks is nearly that observed by Gibbs and Williams so that at this point it seemed possible that the discrepancy might be explained, although a field of 500 volts/cm seemed rather large even for ionic fields in the discharge tube. However, when fields of the same order were used for H_β (plotted in Figs. 2(a) and 2(b)) the resultant curves were no longer doublets but of a form which could hardly escape notice if such fields were present. Hence the form of the curve for H_β should serve as an indicator of the magnitude of the fields present in the discharge tube and would seem to eliminate the possibility of accounting for the results of Gibbs and Williams on H_α by an electric field. In Fig. 2(a) the components of H_β in strong fields (110,000 volts/cm) are given for comparison.

In Figs. 3(b) and 3(c) are plotted the curves for H_α for a field of 1800 volts/cm which is an inter-

[5] Heydenburg, Phys. Rev. **45**, 759 (1934).

mediate field for this line. The strong field case is plotted in Fig. 3(a) for comparison. ($E=180{,}000$ volts/cm.)

It seems probable that for some field between 100 and 400 volts/cm, H_β show a smaller doublet separation, behaving similar to H_α at 500 volts/cm; however fields of this order of magnitude will be too strong for lines higher in the Balmer series, since the splitting due to the Stark effect increases approximately as the square of the total quantum number n. It is to be expected, therefore, that these higher series lines will be even better indicators of the field present in the discharge tube.

In conclusion I wish to express my appreciation to Professor G. Breit, who suggested the problem, and has given many helpful suggestions throughout the progress of the work. I also wish to thank Dr. I. Lowen who helped with some of the computations on H_β.

DECEMBER 15, 1934 PHYSICAL REVIEW VOLUME 46

The Production of Intense Beams of Positive Ions

R. DUDLEY FOWLER AND G. E. GIBSON, *Radiation Laboratory, Department of Physics and Department of Chemistry, University of California*

(Received September 13, 1934)

The theory of the extraction of intense beams of positive ions from the low voltage arc is discussed, and the development of a requisite apparatus described, with which beams of several milliamperes of ions from H_2, He, N_2 and CO_2 have been produced. The influence of the gas pressure and current density in the arc, and of the extractor voltage and geometry on the density of the beams has been studied. The electrostatic divergence, and the magnetic convergence of the beams is discussed, in connection with the observed spreading. Magnetic analyses of the beams from hydrogen have shown them to consist of H_3^+, H_{2-1}^+, H_{3-4}^+, H_2^+, H_{2-1}^+ and H_1^+, the relative composition being a function of pressure. At a pressure of 27 bars the beams consist almost entirely of H_3^+, and at 96 bars pressure, entirely of protons. Magnetic analyses of the beams from N_2, O_2, and CO_2 have also been made. The secondary emission from a monel target has been measured for H_1^+, H_2^+, H_3^+, He^+, N_2^+, N_{2-1}^+ and CO^+, and found to be 1 to 2 per incident ion in all cases. The observed target heating has been used as a rough check on the current measurements.

VERY rapid strides in the study of the atomic nucleus have been made recently, as a consequence of the use of electrically produced beams of high velocity ions[1] to effect nuclear transmutations. Currents of from one-tenth to one hundred microamperes of protons and deutons having energies equivalent to falling through fields of from thirty thousand to three million volts have been used very fruitfully by the various workers in the field. The employment of more intense beams will no doubt enable many new phenomena to be noted, and perhaps permit transmutations on a spectroscopically, if not chemically observable scale. A source of positive ions giving beams of several milliamperes has been developed and will be herein described.

Cockroft and Walton, and their collaborators at Cambridge, use a canal-ray tube as a source of ions. A discharge of twenty to fifty milliamperes is maintained between a perforated iron cathode and the inside of a meter-long iron anode, by a potential difference of from twenty to fifty kilovolts. The discharge tube and its accompanying source of rectified power is maintained at from thirty to nine hundred kilovolts above ground potential, by transformers. A cylindrical tube at ground potential placed coaxially beneath the hole in the cathode accelerates the ions emerging therefrom to a velocity corresponding to the potential difference between ground and the source. The ions are then magnetically deflected through ninety degrees onto the desired target. This method produces working beams up to one hundred microamperes, and has the advantage of operating at low gas pressures.

[1] Cockroft and Walton, Proc. Roy. Soc. **A129**, 477 (1930); Lawrence and Livingston, Phys. Rev. **40**, 19 (1932).

Lawrence and his co-workers derive their fast ions from a cloud produced at the center of the acceleration apparatus by the impact of electrons from a hot tungsten filament. Ions from the cloud are accelerated in a series of twenty thousand volt increments, finally emerging from the accelerators with velocities up to that corresponding to a direct fall through a three million volt field. Beams up to fourteen microamperes are thus produced.

In each type of source, the ions are produced by electron impact and then move towards a negative electrode. The greater number of ions strike the electrode, and are neutralized; a few pass through an orifice of some sort in the electrode, and of these, yet fewer are accelerated to the desired speed.

In the low voltage arc, the current is practically limited only by the electron emissivity of the hot cathode, and the potential drop across the arc, as its name implies, is small—generally not over two hundred volts. A ten-ampere discharge therefore would necessitate the expenditure of two kilowatts of power. If a negative, perforated electrode at fifty thousand volts, inserted in the arc, withdraws to and through itself a total of twenty milliamperes of positive ions, the power expended is one thousand watts. A few watts will be required to heat the arc cathode, so that the aggregate power required is about three and a half kilowatts.

In view therefore, of the comparative ease with which large numbers of positive ions can be produced in the low voltage arc, it was deemed the best source from which to derive more intense ion beams.

The theory of the complicated phenomena occurring during electrical discharges through gases has been treated by Thomson[2] and notably by Langmuir and Compton.[3] In the low voltage arc, ions are generated uniformly throughout most of the space between the cathode and the anode. This region, called the plasma, contains approximately equal numbers of positive ions and electrons, and is therefore relatively field-free, in contradistinction to the regions of high field, contiguous to anode, cathode, and arc walls, called sheaths. Because of the higher mobility of the plasma electrons, the walls of the discharge tube, or floating probes inserted in the plasma, become negatively charged, repelling the advance towards them of electrons, and attracting positive ions. This results in the formation of a region called a positive ion sheath in which the electron concentration is lower than that of the positive ions, and which appears "darker" than the plasma, because fewer atomic excitations occur in it. The anode, or a positively charged probe, similarly repels positive ions, and attracts electrons, with the formation of an electron sheath—the anode dark space.

I. Extraction of Positive Ions From a Plasma

A. The effect of collector voltage

When a probe is made negative with respect to the plasma, a positive ion current of density I_p flows to it, and electrons are repelled; and if the negative potential is made sufficiently great, no electrons reach the probe. The classic experiments of Langmuir and Mott-Smith[4] with probes in discharges in mercury vapor have shown that this occurs when the probe voltage reaches -5 to -10 volts with respect to the surrounding plasma, and that the current flowing to a plane collector is practically independent of applied voltages greater than these values, even up to negative voltages of 1200. The density of the collector current depends only on the number of ions crossing each square centimeter of the surface of the ion sheath, that is, on the random current density I_p of ions passing per second per unit area across any imaginary plane within the plasma.

The surface of a plane sheath is considered by Langmuir[3] as a plane emitter of positive ions, at zero potential. The flow of current between this emitter and a plane collector at potential V is

$$I_p = 5.462 \times 10^{-8} M^{-\frac{1}{2}} V^{\frac{3}{2}} X^{-2} \text{ amp./cm}^2, \quad (1)$$

where M is the "molecular weight" (O = 16) of the ion, X is the thickness of the sheath in cm, and V is expressed in volts.

[2] Thomson, *Conduction of Electricity through Gases*, 3rd Ed., Cambridge Univ. Press, 1933.

[3] Langmuir and Compton, (a) Rev. Mod. Phys. **2**, 123 (1930); (b) Rev. Mod. Phys. **3**, 191 (1931); (c) Langmuir, J. Frank. Inst. **214**, 275 (1932).

[4] Langmuir and Mott-Smith, G. E. Rev. **27**, 449, 538, 616, 762 (1924).

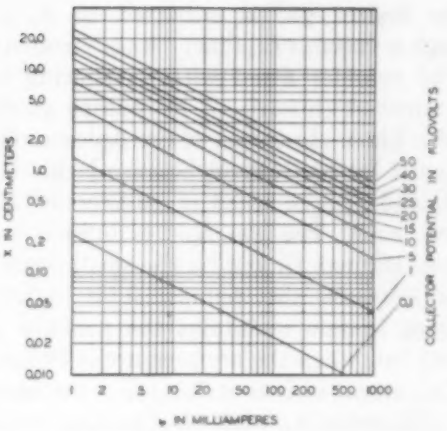

FIG. 1. Sheath thickness and proton current.

In a unipolar discharge, such as the electron flow between a plane cathode and a plane parallel anode, X is constant, and the current between the electrodes is limited, at any prescribed voltage, by the space charge, according to Eq. (1). However, when a plasma serves as an emitter of ions, I_p is predetermined, and X will assume such a value, according to the collector voltage, that Eq. (1) is fulfilled.

Sheath thicknesses as functions of I_p, at various voltages, for protons, are given in Fig. 1. From these curves the sheath thickness for any ionic species may be obtained, by multiplying the value given by the fourth root of the ratio of the ionic charge to its "molecular weight."

B. Effect of the density of the arc current

It would be expected that the random ion current density I_p should be proportional to I_x, the drift current density. (I_x = the current between anode and cathode divided by the cross section of the arc chamber.) The experiments of Langmuir and Mott-Smith,[4] have shown this to be very approximately so, for discharges through mercury vapor at low pressures. The limiting value of I_p will be attained when all the gas molecules become ionized. If the pressure of the gas is p bars, then crossing any unit plane area in the gas there will be

$$n = p/2mv \text{ molecules per sec. per cm}^2, \quad (2)$$

where m is the mass of the molecule, and v its velocity. Now

$$v^2 = 3RT/Nm, \quad (3)$$

where N = Avogadro's number, and R is the gas constant. Whence, substituting $m = M/N$,

$$n = pN(1/12RTM)^{\frac{1}{2}}. \quad (4)$$

If these n molecules all form univalent ions,

$$I_p = ne = pNe(1/12RTM)^{\frac{1}{2}} \quad (5)$$

or evaluating $e = 1.591 \times 10^{-19}$ coulombs, and $R = 8.32 \times 10^7$ ergs per °K per mol,

$$I_p = 3.06p/(MT)^{\frac{1}{2}} \text{ amp./cm}^2. \quad (6)$$

Limiting values of I_p for various ions, at one bar, and at temperatures of 1000°K and 10,000°K, calculated by means of Eq. (6), are given in Table I.

TABLE I. *Limiting values of I_p (amp. per cm²) for various ions at pressure of one bar.*

	I_p (amp./cm²)							
T°K	H_1^+	H_2^+	H_3^+	He^+	CO_2^+	CO^+	N_2^+	N^+
1000	0.0968	0.0684	0.0559	0.0484	0.0146	0.0183	0.0183	0.0259
10000	.0306	.0214	.0177	.0154	.0046	.0058	.0058	.0082

C. Effect of gas pressure

The low voltage arc functions over a limited range of gas pressures. The lower limit occurs when the mean free path for electrons is approximately equal to the distance between the electrodes, and the upper, when the mean free path is so short that the electrons cannot acquire the ionization velocity between collisions.

Over this range it is to be expected that for a constant value of the drift current I_x, I_p should vary linearly with the gas pressure; for the mean free paths of electrons in the plasma varies inversely as the pressure, and the shorter the mean free path, the greater the number of collisions resulting in ionization. The work of Langmuir and Mott-Smith previously cited has shown this to be true for discharges in mercury vapor.

The random ion current density I_p produced in any gas by a predetermined value of I_x, is in general a complicated function of I_x, depending upon the probabilities of ionization by electron, positive ion, and photon impact, at any given pressure.[5]

[5] See reference 3a, pp. 124–135.

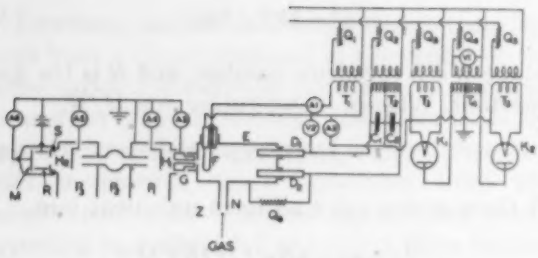

FIG. 2. Schematic diagram of apparatus.

II. EXPERIMENTAL

A. Design and operation of apparatus

Divers forms of apparatus were tried, the most satisfactory of which is schematically represented in Fig. 2. An arc is maintained in the chamber E, between the hot cathode F and anodes D_1 and D_2, and ions from the resulting plasma are extracted by a negatively charged, perforated electrode G. For convenience in measuring, and to eliminate long-path discharges, G is maintained at ground potential and the arc and its power supply at high voltage. The power for the filament and arc currents is obtained from the 220 volt commercial supply by the use of transformers T_1 and T_2, which are insulated between windings for 30,000 volts.

The hot cathode F is heated by a current of 50–75 amperes from T_1 (220 to 10 volts), the current being determined by resistance Q_1, and measured by ammeter A_1. The arc current is supplied by T_2 (220 to 440 volts) and measured by A_2; its value is limited either by resistance Q_2 or by the saturation emission from F. Two anodes, and center-tapping of T_2 allow the arc to run during both halves of the alternating-current cycle. The 500 ohm resistance Q_6 between the metal walls of E and one of the anodes, makes the arc self-starting. The voltage drop across the arc is measured by V_2.

The arc system is maintained at from 10,000 to 22,000 volts (r.m.s. value) positive with respect to G, by T_4 (220 to 44,000 volts) and a full-wave rectifier consisting of kenotrons K_1 and K_2. T_3 and T_5 (220 to 10 volts) supply heating current for the kenotrons. The high voltage d.c. output is adjusted by resistance Q_4, and estimated by voltmeter V_1 across the primary of T_4.

The desired gas is admitted to E, at N, through a variable capillary "leak," from a commercial cylinder fitted with a reducing valve, and removed through G, by pumps at P_1, P_2 and P_3. There pumps are of the Apiezon oil type (designed by Mr. David Sloan, of this laboratory), and have a speed of 80 liters of air per second, each. The gas flow is limited by the channel through G, and by the small connecting tubes between the pumps. This differential pumping system maintains the pressure at P_3 at 0.05 bar, when the arc pressure is 50 bars.

The current of ions striking G is measured by the milliameter A_3, while that passing through G can strike the removable targets H_1 or H_2, and be measured by A_4 or A_5, or pass through a collimating diaphragm S, to a target M, to a magnetic "analyzer," or to high voltage accelerators, as desired.

The actual construction of the apparatus is shown in cross section and to scale by Fig. 3. To insure proper cooling, all metal parts of the arc, and the extractor G, are made of copper. The anodes are insulated from the arc chamber E by glass cylinders M and C; to one of these is sealed a connection to the gas supply, and the other is connected through a stopcock and liquid air trap, to a McLeod gauge.

The cathode F consists of a 50 mil tungsten wire, held by set-screws S_1 and S_2 to the holder D, and the lead P. P is insulated from D, and D from E, by the glass cylinders J and I, respectively. This arrangement greatly facilitates the renewal of the filament.

Water-cooling is effected by three parallel feed systems, consisting of the anodes in series, the two cathode branches in series, and the two arc branches in series. Each system is connected to supply and drain through several feet of heavy-walled rubber tubing. This insulation is quite sufficient, resulting in a power loss of less than two hundred watts.

G is insulated from E by the glass cylinder K, and from the grounded pump system by the hard rubber ring R.

All metal-to-metal connections are either soft or silver soldered, and all metal-to-glass joints made with picein wax.

Targets H_1 and H_2 are made of monel metal, and can be turned in and out of the ion beam by

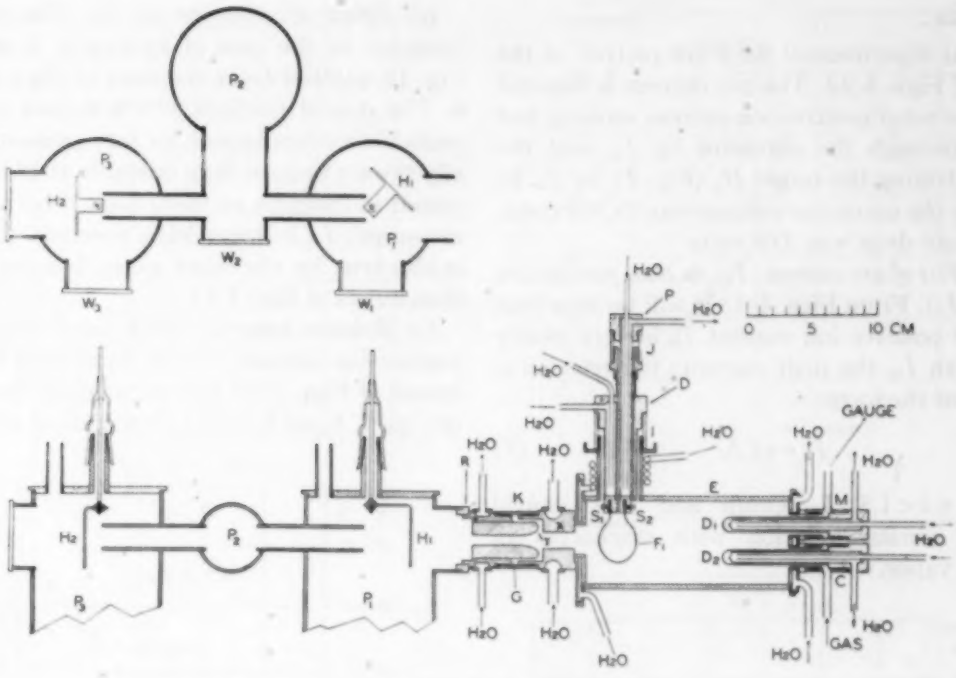

FIG. 3. Detail of apparatus.

means of greased ground joints. Their arrangement, and that of the pumps, is more clearly seen in the inset of Fig. 3, which also shows the glass windows W_1, W_2 and W_3. These windows enable visual observation of the ion beam, and the targets.

The variable gas "leak"[6] is extremely simple and rugged, and allows pressures from one to 100 bars to be maintained in the arc chamber, when the gas cylinder reducing valve is set at 5 to 15 lbs. per sq. in. It consists of a German silver tube, a portion of which is nearly closed by flattening, bent into a U-shaped spring. Flow variation is accomplished by opening or closing the spring with a screw.

Considerable difficulty was at first experienced in the operation of the arc. At certain pressures and currents, the windings of the arc transformer (T_2, Fig. 2) would become shorted. In no case had the transformer been overloaded. Inspection revealed small punctures in the between-turn insulation of both primary and secondary windings, such as would be caused by very high potentials between them. Inasmuch as these punctures occurred even when there was no high voltage applied, they could not have been due to transients from the latter source. Consequently it was assumed that at certain pressures and currents the discharge in the arc chamber became intermittent, the interruptions occurring with very high frequency; this would result in very high values of Ldi/dt in both windings of the arc transformer and so cause between-turn punctures. Intermittent discharge in the electric arc under constant potential has been noted by various workers,[7] and Langmuir[8] and Thomson.[9] Frequencies from several thousand to 10^9 per second have been observed.

Condensers in parallel with the cathode and anodes of the arc prevent di/dt from becoming great in the transformer windings. For this purpose two 2 mfd. condensers, C_1 and C_2 (Fig. 2) were inserted across the terminals of the arc transformer.

[6] Described in Rev. Sci. Inst., January, 1935.

[7] Appleton and West, Phil. Mag. **45**, 879 (1923); Newman, Phil. Mag. **47**, 939 (1924); Clay, Phil. Mag. **1**, 985 (1925); Thomson, Phil. Mag. **11**, 697 (1929); Tonks and Langmuir, Phys. Rev. **33**, 195 (1929); Wood, Phys. Rev. **35**, 673 (1930).

[8] Compton and Langmuir, reference 3a, p. 239.

[9] Thomson, reference 2, p. 447.

B. Results

Typical experimental data are plotted in the curves of Figs. 4–12. The arc current is denoted by I_x, the total positive ion current striking and passing through the extractor by I_p, and the current striking the target H_1 (Fig. 2), by I_u. In each case the extractor voltage was 19,000 r.m.s. and the arc drop was 210 volts.

(*a*) *Effect of arc current* (I_x) *on total positive ion current* (I_p). From Figs. 4–13 it will be seen that the total positive ion current I_p is very nearly linear with I_x, the drift current; the relation is actually of the form

$$I_p = aI_x^b, \tag{7}$$

where $1<b<1.5$. Langmuir and Mott-Smith[4] found a similar relation with discharges in mercury vapor.

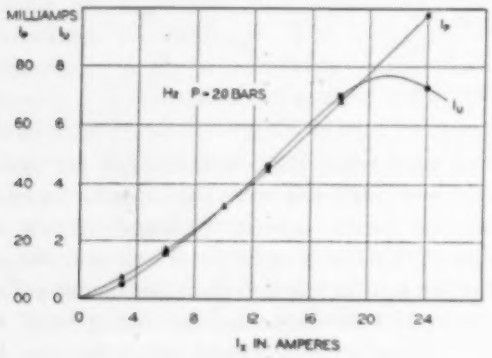

FIG. 4.

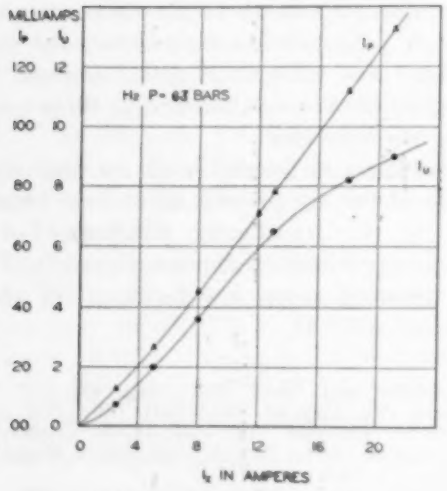

FIG. 6.

(*b*) *Effect of pressure on* I_p. The effect of pressure, in the case of hydrogen, is shown in Fig. 14, plotted from the data of Figs. 4, 5 and 6. The dotted portions of the curves represent probable extrapolations to zero pressure. Actually the arc became very unstable at 18 bars, and ceased to function at 16–17 bars. Over the range measured, I_p is linear with pressure. The same is also true for the other gases, bearing out the statements of Part I–C.

(*c*) *Relation between total* (I_p) *and "useful"* (I_u) *positive ion currents.* It will be noticed from the curves of Figs. 4–13 and particularly from those of Figs. 7, 8 and 9, that I_u is not linear with I_p, as

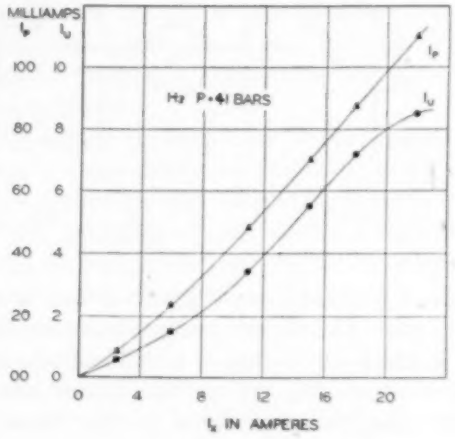

FIG. 5.

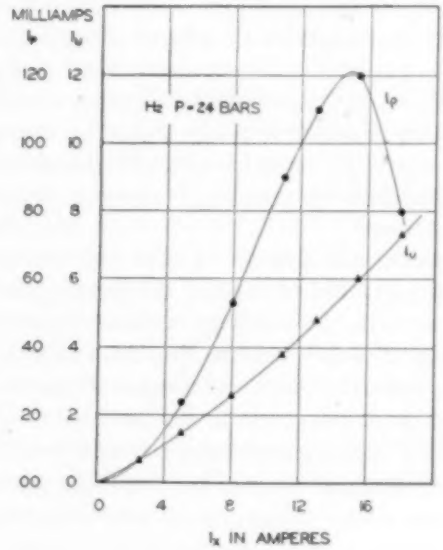

FIG. 7.

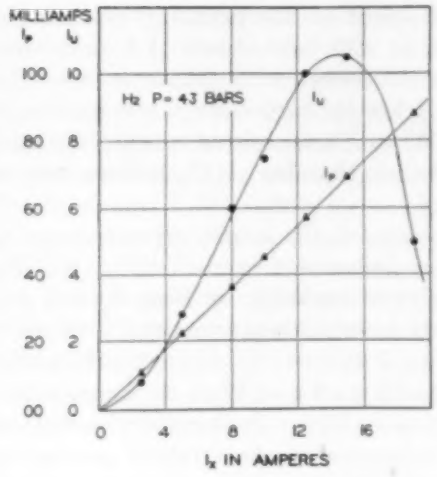

FIG. 8.

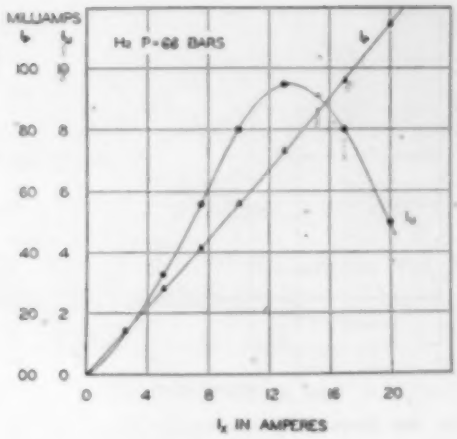

FIG. 9.

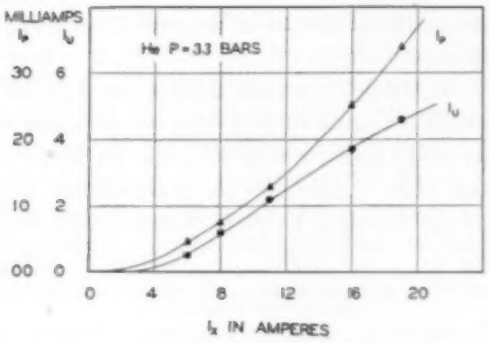

FIG. 10.

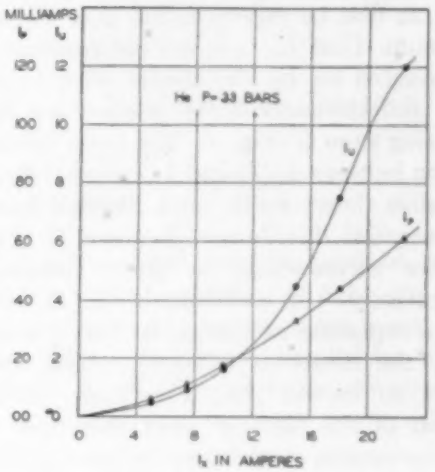

FIG. 11.

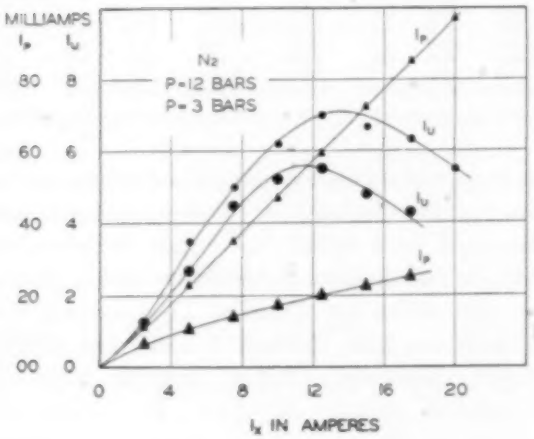

FIG. 12.

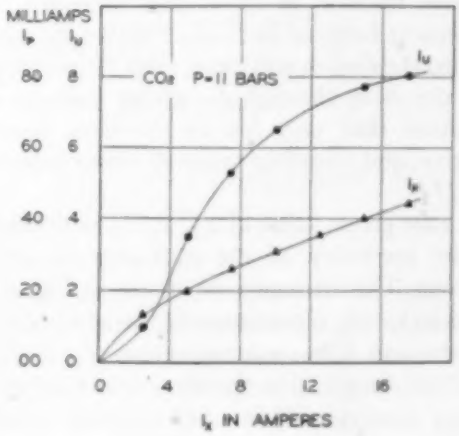

FIG. 13.

FIGS. 4–13. Arc current I_a, total positive ion and useful ion current at various pressures.

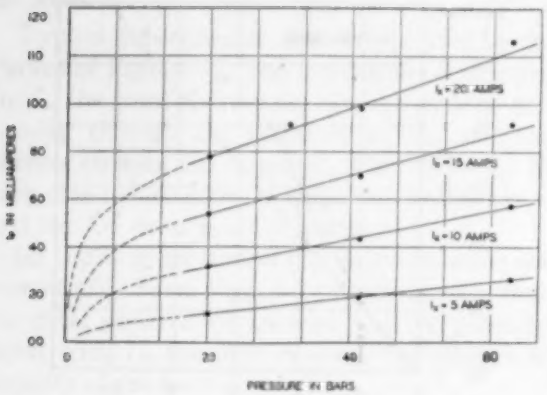

FIG. 14. Arc current I_x *vs.* pressure. (Data of Figs. 4, 5 and 6.)

might at first be expected, but goes through a maximum. That I_u/I_p is not independent of I_p is accounted for by the change with I_p of the shape and thickness of the positive ion sheath extending from G (Fig. 3). The exact functional relation between I_u/I_p and I_p is very difficult to determine theoretically, on a physical basis, as the potential distribution between G (Fig. 3) and its surroundings is quite complicated. Qualitatively, the variation of I_u/I_p with I_p may be explained as follows: At very low values of I_p, the sheath is relatively thick, and its surface so curved that a certain "effective" fraction of the lines of force therefrom to G have curvatures resulting in the passage of ions through G. As I_p increases, the sheath thins, and its curvature changes in such a way that the effective fraction of force lines increases, with consequent increase in I_u/I_p. Further increase in I_p thins the sheath still more, even to its recession into the hole through G, giving rise to such curvature that very few of the force lines are effective, and therefore bringing about a decrease in I_u/I_p.

At any given value of I_p, I_u/I_p is dependent on the geometry of the extractor G and its environs. The arrangement shown in Fig. 3 was found to be the most generally satisfactory. The hole through X has a cross section of 1 cm^{-2} and is 2.5 cm long (I_p is therefore the random ion current density). With a hole through G of the same diameter as that through X, a still higher ratio of I_u to I_p was obtained, I_u even exceeding $I_p - I_u$ at low values of I_p. (Because of the limited speed of the pumping system, the diameter of the hole shown, 7.5 mm, was the largest consistent with pressures over P_3 sufficiently low for high voltage acceleration of the ions.) When X was omitted, and G placed directly into the arc chamber, I_u/I_p became very much smaller.

The ratio I_u/I_p is also dependent on y, the distance between G and X (Fig. 3). This is shown very markedly by Figs. 4, 5, 6 and 10, the data for which were obtained with $y=2$ mm, and Figs. 7, 8, 9 and 11, where the data were obtained with $y=8$ mm. With the larger value of y, I_u/I_p is much higher. Presumably the effect results from extension of the straight portion of the lines of force between G and the sheath surface, which results in a greater number of effective lines.

The difficulties in the way of a systematic study of the influence of geometry on I_u/I_p are obvious.

(*d*) *Effect of extractor voltage on* I_p *and* I_u. Table II contains typical data showing the variation of I_p and I_u with voltage. In I–A it was stated that I_p should be independent of the extractor voltage. Table II shows this to be very far from true. This may be accounted for by the fact that the discharge in the arc chamber is concentrated in a cylindrical region between the cathode and the anodes, and although the plasma fills the entire arc chamber (and extends out through the hole through X), the ion density therein diminishes as the distance from the cylindrical region increases. Increasing the voltage on the extractor G extends the sheath, bringing it nearer to the region of maximum ion density, and therefore increases I_p.

TABLE II. *Typical data showing the variation of* I_p *and* I_u *with voltage in hydrogen. Arc drop 210 volts.*

(a) Distance between G and X, 2 mm. Pressure, 31 bars. $I_x = 18$ amp.				(b) Distance between G and X, 8 mm. Pressure, 50 bars. $I_x = 10$ amp.			
Volts (r.m.s.)	I_p (m.a.)	I_u (m.a.)	I_u/I_p	Volts (r.m.s.)	I_p (m.a.)	I_u (m.a.)	I_u/Ip
10,200	47.5	3.5	0.0736	12,800	28.0	6.0	0.214
13,000	60.0	4.5	.0750	14,000	30.0	6.1	.203
14,000	65.0	5.0	.0767	15,300	33.0	6.3	.190
15,000	70.0	5.5	.0785	16,200	35.0	6.5	.185
16,000	75.0	6.0	.0800	17,600	37.5	6.7	.181
17,000	81.0	6.5	.0803	18,600	42.0	7.0	.166
18,200	87.5	7.5	.0857	21,000	47.5	7.3	.153

In (a) of Table II, I_u/I_p increases with voltage, whereas in (b), it decreases. This may be accounted for by considerations similar to those of the previous section. In obtaining the data of (a), I_x was 18 amperes, and at the lowest voltage the sheath was of less than the optimum thickness for maximum I_u/I_p,; thus increasing the voltage, and therefore the sheath thickness, increases I_u/I_p. The data of (b), however, were taken at the lower value of 10 amperes for I_x, and at the lowest voltage the sheath was already thicker than the optimum value for maximum I_u/I_p, so increase in voltage brought about a decrease in I_u/I_p.

(*e*) *Divergence of the ion beam*

(1) *Natural divergence of an initially parallel beam.* The ions of an originally parallel beam are subject to two forces, at right angles to the initial direction of motion, which deflect them from their parallel courses: (1) the electrostatic force exerted on the particles by the electrostatic field set up by them, resulting in divergence of the beam, and (2), the force exerted on the moving particles by the electromagnetic field caused by them, resulting in convergence of the beam.

The electrostatic field at the periphery of a circular beam of charged particles is easily shown[10] to be

$$E = 2\rho/r \text{ e.s.u.}, \tag{8}$$

where ρ is the density of particles per unit length of a beam of radius r.

$$\text{Now} \qquad I = \rho v, \tag{9}$$

where I is the total charge per second crossing any imaginary plane perpendicularly cutting the beam, and v is the velocity of the ions. Whence the outward force acting on an ion at the periphery of the beam is

$$Ee = m(d^2r/dt^2)_{out} = 2Ie/vr \tag{10}$$

$$\text{whence} \qquad (d^2r/dt^2)_{out} = 2Ie/vrm. \tag{11}$$

The circular electromagnetic field at the periphery of a beam of charged particles is easily shown to be

$$H = 2I/r \text{ e.m.u.} \tag{12}$$

The force exerted on a moving charged particle by the field H is

$$F = Hev \tag{13}$$

and is perpendicular to H; whence the force acting to converge the beam is

$$m(d^2r/dt^2)_{in} = 2Iev/r, \tag{14}$$

$$\text{whence} \qquad (d^2r/dt^2)_{in} = 2Iev/rm. \tag{15}$$

Expressing I in amperes, (15) becomes

$$(d^2r/dt^2)_{in} = Iv/mr\ 2\times10^{-1}\times1.591\times10^{-20} \tag{16}$$

and (11) becomes

$$(d^2r/dt^2)_{out} = I/rvm\ 3\times10^{9}\times4.774\times10^{-10} \tag{17}$$

$$\text{whence} \qquad \frac{(d^2r/dt^2)_{in}}{(d^2r/dt^2)_{out}} = 1/9\times10^{-20}v^2. \tag{18}$$

It is thus evident that when the particles of the beam move with the velocity of light, the outward and inward accelerations are equal and opposite; that is, an initially parallel beam will remain such. At all lesser velocities, the outward acceleration is greater, and the beam will be divergent.

$$\text{Since} \qquad v = 2Ve/m \tag{19}$$

$$\frac{(d^2r/dt^2)_{in}}{(d^2r/dt^2)_{out}} = 2/9\times10^{-20}\frac{Ve}{m}. \tag{20}$$

For protons, this becomes

$$\frac{(d^2r/dt^2)_{in}}{(d^2r/dt^2)_{out}} = 2.13\times10^{-9}V \tag{21}$$

when V is expressed in volts.

Consequently, for 20,000 volt protons, the inward acceleration is only 4.26×10^{-5} times the outward acceleration, and since the latter will be shown to result in a comparatively small divergence, the former may be neglected.

The distances from the origin of an initially parallel beam at which it has doubled, trebled and quadrupled in radius, due to electrostatic

[10] Watson, Phil. Mag. **3**, 849 (1927); Zworykin, J. Frank. Inst. **215**, 546 (1933).

divergence can be shown[11] from (11) to be

$$S_{r=2a}=0.00188A;\quad S_{r=3a}=0.00280A;$$

$$S_{r=4a}=0.00358A;$$

where $$A=aV^{\frac{1}{2}}n^{\frac{1}{2}}/M^{\frac{1}{2}}I^{\frac{1}{2}},$$

where a is the initial radius of the beam, in cm, V is expressed in volts, n is the valence of the ions, M is the "molecular weight" of the ions, and I is expressed in amperes.

For a 5-milliampere beam of 20,000 volt protons, initially of radius 0.375 cm,

$$S_{r=0.75}=16.8\text{ cm};\quad S_{r=1.025}=24.9\text{ cm};$$

$$S_{r=1.5}=31.9\text{ cm}.$$

(2) *Divergence due to non-parallel extraction of the ions.* The current to the target H_2 (Fig. 2) enables the actual spread of the beam to be calculated. In a typical experiment with hydrogen, the current to the target H_1 (Fig. 2) was 5 m.a., and the extractor voltage 20,000, peak value. The diameter of the beam on striking H_2 was 1.5 cm, and the current was 1.25 m.a. Had not the beam been circumscribed to this diameter by the pumping tube between P_2 and P_3 (Fig. 2), its original 5 m.a. would all have struck H_2, in a circular spot of diameter 3.00 cm. This increase in diameter is closely equal to that due to the electrostatic divergence; the ion beam on emerging from the extractor is therefore very nearly parallel.

(*f*) *Magnetic resolution of the beams into their component ions.* For analyses of the beams, the target M (Fig. 2) was removed, and the ions permitted to traverse a 30 cm long glass tube to a rectangular slit. This cut out a 0.1×1.0 cm section of the beam, and allowed it to pass between the poles of a magnet, undeflected to one target, or, bent through an arc of radius 117 cm, to another.

In order to increase the sharpness of the ion "peaks," the extractor voltage was made more nearly uniform by the insertion of a one microfarad condenser between G and the arc chamber (Fig. 3).

Typical data have been plotted in Figs. 15 and 16. In each case the extractor voltage was 16,900, considered as d.c. (12,000 volts, r.m.s. value). The theoretical values of the magnetic field for each ionic species are indicated on the curves.

The curves of Fig. 15 show the constitution of the beams from hydrogen, as a function of the gas pressure. Six peaks have been found: corresponding to H_3^+, H_2^+, H_1^+, H_{3-1}^+ (H_2^+ resulting from the dissociation of H_3^+ after extraction) and H_{2-1}^+ and H_{3-2}^+ (H_1^+ resulting from the dissociation of H_2^+ and H_3^+, respectively, after extraction). It will be noticed that the fields required to deflect the H_{3-2}^+ and H_{2-1}^+ ions were stronger than the calculated fields. This may be accounted for on the assumption that dissociation

---

[11] We are indebted to Mr. J. C. Oxtoby, of the Department of Mathematics, for the following solution of Eq. (11), made at the instigation of Professor Lawrence.

$$d^2r/dt^2=2Ie/vrm=2I/(r2Vm/e).$$

Let
$$4I/(2Vm/e)=b^2$$
then
$$d^2r/dt^2=b^2/2r.$$

Multiplying by $2(dr/dt)dt$, and integrating

$$(dr/dt)^2=b^2\log_e r+c.$$

If the initial radius of the beam is a, $dr/dt=0$, for $r=a$. Therefore
$$(dr/dt)^2=b^2\log_e r/a$$
and
$$dr/dt=b(\log_e r/a)^{1/2}.$$

Now let $y=(\log_e r/a)^{1/2}$; then $y^2=\log_e r/a$
and
$$r=ae^{y^2}$$
and
$$dr/dt=(dr/dy)dy/dt=ae^{y^2}2ydy/dt.$$
Therefore
$$2aye^{y^2}dy/dt=by;\qquad (b/2a)dt=e^{y^2}dy$$
and, since when $t=0$, $y=0$,

$$(b/2a)t=\int_0^y e^{y^2}dy.$$

Now, $S=vt$; whence $bs/2av=\int_0^y e^{y^2}dy$ or

$$\frac{I^{1/2}}{a(2V)^{3/4}(e/m)^{1/4}}S=\int_0^y e^{y^2}dy.$$

This is integrable, in the form of a series

$$\frac{I^{1/2}}{a(2V)^{3/4}(e/m)^{1/4}}S=y+\frac{y^3}{3}+\frac{y^5}{5\times2!}+\frac{y^7}{7\times3!}+\frac{y^9}{9\times4!}+\cdots.$$

It is convenient to express the divergence in terms of the distance from the origin of the beam, at which it has doubled, trebled, and quadrupled, that is, when $r=2a$, $3a$ and $4a$; or when $y=\log_e 2$, $y=\log_e 3$, $y=\log_e 4$. The summation of the first five terms of the above series are as follows:

$$\Sigma^5_{r=2a}=1.07241;\qquad \Sigma^5_{r=3a}=1.5972;\qquad \Sigma^5_{r=4a}=2.0425.$$

Whence, expressing V in volts, I in amperes, m in terms of the "molecular weight" of the ions, and e in terms of n, the number of charges in the ion

$$S_{r=2a}=0.00188aV^{3/4}n^{1/4}/M^{1/4}I^{1/2}$$
$$S_{r=3a}=0.00280aV^{3/4}n^{1/4}/M^{1/4}I^{1/2}$$
$$S_{r=4a}=0.00358aV^{3/4}n^{1/4}/M^{1/4}I^{1/2}.$$

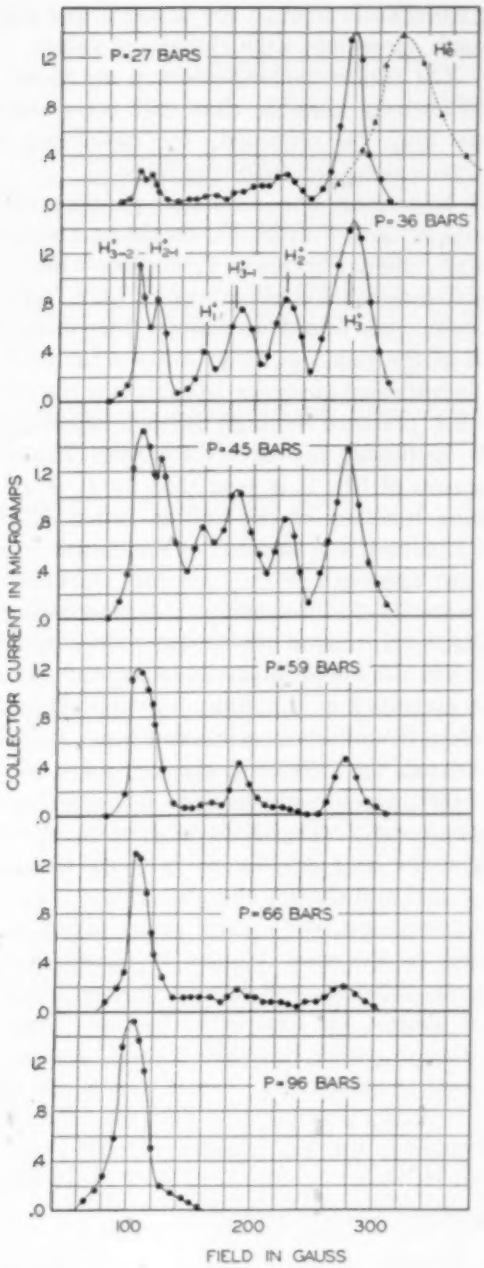

FIG. 15. Current to collector *vs.* magnetic field. The peaks correspond to different ions as indicated in the upper curves.

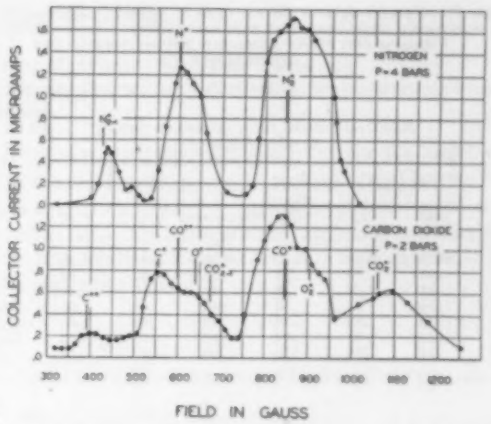

FIG. 16. Current to collector *vs.* magnetic field when N_2 and CO_2 were in the arc space.

of the H_3^+ and H_2^+ took place in the sheath, before the molecular ions had acquired their full 16,900 volts equivalent velocities, so that they fell through a part of the field as H_1^+ ions and consequently acquired higher velocities than they would have as H_2^+ or H_3^+.

The curves of Fig. 15 show that at 27 bars the hydrogen beams consist practically entirely of H_3^+, and at 96 bars, entirely of H_1^+ (H_{3-3}^+, actually, but for nuclear work, involving the further high voltage acceleration of the protons, this is obviously of no significance).

Fig. 16 gives typical data for nitrogen and CO_2. The nitrogen used was obtained from a commercial cylinder, and the curve shows evidence of the presence of oxygen (O^+ and O_2^+). The CO_2 beams contain many different ions, the most likely of which are indicated on the curve.

Experiments were also run on oxygen (pressure, 5 bars, $I_z=10$ amp., $I_u=8$ m.a.), in which peaks corresponding to O^+ and O_2^+ were obtained.

(*g*) *Secondary electron formation.* To estimate the number of secondary electrons emitted from a target by the impact of a positive ion of a given kind, the target used in the magnetic deflection experiments was provided with a guard ring, similar to *R* of Fig. 2. Ions were prevented from striking this ring by a shield similar to *S* of Fig. 2. Some typical data are given in Table III.

From these data it is seen that when floating, the guard ring becomes so negatively charged as to stop the flow of secondary electrons, and that the emitted secondaries have velocities less than 22.5 equivalent volts.

The target H_1 (Figs. 2 and 3) was enclosed by the grounded pumphead P_1, so the conditions in making the measurements of I_u in Figs. 4–13 were similar to those in the previous experiment

TABLE III. *Typical data on the emission of secondary electrons from a monel metal target bombarded with positive ions of various kinds. Voltage of ions 10,900 (condenser between extractor and arc chamber.)*

Ion	Electron current from ground to target, in microamperes						Secondaries per incident ion
	Potential of guard ring with respect to ground, volts						
	−45	−22.5	Floating	Grounded	+22.5	+45	
H_1^+	0.28	0.28	0.28	0.36	0.48	0.48	0.71
H_2^+	.28	.28	.28	.44	.62	.62	1.21
H_3^+	.28	.28	.28	.46	.70	.70	1.50
He^+	.34	.34	.34	.46	.66	.66	0.94
N_2^+	.38	.38	.38	.50	.84	.84	1.21
N_1^+	.32	.32	.32	.44	.72	.72	1.25
CO^+	.28	.28	.28	.40	.72	.72	1.57

with the guard ring grounded. Whence the actual positive ion currents for hydrogen were $I_u \times 28/36$ at the higher pressures (60 bars and above), and $I_u \times 28/46$ at the lower pressures (20–27 bars), and, for helium, $I_u \times 34/46$.

(*h*) *Heating of the targets.* The target H_1 (Fig. 2) was a square of monel metal, $0.05 \times 3 \times 3$ cm. In one experiment with hydrogen at 63 bars arc pressure and $V = 19{,}000$ r.m.s., when I_u measured 11 m.a., a hole 1.5 cm in diameter was melted in this target in a very few seconds (M.P. of monel 1633°K). A measured current of 2 m.a. was enough to heat a 1.5 cm spot on target H_2 (monel, $0.05 \times 4 \times 4$ cm) to a dull red.

Because of the complex relation between the measured and peak values of the ion current and the voltage, the observed heating can only serve as a rough check on the measured secondary formation. Thus, assuming that with the 11 m.a. beam of H_1^+ ions the temperature of the target H_1 (Fig. 2) was 1400°K, and that the total emissivity of monel at this temperature is 35 percent of that from a perfect black-body, the radiation is 128 watts. If the actual ion current (from Table III) is $11 \times 28/36$ m.a., and $V = 19{,}000$ volts (r.m.s.) the power is 162 watts, in rough agreement with the above value.

(*i*) *The further intensification of the beams.* It seems entirely possible that still more intense beams may be obtained, by modifying the apparatus along the following lines:

(1) Increasing the diameter of the orifices through G and X (Fig. 3). Doubling these, for example, should increase I_u to four times the present amount for given values of I_x and V. However, this would necessitate increasing the speed of the pump p_1 (Fig. 3) by a factor of 8, i.e., to 640 e/sec., in order to maintain the necessary low pressure for high voltage acceleration.

(2) Increasing the extractor voltage. From the discussion of (d), it is seen that I_u/I_p is an increasing function of the voltage when I_p is of such a value that extension of the sheath results in closer approach to the optimum thickness for maximum I_u/I_p. Increasing I_p, by increasing I_x, results in thinning of the sheath to less than the optimum thickness, and increasing the voltage again extends it to the optimum value. It should therefore be entirely possible to greatly intensify the beams, by increasing the extractor voltage to 50,000, which could be done by replacing the glass cylinder K (Fig. 3) by a lavite insulator of such shape and size as to prevent flash-over between G and the arc chamber.

In conclusion, our sincere appreciation is expressed to Professor Gilbert N. Lewis for his generous support, and kindly interest; to Professor Ernest O. Lawrence, for the generous donation of a room in the Radiation Laboratory, the loan of equipment that helped in no small part to make possible this research, and, more particularly, for his friendly interest; and to David H. Sloan, for the benefit of many helpful suggestions and discussions.

Collision of Two Light Quanta

G. BREIT* AND JOHN A. WHEELER,** *Department of Physics, New York University*

(Received October 23, 1934)

The recombination of free electrons and free positrons and its connection with the Compton effect have been treated by Dirac before the experimental discovery of the positron. In the present note are given analogous calculations for the production of positron electron pairs as a result of the collision of two light quanta. The angular distribution of the ejected pairs is calculated for different polarizations, and formulas are given for the angular distribution of photons due to recombination. The results are applied to the collision of high energy photons of cosmic radiation with the temperature radiation of interstellar space. The effect on the absorption of such quanta is found to be negligibly small.

TWO simultaneously acting light waves with vector potentials

$$\mathbf{A}_j=\mathbf{a}_j^*\exp\{-(\omega_j t-\mathbf{k}_j\mathbf{r})\}+\mathbf{a}_j\exp\{i(\omega_j t-\mathbf{k}_j\mathbf{r})\} \quad (1)$$

are considered as acting on an electron. Under the influence of the waves a single electron wave function $\psi^{(0)}$ is changed, and the perturbed function may be expanded according to powers of a, a^*. The phenomena of pair production and of recombination have to do with the terms in $a_1^*a_2^*$ and a_1a_2, respectively, as is obvious from the theory of quantization of light waves. We consider first the pair production. We let the function $\psi^{(0)}$ represent an electron in a negative energy state. It is convenient for practical applications to normalize $\psi^{(0)}$ so as to have the electron density equal to unity. It is also unnecessary to use quantized light waves in the pair production problem, since the results with quantized waves are known to be identical with those obtained by means of ordinary waves. As a result of the calculation one finds that at a time t after the application of the waves the wave function contains a term which may be interpreted as referring to an electron in a positive energy state with a momentum and a spin coordinate which are functions of the original momentum and spin and of the momenta and polarizations of the light quanta. The density of electrons corresponding to this wave function may be put into the form

$$(e^2/mc^2)^2|a_1|^2|a_2|^2B|1-\exp(-it\delta W/\hbar)|^2/(\delta W)^2. \quad (2)$$

Here B is a dimensionless number depending on initial momenta and spin and the polarizations of the quanta. δW is the difference in energy of the initial and the final states. Thus if $W=-|W|$ is the energy of the electron in its initial state and if $h\nu_1$, $h\nu_2$ are the energies of the quanta, then

$$\delta W=c(p_2^2+m^2c^2)^{\frac{1}{2}}+W_1-h\nu_1-h\nu_2;\qquad W_1=-W, \quad (3)$$

where

$$\mathbf{p}_2=\mathbf{p}_1+\mathbf{P}_1+\mathbf{P}_2 \quad (4)$$

is the final momentum of the electron and $\mathbf{P}_1$, $\mathbf{P}_2$ are the momenta of the quanta. The total electron density due to the two light quanta is obtained by summing expression (2) over all possible states of negative energy. The equal and opposite spin directions for every $\mathbf{p}_1$ contribute to the density. One is thus only interested in the average for B over the different directions σ of the positron spin. This average will be called $\bar{B}^\sigma$. There are $2p_1^2dp_1d\omega_1\cdot V/h^3$ electronic states of negative energy in the fundamental volume V for which the momentum is $\mathbf{p}_1$ and the direction is within the solid angle $d\omega_1$. Each of these has a density $1/V$. The number of positron electron pairs produced per cm^3 corresponding to the absolute value of positron momentum being between p_1 and p_1+dp_1 in the direction $-\mathbf{p}_1$ and in solid angle $d\omega_1$ is thus obtained from (2) by multiplying it by $2p_1^2dp_1d\omega_1/h^3$. Integrating over dp_1, and making use of

$$d(\delta W)=c^2[p_1/W_1+\mathbf{p}_1\mathbf{p}_2/p_1W_2]dp_1, \quad (5)$$

* Now at Department of Physics, University of Wisconsin.

** National Research Fellow now at Copenhagen.

which follows from (3) and (4), and substituting

$$|a|^2=(c/2\pi\nu^2)I=(hc/2\pi\nu)N, \tag{6}$$

where I is the intensity of each beam and N is the number of light quanta per cm^2 per second, one obtains the probability of pair formation per unit solid angle of the positron and per unit volume of the space in which the light quanta collide, as

$$\frac{2p_1^2(e^2/mc^2)^2N_1N_2\bar{B}^\sigma t}{h\nu_1h\nu_2[p_1/W_1+\mathbf{p}_1\mathbf{p}_2/p_1W_2]}. \tag{7}$$

Here $(-\mathbf{p}_1)$, $\mathbf{p}_2$ are the vectors representing the momenta of the positron and electron, p_1, p_2 are their absolute values and W_1, W_2 are, respectively, the energies of the positron and electron. It is convenient to express the above probability in terms of an effective collision area σ. A convenient definition is to express (7) as $tN_1N_2\sigma/c$. The effective collision area σ thus defined corresponds to a picture of N_1 light quanta per unit area per second traveling through space in which the quanta $h\nu_2$ are thought of as being distributed with their density N_2/c. This definition is arbitrary but convenient for transformations to other frames of reference. It should be noted, however, that if two beams of quanta are shot against each other head-on then the number of pairs produced is

$$A(\sigma/2)\int N_1dt\cdot\int N_2dt, \tag{8}$$

where A is the common cross-section area of the two beams, the factor 1/2 arising from the fact that both beams travel against each other with the velocity of light. The effective collision area for head-on collisions when expressed in terms of the numbers of quanta shot at each other rather than in terms of the density of one of them is thus $\sigma/2$. We have

$$\sigma=\frac{2cp_1^2(e^2/mc^2)^2\bar{B}^\sigma}{h\nu_1h\nu_2[p_1/W_1+\mathbf{p}_1\mathbf{p}_2/p_1W_2]}. \tag{9}$$

The recombination probability of electrons and positrons may also be expressed in terms of the quantity B used in (2). One starts with an electron being in a positive energy state and considers the terms in a_1a_2 according to the method of quantizing light waves. The probability for the electron to jump into the hole may then be calculated for this pair of light waves. Using electron and positron states normalized to 1, i.e., of density $1/V$, a result is obtained which is similar to Eq. (2). It differs from (2) only through the replacement of every $|a|^2$ by the initial expectation of a^+a. Thus the contribution to the emission probability due to the possible cooperation of a pair of light waves is obtained by substituting

$$|a|^2=(c/2\pi\nu^2)I$$

and then letting $\quad I=h\nu c/V. \tag{10}$

Consider a positron with a definite spin and momentum going through an electron distribution also having a definite spin and momentum. In order to obtain the emission probability we must sum expression (2) modified in accordance with (10) over all possible pairs of light quanta. Thus for given momenta of the light quanta 1, 2 each light quantum can have two perpendicular and independent directions of polarization s_1, s_1' and s_2, s_2', respectively, and one obtains contributions to the emission probability due to every possible combination of polarizations. Thus one has the emission probability as a sum of terms

$$(h^2c^4/4\pi^2\nu_1\nu_2)(e^2/mc^2)^2V^{-2}\beta(1,2)\times|1-\exp(-it\delta W/\hbar|^2/(\delta W)^2, \tag{11}$$

where $\beta(1,2)$ should be made to take in turn the values $\beta(s_1, s_2)$, $\beta(s_1, s_2')$, $\beta(s_1', s_2)$, $\beta(s_1', s_2')$. If it happens that the pair production calculation for quanta 1, 2 gives for the assigned positron spin also the assigned electron spin then $\beta(1,2)=B(1,2)$. In general, however,

$$\beta(1,2)=\frac{|(\psi_\sigma^*,\psi_{\sigma'})|^2}{(\psi_{\sigma'}^*\psi_{\sigma'})(\psi_\sigma^*\psi_\sigma)}B(1,2), \tag{12}$$

where ψ_σ, $\psi_{\sigma'}$ are, respectively, the electron state with specified spin and the electron state which arises from the positron state under the action of the light quanta 1, 2. The probability of having recombination in which light quantum 1 has the polarization s_1 while the polarization of light quantum 2 is subject to no restriction is

obtained by omitting $\beta(s_1', s_2)$, $\beta(s_1', s_2')$ from the summation. The result depends then only on the average value

$$\beta(s_1, \bar{s}_2) = \tfrac{1}{2}[\beta(s_1, s_2) + \beta(s_1, s_2')]. \quad (12')$$

Performing the integration over P_1 and allowing $\mathbf{P}_1$ to lie within a small solid angle of $d\Omega_1$ one obtains the number of emissions per second. This number refers to electron and positron densities $1/V$. To reduce to unit electron and positron density the probability must be multiplied by V^2 and it must again be divided by V to reduce to probability of emission in unit volume. The probability of emission per second per cm^3 due to unit electron and positron densities restricting the emission processes to those in which one of the light quantum pair has a direction in $d\Omega_1$ is

$$2c\left(\frac{e^2}{mc^2}\right)^2 \beta(s_1, \bar{s}_2)\frac{\nu_1}{\nu_2}\left[1-\frac{\mathbf{P}_1\mathbf{P}_2}{P_1P_2}\right]^{-1} d\Omega_1. \quad (13)$$

In obtaining the total emission probability from this expression one should be careful not to sum over s_1 and then to integrate over $d\Omega_1$ without dividing the result by two. Otherwise one counts every pair of quanta twice: one time in the order 1, 2 and another time in the order 2, 1. Letting

$$\beta(\bar{s}_1, \bar{s}_2) = \tfrac{1}{2}[\beta(s_1, \bar{s}_2) + \beta(s_1', \bar{s}_2)] \quad (14)$$

the total emission probability is

$$2c\left(\frac{e^2}{mc^2}\right)^2 \int \beta(\bar{s}_1, \bar{s}_2)\frac{\nu_1}{\nu_2}\left(1-\frac{\mathbf{P}_1\mathbf{P}_2}{P_1P_2}\right)^{-1} d\Omega_1. \quad (15)$$

One is usually interested in the passage of positrons with random spins through electron distributions having random spins, and in this case $\beta(\bar{s}_1, \bar{s}_2)$ should be averaged over these spins. Similarly, in the production of pairs one is usually interested in the average of (9) for quanta having random polarizations. One should be careful not to suppose that the average thus entering in (9) $[\bar{B}^\sigma]$ is equal to the average of $\beta(\bar{s}_1, \bar{s}_2)$ which we call $\bar{\beta}(\bar{s}_1, \bar{s}_2)$. In fact, using (12)

$$\bar{\beta}(\bar{s}_1, \bar{s}_2) = \tfrac{1}{2}\bar{B}^\sigma. \quad (16)$$

Thus the total emission probability in all directions per unit volume per second due to unit positron and electron densities is

$$c\left(\frac{e^2}{mc^2}\right)^2 \int \bar{B}^\sigma \frac{\nu_1}{\nu_2}\left(1-\frac{\mathbf{P}_1\mathbf{P}_2}{P_1P_2}\right)^{-1} d\Omega_1 \quad (17)$$

and for light quanta with random polarizations the "density collision cross section" is

$$\bar{\sigma} = 2\left(\frac{e^2}{mc^2}\right)^2 \int \frac{cp_1^2}{h^2\nu_1\nu_2}\bar{B}^\sigma\left[\frac{p_1}{W_1}+\frac{\mathbf{p}_1\mathbf{p}_2}{p_1W_2}\right]^{-1} d\omega_1. \quad (18)$$

If the momenta of the electron and positron are equal and opposite the probability (17) is

$$\tfrac{1}{2}c(e^2/mc^2)^2 \int \bar{B}^\sigma d\Omega_1 \quad (17')$$

and

$$\bar{\sigma} = (e^2/mc^2)^2(cp/W)\int \bar{B}^\sigma d\omega_1. \quad (18')$$

The quantity B was calculated as in Dirac's paper. The method used by him can be applied to any initial state of a free electron. The initial wave functions for an electron having an energy $mc^2 \cosh\theta$ a momentum $\mathbf{p}=mc(\mathbf{p}/p)\sinh\theta$ and two independent spin directions are given by the first two columns of $[-\cosh\theta+(\mathbf{p}/p)\boldsymbol{\alpha}\sinh\theta+\rho_3](1+\rho_3)$. Following the procedure of Dirac[1] the calculation of $\psi^{(2)}$ with such an initial wave function reduces to mechanical operations. The answer comes out as a four row four column matrix, the last two columns of which are automatically zero. The first two columns are the wave functions arising under the influence of (1) from the wave functions represented by the first two columns of $[-\cosh\theta+(\mathbf{p}/p)\boldsymbol{\alpha}\sinh\theta+\rho_3](1+\rho_3)$. In this manner one can obtain the spin properties of $\psi^{(2)}$ as well as its density. At present there seem to be no applications for the spin relations between the initial and final states, and we give therefore only the results for the density. The results take a simple form in the reference system in which the total momentum is zero. In the results listed below the common line of the two quanta is taken to be the x-axis. The direction cosines of the produced positron are called λ, μ, ν. We let the energy of the

[1] P. A. M. Dirac, Proc. Camb. Phil. Soc. **24**, 361 (1930). Although Eq. (28) of Dirac's paper appears to refer to the problem here discussed it does not actually do so, because the negative energy state is kept fixed and the frequency of the quantum is varied.

electron as well as that of the positron be $W=mc^2\cosh\theta$ and

$$C=\cosh\theta,\quad S=\sinh\theta. \tag{19}$$

We obtain

$(\mathcal{E}_1\|y,\ \mathcal{E}_2\|y)$

$$B_{11}=[S^2-2S^2(\nu^2-\mu^2)-S^4(\nu^2-\mu^2)^2 +S^2C^2(1-\lambda^2)]C^{-2}(C^2-\lambda^2S^2)^{-2}, \tag{20.1}$$

$(\mathcal{E}_1\|y,\ \mathcal{E}_2\|z)$

$$B_{\perp}=[C^2-4S^4\mu^2\nu^2 +S^2C^2(1-\lambda^2)]C^{-2}(C^2-\lambda^2S^2)^{-2}. \tag{20.2}$$

Averaging over the angle which one of the electric intensities makes with the y-axis

$$\bar{B}_{11}^{\varphi}=(S^2/2)[C^2+3-2\lambda^2-\lambda^4S^2]C^{-2}(C^2-\lambda^2S^2)^{-2};$$

$$\bar{B}_{\perp}^{\varphi}=\tfrac{1}{2}[C^4+2C^2-1-2\lambda^2S^2-\lambda^4S^4]C^{-2} \times(C^2-\lambda^2S^2)^{-2}. \tag{20.3}$$

If one of the quanta is polarized along y and the other at random

$$B(\mathcal{E}_y,\ \bar{\mathcal{E}})=\tfrac{1}{2}[C^4+2C^2-2-2\lambda^2S^2-\lambda^4S^4 +2(\mu^2-\nu^2)S^2]C^{-2}(C^2-\lambda^2S^2)^{-2}. \tag{20.4}$$

If both quanta are polarized at random

$$B(\bar{\mathcal{E}},\ \bar{\mathcal{E}})=\tfrac{1}{2}[C^4+2C^2-2-2\lambda^2S^2 -\lambda^4S^4]C^{-2}(C^2-\lambda^2S^2)^{-2}. \tag{20.5}$$

For all of the above six conditions Eq. (9) reduces to

$$\sigma=(e^2/mc^2)^2B\tanh\theta \tag{9'}$$

and the number of pairs in which the positron has the direction $(\lambda,\ \mu,\ \nu)$ produced per unit solid angle per unit volume per second is $N_1N_2\sigma/c$. By integration one obtains the number of pairs in all solid angles. The values of σ which correspond to the two cases (20.3) are

$$\bar{\sigma}_{11}=2\pi(e^2/mc^2)^2[-SC^{-3}-\tfrac{3}{2}SC^{-5}-\tfrac{3}{2}\theta C^{-6} +2\theta C^{-4}+2\theta C^{-2}], \tag{21.1}$$

$$\bar{\sigma}_{\perp}=2\pi(e^2/mc^2)^2[-SC^{-3}-\tfrac{1}{2}SC^{-5}-\tfrac{1}{2}\theta C^{-6} +2\theta C^{-4}+2\theta C^{-2}], \tag{21.2}$$

and for random polarizations

$$\bar{\sigma}=2\pi(e^2/mc^2)^2[-SC^{-3}-SC^{-5}-\theta C^{-6} +2\theta C^{-4}+2\theta C^{-2}]. \tag{21.3}$$

Formulas (21.1), (21.2) apply also to (20.1), (20.2). It should be remembered that Eqs. (21) apply to the "density collision cross section" defined in terms of $N_1N_2\bar{\sigma}/c$ and that the total number of pair producing collisions for two beams of quanta each containing n quanta is $n_1n_2\bar{\sigma}/(2A)$ in accordance with Eq. (8).[2]

If the pair production conditions described by Eqs. (20), (21) are viewed from a moving frame of reference, the number of pairs produced per unit volume per unit time remains the same because pair production is an event in four dimensional space and the density of events is Lorentz invariant. Thus

$$N_1'N_2'\sigma'd\omega_1=N_1N_2\sigma d\omega_1, \tag{22}$$

where N' is the number of quanta per cm^2 per sec. in the new frame of reference and σ' is the "density collision cross section" per unit positron solid angle in that frame. For any two light quanta it is possible to perform a Lorentz transformation so that they appear to be equal and opposite. The only case in which this is impossible is that of quanta travelling in the same direction. However, this case is of no interest because it leads to no pair production. If the frequencies of the quanta are ν_1', ν_2' and the angle between their directions is φ then the frequency of either in the frames of zero total momentum is $\nu_1=\nu_2=\nu =(\nu_1'\nu_2')^{1/2}\sin(\varphi/2)$ and $N_1'=(\nu_1'/\nu_1)N_1$, $N_2' =(\nu_2'/\nu_2)N_2$. Hence

$$\sigma'd\omega_1'=\sin^2(\varphi/2)\sigma((\nu_1'\nu_2')^{\frac{1}{2}}\sin(\varphi/2))d\omega_1. \tag{23}$$

The velocity with which the primed system of reference is moving with respect to the unprimed system is $-c^2(\mathbf{P}_1'+\mathbf{P}_2')/(h\nu_1'+h\nu_2')$. From (23) and (20) one can obtain the angular distribution of positrons and electrons by calculating $d\omega_1'/d\omega_1$ by means of the usual formulas

[2] In a forthcoming issue of the Proc. Roy. Soc. the pair production due to collisions of γ-rays and electrons with the electric fields of atoms is treated successfully by Williams by means of Eq. (21.3) which was published in an abstract of a paper read at the Washington meeting of the Physical Society (Phys. Rev. **45**, 766(A) (1934)). The formula in the abstract gives an incorrect value of σ which is twice as large as that given here. Correct results are obtained by Williams using $n_1n_2\sigma/(2A)$ and σ as in (21.3).

for the transformation of momentum and energy. The collision cross section for pair production over all angles depends only on $\int \sigma' d\omega_1$ and one may thus use Eqs. (21) for the calculation of these cross sections for any angle between light quanta by applying

$$\bar{\sigma}' = \sin^2(\varphi/2)\bar{\sigma}((\nu_1'\nu_2')^{\frac{1}{2}}\sin(\varphi/2)). \quad (23')$$

The polarizations of the light quanta are changed by the Lorentz transformation and thus only (21.3) has in general a simple meaning.[3]

Using Eq. (17'), comparing it with Eq. (18') and Eq. (21.3), one obtains the probability of recombination per unit volume per second as

$$c\rho_e\rho_p(\bar{\sigma}/2)(C/S)$$

in the frame of zero momentum in terms of the electron and positron densities ρ_e, ρ_p. Transforming to a frame in which the electrons are at rest one has

$$\rho_e' = (1-\beta^2)^{\frac{1}{2}}\rho_e, \quad \rho_p' = (1+\beta^2)(1-\beta^2)^{-\frac{1}{2}}\rho_p, \quad \beta = v/c$$

and $$\rho_e\rho_p = (1+\beta^2)^{-1}\rho_e'\rho_p' = [C^2/(C^2+S^2)]\rho_e'\rho_p'.$$

As for pair productions the number of recombinations per unit volume per unit time is Lorentz invariant and thus in K' (system where electron is at rest) this number per unit electron and positron density is

$$c(\bar{\sigma}/2)C^2/[S(C^2+S^2)].$$

This is Dirac's recombination formula with Dirac's $\alpha = \cosh 2\theta$. One could also derive (21.3) from Dirac's recombination formula and the relations (17'), (18'). The other formulas (20), (21) require, however, the more detailed calculations, the results of which were reported above.

As has been reported at the Washington meeting, pair production due to collisions of cosmic rays with the temperature radiation of interstellar space is much too small to be of any interest. We do not give the explicit calculations, since the result is due to the orders of magnitude rather than exact relations. It is also hopeless to try to observe the pair formation in laboratory experiments with two beams of x-rays or γ-rays meeting each other on account of the smallness of σ and the insufficiently large available densities of quanta. In the considerations of Williams, however, the large nuclear electric fields lead to large densities of quanta in moving frames of reference. This, together with the large number of nucleii available in unit volume of ordinary materials, increases the effect to observable amounts. Analyzing the field of the nucleus into quanta by a procedure similar to that of v. Weizsäcker,[4] he finds that if one quantum $h\nu$ per cm^2 is incident on a nucleus of charge Ze then the number of pairs produced is[5]

$$\sigma(\xi) = (4/\pi)Z^2\alpha\int_1^{(\xi/2)^{\frac{1}{2}}} \sigma(C)\log\{(\xi/2)^{\frac{1}{2}}C^{-1}\}C^{-1}dC,$$

where $\sigma(C)$ is given by Eq. (21.3), $h\nu = mc^2\xi$ and $\alpha = 2\pi e^2/hc$. The evaluation of the integral shows that $\sigma(\xi)$ is in asymptotic agreement with the corresponding formula of Heitler and Sauter[6] for high ξ.

[3] Two light waves polarized parallel or perpendicular to each other retain their relative polarization when viewed from another frame of reference if they travel in the same direction. If, however, they travel in opposite directions the relative polarization is in general changed. On the other hand, an unpolarized beam remains unpolarized when viewed from any frame of reference. Thus Eq. (21.3) in conjunction with (23') always applies to the collision of a quantum with quanta having random polarizations.

For quanta colliding head-on the relative polarizations are the same as in the frame of zero momentum, and for such quanta Eq. (23') with σ as given by Eqs. (21.1), (21.2) may be applied directly to the calculation of collisions between quanta polarized parallel or perpendicular to each other whether the total momentum is zero or not.

[4] C. F. v. Weizsäcker, Zeits. f. Physik **88**, 612 (1934).

[5] We are very much indebted to Dr. E. J. Williams for permission to quote his results.

[6] W. Heitler and F. Sauter, Nature **132**, 892 (1933). Cf. also J. R. Oppenheimer and M. S. Plesset, Phys. Rev. **44**, 53 (1933).

Thermal Expansion of Bismuth Single Crystals Near the Melting Point

J. W. BUCHTA* AND A. GOETZ, *California Institute of Technology*

(Received September 4, 1934)

Single crystals of Bi *highly purified* by repeated crystallizations show no decline in the coefficient of thermal expansion as the melting point is approached. It is shown that the presence of impurities (Pb, Ag, Cd, Sn) in very small amounts does cause the coefficient to decline and attain negative values in a range of 10° or 20°C below the melting point. On the basis of these observations the discrepancy between previous results by Roberts, and Ho and Goetz concerning the integral (macroscopic) thermal dilatation, and Goetz and Hergenrother, and Jay concerning the lattice expansion of Bi crystals is discussed.

INTRODUCTION

ONE of the major problems of the solid state is the phenomenon of melting. The characteristics of this phenomenon for a crystalline material have not been satisfactorily included in the theories of the crystalline state. It is expected that some information concerning the process of melting could be obtained by studying the physical properties of materials at temperatures near their melting points.

In this investigation the thermal expansion of bismuth single crystals was measured. Bismuth was chosen since earlier work indicated some anomalies in the thermal expansion near the melting point. Roberts[1] and Ho[2] found the thermal expansion macroscopically to decrease in a range of 10° to 30°C below the melting point. Roberts suggested that impurities may be important in causing the lowering of the expansion coefficient but did not state that impurities were known to be present in his crystals.

Determination by Goetz and Hergenrother[3] of the lattice spacing by refraction of x-rays indicated no decrease in the coefficient of thermal expansion as the melting point was approached. However, later measurements by Jay[4] on the crystal lattice spacing differed from those of Goetz and Hergenrother in that no divergence between the macroscopic and the lattice expansion coefficient was found and in that indications of a very rapid decline of the lattice expansion coefficient normal to the principal axis above 250°C were obtained. The powder method was used by Jay. The samples tested were filings from a metal rod which by analysis was given Bi, 99.995 percent; Ag, 0.004 percent; other elements, minute trace. From his measurements Jay concluded that there was no difference between the integral (macroscopic) expansion of a crystal obtained with a dilatometer and that indicated by the change of the atomic spacing within the crystal lattice as measured by x-ray diffraction for the range between room temperature and melting point.

PRODUCTION OF CRYSTALS

The crystals used in this investigation were grown in the apparatus described by Hasler.[5] A vacuum pump was added to the apparatus and the crystals grown in high vacuum. They were at all times protected from mercury vapor by a liquid air trap.

The bulk bismuth used was purchased as commercially pure stock. To obtain very pure materials this was placed in a graphite mold ($1.2\times1.0\times25$ cm) and recrystallized five times. The total time for each crystallization of the rod about 20 cm long was 7 to 18 hours. After each crystallization pieces 2 to 4 cm long were broken off each end of the bar and the remaining material used for the next crystallization. This work and that of Hasler[6] supports the original findings of L. Schubnikof[7] that a large part of the impurities is driven along the molten metal ahead of the region of crystallization and finally deposited near the end of the crystal. After the

* On leave from the University of Minnesota.

[1] J. K. Roberts, Proc. Roy. Soc. **A106**, 385 (1924).

[2] See A. Goetz and R. C. Hergenrother, Phys. Rev. **40**, 643 (1932); A. Goetz and T. L. Ho, Phys. Rev. **43**, 213 (1933); F. Blank, Phys. Zeits. **34**, 353 (1933).

[3] A. Goetz and R. C. Hergenrother, Phys. Rev. **40**, 643 (1932).

[4] A. H. Jay, Proc. Roy. Soc. **A143**, 465 (1934).

[5] M. F. Hasler, Rev. Sci. Inst. **4**, 656 (1933).

[6] Thesis, *The Thermo-electric Analysis of Micro-alloyed Single Crystals of Bismuth*, Cal. Inst. Tech. (1933).

[7] L. Schubnikof and H. T. de Haas, Comm. Univ. of Leyden No. 207c, page 26 (1930).

fifth recrystallization the material was cast in graphite molds (approximately 3×3×150 mm) in a vacuum induction furnace. These polycrystalline casts we shall call Bia. The pieces broken from the larger rod after each recrystallization were also cast in small bars in the induction furnace. This material we shall designate as Bib. The polycrystalline casts were seeded to obtain various orientations of single crystals. They were grown in the apparatus[5] mentioned above and in some cases were recrystallized three or four times to obtain further purification. Specimens 2 cm long were cut from various parts of the final single crystal rods 10 to 24 cm long and used in the dilatometer.

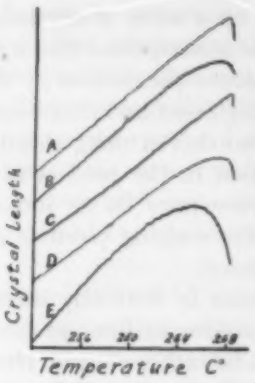

FIG. 1. Curves *A* and *C*; thermal expansion of crystals of pure bismuth. Curves *B*, *D* and *E*; thermal expansion of crystals containing impurities. Curves are displaced and various ordinate scales are used.

THE EXPANSION APPARATUS

The dilatometer is described in detail in a current issue of the *Review of Scientific Instruments*.[6] Its essential parts were an optical lever and a Moll thermorelay to detect the deflections of the light beam. The temperature was measured by means of a platinum resistance thermometer. Recording galvanometers were used so that a length-temperature curve was traced on 5″×7″ photographic paper. Some of the curves are reproduced in Fig. 1. The difference between this method and that which uses an ordinary dilatometer lies in the possibility of recording the thermal dilatation of a specimen over temperature intervals of only a few degrees with a considerable accuracy in spite of the large sensitivity.

DISCUSSION OF RESULTS

The results indicate rather definitely that for pure bismuth crystals there is no decline in the coefficient of expansion up to within three degrees of the melting point. At 268.0 to 268.5° the gravitational load transgresses the elasticity limit of the crystals. This is indicated by the plastic deformation of the lower part of the crystal although occasionally intermediate regions showed this deformation

Typical temperature-length curves are shown in Fig. 1. Curve *A* is the record of a specimen cut from a crystal grown from Bia. The crystal was seeded so that the trigonal axis was perpendicular to the axis of the crystal (P_1 orientation). Except for a small decline in the last degree before collapse there is no change in the coefficient as the crystal is heated above 250°C. Curve *B* is the record of a section cut from the end of a crystal grown from Bib. It had the same orientation as the first crystal. The trace departs from a straight line at 263°C and the coefficient of expansion declines rapidly thereafter.

The crystal used to obtain curve *C* was a cast of Bia which was then recrystallized three times. The end of the material was discarded after the second crystallization and a middle section of the final crystal was used. The trigonal axis was parallel to the crystal length (P_3 orientation). There is no indication of decline of the slope of the line up to the point where the crystal collapsed.

During the course of the work crystals of various orientations were used and similar results obtained. The coefficient, of course, has different numerical values for the various orientations. No attempt was made to obtain precise absolute values of the coefficients. The measurements made agreed with the accepted values of the coefficients for the various orientations. The different slopes of the straight portions of the curves of Fig. 1 are not significant as the dilatometer was set for different sensitivities.

Curve *D* is the record of a section near the end (part of crystal last to solidify) of a very long (24 cm) crystal grown slowly (10 hrs.) from Bib. A middle section of this crystal gave a sharp break such as that in curve *C*.

[5] A. Goetz, J. W. Buchta and T. L. Ho, Rev. Sci. Inst. **5**, 428 (1934).

The results on a score of crystals are all consistent with the assumptions that a small amount of impurity causes the decline of the coefficient near the melting point and that impurities in the molten metal are driven along ahead of the region of crystallization in the process of growing the crystals. In very pure Bi no indication of the approach to the melting point is given by the thermal expansion.

The expansion is evidently affected by *very small* amounts of impurities and their determination proved to be rather elusive. However, it was shown that small amounts of Pb, Ag, Sn and Cd were important. The results of a rough spectroscopic analysis of the specimen used for curves *A*, *B*, *C* and *E* are given in Table I.

TABLE I.

Crystal curve	Percent of impurities Pb	Cu	Ag	Cd	Ca	Al	Mg	Ti
A	0	0.001	0	—	0.1	—	—	—
B	0.05	0.01	0.05	—	0.1	0.001	0.001	0.001
C	0	0.001	0	—	0.1	0.001	0.01	0.01
E	0.001	0.1	0.01	1.0	0.1	—	—	—

Polarograph tests checked the values of the lead content. The traces of Ca, Al, Mg and Ti are probably mechanically included. The samples were tested after they had been melted in the dilatometer.

The decline of the curves for crystals containing impurities is partially but not entirely caused by plastic deformation. If the contraction near the melting point was not carried too far the crystal could be tested again. Curve *E*, Fig. 1, is a second record of a crystal containing some Cd that had been previously heated. Curve *F*, Fig. 2, is the trace obtained at the first heating. The curve departed from a straight line at a lower temperature in the first run than in the second. Some permanent deformation occurred and on cooling the curve was not retraced.

The specimens used for curves *G* and *H*, Fig. 2, have several percent of tin. Curve *G* was obtained on heating and curve *H* on cooling. The phenomenon in the temperature range indicated is at least partially reversible.

It is believed that the present work explains some of the discrepancies of previous experiments, though perhaps not all. There exists

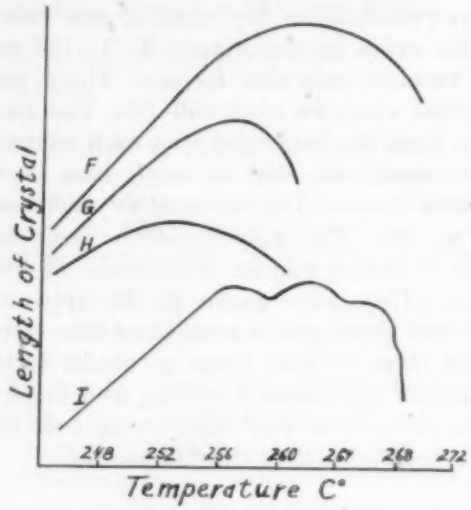

FIG. 2. Curve *F*; thermal expansion of a bismuth crystal containing Cd. Curves *G* and *H*; thermal expansion of a bismuth crystal containing Sn. *G*, heating; *H*, cooling. Curve *I*; thermal expansion of a bismuth crystal containing Ag.

evidently a process within the crystal which causes a decline of the expansion coefficient which is partially, at least, of reversible nature as soon as traces of impurities are present. This decline cannot be traced in the lattice expansion, at least the indications of such an effect found by Jay[4] could not be reproduced by recent tests more accurate than the original measurements by Goetz and Hergenrother.[3] Furthermore, the Bi used by Jay[4] was of an exceptionally high degree of purity (0.004 percent Ag), a concentration for which we should not expect a decline. In order to be certain about this and to decide whether or not the decline of the expansion coefficient characterizes only soluble (or partially soluble) admixtures (Pb and Cd being partially soluble in Bi) and not foreign atoms unable to interpenetrate the crystal lattice (e.g., Ag) a record of a specimen containing not more than 0.5 percent (atomic) Ag was made (curve I, Fig. 2). The Ag was added to Bi which had been purified so that it gave a sharp break in the curve at 268°C. The mixture was then recrystallized once and a center section of the crystal tested. The general characteristics of the curve—a contraction followed by an expansion—could be repeated on the same specimen by carefully heating and cooling it in the region above 256°C. The phenomenon seems to be in suggestive analogy to that described for

the Bi-Pb crystals[9] in the region of the eutectic melting point since the corresponding point for the Bi-Ag system lies at 260°C. Since changes of this type apparently do not affect the regions of the lattice capable of diffraction, they should not be reflected in x-ray measurements.

Our observations establish thus a support for the hypothesis of "decrystallization" by Goetz and Hergenrother[2] which attributes any deviation of the macroscopic qualities from the crystal lattice as seen by x-rays to disturbances caused by foreign atoms even if they are soluble. The mentioned hypothesis suggests, however, a divergence of the two expansions (i.e., a decline of the macroscopic dilatation) even for ideally pure material. The present results do not disprove this possibility since the region of such a decline may be restricted to the very close neighborhood of the melting point which is inaccessible due to plastic deformation of the specimen in the gravitational field.

The authors are indebted to Dr. M. F. Hasler for the spectroscopic and polarographic analyses and to him and Mr. R. C. Kendall for aid in growing the crystals and valuable discussions during the course of the work.

[9] A. Goetz, J. W. Buchta and T. L. Ho, Phys. Rev. **46**, 538 (1934).

DECEMBER 15, 1934 PHYSICAL REVIEW VOLUME 46

The Magnetostriction of Pure and Alloyed Bi Single Crystals*

ALEXANDER WOLF AND ALEXANDER GOETZ, *California Institute of Technology*

(Received August 6, 1934)

The existence of a magnetostrictive effect (Joule effect) in nonferromagnetic substances, first demonstrated by Kapitza for large transient fields, is here shown for steady fields of moderate (20 to 25 kg) values. Pure (99.97 percent) Bi single crystals and crystals with dissolved foreign atoms are used. A recording dilatometer permitted measurements of a change in length of 2.5×10^{-7} cm. The sum of errors amounted to approximately 10 percent. The modulus of magnetostriction (m) is defined by $\Delta l/l=\frac{1}{2}mH^2$. For pure Bi crystals $m=+5.7\times10^{-16}$ (elongation) parallel to trigonal axis and $m=-7.0\times10^{-16}$ (contraction) normal to trigonal axis. Bi crystals with Pb, Sn and Te in concentration within the solubility range were studied. Sn and Pb (electropositive) first cause the contraction normal to the trigonal axis to diminish and finally with increasing concentrations, cause an elongation, Sn being four times as effective as Pb. Parallel to the axis small concentrations of Sn decrease the elongation, larger concentrations increase the elongation. The effect of Pb in this direction is small. Te (electronegative) produced a much larger specific effect but no change in sign. The effect was of the same order of magnitude for the two principal crystal orientations. The data are discussed with special reference to the influence of foreign atoms on the magnetic susceptibility, studied previously by Goetz and Focke. It was found that the change of the stress coefficient of the susceptibility with the concentration of foreign atoms *normal* to the principal axis is inversely proportional to the concentration and furthermore: the variation of the stress coefficient with the concentration is nearly equal to the variation of the susceptibility at higher concentrations, in other words the stress coefficient of the susceptibility is proportional to the susceptibility itself. It is furthermore concluded that the results presented justify the previous assumption of the existence of two types of insertion of foreign atoms in the crystal lattice, i.e., selective adsorption for small concentrations and volume absorption for larger concentrations.

I. INTRODUCTION

THE search for magnetostrictive effects in non-ferromagnetic materials was begun soon after the discovery by Joule in 1847 of the effect in ferromagnetic materials. Aubel[1] in his review quotes a number of attempts[2–6] to detect the phenomenon. All gave negative results as did more recent work of Hobbie,[7] Schulze[8] and Bryan and Heaps.[9] Kapitza[10, 11] was the first

* Partly contained in: A. Wolf, Thesis, Cal. Inst. of Tech. 1933; A. Wolf and A. Goetz, Phys. Rev. **43**, 213 (1933).

[1] Aubel, Phys. Rev. **16**, 60 (1903).
[2] S. Bidwell, Phil. Trans. **179**, 205 (1888).
[3] Grimaldi, J. de physique **8**, 552 (1889).
[4] Aubel, J. de physique **1**, 422 (1892).
[5] Knott, Nature **61** (1899).
[6] A. P. Wills, Phys. Rev. **15**, 1 (1902).
[7] J. R. Hobbie, Phys. Rev. **19**, 456 (1922).
[8] A. Schulze, Zeits. f. Physik **50**, 448 (1928).
[9] A. B. Bryan and C. W. Heaps, Phys. Rev. **37**, 466 (1931).
[10] P. Kapitza, Nature **124**, 53 (1929).
[11] P. Kapitza, Proc. Roy. Soc. **A135**, 537 (1932).

to observe a positive result for Bi crystals. He used extreme fields (250–300 kg) of brief duration (10^{-2} sec.), thus detecting the small effect which the previous workers had failed to find.

This investigation is closely related to the work on crystal-diamagnetism on Bi crystals by Goetz and Focke[12–15] where a quantitative study of the influence of foreign atoms inserted into a metallic crystal lattice was made. It is thus of interest to investigate in what manner the changes of susceptibility caused in a crystal by inserted admixtures are reflected in the magnetostrictive effect; as such this investigation follows the lines of the general research program in this laboratory.

An additional purpose was to supplement the results of Kapitza concerning Bi crystals in a stationary magnetic field of moderate intensity (about 25 kg) in contradistinction to Kapitza's transient field of high intensity.

II. The Apparatus

(a) Method of measurement

The magnetostrictive effects in Bi are very much more difficult to measure than those in ferromagnetic substances. With fields of about three thousand gauss, the effect $(\Delta l/l)$ in Ni is of the order of 3×10^{-5}, in Bi it is of the order of 3×10^{-9}. With a powerful solenoid producing a magnetic field of 25 kg the effect is still 100 times smaller than the magnetostriction of a ferromagnetic material in a moderate field. The extraneous disturbances on the apparatus produced by increasing the magnetic field are augmented to a marked extent. These disturbances are, principally the heating, transient currents induced by the field, vibration of the necessary rotating machinery, etc.

The essentials of the method of measurement are shown in Fig. 1. The change in length of the crystal *Cr* relative to that of a neutral material *N* rotates the mirror *M*. A beam of light from a fixed slit is reflected by the mirror and then focussed on the Moll-thermorelay *Th*. This is a differential thermocouple, Constantan *C* between copper *Cu* ribbons of low heat capacity (1μ thick) mounted in an evacuated glass bulb. The bulb is mounted on a micrometer stage and may be adjusted so that the beam of light from the mirror *M* heats each junction *C–Cu* equally. A slight displacement of the beam from this position results in a current through the galvanometer *G*.

The sensitivity of the arrangement depends upon the intensity of the light and the sensitivity of the galvanometer. As used, a motion of about 0.0007 mm of the spot of light gave a galvanometer deflection of 1 mm. The magnification of the optical lever was about 300 times, giving a total magnification of 1 : 400,000. With crystals 10 cm long a strain of 2.5×10^{-3} corresponded to 1 mm on the galvanometer scale.*

In addition to high sensitivity, the method offers advantages over microscopic or telescopic methods in that the readings can be recorded photographically. Also there is no indeterminacy caused by diffraction. The thermorelay integrates over the total beam and is not handicapped by a limited "resolving power." The image on the ribbon was 2–3 mm wide. The lack of mechanical magnifying levers made the set-up insensitive to mechanical vibration and permitted a 500 kw motor generator set to be located in the same room.

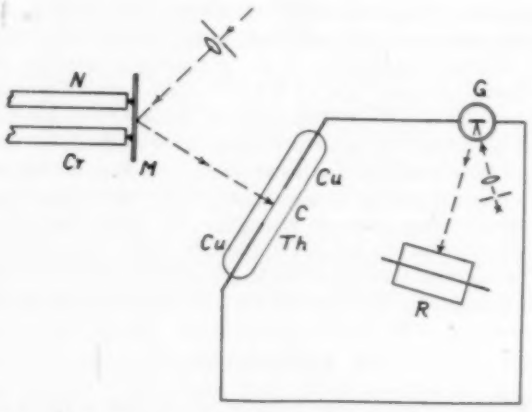

FIG. 1. Scheme of the magnetostriction—dilatometer. (*Cr*, crystal; *N*, neutral frame; *M*, mirror; *Th*, thermorelay; *G*, galvanometer; *R*, photographic recorder.) The full drawn line indicates the electric recording circuit, the dashed lines the optical paths.

[12] A. B. Focke, Phys. Rev. **36**, 319 (1930).
[13] A. Goetz and A. B. Focke, Phys. Rev. **38**, 1569 (1931).
[14] A. Goetz and A. B. Focke, Science **74**, 603 (1931).
[15] A. Goetz and A. B. Focke, Phys. Rev. **45**, 170 (1934).

* It may be mentioned that an interferometer method could hardly be used for these experiments since the entire effect under investigation would have produced a shift of only one-tenth of a fringe in the visible region.

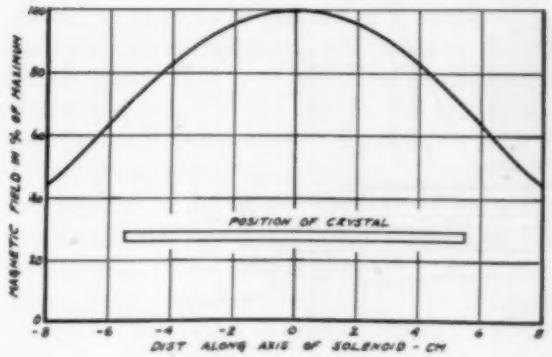

FIG. 2. Longitudinal field distribution along the axis of the solenoid.

(b) The magnet

The magnet used was a large 500 kw solenoid installed at the physical laboratory of the Mount Wilson Observatory constructed by Dr. J. A. Anderson. It consists of two coaxial coils of heavy copper tape which are connected parallel. The coils are enclosed in a brass shell leaving a central opening 2 inches in diameter. The cooling medium is transformer oil pumped at high speed through the interspace of the windings and through pipe slings immersed in a large water tank. The maximum current for which the solenoid is designed is 4000 amp. at 125 volts, which is supplied by a motor generator set mentioned above. The maximum field at the center of the coil is 28 kg, since however the coil is short the inhomogeneity of the field is large as shown in Fig. 2.

(c) Description of the dilatometer

The essential part of the apparatus is the framework in which the crystal is mounted, and the arrangement whereby the magnetostriction is transformed into the rotation of a mirror. This part of the apparatus, is shown in Fig. 3.

A brass block (1) is held rigidly in the wooden piece (2), which in turn is bolted to an outside wooden framework, not shown in Fig. 3. Two fused quartz tubes (3) are cemented in the brass block. Aluminum disks (4 to 10) are cemented to the quartz tubes, forming a rigid frame. The disk (9) holds a copper cup (11) in which one end of the crystal (12) is fixed with Wood's metal. The other end of the crystal is fixed similarly in a copper cup (13), cemented in turn to the fused quartz tube (14), which extends to the right, passing freely through the brass block (1).The left end of tube (14) is held in a brass ring (15), which has soldered to it radially four thin bronze wires (16), which in turn are soldered to the heads of four pins (17) screwed into the aluminum disk (4). This feature of the apparatus is best seen in the section in the lower center of Fig. 3. It is seen that the left end of tube (14) is free to move through small distances to the right or left. The right end of this tube carries a small brass block (18). To the right face of this block is clamped a very thin bronze strip (19). The upper end of this strip is clamped to the face of a brass block (20), cemented onto the quartz tubes (3) which form the main framework. The vertical clearance between (18) and (20), which is also the free length of the bronze strip (19) is 3 mm. Along the center of the free part of the bronze strip (19) is soldered a copper wire (21), which carries a 5/8-inch galvanometer mirror (22). This part of the apparatus is shown best in the section on the lower right of Fig. 3.

It is seen that the central quartz tube (14) is constrained to a small horizontal motion, which, however, is amply sufficient to permit the crystal under test to expand and contract freely. It can be readily seen that a change in the length of the crystal results in a horizontal motion of the brass block (18) relative to (20), and that the bronze strip transforms this motion into the rotation of the mirror (22) around a horizontal axis. The movement is entirely free from friction and there is no possibility of lost motion.

For purposes of calibration (see later) it was necessary to raise the temperature of the crystal by about 0.2°. This could be accomplished by means of a heating coil (23) extending over the full length of the crystal and being conducted through the holes in the aluminum disks. Holes (24) on the opposite side of the crystal hold insulating bushings, which carry the leads of a platinum resistance thermometer wound concentrically with the crystal on four mica frames (25), attached to the aluminum disks (5, 6, 7, 8). A section showing the mica frames can be seen on the lower left of Fig. 3. The platinum thermometer is spread out over the full length of the crystal, so as to obtain an average of temperature, in case of a temperature gradient. The

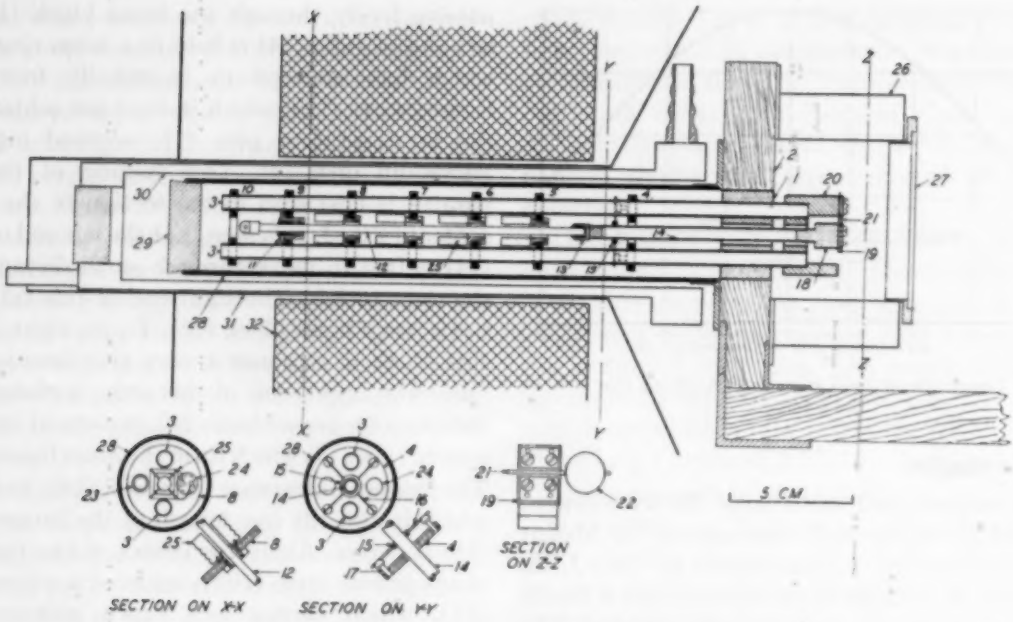

FIG. 3. Detail of the magnetostriction dilatometer.

thermometer also is needed for purposes of calibration.

The apparatus described above forms a distinct unit, which does not come in direct contact with the solenoid. It is protected on the right by a water-jacket (26) with a glass window (27) in front of the moving mirror. On the left the apparatus is covered by a glass tube (28) closed with a cork (29). Between the above unit and the solenoid is interposed a water-jacket (30), intended to maintain the crystal at a uniform temperature. The outer shell of the solenoid (31), and the position of the coils (32), are indicated on the figure. The optical system (Fig. 4) consists of a series street-lighting lamp A which is the source of energy for operating the thermorelay G. C is a horizontal slit, B, D are convex lenses. The cylindrical lens F is placed just in front of the thermorelay with its axis parallel to the ribbon in the thermorelay.

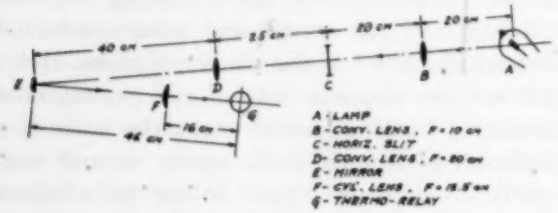

FIG. 4. Optical path between dilatometer and thermorelay.

The deflection of the galvanometer in the thermorelay circuit is recorded in a photographic recorder (Fig. 1) driven by a clockwork. A timing device makes a mark on the paper at intervals of 15 seconds.

III. THE CRYSTALS

The crystals used for this investigation had to be very uniform over a considerable length. They were grown after the method described by Goetz[16] and Goetz and Focke.[15] They were rods 2–3 mm in diameter and at least 120 mm long.

The metal was the brand of the Merck Chemical Co. Two separate lots designated as Bi H and Bi J were used. They are presumed to have not more than 0.03 percent impurities or found in lots E and F which were used in the magnetic measurements[15] since H and J had the same magnetic anisotropy. A spectroscopical analysis of E and F has been published.[15]

Two principal crystallographic orientations were studied. Following a designation given previously[17] P_1 crystals had the trigonal axis

[16] A. Goetz, Phys. Rev. **35**, 193 (1930).
[17] A. Goetz and M. F. Hasler, Phys. Rev. **36**, 1752 (1930).

normal to the axis of the rod. For this case two variations of second order are possible: (a). One of the binary axis [111] in plane with the axis of the rod (P_1 0°); (b) one of the binary axis [111] normal to the axis of the rod (P_1 30°).

The other orientation (P_3) had the trigonal axis parallel to the axis of the rod, no secondary variations are possible in this case in a field symmetrical to the axis of the rod.

IV. The Measurement

(a) Calibration of the apparatus

The apparatus was calibrated by changing the temperature of the crystal in its mountings approximately 0.2° and measuring the corresponding deflection of the thermorelay galvanometer. The sensitivity of the apparatus can then be calculated since the expansion coefficient of the crystal and the temperature interval are known.

The coefficients of thermal expansion of Bi crystals were taken from the measurements of Ho and Goetz[18] and correction was made for the expansion of the frame.

The *Pt* thermometer measures the variation of the air temperature, with which the temperature of the crystal does not coincide until the elapse of a certain time interval. This was found to be at least one hour, a time much too long for maintaining constant conditions within the other parts of the apparatus due to unavoidable gradual distortions. In order to eliminate this uncertainty the calibration was accomplished by changing the current supplied to the heating coil at 6 to 10 minute intervals. The resulting temperature variation of the air is somewhat as shown in Fig. 5, where curve *A* shows the air temperature recorded against time. The temperature of the crystal, as reflected by the record of the thermorelay galvanometer, is shown by curve *B*. Although the temperature of the crystal lags behind the air-temperature the former is known at any of the peaks C_1, C_2, etc., since at the point where the temperature variation of the crystal changes sign, the crystal temperature must equal the air temperature. Hence the galvanometer deflection *D* corresponds to a change in temperature ΔT, as shown in the figure.

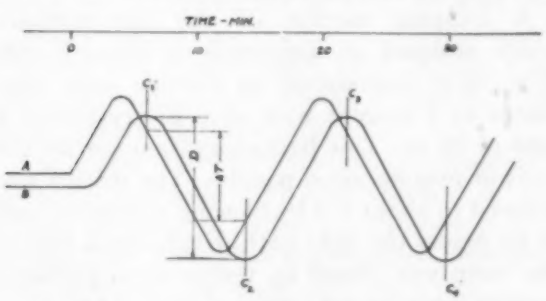

FIG. 5. Time-temperature diagram for the purpose of calibration. (*A*, air temperature measured by thermometer; *B*, crystal temperatures measured by thermorelay.)

If a drift occurs because of deformations of the apparatus, this can be recognized since in that case alternate peaks C_1, C_3, C_5, etc. do not occur at the same temperature. A proper correction can then be applied, since the time-drifts, as found, were always unidirectional, and their rate was practically constant for any given calibration. The great advantage of the method is found in its speed, which permits one to obtain a number of points on the calibration curve in such a short time that an external distortion-drift can be corrected for. In most calibrations about 12 points were used.

The method of calibration described above does not involve the measurement of the length of the crystal, which is one of the serious sources of error in most investigations of magnitostriction, particularly those made on short samples.

(b) Magnetostriction tests

The magnetostriction tests were carried out on a time-schedule, and Fig. 6 shows typical records of such measurements.

The marks at the top indicate the 15-second intervals. The time-axis runs from left to right. The line in the center is a record made by the thermorelay galvanometer. Deflections downward indicate an expansion of the crystal tested, deflections upward indicate contraction. The two sets of large deflections, extending almost across the records are the calibration of the lamp intensity, being checked just before and just after each test, because of the dependence of the total sensitivity on the light intensity. On the records shown in the figures these deflections were produced by a vertical displacement of the mi-

[18] A. Goetz and R. C. Hergenrother, Phys. Rev. **40**, 643 (1932).

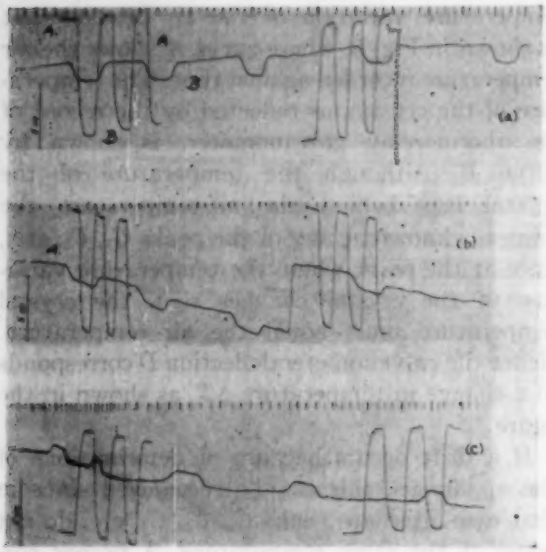

FIG. 6. Magnetostriction records. (The points *A* designate the moment, when the field current was started, the points *B* when the field was taken off. On the same record are the calibration curves of the intensity of the light source for the thermorelay, indicating also the temperature drift inside the dilatometer.)

crometer stage of the thermorelay of 0.056 mm.

The magnetostriction in Fig. 6a is an expansion, $(\Delta l/l)$ of 34×10^{-6}. This was the largest effect observed in any of the tests. Fig. 6b shows an expansion of 19×10^{-6}. Fig. 6c shows a contraction of 22.5×10^{-6}. A fairly rapid thermal expansion of the crystal can be seen in Fig. 6b. In order that the line should not drift off the paper, the thermorelay was displaced about the middle of the record.

Immediately after each test of the type described above a mirror was attached with wax to the face of the glass window (27, Fig. 3) in front of the rotating mirror (22, Fig. 3), and the identical procedure was gone through again. This is equivalent to conducting the test with the rotating mirror effectively locked. Any deflection of the thermorelay galvanometer obtained in this way is ascribable to a deformation in some part of the apparatus outside the solenoid, and should be subtracted from the deflection observed in the magnetostriction test. Such effects were actually found. Their magnitude varied from zero to about 1 mm, i.e., they were equivalent to a magnetostriction of from zero to 2.5×10^{-6}.

(c) Discussion of errors

There are two chief sources of error, *viz*, (a) imperfections in the crystals and (b) observational errors.

(a) There is little question as to the perfection of the crystals used in this investigation, so long as only crystals of pure bismuth are concerned except that the principal axis of the P_3 crystals was inclined about 4° from the axis of the rods instead of being parallel. Kapitza's[11] work shows that this introduced a negligible error of about 0.3 percent.

The amounts of impurities given for the alloyed crystals are the amounts added to the melt from which the crystal was grown. Previous experiments[15] indicate that in the P_1 crystals grown rapidly (6 mm per min.) the impurity is uniformly distributed. The P_3 crystals were grown more slowly (1 mm per min.) and the curves showing the effect of impurities are drawn from points which represent the average magnetostriction for a certain range of impurity, rather than the magnetostriction for a specific amount of impurity.

(b) The observational error can be estimated as follows: An uncertainty of 1 percent in the coefficients of thermal expansion introduces a corresponding error in the calibration and accordingly in the final result.

The measurement of the magnetic field involved an error of about 2 percent, hence 4 percent in the magnetostriction. The error was of this magnitude since the coil gradually short circuited in the later part of the investigation and the field intensity was calculated by interpolation between successive calibrations.

A creeping motion of the galvanometer which attained an amplitude of about 1 mm (Fig. 6a–c) introduced an average error estimated at 5 percent with pure Bi crystals in a field of 26 kg. This background motion set the limit of magnification possible. The motion was reduced to about 1/3 by blowing a broad stream of air across the light path. Evidently a part of the creep was caused by temperature gradients causing irregular diffraction of the light beam.

The total error then is about 10 percent in measurements on pure Bi in a field of 26 kg. The error may be slightly larger when weaker fields or alloyed crystals are used.

The magnetostriction of the frame work was checked and was found unmeasurably small.

The elastic deformation of the crystal due to mechanical stress by its mountings was found to be only 2 percent of the magnetostrictive deformation. Since an identical strain is applied by the thermal dilatation during the calibration (see 3a) no correction is necessary.

The effect of the inhomogeneity of the field of the solenoid (l.b. Fig. 2) along the crystal can be compensated by taking the root-mean-square value, assuming the quadratic dependence of the magnetostrictive effect on the field.

The deformation caused by the ponderomotoric forces acting upon a diamagnetic substance in an inhomogeneous field can be neglected as it results in the worst case (direction of smallest modul and largest susceptibility) in an elongation of 0.15 percent of the magnetostriction. Since the crystal is mounted symmetrically to the solenoid a one-sided force is avoided.

Despite the water-jacket surrounding the apparatus it was found impossible to maintain the crystal at a uniform temperature during a magnetostriction test. This is not surprising, since the outside temperature of the solenoid increased during the test from 25°C to about 50°C. So long, however, as the temperature drift of the crystal remained uniform, no error was introduced into the measurement, since the temperature drift resulted only in an inclination of the base-line from which magnetostriction was measured, as can be seen on the records (Fig. 6).

If, while the field is on, a change takes place in the rate of change of temperature, this can be recognized on the record by the fact that the inclination of the base-line is different before and after the field is established. Since at least four tests are made on each crystal, no serious error should arise from this source.

The temperature of the crystal is increased also when the magnetic field is established or destroyed, because of induction currents in the crystal. The corresponding elongation, however, is not over 0.01 percent of the total effect.

Finally the magneto-caloric effect (Langevin[19]) has to be considered, which depends upon the temperature coefficient of the susceptibility determined by Goetz and Focke.[15] In case of an ideally adiabatic process the effect would cause a thermal contraction of 0.5 percent of the total effect for P_2 and 1 percent for P_1. Since the real process is practically isothermal the actual error will be very much smaller and can be neglected.

[19] P. Langevin, Ann. de chim. et phys. **5**, 123 (1905).

V. Results

(a) Definition of the modulus of magnetostriction

The term "magnetostriction" as used throughout this paper designates only one of the several known phenomena of magnetostriction: the so-called Joule-effect. This is the change in the length of a long rod ($\Delta l/l$) when subjected to the action of a homogeneous longitudinal magnetic field.

The longitudinal stress p thus caused in the rod can then be expressed in terms of the field strength H, the susceptibility χ, Young's modulus Y and Poisson's ratio σ (χ, Y, σ with reference to the direction of p in an anisotropic substance) by:

$$p=-\int(Y\partial\chi/\partial p+\chi(1-2\sigma))HdH. \quad (1)$$

And since $\Delta l/l=p/Y$ and Y can be assumed to be invariant with H:

$$\Delta l/l=-\int(\partial\chi/\partial p+(\chi/Y)(1-2\sigma))HdH. \quad (2)$$

Since in case of a non-ferromagnetic substance $d\chi/dH=0$ at room temperature, $\partial\chi/\partial p$ is independent of H, and Eq. (2) reduces thus by integration to:

$$\Delta l/l=-\tfrac{1}{2}H^2(\partial\chi/\partial p+\chi/Y(1-2\sigma))$$
$$=-\tfrac{1}{2}H^2m, \quad (3)$$

where m shall be called the *modulus of magnetostriction*, since it is independent of H (if the invariance of Young's modulus with the field can be taken for granted). From experimental data the modulus of magnetostriction can thus be derived as:

$$m=2\Delta l/(l\cdot H^2). \quad (4)$$

The second term in Eq. (3) is negligibly small in case of Bi, since for a pure P_1-crystal $\chi/Y=1.05\times10^{-6}\times9.8\times6.17\times10^{-12}$, [15, 20] whereas σ is

[20] P. W. Bridgman, Proc. Am. Acad. Sci. **60**, 305 (1925).

about 0.25, the total being smaller than 10^{-17}, whereas the experimental value of m is larger than 10^{-16}. Thus in our case the modulus of magnetostriction can be defined with an accuracy higher than the experimental error (i.e., <10 percent) as:

$$m = 2\Delta l/lH^2 = \partial\chi/\partial p. \qquad (4a)$$

(b) Magnetostriction in single crystals of pure bismuth

In the case of pure bismuth magnetostriction tests were made on five crystals. The results are given in Table I, which is self-explanatory. The most striking fact about the results is that *magnetostriction is positive* (increase in length) *parallel to the trigonal axis* (P_3 crystals), *and negative at right angles to the trigonal axis* (P_1 crystals).

TABLE I. *Longitudinal magnetostriction in Bi crystals.* (Pure Bi.) ($T = 25°$C.)

A, crystal orientation; B, designation of Bi; C, temperature coefficient of expansion; D, magnetic field; E, longitudinal magnetostriction; F, modulus of magnetostriction.

A	B	C ($\times 10^6$)	D (gauss)	E ($\Delta l/l \times 10^6$)	F ($m \times 10^{16}$)
P_1, 30°	H	11.6	13,700	− 5.	
			19,300	−10.	
			25,900	−22.5	−6.65
P_1, 0°	H	11.6	14,200	− 6.	
			20,100	−13.5	
			26,000	−24.5	−7.3
P_3	H	15.9	13,600	+ 6.5	
			20,500	+13.	
			26,000	+19.5	+5.7
P_1, 0°	J	11.6	25,750	−22.5	−6.8
P_3	J	15.9	12,350	+ 6.5	
			18,700	+11.	
			24,000	+16.	+5.65

Since it was not possible to check all crystals with exactly the same field intensities, the best comparison between the crystals is obtained from the moduli of magnetostriction, m (4a). The agreement between each pair of crystals of like orientation is extremely close. The difference between the moduli of the two P_3 crystals is only 1 percent; the difference between the two P_1, (0°), crystals is 7 percent.

The modulus of the P_1, (30°), crystal is within the limits of experimental error the same as that of the P_1 (0°) crystals.

The accuracy of the present investigation is not sufficient to distinguish between the two azimuthal orientations. Hence no further tests were made on crystals of the P_1, (30°), orientation.

TABLE II. *Moduli of magnetostriction in pure Bi crystals.* ($T = 25°$, $H = 25$ kg.)

Crystal orientation	P_1, 0°	P_3
Modulus "m"—this exp.	-7.05×10^{-16}	5.7×10^{-16}
" " Kapitza	−7.3 "	6.5 "
Difference	3.5%	11.5%

Fig. 7 shows the magnetostriction values from Table I as function of the field strength; for comparison the values obtained by Kapitza[11] are added. Although the latter's work is not very accurate in the range of the smaller fields, there is good agreement. A comparison of the two investigations can also be made on the basis of the moduli of magnetostriction, as shown in Table II.

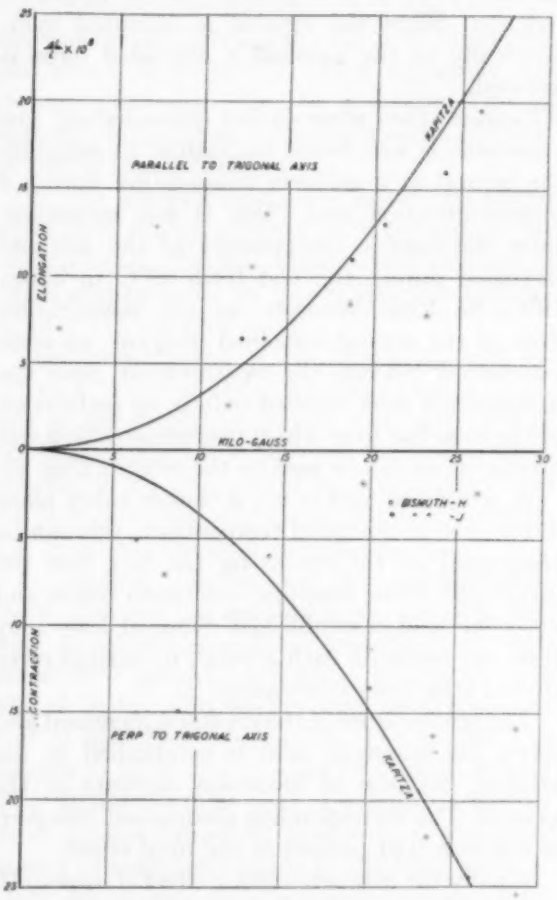

FIG. 7. Magnetostriction diagram as function of the field strength. (The full-drawn curve is computed from the values by Kapitza; the points shown represent the values obtained for pure Bi in this investigation.)

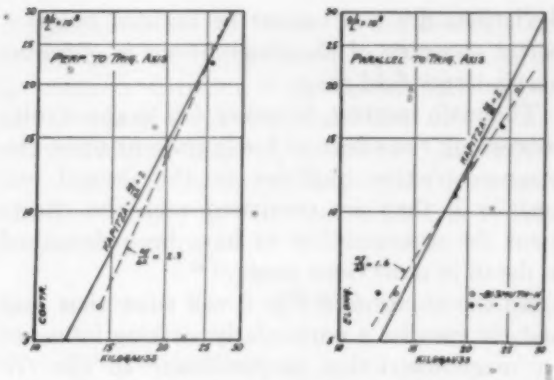

FIG. 8. Logarithmic magnetostriction diagram. (The full-drawn line represents Kapitza's H^2-dependence, the dashed line through the observed points indicates the closest straight line.)

The agreement is seen to be quite good when one considers that the present work does not claim an accuracy of over 10 percent, and Kapitza considers his limiting error as about 8 percent in his strong fields, and probably greater in the range which is here represented.

In order to check the theoretical expression for magnetostriction as a function of the magnetic field, the data of Table I were plotted on a logarithmic scale in Fig. 8. It is seen that the points lie practically on straight lines. From the inclination of the lines one obtains the equation:

$$\Delta l/l = k \cdot H^n. \tag{5}$$

where $n=2.3$ for P_1 crystals (Fig. 8a), $n=1.6$ for P_3 (Fig. 8b) and $k=$const. depending on crystal orientation. This appears to be valid between 15 and 25 kg.

Kapitza[11] obtained $n=2$ valid at least up to 100 kg. The present work, however, does not actually contradict Kapitza's, since the accuracy of both investigations drops so rapidly with decreasing magnetic fields that a definite determination of the exponent of H is not possible in weak fields.

(c) Magnetostriction in single crystals of alloyed bismuth

In order to determine the effect of foreign atoms on the magnetostriction of a bismuth crystal, tests were made on 22 crystals of bismuth containing various amounts of tin, lead or tellurium. These elements were selected on account of their mutual relations of valency configuration as discussed at length in a previous paper.[15]

The alloyed crystals were tested only in the maximum available magnetic field. Since this was not always the same, the effect of the impurities can be obtained only from a comparison of the moduli of magnetostriction which are listed in the second column from the right in Table III. The last column of the table gives the "percent magnetostriction," which is obtained by dividing the actual modulus of a crystal by the modulus of the crystal of the same orientation, but containing no impurity. The "percent magnetostriction" is plotted against the impurity in Fig. 9.

VI. Discussion

The described results obtained for pure Bi crystals show that our values of the modulus of magnetostriction agree for field strengths between 20 and 25 kg with those obtained by Kapitza[11] as well as one could expect within the margin of experimental error. This agreement proves that his method of transient fields of very short duration is equivalent to the usual

TABLE III. *Longitudinal magnetostriction in bismuth single crystals. The effect of impurities.*

A, Crystal orientation; B, designation of Bi; C, type of impurity; D, amount of impurity;* E, temperature coefficient of expansion; F, magnetic field; G, longitudinal magnetostriction; H, modulus of magnetostriction; I, percent magnetostriction.**

A	B	C	D	E	F	G	H	I
			(% at)	($\times 10^6$)	(gauss)	$\left(\frac{\Delta L}{L}\times 10^6\right)$	(m $\times 10^{12}$)	(%)
P_1, 0°	*H*	—	—	11.6	26,000	−24.5	− 7.3	100
P_3	"	—	—	15.9	26,000	+19.5	+ 5.7	100
P_1, 0°	"	Te	0.3	11.6	25,750	− 6.5	− 1.9	26
"	"	Te	0.2	11.6	25,750	− 7	− 2.1	29
"	"	Te	0.1	11.6	25,750	− 9.5	− 2.9	40
"	*J*	—	—	11.6	25,750	−22.5	− 6.8	100
"	"	Te	0.05	11.6	25,750	−11	− 3.3	48
"	"	Sn	0.1	11.6	25,750	−17	− 5.1	75
"	"	Te	0.01	11.6	25,750	−19	− 5.7	83
"	"	Sn	2.5	12.5	25,750	+34	+10.3	−151
"	"	Sn	1.0	12.0	25,750	+19	+ 5.7	− 84
"	"	Sn	5.0	12.9	25,750	+33.5	+10.1	−149
"	"	Sn	0.5	11.6	25,750	+12	+ 3.6	− 53
P_3	"	Sn	0.9	15.0	25,750	+12	+ 3.6	64
"	"	Sn	4.4	14.7	25,750	+22	+ 6.6	119
"	"	Te	0.09	15.9	25,750	+15	+ 4.5	80
"	"	Te	0.24	15.9	25,750	+ 5	+ 1.5	27
"	"	Pb	1.0	16.4	24,000	+14.5	+ 5.1	90
"	"	—	—	15.9	24,000	+16	+ 5.55	100
"	"	Te	0.09	15.9	23,450	+10.5	+ 3.8	67
"	"	Sn	0.44	15.9	22,650	+12.5	+ 4.8	86
"	"	Sn	2.4	15.2	21,850	+13.5	+ 5.7	102
"	"	Pb	2.56	16.5	21,750	+14	+ 5.9	104
P_1, 0°	"	Pb	1.0	12.2	21,000	− 6	− 2.8	42
"	"	Pb	2.56	12.8	20,800	+ 5.5	+ 2.5	− 36
"	"	Pb	4.9	13.1	20,400	+15	+ 7.2	−105
P_3	"	Pb	4.9	16.7	20,400	+ 9	+ 4.3	78
"	"	Pb	2.56	16.5	20,400	+11.5	+ 5.5	99

* Expressed in atomic percent, i.e., number of foreign atoms per 100 atoms of bismuth.

** Modulus of magnetostriction expressed in percent of modulus for crystal of same orientation, but without the impurity.

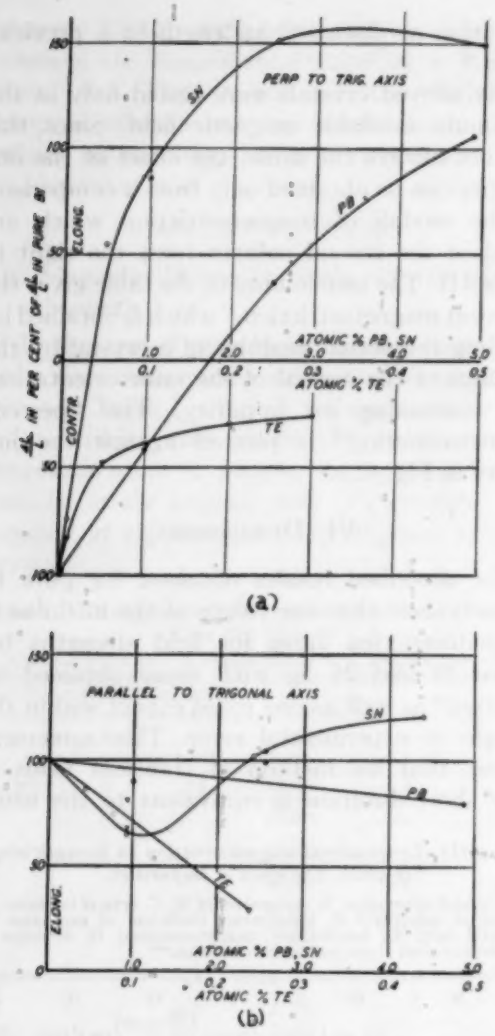

FIG. 9. Diagram showing the magnetostriction of alloyed Bi crystals relative (in percent) to the magnetostriction of pure Bi as function of the concentration of the admixture. Solid circle, *Pb*; circle, *Sn*; triangle, *Te*.

method of permanent fields under isothermal conditions, i.e., that the magnetostriction in a real crystal is an effect which does not involve a time lag larger than 10^{-2} sec.—a fact not necessarily anticipated in view of the structural differences between a real and an ideal crystal.

The only discrepancy between Kapitza's value and ours is the difference in the value of n in Eq. (5), consisting of a larger field dependence of the magnetostriction in the direction perpendicular to the trigonal axis and a smaller parallel to the axis than predicted by the simple thermodynamic theory. To what extent those deviations are real cannot be decided unless a better accuracy of the observations is obtained over a larger field range.

The main interest, however, lies in the results concerning the effect of foreign atoms upon the magnetostrictive qualities of the crystal, especially if they are compared with the effects upon the susceptibility as have been described in detail in a previous paper.[15] *

An examination of Fig. 9 will show that lead and tin exercise a particularly striking influence on magnetostriction *perpendicular* to the trigonal axis (P_1 crystals). About 0.4 percent of tin, or about 2 percent of lead reduced the magnetostriction to zero, and greater amounts of these elements actually reverse the sign of the effect. It should also be pointed out that the curves for lead and tin are identical except for the horizontal scale. It requires almost exactly five times as much lead as tin to change the magnetostriction perpendicular to the trigonal axis by a given amount.

The effect of lead and tin on magnetostriction *parallel* to the trigonal axis (P_3 crystals) (Fig. 9b) is much smaller than in the case of P_1 crystals, and more complicated in character; thus no definite conclusion as to the ratio of the relative effects of the two admixtures can be reached.

The influence of the electronegative admixture Te is very much larger and different in character from that of Pb and Sn since no reversal in the sign of magnetostriction normal to the trigonal axis takes place.

A closer insight into the nature of these phenomena can be obtained by the following consideration: it has been shown before (*Va* Eq. (4)) that the modulus of magnetostriction is equivalent to a change in the susceptibility $(\partial\chi/\partial p)$ (longitudinal) under the elastic deformation produced by the stress (p). If one assumes in analogy to Kapitza's considerations that the application of stress and the change in the rela-

* The great influence of admixtures in small concentrations was already observed by Kapitza when he replaced the pure Bi by a metal, the spectroscopic test of which showed traces of Pb and Ag; Kapitza mentions Kahlbaum as source of this metal which corresponds to our Bi "D", of which an analysis is given previously.[16] The admixtures have the tendency in both principal orientations to decrease the magnetostrictive effect. Our results conducted on a quantitative basis over a much larger range of concentrations confirm this observation.

tive positions of the atoms in the lattice thus caused, does not change the general character of the electron distribution within the lattice, one should expect the stress coefficient (ω') of the susceptibility to be proportional to the susceptibility itself. If the susceptibilities in a certain direction within the crystal without and with stress are χ_0 and χ_p:

$$\chi_p = \chi_0(1+\omega' p) \qquad (6)$$

one obtains the relation:

$$m = \partial\chi/\partial p = \chi_0 \cdot \omega', \quad \text{and} \quad \omega' = m/\chi_0. \qquad (7)$$

This consideration is applicable only if moduli of crystals are compared for which one has reason to assume a similar electron configuration. One such case is the comparison of the same crystals at different temperatures, as attempted by Kapitza;[11] another is the comparison of crystals at the same temperature containing admixtures in different concentrations within the region of solubility. This case seems to be of special interest, since the very large influence of admixtures upon the susceptibility of Bi crystals is known quantitatively.

Fig. 10 represents $\chi_\perp$ and $\chi_{||}$ as function of the (logarithmic) concentration of the admixtures used in this investigation for room temperature.*

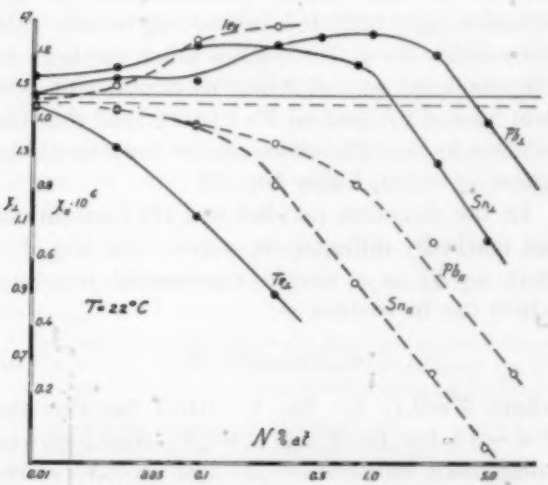

FIG. 10. $\chi(N)$ diagram for $T=22°C$.[18] The abscissa is on a logarithmic scale (0.01 percent at. to 10 percent at.); the ordinate has two scales: the left refers to $\chi_\perp$ (full drawn curves, solid circle), the right refers to $\chi_{||}$ (dashed curves, circle) respectively. The horizontal lines represent the values of $\chi_\perp$ and $\chi_{||}$ for pure crystals.

TABLE IV.

Metal	Orient	% at	χ (10^6)	χ_r	m (10^{16})	m_r	$m_r/\chi_r=\omega$
Bi	⊥	0.0	1.48	100	− 7.0	100	1.00
Bi+Te	⊥	0.01	1.48	99.8	− 5.7	83	0.835
"		0.05	1.23	83.2	− 3.3	48	0.577
"		0.1	1.12	75.5	− 2.9	40	0.53
"		0.2	0.96	65.0	− 2.1	29	0.45
"		0.3	0.87	59.0	− 1.9	26	0.442
Bi+Sn	⊥	0.1	1.66	112	− 5.1	75	0.67
"		0.5	1.60	108	+ 3.6	− 53	−0.49
"		1.0	1.55	104.5	+ 5.7	− 84	−0.80
"		2.5	1.28	86.5	+10.3	−151	−1.75
"		5.0	1.06	71.5	+10.1	−149	−2.08*
Bi+Pb	⊥	1.0	1.66	112	− 2.8	42	0.375
"		2.56	1.60	108	+ 2.5	− 36	−0.33
"		4.9	1.35	91.0	+ 7.2	−105	−1.15**
Bi	||	0.0	1.05	100	+ 5.7	100	1.00
Bi+Te	||	0.09	1.24	118	+ 3.8	67	.568
"		0.09	1.24	118	+ 4.5	80	0.677
"		0.24	1.26	120	+ 1.5	27	0.225
Bi+Sn	||	0.44	0.75	71.2	+ 4.8	86	1.20
"		0.9	0.50	47.5	+ 3.6	64	1.35
"		2.4	0.38	36	+ 5.7	102	2.84
"		4.4	0.08	24	+ 6.6	119	5.0*
Bi+Pb	||	1.0	0.97	86	+ 5.1	90	1.05
"		2.56	0.65	62	+ 5.5	99	1.6
"		4.9	0.36	34	+ 4.3	78	2.3**

* Interpolated from crystal (224/21[10]).
** Extrapolated for 1.63% Sn[10] = 4.9% Pb.

If the suffix (p) refers to the pure crystal and the suffix (r) indicates the relative value, the following definitions can be chosen:

$$\chi_r = \chi/\chi_p; \quad m_r = m/m_p; \quad \omega = m_r/\chi_p;$$

$$\omega = \omega' \cdot \chi_p/m_p. \qquad (9)$$

Table IV represents the numerical values of χ, χ_r, m, m_r, and ω, taken from Table III and from interpolations of Fig. 10. The functions $\omega_\perp(N)$ and $\omega_{||}(N)$ are given in Figs. 11a and 11b, respectively, in full drawn lines and solid circle, for comparison the values for $m_r(N)$ are added

* The similarity in the effect of Pb and Sn is obvious, as is the difference of the effect in different orientations: for small concentrations ($<N_0$) $\chi_\perp$ is increased, for large concentrations ($>N_0$) it is decreased. The values of N_0 are: for Pb 3.75 percent (at.), for Sn 1.24 percent (at.), in quantative agreement to previous findings (Goetz and Focke) that the effect of Pb is one-third of that of Sn (since $N_{0\,Pb}/N_{0\,Sn}=3.0_3$.

In contradistinction to $\chi_\perp$, $\chi_{||}$ is *only* decreased by Pb and Sn; for higher concentrations $d\chi/dN^{16}$ is the *same* in both orientations for Pb and Sn. This part of $\chi(N)$ can be described by:

$$\chi_{||} \sim \chi_\perp \sim \ln\,[N_0/N^b] \cdots (b=1.32) \qquad (8)$$

where N_0 is the concentration for which $\chi_r=100$ and $N\neq 0$.

The electronegative admixture Te increases $\chi_{||}$ and decreases $\chi_\perp$, i.e., it affects the crystal qualitatively in the opposite way than Sn and Pb.

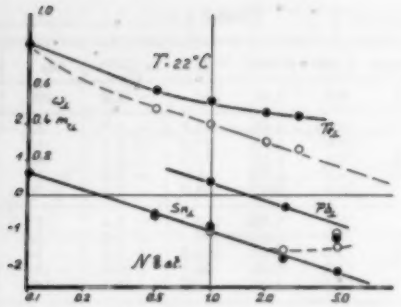

FIG. 11a. $\omega_\perp(N)$ diagram. The ordinate is on a linear scale; the left numbers refer to Pb and Sn, the right to Te. The abscissa is on a logarithmic scale (0.1 percent at. to 10 percent at.). For comparison the values of $m_{r\perp}(N)$ (Table IV) are added in dashed lines and circles. The numerical values of the ordinate have to be multiplied by 100 to obtain the values of $m_{r\perp}$.

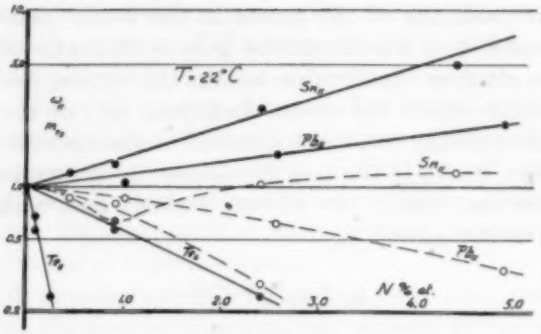

FIG. 11b. $\omega_{||}(N)$ diagram. The ordinate is on a logarithmic, the abscissa on a linear scale (0 percent to 5 percent at.). For comparison, the values of $m_{r||}(N)$ (Table IV) are added in dashed lines and circles. The numerical values of the ordinate have to be multiplied by 100 to obtain the values of $m_{r||}$. In order to show the linearity for Te, the values are plotted twice: once on the regular scale, solid circle, and once on a ten-fold N-scale, cross circle.

in dashed lines and circle. For the direction normal to [111] the electropositive admixtures follow definitely a function of the form:

$$\omega_\perp = C - \delta \ln N = \ln [N_0/N^\delta] \qquad (10)$$

where δ is the same for Pb and Sn ($\delta = 1.4 \pm 0.3$) and N_0 equals 0.25 percent at. for Sn and 1.60 percent at. for Pb.

The analogy between $\chi_\perp(N)$ for higher concentrations (Eq. (8)) and $\omega_\perp(N)$ (Eq. 10)) is obvious; both functions are the same and within the limits of experimental error b equals δ. The differentiation of Eq. (8) and Eq. (10) results accordingly in:

$$d_\perp\chi/dN = -b/N; \quad d\omega_\perp/dN = -\delta/N;$$

$$dm_\perp/dN = -\chi_{0\perp} \cdot m_p \cdot \delta/\chi_p \cdot N \qquad (11)$$

and

$$d\omega_\perp/d\chi_\perp = \delta/b = \text{const.} \sim 1. \qquad (11a)$$

Hence: *the change of the stress coefficient of the susceptibility with the concentration of foreign atoms is inversely proportional to the concentration;* furthermore: *the variation of the stress coefficient with the concentration is nearly equal to the variation of the susceptibility at higher concentrations,* or: *the stress coefficient of the susceptibility is proportional to the susceptibility itself.**

* This relation is proved quantitatively by the validity of:

$$\chi_1 + \omega_1\left[\frac{\chi_2-\chi_1}{\omega_1-\omega_2}\right] = C_{12} = \chi_2 + \omega_2\left[\frac{\chi_3-\chi_2}{\omega_2-\omega_3}\right] = C_{23}$$

$$= \chi_3 + \omega_3\left[\frac{\omega_1-\omega_2}{\chi_3-\chi_1}\right] = C_{31}, \text{ etc.} \qquad (12)$$

where χ and ω refer only to $\perp$[111] and where the indices mean corresponding values of χ and ω (Table IV) for Pb *and* Sn. The variation among the values of C_{nm} thus obtained is ≤ 5 percent.

The comparison of $m_{r\perp}(N)$ and $\omega_\perp(N)$ in Fig. 11a shows that the function in Eq. (10) does not hold as well for the former as for the latter. (See footnote to page 1105.)

The validity of the function is limited to large concentrations of admixtures for $\chi_\perp(N)$ and probably also for $\omega_\perp(N)$ if measurements for sufficiently small concentrations were available. For $\chi_\perp(N)$ the relation ceases to be valid below 0.9 percent Sn and 2.7 percent Pb (Fig. 10), i.e., in the region where the admixtures cause an increase of the crystal diamagnetism in one direction ($\chi_\perp > 100$). It is interesting to note that the validity for $\chi_\perp(N)$ reaches much further—to the smallest concentrations measured (0.1 percent Sn and 1.0 percent Pb.) It is trivial that the relation in Eq. (12) holds only for concentrations where $\chi_\perp$ *and* $\omega_\perp$ follow Eq. (11).

In the direction parallel to [111] conditions are markedly different: it is seen from Fig. 11b that $\omega_{||}(N)$ is a simple exponential function, which can be written as:

$$\omega_{||} = \omega_{p||}(1 + N^{\delta'}) \qquad (13)$$

where $\delta' = 0.17$ for Sn; $\delta' = 0.072$ for Pb; and $\delta' = -3.4$ for Te ($\delta'_{Sn}/\delta'_{Pb} = 2.4$). Also here the comparison between $\omega_{||}(N)$ and $m_{r||}(N)$ shows that the simple exponential relation does definitely *not* hold for the former, e.g., the minimum

at $Sn_{||}=0.9$ percent for $m_{r||}$ disappears for $\omega_{||}$.*

If there is a relation between $\chi_{||}(N)$ and $\omega_{||}(N)$ it is not a simple one. As is seen from Fig. 11 the $\chi_{||}(N)$ relation (Eq. (8)) holds for $N_{Sn} \geq 0.3$ percent; $N_{Pb} \geq 1$ percent (i.e., approximately one-third of the corresponding concentration of $\chi_{\perp}$), whereas $\omega_{||}(N)$ follows a simple function (Eq. (13)) for all concentrations.

The most marked result is the fact that the electropositive admixtures affect the crystal differently in different directions. The difference consists in the fact that parallel to [111] $\omega_{||}(N)$ is the same function beginning at the smallest concentration, whereas $\omega_{\perp}(N)$ shows a threshold for small concentrations $[\omega_{\perp}(N)]_{I}$ and for large concentrations $[\omega_{\perp}(N)]_{II}$. This can be interpreted that the disturbance of the electron configuration by the foreign atom is changed in character with increasing concentration.

Assuming the Ehrenfest-Raman[21, 22, 23] theory about the electron mechanism of crystal diamagnetism and the hypothesis by Goetz and Focke[15] concerning the process of electron scattering caused by foreign atoms dissolved in the lattice, the insertion of electropositive admixtures below the "critical concentration" follows approximately equidistant sets of planes with a large component parallel to [111], e.g., $(11\bar{1})$ or (110). Thus scattering walls in certain directions throughout the crystal are produced which affect the electromagnetic qualities accordingly. As long as N is small enough to saturate only such planes, only one direction in the crystal is affected. If, however, N is larger—so that the foreign atoms spread statistically over the whole volume of the crystal—the effect becomes similar in all directions.

The results of this investigation prove to be in good agreement with those conclusions, since the function of $\omega_{||}(N)$ for Pb and Sn is continuous, whereas there exist two forms for $\omega_{\perp}(N)$.* The validity of $[\omega_{\perp}(N)]_{I}$ is thus restricted to the region of selective adsorption of foreign atoms, whereas $[\omega_{\perp}(N)]_{II}$ holds for the region of volume absorption. At present our data for m are not sufficient to give a quantitative evaluation of $[\omega_{\perp}(N)]_{I}$ except for the fact that $\delta > 0$.

The agreement with the electropositive admixture Te in the sense of this hypothesis is much less satisfactory, probably due to the incomensurability of the solution Bi+Sn (or Pb) and $Bi+Bi_2Te_3$.

Generally speaking, there are two handicaps which so far prevent a closer insight into the relation between crystal diamagnetism and magnetostriction: first, the absence of measurements of N at temperatures low enough to render the determination of N_e sufficiently exact; second, the indeterminacy of N in the solid crystal, about which subject a detailed investigation will be published soon from our laboratory.

Nevertheless, the present results support sufficiently the assumption that the effect of Sn and Pb in Bi in the region of selective adsorption ($<N_e$) is characterized by a disturbance of the electron configuration parallel to the principal axis, and in the region of volume absorption ($>N_e$) by a uniform disturbance which does not change any more the character of the electron lattice. Accordingly, the latter concentrations only show a proportionality between the coefficient of stress and the susceptibility. Thus the existence of the two types of insertion of foreign atoms in the crystal lattice seems to find another support.

In conclusion the authors wish to express their sincere obligation to Dr. W. S. Adams, Director of the Mt. Wilson Observatory and to Dr. A. S. King for the permission to use the solenoid, and their sincere thanks to Dr. A. B. Focke and Mr. J. H. Darlington for their help in preparing most of the crystals in this work.

* The probability that this be caused by a faulty crystal is minimized by the fact that an entirely different set of crystals was used for the determination of $\chi_{||}(P_1)$ (Gouy method) and $m_{||}$ (P_3).

[21] P. Ehrenfest, Physica **5**, 388 (1925).
[22] P. Ehrenfest, Zeits. f. Physik **58**, 719 (1929).
[23] C. V. Raman, Nature **123**, 945; **124**, 412 (1929).

* For a detailed discussion of these directional relations reference is made to[15] Chapter 7.

LETTERS TO THE EDITOR

Prompt publication of brief reports of important discoveries in physics may be secured by addressing them to this department. Closing dates for this department are, for the first issue of the month, the twentieth of the preceding month; for the second issue, the fifth of the month. The Board of Editors does not hold itself responsible for the opinions expressed by the correspondents.

Discontinuities of Magnetoresistance

In a recent paper[1] the writer has described experiments in which sudden jumps of resistance were found to be associated with jumps of magnetization in a strained nickel wire. Alocco and Drigo[2] have studied the magnetoresistance of nickel and observed apparent discontinuities which they found were due to disturbance of bridge balance arising from induced electromotive forces. They suggest that the writer's results may be similarly explained.

As a matter of fact the writer was well aware of the source of error mentioned by Alocco and Drigo, having previously performed experiments on the phenomenon.[3] Hence special precautions were taken to eliminate the spurious effect. When the balance of the bridge was disturbed by the resistance jump, the galvanometer suffered a permanent deflection of about 200 mm, superposed on a steady drift, due to temperature changes, of about 4 mm per minute. Any induced e.m.f. would, of course, have thrown the bridge out of balance only temporarily. The period of the galvanometer used was sufficiently short and the temperature drift was sufficiently small so that the bridge could be rebalanced by adjustment of resistance arms, and the resistance jump calculated in this way. In the interests of accuracy, however, a method involving the reading of galvanometer deflections was actually used.

It seems probable that Alocco in his work[4] did not find discontinuities of magnetoresistance because his specimens did not exhibit sufficiently large jumps. His hysteresis loop for nickel is quite like the writer's, but he has indicated observed points on the steep branch where the writer was unable to obtain them because of the large discontinuity.

C. W. HEAPS

The Rice Institute,
November 18, 1934.

[1] C. W. Heaps, Phys. Rev. **45**, 320 (1934).
[2] G. Alocco and A. Drigo, N. Cimento **11**, 224 (1934).
[3] C. W. Heaps, Phys. Rev. **43**, 945 (1933).
[4] G. Alocco, N. Cimento **10**, 153 (1933).

An Equation for X-Ray Crystal Curves

Parratt[1] has found that the shapes of all $(1, -1)$ curves of calcite and quartz are symmetrical and fall between the Gaussian error function and the classical dispersion shape revived by Hoyt.[2] Both of these curves may be expressed in the form $1/y=1+Bx^2+Cx^4+\cdots$, where $y=1$ when $x=0$ and $y=1/2$ when $x=1$. In the case of the classical dispersion shape, which is a witch, $B=1$, the remaining constants being zero. A closer approximation may be had by evaluating one more constant, C. The half maximum condition gives $B=C-1$. The curve may be made to pass through a third point x, by properly choosing C. Let the value of $1/y$ at x be z. Then the solutions of B and C are

$$B=(x^4+1-z)/(x^4-x^2), \qquad C=(z-x^2-1)/(x^4-x^2).$$

Fig. 1 shows a family of curves of the form of $1/y=1+(1-C)x^2+Cx^4$. A comparison of these curves with Figs. 5 and 6 in Parratt's[1] paper will show a remarkable resemblance (most crystal curves using values of C between 0 and 1/4).

There is need to check the equation for larger values of x. The writer used data on calcite crystal pair No. 2,[3] which

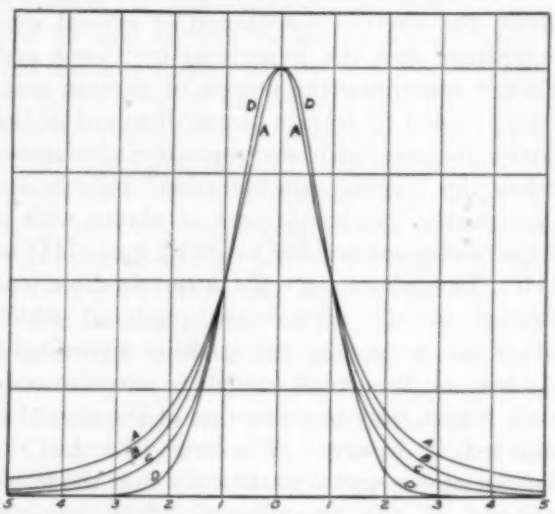

FIG. 1. Curves A, B and C of form $1/y=1+(1-C)x^2+Cx^4$ with C equal 0, 1/12 and 1/4. Curve A shows the classical dispersion shape and curve D the Gaussian error function.

gave a full width at half maximum of 5.2 seconds at $\lambda=0.71$A. The value of C at $x=2$ was 0.1 but was zero from $x=4$ to $x=12$.

An interesting case of a variable C is where a cracked crystal has two planes each represented by a witch but displaced $\pm\alpha$. The average of the two witches will have a maximum ordinate equal to $1/(1+\alpha^2)$ while the other ordinates will be little effected. The drop in the maximum forces the adoption of a greater half maximum width, which gives a finite value for C for small values of x, but reduces to zero for large values of x.

The writer has checked mathematically the rule that if the shapes of both crystals and x-ray lines are witches, the

width of the experimental curve should be the sum of the two widths. Therefore, the failure of this rule[4] must be linked with the failure of the original curves to be witches. The exact law of correction, then, should depend on the departure from the witch and hence on the constant G. This should be determined by using moderate values of x, as the effect on the width is negligible for large values of x.

ROY C. SPENCER

Brace Laboratory of Physics,
University of Nebraska,
November 20, 1934.

[1] Parratt, Rev. Sci. Inst. **5**, 395 (1934).
[2] Hoyt, Phys. Rev. **40**, 477 (1932).
[3] Spencer, Phys. Rev. **38**, 630 (1931).
[4] Parratt, Phys. Rev. **46**, 749 (1934).

Rectifying Effect in Chrome Cast Iron

I recently noted an apparent rectifying effect in chrome cast iron similar to that of the "Kuprox" rectifiers.

In melting the metal, which contained about 14 percent chromum and 2 percent carbon, it was made the anode in a 220 volt d.c. arc furnace; a graphite rod serving as cathode. When fusion was nearly complete, current was accidentally shut off and the metal cooled. Its surface was badly oxidised as a result of opening the furnace while still hot.

On attempting to start the arc again it was found that no current would pass. But after reversing the polarity so that the metal became the cathode, current readily passed, an arc was struck and the metal was heated to seven or eight hundred degrees in this manner. It was then found that current would again pass in the original direction.

The metal was contained in a magnesia-lined bowl through the bottom of which a steel bar extended, serving as conductor. The cathode extended vertically downward through a hole in the cover.

I have seen no notice of such a rectifying effect in chrome cast iron; which effect seems rather strange in view of the fact that the black iron oxide which is formed on hot iron is a conductor even when cold. The effect seems to have been due to the presence of the chromium, whose oxide (Cr_2O_3) does not conduct until heated to a temperature in excess of one thousand degrees. On the other hand I have noticed that some chromium-iron ores which are relatively rich in iron conduct very readily when cold. Time was not available in which to investigate this phenomenon further.

LEO G. HALL

Spalding Machinery Company,
Chicago, Illinois,
November 24, 1934.

Gamma-Rays from Boron Bombarded with Deutons

Using a Wilson cloud chamber in a magnetic field of 1000 gauss we have studied the spectrum of recoil electrons produced by the gamma-rays from boron bombarded with deutons, and have found it to consist of components of at least five different energies.

A total of 6500 photographs was obtained, of which 1500 were taken with a carbon sheet 1 mm thick across the center of the chamber, 4000 with a 0.25 mm lead sheet, and 1000 with a 3 mm lead sheet. Where the thin absorber was used, it was possible to identify the tracks of recoil electrons and electron pairs which originated in the thin material. Below are shown the energy spectra of the electrons from the thin carbon absorber (Fig. 1), and of those ejected in the forward direction from the glass walls of the chamber (Fig. 2).

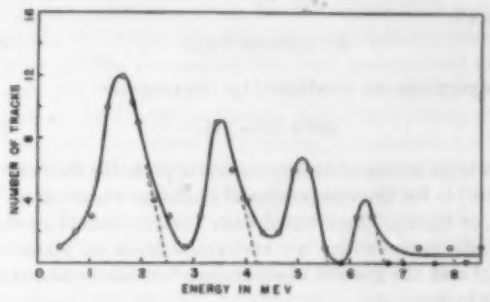

FIG. 1. Energy spectrum of negative electrons ejected from a 1 mm carbon absorber by the gamma-radiation from boron bombarded with deutons. Ordinates represent the number of tracks in a 0.3 m.e.v. energy interval.

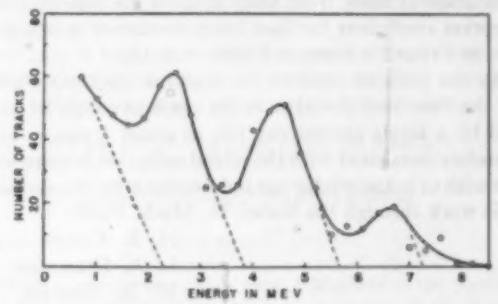

FIG. 2. Energy spectrum of negative electrons ejected from the glass wall of the chamber by the gamma-radiation from boron bombarded with deutons. Ordinates represent the number of tracks in a 0.3 m.e.v. energy interval.

The spectrum in Fig. 1 indicates gamma-ray lines of roughly 2, 4, 5.5 and 7 m.e.v., the intercepts of the curves extrapolated down to the axis being 2.4, 4.2, 5.6 and 6.7 m.e.v., and in addition an appreciable number of tracks of higher energy, extending up to more than 10 m.e.v. The spectrum from the thick glass absorber (Fig. 2) indicates the same lines, and is less subject to statistical fluctuation, since it is composed of a larger number of tracks. It gives intercepts at 2.3, 3.9, 5.6 and 7.2 m.e.v. Here, however, the 2 and 4 m.e.v. lines are not so clearly resolved, and the extrapolation of the 2 m.e.v. line down to the axis obviously cannot be accurate. The presence of four lines of approximately the above energies is further confirmed by the spectra of electrons and of electron pairs from the lead absorbers, the plots of which are not shown. Tracks of very high energy appeared relatively more frequently when the lead absorber was used, and a number of pairs were found having total energies as high as 10 m.e.v.

The 2, 4 and 7 m.e.v. lines can be correlated with differences in energy of proton groups observed by Cockroft and Walton,[1] which indicate lines at 2.2, 4.5 and 6.8 m.e.v. The reaction producing the protons, and hence also these gamma-ray lines is probably

$$B^{10}+H^2 \rightarrow B^{11}+H^1. \quad (1)$$

The 5.5 m.e.v. line has been found associated with the formation of C^{13} in the case of beryllium bombarded with alpha-particles,[2] and therefore it seems reasonable to ascribe it also in this case to the reaction in which C^{12} is produced:

$$B^{11}+H^2 \rightarrow C^{12}+n^1. \quad (2)$$

Alpha-particles are produced, by the reaction

$$B^{10}+H^2 \rightarrow 3\ He^4 \quad (3)$$

with a large excess of energy, and it is probable that this is responsible for the component of radiation observed at 10 m.e.v. or higher. There has already been an indication that the alpha-particle has an excitation level at about 12 m.e.v.,[3] and the present observations furnish confirmation of this hypothesis.

The absorption coefficient in lead which we previously determined for the gamma-radiation from boron bombarded with deutons[4] is entirely consistent with the above combination of lines, if we keep in mind the fact that the absorption coefficient for lead has a minimum at about 3 m.e.v. and rises for energies higher than this.[5]

Also the ratio of positive to negative electrons (0.05) from the thin lead absorber is the same as would be produced by a single gamma-ray line of about 5 m.e.v., and is therefore consistent with the mixed radiation in question.

We wish to acknowledge our indebtedness for the support of this work through the Seeley W. Mudd Fund.

H. R. Crane
L. A. Delsasso
W. A. Fowler
C. C. Lauritsen

Kellogg Radiation Laboratory,
California Institute of Technology,
December 1, 1934.

[1] Cockroft and Walton, Proc. Roy. Soc. **A144**, 704 (1934).
[2] Becker and Bothe, Zeits. f. Physik **76**, 421 (1932).
[3] Lauritsen and Crane, Phys. Rev. **46**, 537 (1934).
[4] Lauritsen and Crane, Phys. Rev. **45**, 493 (1934).
[5] Crane, Delsasso, Fowler and Lauritsen, Phys. Rev. **46**, 531 (1934).

Capture of Charged Particles by Nuclei Due to Emission of Gamma-Radiation

According to the experiments of Lea[1, 2] and more definitely according to Chadwick and Goldhaber[3] a proton and a neutron may unite to form a deuton emitting a γ-ray in the process. It appears probable that a nucleus and a proton may unite also in other cases, and that the excess energy may be emitted as γ-radiation. Thus, the formation of N^{13} by proton bombardment of C may perhaps be due to the reaction $C^{12}+H^1 \rightarrow N^{13}+\gamma$. We calculated the probability of such processes, and we can account without difficulty for collision cross sections of the order of 10^{-29} cm^2 and higher for 500 kv protons supposedly captured by C with the emission of approximately 7×10^6 e.v. γ-rays. We discuss first an approximate formula for the effective collision cross section σ at a given velocity v of the protons

$$\sigma = 5.08(c/v)(1+\eta^2)(R^6/\lambda^3\Lambda^2)P^2\cdot\pi R^2\xi/(e^\xi-1). \quad (1)$$

Here

$$P = 1+(5/12)\kappa R\eta+(1/14)(\kappa R\eta)^2(1-1/\eta^2) + (1/144)(\kappa R\eta)^3(1-7/2\eta^2)+\cdots,$$

$$\eta = Zc/\text{“}137\text{”}v, \quad \xi = 2\pi\eta, \quad \kappa = 2\pi/\Lambda, \quad \Lambda = h/mv.$$

λ = wave-length of γ-rays, Λ = wave-length of incident protons, R = nuclear radius. This formula is rough, but is often useful in estimating σ. Two approximations are involved in its derivation: (1) that of neglecting the effect of the nuclear potential well on the wave function of the proton before capture, (2) that of taking the wave function of the proton after capture to be constant through a sphere of radius R and zero outside that sphere. The values of σ obtained from this formula for 520 kv protons incident on carbon for $h\nu = 14mc^2 \leqq 7\times10^6$ e.v. are:

σ(cm^2)
$= 1.3\times10^{-28}$ 2.2×10^{-29} 2.3×10^{-30} 1.0×10^{-31} 6.1×10^{-34}

for R(cm)
$= 1.0\times10^{-13}$ 0.8×10^{-13} 0.6×10^{-13} 0.4×10^{-13} 0.2×10^{-13}.

The dependence on v is primarily determined by $e^{-\xi}$. The mean collision cross section for solid targets is

$$\bar{\sigma} = v^{-2}\int_0^v 3\sigma(v)v^2dv.$$

For $R = 0.4\times10^{-13}$ cm. The ratio $\bar{\sigma}/\sigma$ has the approximate values 0.26 at 1020 kv and 0.34 at 520 kv.

The above formula is simple but not accurate. Without approximations except those inherent to a central field treatment one finds for the dipole radiation due to a transition to a captured s state:

$$\sigma = 3.36\frac{c}{v}\frac{1+\eta^2}{(\kappa\lambda)^3}\frac{\xi}{e^\xi-1}\cdot\frac{1}{\kappa^3}\left|\int_0^\infty \rho\Psi(\rho)\bar{f}_1(\rho)d\rho\right|^2, \quad (2)$$

where Ψ represents the captured state, $\rho = \kappa r$, $\int\Psi^2(\rho)d\rho = 1$ and $\bar{f}_1$ is the function which replaces the regular power series solution in a Coulomb field beginning with ρ^2 for $l=1$. If the well is absent $\bar{f}\rightarrow f = \rho^2(1+\cdots)$. The ratio $|\bar{f}/f|^2$ at boundary of well is $[(1-FG\delta)^2+F^4\delta^2]^{-1}_{r=R}$, where F, G are, respectively, the regular and irregular radial functions asymptotic at ∞ to sin $(\rho+\epsilon)$, cos $(\rho+\epsilon)$. The quantity $\delta = (F'/F-\bar{f}'/\bar{f})$.

Formula (2) gives larger values of σ than Eq. (1). Thus for a well with a depth of about 20×10^6 e.v. and a radius $R = 0.33\times10^{-13}$ cm the approximate values of σ are as follows:

Energy (kv)	900	730	580	440
$\sigma(10^{-30}$ cm$^2)$	3.9	2.7	1.7	0.94

The more accurate Eq. (2) gives a less rapid decrease of the

probability with decreasing velocity and thus $\bar{\sigma}/\sigma$ is somewhat larger than for Eq. (1).

A yield of 500 disintegrations per 2 microamperes at 900 kv corresponds to $\bar{\sigma}=2.8\times10^{-31}$ cm². There appears thus to be no difficulty in accounting for either the Cambridge[4] or the Pasadena[5] results on C on the basis of γ-radiation. Since the γ-radiation itself has not been detected and since the alternative explanation of Lauritsen and Crane $C^{13}+H^1\rightarrow N^{13}+n$ appears to be also possible we do not attempt to draw a definite conclusion as to the way in which N^{13} is formed.

Hafstad and Tuve[6] found a very intense induced radioactivity when C was bombarded by deutons at 1000 kilovolts but were able to show that the effect with protons at the same voltage (using magnetic analysis of the beam) was less than 1/8000 of the deuton effect. They have recently informed us[7] that preliminary observations using more intense proton beams indicate a real proton effect of 1/7000 to 1/14,000 of the deuton effect at 900 kilovolts, and estimate that a 2 microampere beam of protons at 900 kilovolts gives rise to an equilibrium emission of roughly 1000 positrons per second in the total solid angle 4π. There is thus qualitative agreement as to order of magnitude of the effect between the three groups of experimenters.

We made use above of some unpublished calculations of Dr. John A. Wheeler giving F and G in tabular form, and we are very much indebted to him for making these tables available to us. We are also very grateful to G. Gamow, M. A. Tuve and L. R. Hafstad for a discussion of the theoretical and experimental evidence for $C+H^1\rightarrow N^{13}$.

G. Breit and F. L. Yost

Physical Laboratory,
University of Wisconsin,
December 3, 1934.

[1] D. E. Lea, Nature **133**, 24 (1934).
[2] H. S. W. Massey and C. B. O. Mohr, Nature **133**, 211 (1934). Calculations of the probability of the effect observed by Lea are reported, and it is concluded that it is improbable that the effect is due to γ-ray emission.
[3] J. Chadwick and M. Goldhaber, Nature **134**, 237 (1934). Calculations of Bethe and Peierls are quoted here. These account for the photon emission of Chadwick and Goldhaber but do not account for the large capture effect observed by Lea.
[4] J. D. Cockroft, C. W. Gilbert and E. T. S. Walton, Nature **133**, 328 (1934).
[5] H. R. Crane and C. C. Lauritsen, Phys. Rev. **45**, 497 (1934). Cf. also H. R. Crane and C. C. Lauritsen, Phys. Rev. **45**, 430 (1934); and C. C. Lauritsen and H. R. Crane, Phys. Rev. **45**, 345 (1934).
[6] L. R. Hafstad and M. A. Tuve, Phys. Rev. **45**, 902 (1934).
[7] Reported in the discussion at the Inter. Conf. on Physics, London, Oct., 1934.

A Criticism of Dr. L. G. H. Huxley's Theory of the Origin of Cosmic Rays

In a recent paper, L. G. H. Huxley[1] has developed in detail a theory of the origin of cosmic rays in which the rays are treated as charged particles, distributed uniformly at infinity and starting with negligible velocity, which move in the field of an earth which is a uniformly magnetized sphere carrying an electric charge opposite in sign to the charge of the particles. The suggestion of a charged Earth attracting the particles, and thus accounting for their huge energies, has been previously put forward by Johnson.[2] Apart from difficulties of a general nature such as are suggested by Huxley himself which this theory would have to meet, it appears to the writer that Huxley's analysis is incorrect, and the object of this note is to point out this fact.

Taking, with Huxley, polar coordinates (r, θ, ϕ) at the Earth's center, with the polar axis the Earth's magnetic axis, and employing special relativity dynamics, the velocity v of the particle and the azimuthal velocity ϕ are easily expressed as functions of r only by means of well-known integrals of the equations of motion. The assumption is then made that *at the Earth's surface the component of velocity $r\dot{\theta}$ is negligibly small compared with the other two components.* The expressions for v and $\dot{\phi}$ mentioned above then enable the velocity and direction of motion of the particle at the Earth's surface to be found in terms of the latitude and the constants defining the particle and the Earth. Most of Huxley's results relating to intensity of the radiation, etc., depend on the above assumption. Concerning this, Huxley merely says (Reference 1, p. 977): "as, however, the particles approach the Earth radially over the greater part of their orbits, it is evident that $\dot{r}\ll r\dot{\theta}$ throughout the motion."[3] However, this hardly seems enough; certainly the *initial* motion is radial, but the action of the magnetic field will gradually impart θ- and ϕ-components to the velocity, and there does not seem to be any evident reason why the former should be negligible compared with the latter.

We can, in fact, show that the assumption is in general wrong in the following manner: the complete equations (after elimination of $\dot{\phi}$) can be reduced to the form

$$\dot{r}^2+r^2\dot{\theta}^2=c^2[1-(m_0/m)^2]-(e\mu\sin\theta/cr^2m)^2, \tag{1}$$

$$d(mr^2\dot{\theta})/dt=-e^2\mu^2\sin\theta\cos\theta/c^2r^4m, \tag{2}$$

where
$$m=m_0+eQ/c^2r, \tag{3}$$

in which e, m_0 are the charge and rest-mass of the particle, and Q, μ the charge and magnetic moment of the Earth. These equations are given implicitly by Huxley.

We further assume, with Huxley,

$$|Q|>|\mu|/a\ll m_0c^2a/|e|, \tag{4}$$

where a is the Earth's radius; the first part of (4) is necessary for particles to reach the magnetic equator, and the second part is true for electrons or (less so) for protons. We now integrate (1) and (2) approximately under the assumption $r\dot{\theta}\ll\dot{r}$. We may then neglect $\dot{\theta}$ in (1). Then writing $d/dt=\dot{r}d/dr$ in (2) and substituting for $\dot{r}$ from (1), we obtain

$$d(mr^2\dot{\theta})/dt=-(e^2\mu^2\sin\theta\cos\theta/cr^2)\times[e^2Q^2r^2+2m_0c^2eQr^3-e^2\mu^2\sin^2\theta]^{-\frac{1}{2}}. \tag{5}$$

Denoting by a suffix E the value of a quantity taken at the Earth's surface $(r=a)$, $(mr^2\dot{\theta})_E$ is then given by integrating the righthand side of (5) with respect to r from ∞ to a. In this integration, θ may be given an approximately constant mean value because of our assumption $r\dot{\theta}\ll\dot{r}$, and further (4) shows that the second term in the square root

can be treated as negligible compared with the first. Thus

$$(mr^2\dot{\theta})_E \sim -(e^2\mu^2 \sin\theta\cos\theta/cQ)\int_\infty^{r_0} r^{-3}(r^2-\mu^2\sin^2\theta/Q^2)^{-\frac{1}{2}}dr$$
$$= (1/c)eQ\cot\theta[1-(1-\mu^2\sin^2\theta/Q^2a^2)^{\frac{1}{2}}]$$

or, from (3) and (4),

$$(r\dot{\theta})_E \sim c\cot\theta[1-(1-\mu^2\sin^2\theta/Q^2a^2)^{\frac{1}{2}}].$$

On the other hand, from (1)

$$\dot{r}_E \sim c[1-(\mu\sin\theta/Qa)^2],$$

so that $(r\dot{\theta}/\dot{r})_E \sim \cot\theta[(1-\mu^2\sin^2\theta/Q^2a^2)^{-\frac{1}{2}}-1]$.

Thus the assumption $(r\dot{\theta})_E \ll \dot{r}_E$ is only justifiable provided we make the further assumption $|Q| \gg |\mu|/a$, or if θ is near 0 or π or $\pi/2$, i.e., in the neighborhood of the magnetic poles or magnetic equator.[4] The assumption $|Q| \gg |\mu|/a$ would, however, as Huxley has shown, result in the intensity of the radiation not varying appreciably with latitude, and is therefore to be rejected. ($|Q| = |\mu|/a$ corresponds to an Earth-potential of about 6×10^{10} volts, and the value adopted by Huxley as most probable is about 7 or 8×10^{10} volts.)

It thus appears that Huxley's analysis is based on an over-simplification of the problem considered by him, and that consequently his results are not reliable, for the directions of motion of the particles at intermediate latitudes, and consequently their relative intensity there, and the minimum energies with which they can arrive, will require corrections of an unknown amount due to the non-smallness of $r\dot{\theta}$ there. It is not maintained, of course, that the hypothesis of a charged Earth is ruled out, but that Huxley's theory based on it is inadequate. In one respect, the theory is improved by the above criticism; for according to Huxley the rays should all arrive at the Earth approximately in the East-West vertical plane at any point (the direction depending on the sign of e), contrary to observation. This fact alone would seem to rule out Huxley's original form of the theory. This difficulty still seems to remain at the equator, however (but see note (4)).

Incidentally, it would appear that the somewhat obscure theory of Lemaitre and Vallarta[5] which assumes a magnetised but uncharged Earth with a homogeneous and isotropic distribution of particle-velocities at infinity, is also an oversimplification of the problem, as shown by Störmer's detailed criticism,[6] and that consequently their results also are untrustworthy.

A. F. Stevenson

Department of Applied Mathematics,
University of Toronto,
December 3, 1934.

[1] L. G. H. Huxley, Phil. Mag. **18**, 971 (1934); also Nature **134**, 418, 571 (1934).

[2] T. H. Johnson, Phys. Rev. **45**, 569 (1934).

[3] Huxley then attempts to show that $r\dot{\theta} \ll r\sin\theta\dot{\phi}$ at the Earth's surface follows from this, but there is an obvious slip in one of his equations which invalidates his argument. However, since $r\sin\theta\dot{\phi}$ and v have been shown to be of the same order of magnitude at the Earth's surface, this would follow automatically from the assumption $r\dot{\theta} \ll v$, were this true.

[4] The "θ" here is, however, a kind of mean value, so that this last conclusion is only valid provided it can be shown that particles which arrive at the equator (or poles) have necessarily started in the equatorial plane (or on the polar axis). This is evidently assumed by Huxley, but seems to require justification.

[5] Lemaitre and Vallarta, Phys. Rev. **43**, 87 (1933); Vallarta, ibid. **44**, 1 (1933).

[6] Störmer, Phys. Rev. **45**, 835 (1934).

Author Index to Volume 46

References with (A) are to abstracts of papers presented at meetings of the Physical Society. References with (L) are to Letters to the Editor.

Adel, Arthur. Vibrational isotope effects in three particle systems. Part II—222

——— **and V. M. Slipher.** Concerning the carbon dioxide content of the atmosphere of the planet Venus—240(L)

——— **and V. M. Slipher.** Constitution of the atmospheres of the giant planets—902

——— **and V. M. Slipher.** On the identification of the methane bands in the solar spectra of the major planets—240(L)

Agruss, M. (see Grosse, A. v.)—241(L)

Albers, V. M. (see Knorr, H. V.)—336(A)

——— **and H. V. Knorr.** Fluorescence and photodecomposition in solutions of chlorophyll *a*—336(A)

Anderson, Carl D. and Seth H. Neddermeyer. Energy-loss and the production of secondaries by cosmic-ray electrons—325(A)

Anderson, O. E. Hyperfine structure in the arc spectrum of lanthanum—325(A)

——— Nuclear magnetic moment of lanthanum—473

Applegate, Lindsay M. (see Soltau, David L.)—32

Arvin, M. J. (see Loomis, F. W.)—286

Baade, W. and F. Zwicky. Remarks on super-novae and cosmic rays—76(L)

Babcock, Harold D. Wave numbers of infrared spectral lines beyond λ10,000—382

——— (see Russell, Henry Norris)—826(L)

Bacher, Robert F. Survey of experimental hyperfine structure material. Values of nuclear magnetic moments and a discussion of their origin—340(A) (Title only)

——— **and S. Goudsmit.** Atomic energy relations. I—948

Badger, Richard M. Remarks on the band spectrum of sulfur and the statistics of the sulfur nucleus—1025(L)

Balamuth, Lewis. Erratum. New method for measuring elastic moduli and the variation with temperature of the principal Young's modulus of rocksalt between 78°K and 273°K—933

Ballard, Stanley S. Nuclear mechanical moment of columbium—327(A)

——— Nuclear moments of columbium from hyperfine structure—806

——— Nuclear spin of columbium—233(L)

Band, William. Transition in aluminum at 79°C—934(L)

Barker, E. F. (see Nielsen, A. H.)—970

——— (see Sleator, W. W.)—336(A)

Barnes, B. T. (see Forsythe, W. E.)—339(A)

Barnes, S. W. (see Richtmyer, F. K.)—352; 843

Barnett, S. J. Some remarkable multiple sunset flashes in Southern California—75(L)

Barrows, W. M. and J. B. Green. Zeeman effect of the spectra of arsenic—335(A)

Bartlett, James H., Jr. Negative protons in the nucleus?—435(L)

Barton, Vola P. and Geo. A. Lindsay. Dependence of secondary structure in x-ray absorption on crystal form—362

Beams, J. W. (see Flowers, J. W.)—338(A)

Bear, Richard S. (see Spedding, Frank J.)—308; 975

Bearden, J. A. (see Gottling, P. F.)—435(L)

——— (see Wheeler, J. A.)—755

——— **and C. H. Shaw.** Absolute x-ray wave lengths by refraction in quartz—759

Beeck, Otto. Existence of a sharp temperature threshold for catalytic decomposition of molecules on a hot platinum surface and the nature of this decomposition—331(A)

Benz, Carl A. and G. W. Stewart. Cybotactic condition of isopentane in the region of the critical point—703

Berkey, Donald K. Comments on letter of R. J. Stephenson—74(L)

Birge, Raymond T. (see Deming, W. Edwards)—1027(L)

Bjorksted, William (see Whitaker, M. D.)—629(L)

Bleakney, Walker, G. P. Harnwell, W. Wallace Lozier, Philip T. Smith and H. D. Smyth. Production and identification of helium of mass three—81(L)

Bless, A. A. Variation of the dielectric constant of a viscous dielectric with temperature and with frequency—340(A)

Blewett, J. P. (see Smyth, H. D.)—276

Bloch, F. Contribution to the theory of the Compton-line—674

Bock, C. D. (see Zeleny, J.)—318(L)

Boeker, G. F. (see Wills, A. P.)—907

Bonner, Lyman G. Vibrational spectrum of water vapor—458

Bonner, T. W. and L. M. Mott-Smith. Energy spectra of the neutrons from the disintegration of fluorine, boron and beryllium by alpha-particles—258

Boorse, Henry A. Magnetic double refraction in liquids—187

Boucher, P. E. (see Griffith, M. F.)—341(A)

Bowen, I. S. Singlet lines of Cl IV—377

——— Spectra of potassium, K IV and K V, and of calcium Ca V and Ca VI—791

———, **R. A. Millikan and H. Victor Neher.** Very high altitude survey of the effect of latitude upon cosmic-ray intensities and an attempt at a general interpretation of cosmic-ray phenomena—641

Boyce, J. C. Spectra of neon in the extreme ultraviolet—378

Bozorth, R. M. Theory of the heat treatment of magnetic materials—232(L)

——— (see McKeehan, L. W.)—527(L)

Bradley, Charles A., Jr. (see McKellar, Andrew)—664

——— **and Andrew McKellar.** On the photographic infrared absorption spectrum of mono-deutero acetylene—236(L)

——— **and Andrew McKellar.** On the photographic infrared vibration-rotation spectrum of mono-deutero acetylene—341(A)

Brady, James J. Energy distribution of photoelectrons as a function of the thickness of a potassium film—768
Bramley, Arthur. Annihilation of the proton—438(L)
Brandt, W. H. (see Loomis, F. W.)—79(L)
Brasefield, C. J. (see Zeleny, J.)—318(L)
Breit, G. Nuclear stability and isotope shift—319(L)
——— Theory of the effect of a nuclear moment on the state of the atom—340(A) (Title only)
——— **and I. S. Lowen.** Radiation damping and the polarization of fluorescence radiation—590
——— **and I. I. Rabi.** On the interpretation of present values of nuclear moments—230(L)
——— **and John A. Wheeler.** Collision of two light quanta—1087
——— **and F. L. Yost.** Capture of charged particles by nuclei due to emission of gamma-radiation—1110(L)
Brewer, A. Keith and P. D. Kueck. Relative abundance of the isotopes of lithium, potassium and rubidium—894
Brewington, G. P. Secondary structure of x-ray absorption edges from elements in certain cubic crystals—861
Bridgman, P. W. Melting parameters of nitrogen and argon under pressure, and the nature of the melting curve—930
Brinsmade, J. B. Honors work in physics at Williams College—939(A) (Title only)
Broxon, James W. (see Jordan, A. R.)—66
Buchta, J. W. (see Goetz, A.)—538(L)
——— **and A. Goetz.** Thermal expansion of bismuth single crystals near the melting point—1092
Bullard, Persis (see McDowell, Louise S.)—939(A)
Byrne, J. F. (see Myers, F. E.)—777

Cady, Willoughby M. Second-order calculation of H_e I $2s2p\ ^{1,3}P$—439(L)
Carpenter, David W. and Walter M. Nielsen. Effect of temperature and pressure on the mercury afterglow—607
Carr, Laurence H. *L* absorption discontinuities of bismuth—92
Cerwin, Stephen S. Sparking potentials at low pressures—1054
Chaffee, Milton A. (see Livingston, M. Stanley)—330(A)
Cheng, Y. F. Polarization of general x-radiation from thick targets—243
Cinnamon, C. A. Thermal resistivity and the Wiedemann-Franz ratio of single crystal zinc—215
Claus, W. D. (see Jauncey, G. E. M.)—941
Coates, Wesley M. Production of x-rays by swiftly moving mercury ions—542
——— (see Sloan, David H.)—539
Cohen, Victor W. Nuclear spin of caesium—713
——— (see Rabi, I. I.)—707
Cohn, Willi M. Investigations of the polarization and the spectrum of the sky light during the total solar eclipses of August 31, 1932, at Gray, Me., and February 14, 1934, at Losap Islands, in the South Seas—328(A)
Colby, M. Y. and Sidon Harris. X-ray study of a long x-cut quartz crystal vibrating under the transverse piezoelectric effect—445
Compton, Karl T. Scientific problems of the nation—939(A) (Title only)
Copeland, Paul L. Correlation between variation of secondary electron emission and atomic number—167
Copley, M. J. and T. E. Phipps. Reflection coefficient of electrons—144(L)
Cox, R. T. (see Myers, F. E.)—777
Cram, S. Winston. Molecular spectrum of cadmium vapor—205
Crane, H. R. (see Lauritsen, C. C.)—537(L)
———, **L. A. Delsasso, W. A. Fowler and C. C. Lauritsen.** High energy gamma-rays from lithium and fluorine bombarded with protons—531(L)
———, **L. A. Delsasso, W. A. Fowler and C. C. Lauritsen.** Gamma-rays from boron bombarded with deutons—1109(L)
Cravath, Austin M. Further studies on the motion of photoelectrons in a gas—323(A)
——— Terminal energy distribution of electrons driven through a gas by an electric field—332(A)
Crawford, F. H. and T. Jorgensen, Jr. Band spectra of LiH, LiD and NaD—939(A)
——— **and T. Jorgensen, Jr.** Band spectrum of LiH and LiD—746(L)
——— **and P. M. Tsai.** Note on new bands of ionized nitrogen molecule—935(L)
Crawley, C. B. (see Houston, W. V.)—329(A)
Cross, Paul C. Structure of the hydrogen sulfide molecule from a new vibration-rotation band at 10,100A—536(L)
Curtis, Roger W. Experimental determination of ultrasonic absorption and reflection coefficients in air and in carbon dioxide—811

Dahl, O. (see Tuve, M. A.)—1027(L)
Dahlstrom, R. K. and Jos. E. Henderson. Changes in the energy distribution of thermionically emitted electrons produced by high electrical fields—323(A)
Danforth, W. E. Concerning the recovery time of Geiger-Mueller counters—1026(L)
Davis, H. M. (see Glockler, George)—535(L)
Delsasso, L. A. (see Crane, H. R.)—531(L), 1109(L)
Deming, W. Edwards and Raymond T. Birge. On the statistical theory of Errors—1027(L)
Dempster, A. J. Emission of ions and electrons from heated sources—165
——— Sparking potentials at low pressures—728
Dershem, Elmer. Proposed high resolving power x-ray grating spectrometer—337(A)
Dickinson, Beryl H. Specific isotope effect in the hyperfine spectrum of the lead atom—598
Dix, C. H. Electrons and positrons—329(A)
Doan, G. E. and A. M. Thorne. Arcs in inert gases. II—49
Doan, Richard L. Curved-crystal x-ray spectrograph and demountable secondary-radiation tube for analytical work—337(A)
DuBridge, L. A. (see Smith, R. E.)—339(A)
——— **and A. G. Hill.** Energy distribution of photoelectrons from sodium and the photoelectric determination of h/e—339(A)
Duffendack, O. S. and J. H. Manley. Action cross section in collisions of the second kind—336(A)

——— **and J. S. Owens.** Quenching of mercury resonance radiation by hydrogen, carbon monoxide and nitrogen—417

DuMond, Jesse W. M. and Bernard B. Watson. Curved quartz crystal x-ray spectrograph—316(L)

Dunham, Theodore, Jr. Use of Schmidt cameras in plane grating spectrographs—326(A)

Dunnington, Frank G. Establishment of a precision high frequency standard capable of delivering considerable power—331(A)

Dushman, Saul. Relationship of science and industry—939(A) (Title only)

Eastman, E. D. Energy of removal of neutrons and alpha-particles from nuclei and alpha-instability below the radio-elements—238(L)

——— Energy and stability related to composition of atomic nuclei—1

——— Heights of nuclear potential barriers—744(L)

Eaton, William W. (see Pollard, Ernest)—528(L)

Eckart, Carl. Kinetic energy of polyatomic molecules—383

Ellett, Alexander. Measurement of nuclear moments and spin through the polarization of resonance radiation—340(A) (Title only)

——— **and N. P. Heydenburg.** Nuclear magnetic moments from the polarization of resonance radiation. Sodium, $3^2S_{1/2}-4^2P_{3/2,\,1/2}$—583

Ellis, C. B. Simplified interval sorter for spectral analysis—341(A)

Elmore, W. C. (see McKeehan, L. W.)—226(L); 529(L)

Evans, Robley D. Improved technique for determination of radon and radium in liquids—328(A)

——— Ionization currents produced by radon, Ra A and Ra C′ in cylindrical ionization chambers—937(A)

——— Thermionic pentode controlled constant-voltage rectifiers—324(A)

Fender, F. G. and J. P. Vinti. Doubly-excited states in helium—77(L)

Finkelnburg, Wolfgang. Continuous electron radiation in flames and arcs—330(A)

——— Spectra of O_4 and other polyatomic polarization molecules—326(A)

Fitzgerald, Sister M. Ambrosia and R. A. Sawyer. Fifty-three electron spectra of caesium and barium: Cs III and Ba IV—576

Flowers, J. W. and J. W. Beams. Initiation of discharges in ion free gases—338(A)

Focke, Alfred B. Segregation of polonium in bismuth crystals—623

Forsythe, W. E. and B. T. Barnes. Energy distribution in the spectrum of some incandescent lamps—339(A)

Fowler, R. Dudley and G. E. Gibson. Production of intense beams of positive ions—1075

Fowler, W. A. (see Crane, H. R.)—531(L), 1109(L)

Fox, Marvin (see Millman, Sidney)—320(L)

Fredrickson, W. R. and Martin E. Hogan, Jr. Ultraviolet bands of beryllium chloride—454

Freed, Simon. On the velocity of light—1025(L)

Froman, Darol K. (see Stearns, J. C.)—535(L)

Furry, W. H. Approximate wave functions for high energy electrons in Coulomb fields—391

Gamow, George. General nuclear problem—340(A) (Title only)

Gans, David M. (see Harkins, William D.)—397; 827(L)

Gibbs, R. C. (see Ruedy, J. E.)—880

Gibson, G. E. (see Fowler, R. Dudley)—1075

——— **and Angus Macfarlane.** Absorption spectrum of arsenic—1059

Gingrich, N. S. (see Warren, B. E.)—368

——— **and B. E. Warren.** Interpretation of x-ray diffraction patterns of a fluid at various densities—248

Glockler, George. Estimated electron affinities of the light elements—111

——— **and H. M. Davis.** Acetylene bond frequency in heavy acetylene (C_2D_2)—535(L)

——— **and Charles Morrell.** Fundamental frequencies of acetylene—233(L)

Goble, A. T. Four vector problem and intensities in platinum-like spectra—334(A)

Goetz, Alexander (see Buchta, J. W.)—1092

——— (see Wolf, Alexander)—1095

———, **J. W. Buchta and T. L. Ho.** Thermal expansions of alloyed Bi crystals in the region of the eutectic melting point—538(L)

Goldsmith, H. H. Disintegration of H^3 and the stellar abundance of H^2 and H^3—78(L)

Gottling, P. F. and J. A Bearden. Ruled grating wave-length of the copper $K\alpha_1$-line—435(L)

Goudsmit, S. (see Bacher, R. F.)—948

Granath, L. P. and R. K. Stranathan. Magnetic moment of caesium determined from the hyperfine structure of the $6p\ ^2P_{1/2}$ state—317(L)

Green, J. B. (see Barrows, W. M.)—335(A)

——— **and R. A. Loring.** Paschen-Back effect. II. *JJ*-coupling (approx.)—335(A); 888

Griffith, M. F. and P. E. Boucher. Behavior of photovoltaic cells under x-radiation—341(A)

Grosse, A. v. and M. Agruss. Chemistry of element 93 and Fermi's discovery—241(L)

Guernsey, Marjorie L. Spectrum of gallium oxide—114

Hagen, J. P. (see Van Dyke, K. S.)—939(A)

Hahn, T. M. Absorption of monochromatic x-rays of short wave-length—149

Hall, Harvey and William Rarita. On the photoelectric effect for the *L*-shell—143(L)

Hall, Leo G. Rectifying effect in chrome cast iron—1109(L)

Halpern, Otto and Em. Wasser. Direct experimental test of the principle of spectroscopic stability—177

Hanson, Isabel. Intensity measurements in the Raman spectrum of carbon dioxide—122

Hare, Donald G. (see Kirkpatrick, Paul)—831

Harkins, William D. and David M. Gans. Artificial radioactivity and the conversion of kinetic into γ-ray energy associated with nuclear disintegration by neutrons—827(L)

Harkins, William D. and David M. Gans. Inelastic collisions with changes of mass and the problem of nuclear disintegration with capture or non-capture of a neutron or another nuclear projectile—397
Harnwell, G. P. (see Bleakney, Walker)—81(L)
———, **H. D. Smyth and Wm. D. Urry.** Purification and spectroscopic evidence for He_2^3—437(L)
Harris, Sidon (see Colby, M. Y.)—445
Hartree, D. R. Approximate wave functions and atomic field for mercury—738
Harvey, G. G. Effect of pressure on the intensity of x-rays scattered from nitrogen at small angles—441
———, **P. S. Williams and G. E. M. Jauncey.** Quantitative test of the Waller-Hartree theory of x-ray scattering applied to the diffuse scattering from crystals—365
Heaps, C. W. Discontinuities of magnetoresistance—1108 (L)
Hebb, M. H. (see Van Vleck, J. H.)—17; Errata—929
Heil, L. M. Calculation of mass scattering coefficients—58
Heller, Gabriel and Lloyd Motz. Averages over portions of configuration space—502
Henderson, Jos. E. (see Dahlstrom, R. K.)—323(A)
Henderson, M. C. Amplifier and recording apparatus for alpha-particles, high speed protons and neutrons—324(A)
——— (see Lawrence, E. O.)—324(A)
——— (see Livingston, M. S.)—325(A)
———, **M. S. Livingston and E. O. Lawrence.** Transmutation of fluorine by proton bombardment and the mass of fluorine 19—38
Hergenrother, R. C. (see Hughes, A. L.)—180
Herzfeld, K. F. and Maria Goeppert Mayer. On the theory of fusion—995
Heydenburg, N. P. Influence of the Stark effect on the fine structure of the Balmer lines of hydrogen—1069
——— Nuclear magnetic moment of caesium from the polarization of resonance radiation—802
——— (see Ellett, A.)—583
Hill, A. G. (see DuBridge, L. A.)—339(A)
Hill, Harry. Hyperfine structure in silver—536(L)
Ho, T. L. (see Goetz, A.)—538(L)
Hogan, Martin E., Jr. (see Fredrickson, W. R.)—454
Holzer, Robert E. Excitation of light by alkali ions—280
Houston, W. V. (see Kinsler, L. E.)—533(L)
——— **and C. B. Crawley.** Electronic functions for a metallic crystal—329(A)
Hoyt, H. C. and Geo. A. Lindsay. Simple method for demonstrating and measuring approximately the index of refraction of x-rays—337(A)
Hsiung, David S. Coincidence test of the corpuscular hypothesis of cosmic-rays—334(A); 653
Hubbard, J. C. Errata:—Acoustic resonator interferometer—525
Hughes, A. L. and R. C. Hergenrother. Electron scattering by atomic electrons—180
Hulburt, E. O. Analysis of the recent measurements of the ionosphere—822(L)
Hull, Robert B. Crystal structure of nickelous acetate tetrahydrate—329(A)
Huxford, W. S. and Olav Maseng. Spectroscopic study of restriking phenomena in the a.c. copper arc—338(A)

Inglis, D. R. Non-orthogonal wave functions and ferromagnetism—135
——— (see Landé, Alfred)—76(L)

Janes, R. B. Magnetic susceptibilities of powdered crystals—338(A)
Jauncey, G. E. M. Note on the structure of the Compton modified band—667
——— (see Harvey, G. G.)—365
——— **and W. D. Claus.** Diffuse scattering of x-rays from sylvine—More exact measurements—941
Jenkins, F. A. (see Nolan, Philip)—327(A)
Jewitt, T. N. Ionization potentials of formaldehyde and halogen derivatives of methane—616
Johnson, E. A. (see Meyer, R. C.)—143(L)
Johnston, Helen (see Murphy, G. M.)—95
Jordahl, O. M. Information concerning crystal structure from data on magnetic susceptibilities—79(L)
Jordan, A. R., James W. Broxon and Frank C. Walz. Dependence of the dielectric coefficient of air upon pressure and frequency—66
Jorgensen, T., Jr. (see Crawford, F. H.)—746(L); 939(A)
Jungers, J. C. (see Lind, S. C.)—825(L)

Kaplan, Joseph. Band spectrum of nitrogen—631(L)
——— New band systems in nitrogen—534(L)
——— New bands in nitrogen—534(L)
——— New second-positive bands in nitrogen—326(A)
——— **and Leo D. Levanas.** New members of the Lyman-Birge-Hopfield system—331(A)
Kellogg, J. M. B. (see Rabi, I. I.)—157; 163
Kennard, E. H. and E. Ramberg. Origin of $K\alpha$-satellites—1040
——— **and E. Ramberg.** Self-consistent field and some x-ray terms of the sodium atom—1034
King, Arthur S. (see Russell, Henry Norris)—1023
King, Louis V. On the mathematical analysis of cosmic-ray data—154
King, Robert B. Photographic photometry of iron multiplets in electric furnace spectra—327(A)
Kinsey, B. B. (see Thornton, R. L.)—324(A)
Kinsler, L. E. Zeeman effect in neon—533(L)
——— **and W. V. Houston.** Zeeman effect in helium—533(L)
Kirkpatrick, D. E. (see Salant, E. O.)—318(L)
Kirkpatrick, Paul (see Ross, P. A.)—668
——— **and Donald G. Hare.** Depth distribution of origins of characteristic x-rays from thick targets—831
Knorr, H. V. (see Albers, V. M.)—336(A)
——— **and V. M. Albers.** Fluorescence and photodecomposition in solutions of chlorophyll *b*—336(A)
Koontz, Philip G. (see Watson, William W.)—32
Korff, S. A. Penetrating power of asymmetric component of cosmic radiation—74(L)
Kruger, P. Gerald and W. E. Shoupp. Deepest terms in ions of the isoelectronic sequences Ni I to Kr IX and Pd I to Xe IX—124

——— **and S. G. Weissberg.** Ionization potentials in the isoelectronic sequence A I to Mn VIII—336(A)
Kueck, P. D. (see Brewer, A. Keith)—894
Kurie, Franz N. D. Disintegration with the emission of protons induced by neutrons—330(A)
——— Loss in energy in the disintegration of nitrogen by neutrons—324(A)
Kusch, P. (see Loomis, F. W.)—292

LaCoste, Lucien J. B. Rotational wave equation of tetramethylmethane for zero potential and a generalization—718
Lamar, E. S. and Overton Luhr. Proton production in the low voltage arc—87
Landé, Alfred. Is the neutron an elementary particle?—334(A)
——— Nuclear magnetic moments and their origin—477
——— **and D. R. Inglis.** Magnetic moment of the neutron —76(L)
Langer, R. M. Passage of charged particles through the magnetic field and the atmosphere of the earth—330(A)
Langseth, A. and J. Rud Nielsen. Polarization and intensity measurements in the Raman spectrum of carbon dioxide—1057
Larrick, Lewis. Nuclear magnetic moments from the polarization of resonance radiation. Sodium, $3^2S_{1/2} - 3^2P_{3/2,\ 1/2}$—581
Lauritsen, C. C. (see Crane, H. R.)—531(L), 1109(L)
——— **and H. R. Crane.** Evidence of an excited state in the alpha-particle—537(L)
——— **and J. R. Oppenheimer.** On the scattering of the Th C″ γ-rays—80(L)
Lawrence, Ernest O. Radioactive sodium produced by deuton bombardment—746(L)
——— (see Henderson, M. C.)—38
——— (see Livingston, M. S.)—325(A)
———, **M. C. Henderson and M. S. Livingston.** Transmutation of fluorine by proton bombardment and the mass of fluorine 19—324(A)
LeGalley, Donald P. (see Locher, Gordon L.)—1047
Levanas, Leo D. (see Kaplan, Joseph)—331(A)
Lewis, Gilbert N. Genesis of the elements—897
Lewis, William. Growing and testing large single crystals of ice—328(A)
Libby, W. F. Absence of low energy radiations from potassium and rubidium—745(L)
——— Radioactivity of neodymium and samarium—196
Lind, S. C., J. C. Jungers and C. H. Shiflett. Polymerization of heavy acetylene by alpha-rays—825(L)
Lindsay, Geo. A. (see Barton, Vola P.)—362
——— (see Hoyt, H. C.)—337(A)
Linford, Leo H. Emission of secondary electrons from various metal targets—325(A)
Liska, John W. Efficiencies of ionization of helium and mercury by electron impact at high voltages—169
Livingston, M. Stanley (see Henderson, M. C.)—38
——— (see Lawrence, E. O.)—324(A)
——— **and Milton A. Chaffee.** Production of high voltage x-rays for medical uses—330(A)
——— **and Edwin McMillan.** Production of radioactive oxygen—437(L)
———, **M. C. Henderson and E. O. Lawrence.** Radioactivity induced by neutron bombardment—325(A)
Locher, Gordon L. and Donald P. LeGalley. Measurement of absolute x-ray intensities and absolute sensitivity of x-ray film with a Geiger-Müller counter—1047
Loeb, Leonard B. Energy of detachment of electrons from negative ions in oxygen—323(A)
Longacre, Andrew. Scattering of lithium ions by a polycrystalline nickel surface—407
Loomis, F. W. and M. J. Arvin. Band spectrum of NaK—286
——— **and W. H. Brandt.** OH^+ bands—79(L)
——— **and P. Kusch.** Band spectrum of caesium—292
Loring, R. A. (see Green, J. B.)—335(A); 888
Loughridge, Donald H. (see Soltau, David L.)—328(A)
——— **and Harold C. Trueblood.** Organic liquids suitable for cloud expansion work—323(A)
Lowen, I. S. (see Breit, G.)—590
Lozier, W. Wallace. Heat of dissociation of CO and the electron affinity of O—268
——— (see Bleakney, Walker)—81(L)
Luhr, Overton (see Lamar, E. S.)—87

MacDonald, J. K. L. On the modified Ritz variation method—828(L)
Macfarlane, Angus (see Gibson, G. E.)—1059
Manley, J. H. (see Duffendack, O. S.)—336(A)
Mann, M. M. and Walter M. Nielsen. Effect of hydrogen on the afterglow in mercury vapor—991
Manning, Millard F. Energy levels for a potential function having symmetrical double minima and applications to the NH_3 and ND_3 molecules—335(A)
Margenau, Henry. Complex neutron—107
——— Nuclear energy levels and the model of a potential hole—613
——— **and E. Pollard.** Progression of nuclear resonance levels with atomic number—228(L)
Marton, L. Electron microscopy of biological objects—527(L)
Maseng, Olav (see Huxford, W. S.)—338(A)
Mason, R. C. Arcs in rare gases—630(L)
Mayer, Maria Goeppert (see Herzfeld, K. F.)—995
McDowell, Louise S., Persis Bullard and Marian E. Whitney. Effect of frequency of impressed electromotive force upon the power loss and dielectric constant of various glasses—939(A)
McKeehan, L. W. and R. M. Bozorth. Hysteresis losses and the area of the hysteresis loop—527(L)
——— **and W. C. Elmore.** Surface magnetization in ferromagnetic crystals—226(L); II—529(L)
McKellar, Andrew (see Bradley, C. A.)—236(L); 341(A)
——— **and Charles A. Bradley, Jr.** On the near infrared absorption spectrum of mono-deutero-acetylene—664
McMillan, Edwin. Absorption measurements of hard gamma-rays from fluorine bombarded by protons—325(A)
——— Some gamma-rays accompanying artificial nuclear disintegrations—868

McMillan, Edwin (see Livingston, M. Stanley)—437(L)
McMillen, J. Howard. Elastic electron scattering in potassium—983
Merrill, Robert A. Spectral multiplets arising from configurations of the type $d^k msns$. ($k = 1 \cdots 9$)—334(A)
——— Spectral multiplets belonging to configurations of the type $d^k ms$ and $d^k msns$—487
Meyer, R. C. and E. A. Johnson. Measurement of flicker effect—143(L)
Miller, F. M. (see Ufford, C. W.)—283
Millikan, Robert A. General interpretation of cosmic-ray effects—329(A)
——— (see Bowen, I. S.)—641
Millman, Sidney, Marvin Fox and I. I. Rabi. Spin and magnetic moment of the potassium K^{39} nucleus—320(L)
Mitchell, Allan C. G. (see Whitaker, M. D.)—629(L)
——— **and Edgar J. Murphy.** Mean life of the 7^3S_1 state of mercury from polarization measurements on the visible triplet—53
Møller, Chr. and M. S. Plesset. Note on an approximation treatment for many-electron systems—618
Moore, Charlotte, E. (see Russell, Henry Norris)—826(L)
More, Kenneth R. Nuclear mechanical moment of cobalt—327(A); 470
Morrell, Charles (see Glockler, George)—233(L)
Morrow, John A. Precision determinations of the variation of the dielectric constant of benzene with temperature—340(A) (Title only)
Mott-Smith, L. M. (see Bonner, T. W.)—258
Motz, Lloyd (see Heller, Gabriel)—502
Mulliken, Robert S. Halogen molecules and their spectra. *J-J*-like coupling. Molecular ionization potentials—549
——— Hopfield's Rydberg series and the ionization potential and heat of dissociation of N_2—144(L)
——— Measurement of nuclear spin and statistics by means of band spectra—340(A) (Title only)
Murphy, Edgar J. (see Mitchell, Allan C. G.)—53
Murphy, G. M. and Helen Johnston. Nuclear spin of deuterium—95
Myers, F. E., J. F. Byrne and R. T. Cox. Diffraction of electrons as a search for polarization—777

Neddermeyer, Seth H. (see Anderson, Carl D.)—325(A)
Neher, H. Victor (see Bowen, I. S.)—641
Nielsen, A. H. and E. F. Barker. Infrared spectrum of methyl chloride—970
Nielsen, Harald H. Infrared absorption spectrum of formaldehyde. Part I—117
Nielsen, J. Rud (see Langseth, A.)—1057
Nielsen, Walter M. (see Carpenter, David W.)—607
——— (see Mann, M. M.)—991
Nolan, Philip and F. A. Jenkins. Intensities in the 3400 band of phosphorous hydride—327(A)
Nordsieck, Arnold. Neutron collisions and the beta-ray theory of Fermi—234(L)
Nottingham, W. B. Application of the Forsythe-Watson temperature scale for tungsten—341(A)
——— Experiments with the copper arc—630(L)
——— Thermionic electron emission from tungsten—339(A)

O'Bryan, H. M. Optical constants and the conduction electrons of beryllium and silicon—336(A)
Oldenberg, O. On abnormal rotation of molecules—210
Oppenheimer, J. R. (see Lauritsen, C. C.)—80(L)
Osterberg, H. (see Roebuck, J. R.)—340(A); 785
Ostrofsky, M. Application of the Dirac vector model to the d^3 configuration—604
Owens, J. S. (see Duffendack, O. S.)—417

Parker, Allan E. Band systems of BaCl—301
Parratt, Lyman G. Natural x-ray line widths: correction for finite resolving power—749
Paton, R. F. Protons emitted from boron and phosphorus bombarded by high energy alpha-particles—229(L)
Patterson, A. L. Fourier series method for the determination of the components of interatomic distances in crystals—372
Payne, J. Fred, Jr. Effect of x-rays on the dielectric constant of various liquids—340(A)
Pearsall, Anna W. Intensities of satellites of $L\beta_2$—694
Peckham, A. L. (see Rusk, R. D.)—425
Peoples, James A., Jr. (see Slack, Francis G.)—724
Phelps, William D. *M*-series absorption spectrum of metallic bismuth—357
Phipps, T. E. (see Copley, M. J.)—144(L)
Plesset, M. S. (see Møller, Chr.)—618
Podolsky, Boris. Interpretation of e^2/mc^2 and h/mc—734
Polk, O. E. Ionization of air by alpha- and beta-rays as a function of pressure—405
Pollard, Ernest (see Margenau, H.)—228(L)
——— (see Zeleny, J.)—318(L)
——— **and William W. Eaton.** Attempts to detect the emission of deutons in nuclear transmutations—528(L)
Poppy, Willard J. Electrical resistivities of single and optically mosaic zinc crystals—815
Powell, W. M., Jr. Photoelectric measurements of the absorption of fused and crystalline quartz between 1633 and 1463A—43
Price, W. C. Absorption spectra of formaldehyde and hydrogen cyanide in the far ultraviolet—529(L)

Quarles, Gilford G. Dispersion of the electro-optical Kerr effect in carbon dioxide—692

Rabi, I. I. Measurement of nuclear spin and moments by method of molecular beams—340(A) (Title only)
——— (see Breit, G.)—230(L)
——— (see Millman, Sidney)—320(L)
——— **and V. W. Cohen.** Measurement of nuclear spin by the method of molecular beams. The nuclear spin of sodium—707
———, **J. M. B. Kellogg and J. R. Zacharias.** Magnetic moment of the deuton—163; of the proton—157
Ramberg, E. (see Kennard, E. H.)—1034, 1040
——— (see Richtmyer, F. K.)—843
Rarita, William (see Hall, Harvey)—143(L)
Read, D. N. Rotational and vibrational structure of the fourth positive bands of carbon monoxide—571
Reeves, Ralph L. (see Slack, Francis G.)—724
Reinhart, Raymond E. Large Barkhausen discontinuities and their propagation in Ni-Fe alloys. II—483

Richtmyer, F. K. and S. W. Barnes. Natural widths of the *K*-series of W(74)—352
———, **S. W. Barnes and E. Ramberg.** Widths of the *L*-series lines and of the energy levels of Au(79)—843
Rieke, F. F. Anomalous rotation of HgH molecules—236(L)
Robertson, H. P. Indeterminacy relation for several observables and its classical interpretation—794
Rodine, Milward T. Thermal conductivities of bismuth single crystals as influenced by a magnetic field—910
Roebuck, J. R. and H. Osterberg. Joule-Thomson effect in argon—785
——— **and H. Osterberg.** Joule-Thomson effect in nitrogen argon and in mixtures of nitrogen and helium—340(A)
Rosenthal, Jenny E. Vibrations of tetrahedral pentatomic molecules. Part III. Comparison with experimental data. Part IV. Isotopic shifts—730
Ross, P. A. and Paul Kirkpatrick. Effect of electron binding upon the magnitude of the Compton shift—668
Ross, William H. Magnetic susceptibilities of dilute solid solutions of nickel in copper at various temperatures—46
Rudberg, Erik. Vapor pressure of calcium between 500 and 625°C—763; 937(A)
Ruedy, J. E. and R. C. Gibbs. Arc spectrum of selenium—880
Rusk, R. D. and A. L. Peckham. Asymmetry of collector currents—425
Russell, Henry Norris. Spectrum and ionization potential of radium—989
——— **and Arthur S. King.** Arc spectrum of europium—1023
———, **Harold D. Babcock and Charlotte E. Moore.** Series lines of magnesium in the solar spectrum—826(L)

Salant, E. O. and D. E. Kirkpatrick. Vibration-rotation bands of hydrogen fluoride—318(L)
Sandström, Arne. Absorption of hard x-rays and the laws of Jönsson—825(L)
Sawyer, R. A. (see Fitzgerald, Sister M. Ambrosia)—576
Scott, F. A. Measurement of the energy of a beta-ray of radium B—633
Seitz, F. (see Wigner, E.)—509
Semat, Henry. Structure and width of the L_{III} absorption limits of tantalum, tungsten and gold—688
Serber, Robert. Energies of some hydrocarbon molecules—335(A)
Shaw, C. H. (see Bearden, J. A.)—759
Shiflett, C. H. (see Lind, S. C.)—825(L)
Shih, J. W. Magnetic properties of iron-cobalt single crystals—139
Shortley, George H. General sum rule in intermediate coupling—938(A)
Shoupp, W. E. (see Kruger, P. Gerald)—124
Slack, Francis G. Verdet constant of heavy water—945
———, **Ralph L. Reeves and James A. Peoples, Jr.** Effect of concentration, temperature and wave-length of light upon the Verdet constant of cerous chloride solutions—724
Sleator, W. W. and E. F. Barker. Infrared absorption bands of heavy water vapor—336(A)
Slipher, V. M. (see Adel, Arthur)—240(L); 902
Sloan, David H. and Wesley M. Coates. Recent advances in the production of heavy high speed ions without the use of high voltages—539
Smith, Lloyd P. Determination of x-ray line shapes by a double crystal spectrometer—343
Smith, Philip T. (see Bleakney, Walker)—81(L)
——— (see Tate, John T.)—773
Smith, R. E. and L. A. DuBridge. Photoelectric emission from thoriated tungsten—339(A)
Smyth, H. D. (see Bleakney, Walker)—81(L)
——— (see Harnwell, G. P.)—437(L)
——— **and J. P. Blewett.** Ionization of carbon disulphide by electron impact—276
Soller, Walter. Interpolation equation for photo-densitometer charts of x-ray diffraction patterns—331(A)
Soltau, David L., Donald H. Loughridge and Lindsay M. Applegate. Variable frequency generator for furnishing odd harmonics of 60 cycle current of pure sinusoidal form—328(A)
Spangler, Ross D. Cybotactic condition of ethyl ether in the region of the critical point—698
Spedding, Frank H. and Richard S. Bear. Absorption spectra of the samarium ion in solids. IV. Absorption of $Sm(C_2H_5SO_4)_3 \cdot 9H_2O$ and partial energy level diagrams for the Sm^{+++} ion as it exists in hydrated crystalline samarium ethylsulfate, samarium iodide and samarium perchlorate—308. V. The absorption spectrum and energy levels of the Sm^{+++} ion as it exists in monoclinic crystals of $Sm_2(SO_4)_3 \cdot 8H_2O$—975
Spencer, Roy C. Equation for x-ray crystal curves—1108(L)
——— Factors causing deviations in x-ray ionization measurements—337(A)
Stabler, H. P. Symmetry of the thermoelectric effects in single crystals—938(A)
Stearns, J. C. and Darol K. Froman. Azimuthal asymmetry of cosmic radiation on Mount Evans, Colorado—535(L)
Stephens, W. E. Elastic scattering of fast electrons in mercury and agreement with Mott's theory—935(L)
Stephenson, R. J. Fluorescence x-ray yields from *K* shells of atoms—73(L)
Stevenson, A. F. Criticism of Dr. L. G. H. Huxley's theory of the origin of cosmic rays—1111(L)
Stewart, G. W. (see Benz, Carl A.)—703
Stoddard, K. B. Direct and fluorescence excitation of the *K*-level in thick targets of copper—837
Stranathan, R. K. (see Granath, L. P.)—317(L)
Stratton, J. A. Spheroidal functions—938(A)
Street, J. C. and R. H. Woodward. Counter calibration and cosmic-ray intensity—938(A); 1029
——— **and R. T. Young, Jr.** Transition effects in the cosmic radiation—823(L); 938(A)
Strong, John. Anomalous behavior of diffraction gratings coated by evaporation—326(A)
Suits, C. G. Experiments with arcs at atmospheric pressure—252
——— Observations on the velocity of sound in arcs—339(A)

Swann, W. F. G. Relation of the primary cosmic radiation to the phenomena observed—828(L)
——— Significance of J. Clay's ionization depth data in relation to the nature of the primary cosmic radiation—432

Tate, John T. (see Vaughan, Alfred L.)—327 (A)
——— **and Philip T. Smith.** Ionization potentials and probabilities for the formation of multiply charged ions in the alkali vapors and in krypton and xenon—773
Thomassen, L. (see Wilson, J. E.)—337(A)
Thorne, A. M. (see Doan, G. E.)—49
Thornton, R. L. and B. B. Kinsey. Production of high velocity lithium ions—324(A)
Tilles, Abe. Survey of time lag of sparkover in a uniform field—1015
Tonks, Lewi. Pressure of plasma electrons and the force on the cathode of an arc—278
Torrance, C. C. Hartree fields of carbon—388
Trawick, M. W. Spectra of columbium V and molybdenum VI—63
Trueblood, Harold C. (see Loughridge, Donald H.)—323(A)
Tsai, P. M. (see Crawford, F. H.)—935(L)
Tuve, M. A., O. Dahl and C. M. Van Atta. Low-power positive-ion source of high intensity—1027(L)

Uehling, E. A. Transport phenomena in Einstein-Bose and Fermi-Dirac gases. II—917
Ufford, C. W. and F. M. Miller. Relative multiplet transition probabilities from spectroscopic stability—283
Uhlenbeck, G. E. (see Wolfe, Hugh C.)—237(L)
Urry, Wm. D. (see Harnwell, G. P.)—437(L)
Utterback, C. L. and Henry Wirth. Ultramicrometer—328(A)

Valasek, Joseph (see Zeleny, Anthony)—450
Van Atta, C. M. (see Tuve, M. A.)—1027(L)
Van Dyke, K. S. and J. P. Hagen. Decrement investigations of quartz resonators—939(A)
Van Vleck, J. H. Magnetic dipole radiation and the atmospheric absorption bands of oxygen—334(A)
——— **and M. H. Hebb.** On the paramagnetic rotation of tysonite—17; Errata—929
Van Voorhis, S. N. Small-angle inelastic scattering of electrons in helium, hydrogen and mercury—480
Varian, Russell H. Contribution to the theory of barrier layer cells—1051
Varney, Robert N. Ionization by positive alkali ions as measured by a balanced space-charge method—235(L)
——— Ionization by positive alkali ions in noble gases using a balanced space-charge method—322(A)
Vaughan, Alfred L., John H. Williams and John T. Tate. Isotopic abundance ratios of C, N, A, Ne and He—327(A)
Vernoff, S. N. On the study of cosmic rays at the great altitudes—822(L)
Vigness, C. Irwin. Inverse piezoelectric properties of Rochelle salt—255
Vinti, J. P. (see Fender, F. G.)—77(L)

Walerstein, I. High series terms in the arc spectrum of mercury—874
——— $^3S_1$ and $^3D_{3,\,2,\,1}$ terms in mercury—335(A)
Walz, Frank C. (see Jordan, A. R.)—66
Warren, B. E. (see Gingrich, N. S.)—248
——— **and N. S. Gingrich.** Fourier integral analysis of x-ray powder patterns—368
Wasser, Em. (see Halpern, Otto)—177
Watson, Bernard B. (see DuMond, Jesse W. M.)—316(L)
Watson, W. H. Quantum theory of electromagnetic fields—936(L)
Watson, William W. Mass ratios of isotopes from band spectra—319(L)
——— Spectrum of calcium deuteride—939(A)
——— **and Philip G. Koontz.** Nitrogen molecular spectra in the vacuum ultraviolet—32
Weissberg, S. G. (see Kruger, P. Gerald)—336(A)
Weyl, Hermann. Observations on Hilbert's independence theorem and Born's quantization of field equations—505
Wheeler, John A. (see Breit, G.)—1087
——— **and J. A. Bearden.** Variation of the K resonating strength with atomic number—755
Whitaker, M. D., William Bjorksted and Allan C. G. Mitchell. Preliminary report on a quick method of depositing polonium on silver—629(L)
White, Harry J. Some improvements in the technique of Kerr cells—323(A)
——— Study of the initial stages of spark discharges in gases—99; 330(A)
White, T. N. Measurement of the x-ray absorption coefficient of xenon—865
Whitelaw, Neill G. Temperature variation of the second virial coefficient for helium—340(A)
Whitford, Albert E. Highly ionized potassium and calcium spectra—793
Whitney, Marian E. (see McDowell, Louise S.)—939(A)
Wigner, E. On the interaction of electrons in metals—1002
——— **and F. Seitz.** On the constitution of metallic sodium. II—509
Wilhelmy, E. Quadrupole lines in the K-series of ruthenium—130
Williams, Clarke. Thermal expansion and the ferromagnetic change in volume of nickel—1011
Williams, E. H. Magnetic properties of rare earth salts—133
Williams, John H. (see Vaughan, Alfred L.)—327(A)
Williams, P. S. Diffuse scattering of x-rays from sodium fluoride. III. Using sensible monochromatic radiation—83
——— (see Harvey, G. G.)—365
Williams, Robley C. Properties of evaporated films of aluminum over chromium—146(L)
Wills, A. P. and G. F. Boeker. Dependence of the diamagnetism of water upon its temperature—907
Wilson, E. Bright, Jr. Partial interpretation of the Raman and infrared spectra of benzene—146(L)
Wilson, J. E. and L. Thomassen. X-ray investigation of lattice recovery of metals after cold-working—337(A)
Wirth, Henry (see Utterback, C. L.)—328(A)

Witmer, Enos E. On the doublet separation in the normal state of nitric oxide and its thermodynamic quantities—629(L)

Wolf, Alexander and Alexander Goetz. Magnetostriction of pure and alloyed Bi single crystals—1095

Wolfe, Hugh C. and G. E. Uhlenbeck. Spontaneous disintegration of proton or neutron according to the Fermi theory—237(L)

Woodward, R. H. (see Street, J. C.)—938(A); 1029

Wu, Ta-You. Energy states of doubly excited helium—239(L)

——— Infrared spectra of the chlorine derivatives of ethylene C_2H_4—465

Wulf, Oliver R. Pressure broadening in the gamma-bands of nitric oxide—316(L)

Yost, F. L. (see Breit, G.)—1110(L)

Young, R. T., Jr. (see Street, J. C.)—823(L); 938(A)

Zabel, R. M. Scattering of hydrogen and helium beams in mercury vapor—411

Zacharias, J. R. (see Rabi, I. I.)—157; 163

Zaikowsky, W. M. On the development of the intermolecular and intramolecular chains in oxidation of *n*-hexan—329(A)

Zeleny, Anthony and Joseph Valasek. Variation of the dielectric constant of Rochelle salt crystals with frequency and applied field strength—450

Zeleny, J., C. J. Brasefield, C. D. Bock and E. C. Pollard. Alpha-particles from lithium ions striking hydrogen compounds—318(L)

Zener, Clarence. Ferromagnetism and liquid mixtures—824(L)

Ziegler, G. E. Crystal structure of lithium sulphate monohydrate—338(A)

Zinn, Walter H. Two-crystal study of the structure and width of *K* x-ray absorption limits—659

Zwicky, F. (see Baade, W.)—76(L)

Analytic Subject Index to Volume 46

References with (A) are to abstracts of papers presented at meetings of the Physical Society. References with (L) are to Letters to the Editor.

Absorption coefficient (see also **X-ray, absorption**)
Of hard γ-rays from F bombarded by protons, E. McMillan—325(A); 868
Of hard x-rays and the laws of Jönsson, A. Sandström—825(L)
Absorption and reflection of light (see also **Spectra, absorption**)
In fused and crystalline quartz between 1633 and 1463A, W. M. Powell, Jr.—43
Accommodation coefficient
Pressure of plasma electrons, L. Tonks—278
Acoustics
Errata:—Acoustic resonator interferometer, J. C. Hubbard—525
Ultrasonic absorption and reflection coefficients in air and in CO_2, R. W. Curtis—811
Velocity of sound in arcs, C. G. Suits—339(A)
Affinity
Detachment of electrons from O_2, L. B. Loeb—323(A)
Electron affinities of light elements, G. Glockler—111
Electron affinity of O, W. W. Lozier—268
Afterglow
In Hg, effect of H_2, M. M. Mann, W. M. Nielsen—991
In Hg vapor, effect of temperature and pressure, D. W. Carpenter, W. M. Nielsen—607
Arcs (see also **Discharge of electricity in gases**)
Dependence on boiling point of electrodes, C. G. Suits—252; W. B. Nottingham—630(L)
Pressure of plasma electrons, L. Tonks—278
Spectroscopic study of restriking phenomena, W. S. Huxford, O. Maseng—338(A)
Temperature from velocity of sound in arcs, C. G. Suits—339(A)
Unstable arcs in pure inert gases, G. E. Doan, A. M. Thorne—49; R. C. Mason—630(L)
Astrophysics
Atmospheres of the giant planets, A. Adel, V. M. Slipher—902
CO_2 in atmosphere of Venus, A. Adel—240(L)
Genesis of the elements, G. N. Lewis—897
Methane in solar spectra of major planets, A. Adel, V. M. Slipher—240(L)
Series lines of Mg in solar spectrum, H. N. Russell, H. D. Babcock, C. E. Moore—826(L)
Stellar abundance of H^2 and H^3, H. H. Goldsmith—78(L)
Super-novae and cosmic rays, W. Baade, F. Zwicky—76(L)
Atmospheric electricity (see **Meteorology**)
Atomic and molecular beams
Scattering of H and He beams in Hg vapor, R. M. Zabel—411
Scattering of Li ions by a polycrystalline Ni, A. Longacre—407
Barkhausen effect (see **Magnetic properties**)
Barrier-Layer photo-cells
Theory of direction of flow, R. H. Varian—1051
Chemical reactions
Intermolecular and intramolecular chains in oxidation of *n*-hexan, W. M. Zaikowsky—329(A)
Temperature threshold for catalytic decomposition of molecules on hot Pt, O. Beeck—331(A)
Collisions of second kind
Mg atoms and Ne, O. S. Duffendack, J. H. Manley—336(A)
Hg atoms and H_2, CO and N_2, O. S. Duffendack, J. S. Owens—417
Combustion (see **Chemical reactions**)
Compton effect (see **X-rays, diffraction, scattering, etc.**)
Constants, physical, standards
Interpretation of e^2/mc^2 and h/mc, B. Podolsky—734
Photoelectric determination of h/e, L. A. DuBridge, A. G. Hill—339(A)
Velocity of light, anomalies, S. Freed—1025(L)
Cosmic radiation
Absorption measurements of hard γ-rays from F bombarded by protons, E. McMillan—325(A)
Analysis of data, L. V. King—154
Annihilation of the proton, A. Bramley—438(L)
Azimuthal asymmetry on Mount Evans, J. C. Stearns, D. K. Froman—535(L)
Coincidence test of the corpuscular hypothesis, D. S. Hsiung—334(A); 653
Counter calibration and ray intensity, J. C. Street, R. H. Woodward—938(A); 1029
General interpretation, R. A. Millikan—329(A)
At the great altitudes, S. N. Vernoff—822(L)
High altitude survey of the effect of latitude; general interpretation, I. S. Bowen, R. A. Millikan, H. V. Neher—641
Ionization of air by α- and β-rays as function of pressure, O. E. Polk—405
Ionization depth data, nature of the primary radiation, W. F. G. Swann—432; 828(L)
Origin, criticism of Huxley's theory, A. F. Stevenson—1111(L)
Passage of particles through magnetic field and atmosphere of the earth, R. M. Langer—330(A)
Penetrating power of asymmetric component, S. A. Korff—74(L)
Production of secondaries by cosmic-ray electrons; energy loss, C. D. Anderson, S. H. Neddermeyer—325(A)
Recovery time of G-M counters, W. E. Danforth—1026(L)
Super-novae as source, W. Baade, F. Zwicky—76(L)
Transition effects, air to Pb, J. C. Street, R. T. Young, Jr.—823(L); 938(A)

Crystalline state
Absorption of light in quartz, W. M. Powell, Jr.—43
Constitution of metallic Na, E. Wigner, F. Seitz—509
Decrement of quartz resonators, K. S. Van Dyke, J. P. Hagen—939(A)
Dielectric constant of Rochelle salt crystals, A. Zeleny, J. Valasek—450
Electrical resistivities of single and mosaic Zn crystals, W. J. Poppy—815
Electronic functions for a metallic crystal, W. V. Houston, C. B. Crawley—329(A)
Electrons in metals, E. Wigner—1002
Inverse piezoelectric properties of Rochelle salt, C. I. Vigness—255
Magnetic properties of Fe-Co single crystals, J. W. Shih —139
Magnetic susceptibilities of powdered crystals, R. B. Janes—338(A)
Magnetization in ferromagnetic crystals, L. W. McKeehan, W. C. Elmore—226(L); 529(L)
Magnetostriction of pure and alloyed Bi single crystals, A. Wolf, A. Goetz—1095
Melting parameters of N and A under pressure, nature of the melting curve, P. W. Bridgman—930
Paramagnetic rotation of tysonite, J. H. Van Vleck, M. H. Hebb—17; Errata—929
Segregation of Po in Bi crystals, A. B. Focke—623
Single crystals of ice, W. Lewis—328(A)
Spectra of Sm ion in solids, F. H. Spedding, R. S. Bear—308; 975
Susceptibilities of solutions of Ni in Cu, W. H. Ross—46
Theory of fusion, K. F. Herzfeld, M. Goeppert Mayer—995
Thermal conductivities of Bi single crystals in a magnetic field, M. T. Rodine—910
Thermal expansion of alloyed Bi crystals near eutectic melting point, A. Goetz, J. W. Buchta, T. L. Ho—538(L)
Thermal expansion of Bi near melting point, J. W. Buchta, A. Goetz—1092
Thermoelectric effects in single crystals, H. P. Stabler—938(A)
Transition in Al at 79°C, W. Band—934(L)
Wiedemann-Franz ratio of single crystal Zn, C. A. Cinnamon—215
X-ray investigation of lattice recovery after cold-working, J. E. Wilson, L. Thomassen—337(A)
X-ray study of a vibrating quartz crystal, M. Y. Colby, S. Harris—445
Critical potentials (see **Potentials, critical**)
Crystals, structure
From data on magnetic susceptibilities, O. M. Jordahl—79(L)
Fourier integral analysis of x-ray powder patterns, B. E. Warren, N. S. Gingrich—368
Fourier series method for the determination of interatomic distances, A. L. Patterson—372
Of lithium sulphate monohydrate, G. E. Ziegler—338(A)
Of nickelous acetate tetrahydrate, R. B. Hull—329(A)
Photo-densitometer charts of diffraction patterns, W. Soller—331(A)
Cybotactic state
Of ethyl ether in region of critical point, R. D. Spangler—698
Of isopentane in region of critical point, C. A. Benz, G. W. Stewart—703

Diamagnetism (see **Magnetic properties**)
Dielectric constants (see **Dielectrics and dielectric properties**)
Dielectrics and dielectric properties
Dielectric coefficient of air, variation with pressure and frequency, A. R. Jordan, J. W. Broxon, F. C. Walz—66
Effect of x-rays on dielectric constant of liquids, J. F. Payne, Jr.—340(A)
Frequency and applied field strength variations of constant in Rochelle salt, A. Zeleny, J. Valasek—450
Power loss and dielectric constant of various glasses, L. S. McDowell, P. Bullard, M. E. Whitney—939(A)
Of tung oil, variation with temperature and frequency, A. A. Bless—340(A)
Diffraction of electrons (see **Electron diffraction**)
Diffraction of molecules (see **Atomic and molecular beams**)
Discharge of electricity in gases (see also **Arcs; Electrons in gases**)
Current in different directions, R. D. Rusk, A. L. Peckham—425
Excitation of light by alkali ions, R. E. Holzer—280
Initial stages of spark discharges, H. J. White—99; 330(A)
Mechanism of spark discharge; time lags, A. Tilles—1015
Pressure of plasma electrons, L. Tonks—278
Reflection coefficient of electrons, M. J. Copley, T. E. Phipps—144(L)
Source of positive ions, R. D. Fowler, G. E. Gibson—1075
Sparking potentials at low pressures, S. S. Cerwin—1054
Disintegration of nucleus (see also **Radioactivity**)
α-particles from Li, J. Zeleny, C. J. Brasefield, C. D. Bock, E. C. Pollard—318(L)
Attempts to detect emission of deutons, E. Pollard, W. W. Eaton—528(L)
Of B, γ-rays emitted, H. R. Crane, L. A. Delsasso, W. A. Fowler, C. C. Lauritsen—1109(L)
Capture of charged particles by nuclei due to emission of γ-radiation, G. Breit, F. L. Yost—1110(L)
Conversion of kinetic into γ-ray energy; disintegration by neutrons, W. D. Harkins, D. M. Gans—827(L)
Disintegration of H^3, H. H. Goldsmith—78(L)
Emission of protons induced by neutron bombardment, F. N. D. Kurie—330(A)
Energy spectra of neutrons from the disintegration of F, B and Be, T. W. Bonner, L. M. Mott-Smith—258
Excited state in the α-particle, C. C. Lauritsen, H. R. Crane—537(L)
Of F by H^+, M. C. Henderson, M. S. Livingston, E. O. Lawrence—38

Disintegration of nucleus (Continued)
Of F, mass of F^{19}, E. O. Lawrence, M. C. Henderson, M. S. Livingston—324(A)
γ-rays accompanying artificial disintegrations, E. McMillan—325(A); 868
γ-rays from Li and F bombarded with protons, H. R. Crane, L. A. Delsasso, W. A. Fowler, C. C. Lauritsen —531(L)
High velocity Li ions, R. L. Thornton, B. B. Kinsey—324(A)
Inelastic collisions with changes of mass, W. D. Harkins, D. M. Gans—397
Of N by neutrons, F. N. D. Kurie—324(A)
Organic liquids for cloud expansion work, D. H. Loughridge, H. C. Trueblood—323(A)
Proton production in the low voltage arc, E. S. Lamar, O. Luhr—87
Protons from B and P bombarded by α-particles, R. F. Paton—229(L)
Radioactive O, M. S. Livingston, E. McMillan—437(L)
Radioactive Na, E. O. Lawrence—746(L)
Recording apparatus for α-particles, protons and neutrons, M. C. Henderson—324(A)
Source of positive ions, R. D. Fowler, G. E. Gibson—1075
Dissociation, heat of (see also **Molecular structure and constants**)
Of CO, W. W. Lozier—268
Of CS_2, H. D. Smyth, J. P. Blewett—276
Energies of some hydrocarbon molecules, R. Serber—335(A)
Of N_2, R. S. Mulliken—144(L)

Efficiency of ionization
Of He and Hg at high voltages, J. W. Liska—169
Of multiply charged ions in the alkali vapors and in Kr and Xe, J. T. Tate, P. T. Smith—773
Elasticity
Erratum, elastic moduli of rocksalt, L. Balamuth—933
Electrets
Neutron collisions, theory of, A. Nordsieck—234(L)
Electrical conductivity and resistance
Of single and mosaic Zn crystals, W. J. Poppy—815
Electromagnetic theory
And interpretation of e^2/mc^2 and h/mc, B. Podolsky—734
Quantization of field equations, H. Weyl—505
Quantum theory of electromagnetic fields, W. H. Watson—936(L)
Electron diffraction (see also **Scattering of electrons**)
Search for polarization, F. E. Myers, J. F. Byrne, R. T. Cox—777
Electron lenses
Microscopy of biological objects, L. Marton—527(L)
Electrons in gases
Motion of photoelectrons, A. M. Cravath—323(A)
Terminal energy distribution, A. M. Cravath—332(A)
Electrons in metals
In Be and Si, H. M. O'Bryan—336(A)
Constitution of metallic Na, E. Wigner, F. Seitz—509
Interactions in an electron gas, E. Wigner—1002
Theory of barrier layer cells, R. H. Varian—1051
Electrons, secondary
From metal targets bombarded by 1.3 MEV Hg ions, L. H. Linford—325(A)
Production by cosmic-rays, C. D. Anderson, S. H. Neddermeyer—325(A)
Variation with atomic number, P. L. Copeland—167
Electron tubes (see **Vacuum tubes**)
Electro-optical effects (see also **Photoelectric effect and properties**)
Dispersion of Kerr effect in CO_2, G. G. Quarles—692
E/m
From Zeeman effect in He, L. E. Kinsler, W. V. Houston —533(L)
From Zeeman effect in Ne, L. E. Kinsler—533(L)
Energy states of atoms (see also **Spectra, atomic**)
Doubly excited He, T.-Y. Wu—239(L)
Doubly excited states in He, F. G. Fender, J. P. Vinti—77(L)
Equations of state
Melting parameters of N and A under pressure, nature of the melting curve, P. W. Bridgman—930
Theory of fusion, K. F. Herzfeld, M. G. Mayer—995
Errata
Acoustic resonator interferometer, J. C. Hubbard—525
Magnetic moment of the neutron, A. Landé, D. R. Inglis—76(L)
New method for measuring elastic moduli and the variation with temperature of the principal Young's modulus of rocksalt between 78°K and 273°K, L. Balamuth—933
On the paramagnetic rotation of tysonite, J. H. Van Vleck, M. H. Hebb—929
Excitation of atoms and molecules
Mean life of the 7^3S_1 state of Hg, A. C. G. Mitchell, E. J. Murphy—53

Ferromagnetism (see **Magnetic properties**)
Field currents
Of Balmer lines and Stark effect, N. P. Heydenburg—1065
Fluorescence
And photodecomposition in solutions of chlorophyll *a* and *b*, V. M. Albers, H. V. Knorr—336(A)

Gases (see **Kinetic theory**)

Heat of dissociation (see **Dissociation**)
High voltage tubes and machines
Heavy high speed ions without the use of high voltages, D. H. Sloan, W. M. Coates—539
Hyperfine structure (see also **Nuclear moments and spin**)
Of La I, O. E. Anderson—325(A)
In Pb, B. H. Dickinson—598
In Ag, H. Hill—536(L)

Instruments (see **Methods and instruments**)
Ionization by ions (see also **Ionization potentials**)
α- and β-rays ionization of air, variation with pressure, O. E. Polk—405

Balanced space-charge method, R. N. Varney—235(L); 322(A)
Excitation of light by alkali ions, R. E. Holzer—280
Ionization by radon, Ra A and Ra C′ in clyindrical chambers, R. D. Evans—937(A)

Ionization potentials
Of CS_2, H. D. Smyth, J. P. Blewett—276
Of Eu, H. N. Russell, A. S. King—1023
Of formaldehyde and halogen derivatives of methane, T. N. Jewitt—616
Iso-electronic sequence A I to Mn VIII, P. G. Kruger, S. G. Weissberg—336(A)
Molecular ionization potentials, R. S. Mulliken—549
Of multiply charged ions in the alkali vapors and in Kr and Xe, J. T. Tate, P. T. Smith—773
Of N_2, R. S. Mulliken—144(L)
Of Ra, H. N. Russell—989

Ions, high speed
Source, of high intensity, M. A. Tuve, O. Dahl, C. M. Van Atta—1027(L)

Isotopes
Abundance ratios of C, N, A, Ne and He, A. L. Vaughan, J. H. Williams, J. T. Tate—327(A)
Isotopic shifts in pentatomic molecules, J. E. Rosenthal—730
Mass ratios from band spectra, W. W. Watson—319(L)
Nuclear stability and isotope shift, G. Breit—319(L)
Relative abundance of Li, K and Rb isotopes, A. K. Brewer, P. D. Kueck—894
Spectroscopic evidence for He_2^3, G. P. Harnwell, H. D. Smyth, W. D. Urry—437(L)
Vibrational isotope effects, A. Adel—222

Joule-Thomson effect (see **Kinetic theory of gases**)
In A, J. R. Roebuck, H. Osterberg—785

Kinetic theory of gases
Joule-Thomson effect in A, J. R. Roebuck, H. Osterberg—340(A); 785
Second virial coefficient of He, N. G. Whitelaw—340(A)
Transport phenomena in Einstein-Bose and Fermi-Dirac gases, E. A. Uehling—917
Ultrasonic absorption and reflection coefficients in air and in CO_2, R. W. Curtis—811

Magnetic properties
Barkhausen discontinuities and their propagation, R. E. Reinhart—483
Diamagnetism of water temperature effect, A. P. Wills, G. F. Boeker—907
Ferromagnetic change in volume of Ni, C. Williams—1011
Ferromagnetism and liquid mixtures, C. Zener—824(L)
Ferromagnetism and non-orthogonal wave functions, D. E. Inglis—135
Heat treatment of magnetic materials, R. M. Bozorth—232(L)
Hysteresis losses and the hysteresis loop, L. W. McKeehan, R. M. Bozorth—527(L)
Of Fe-Co single crystals, J. W. Shih—139
Magnetic susceptibilities and crystal structure, O. M. Jordahl—79(L)
Magnetoresistance discontinuities, C. W. Heaps—1108(L)
Magnetostriction of pure and alloyed Bi single crystals, A. Wolf, A. Goetz—1095
Paramagnetic rotation of tysonite, J. H. Van Vleck, M. H. Hebb—17; Errata—929
Of powdered crystals, R. B. Janes—338(A)
Of rare earth salts, susceptibility and water content, E. H. Williams—133
Surface magnetization in ferromagnetic crystals, L. W. McKeehan, W. C. Elmore—226(L); 529(L)
Susceptibilities of dilute solid solution of Ni in Cu, W. H. Ross—46

Magneto-optical effects
Paramagnetic rotation of tysonite, J. H. Van Vleck, M. H. Hebb—17; Erratum—929
Verdet constant of $CeCl_3$; effect of concentration, temperature and wave-length, F. G. Slack, R. L. Reeves, J. A. Peoples, Jr.—724
Verdet constant of heavy water, F. G. Slack—945

Mean life
Of the 7^3S_1 state of Hg, A. C. G. Mitchell, E. J. Murphy—53

Mechanics, quantum-atomic structure and spectra
Calculation of atomic energy levels, R. F. Bacher, S. Goudsmit—948
Dirac vector model and d^4 configuration, M. Ostrofsky—604
Hartree fields of C, C. C. Torrance—388
Second-order calculation of He I $2s2p\,^{1,3}P$, W. M. Cady—439(L)
Self-consistent field for Na atom, E. H. Kennard, E. Ramberg—1034
Spectral multiplets, Dirac vector model, R. A. Merrill—487
Wave functions and atomic field for Hg, D. R. Hartree—738

Mechanics, quantum—general
Averages over portions of configuration space, G. Heller, L. Motz—502
Capture of particles by nuclei, emission of γ-ray, G. Breit, F. L. Yost—1110(L)
Collision of two light quanta, G. Breit, J. A. Wheeler—1087
Electrons and positrons, Dirac theory, C. H. Dix—329(A)
Indeterminacy relation for several observables, H. P. Robertson—794
Many-electron systems, approximation treatment, C. Møller, M. S. Plesset—618
Modified Ritz variation method, J. K. L. MacDonald—828(L)
Non-orthogonal wave functions and ferromagnetism, D. R. Inglis—135
Nuclear energy levels and a model, H. Margenau—613
Quantization of field equations, H. Weyl—505; W. H. Watson—936(L)

Mechanics, quantum—general (Continued)
Spheroidal functions, general equation, J. A. Stratton—938(A)
Test for spectroscopic stability, O. Halpern, E. Wasser—177
Transport phenomena in Einstein-Bose and Fermi-Dirac gases, E. A. Uehling—917
Wave functions for high energy electrons in Coulomb fields, W. H. Furry—391
Mechanics, quantum—molecular structure and spectra
Kinetic energy of polyatomic molecules, C. Eckart—383
Potential function having symmetrical double minima, M. F. Manning—335(A)
Rotational wave equation of tetramethylmethane, L. J. B. LaCoste—718
Mechanics, quantum—of solid bodies
Constitution of metallic Na, E. Wigner, F. Seitz—509
Electronic functions for a metallic crystal, W. V. Houston, C. B. Crawley—329(A)
Radiation damping and polarization, G. Breit, I. S. Lowen—590
Metals (see also **Crystalline state**)
Transition in Al at 79°C, W. Band—934(L)
Meteorology
Analysis of measurements of the ionosphere, E. O. Hulburt—822(L)
Multiple sunset flashes, S. J. Barnett—75(L)
Methods and instruments
Behavior of diffraction gratings coated by evaporation, J. Strong—326(A)
Capacity-resistance bridge, A. R. Jordan, J. W. Broxon, F. C. Walz—66
Compensator to measure double refraction, H. A. Boorse—187
Constant-voltage rectifier, R. D. Evans—324(A)
Curved crystal x-ray spectrograph, R. L. Doan—337(A)
Curved quartz crystal x-ray spectrograph, J. W. M. DuMond, B. B. Watson—316(L)
Deposition Po on Ag, M. D. Whitaker, W. Bjorksted, A. C. G. Mitchell—629(L)
Determination of Rn and Ra in liquids, R. D. Evans—328(A)
Evaporated films of Al over Cr, R. C. Williams—146(L)
G-M counter calibration, J. C. Street, R. H. Woodward—938(A); 1029
Heavy high speed ions without the use of high voltages, D. H. Sloan, W. M. Coates—539
High velocity Li ions, R. L. Thornton, B. B. Kinsey—324(A)
High voltage x-rays for medical uses, M. S. Livingston, M. A. Chaffee—330(A)
Index of refraction of x-rays, H. C. Hoyt, G. A. Lindsay—337(A)
Intensity measurements in Raman spectrum, I. Hanson—122
Magnetic field with high gradient, I. I. Rabi, J. M. B. Kellogg, J. R. Zacharias—157
Organic liquids for cloud expansion work, D. H. Loughridge, H. C. Trueblood—323(A)
Photographic photometry of electric furnace spectra, R. B. King—327(A)
Positive ion source of high intensity, M. A. Tuve, O. Dahl, C. M. Van Atta—1027(L)
Precision frequency standard of high power, F. G. Dunnington—331(A)
Proton production in the low voltage arc, E. S. Lamar, O. Luhr—87
Recovery time of G-M counters, W. E. Danforth—1026(L)
Quartz used in instruments, W. M. Powell, Jr.—43
Recording apparatus for α-particles, protons and neutrons, M. C. Henderson—324(A)
Rectifying effect in chrome cast iron, L. G. Hall—1109(L)
Schmidt cameras in plane grating spectrographs, T. Dunham, Jr.—326(A)
Simplified interval sorter for spectral analysis, C. B. Ellis—341(A)
Source of positive ions, R. D. Fowler, G. E. Gibson—1075
Spheroidal functions, general equation, J. A. Stratton—938(A)
Statistical theory, W. E. Deming, R. T. Birge—1027(L)
Technique of Kerr cells, H. J. White—323(A)
Ultramicrometer, C. L. Utterback, H. Wirth—328(A)
Variable frequency generator for odd harmonics of 60 cycle, D. L. Soltau, D. H. Loughridge, L. M. Applegate—328(A)
X-ray intensities by use of G-M counter, G. L. Locher, D. P. LeGalley—1047
Molecular structure and constants (see also **Spectra, molecular and Raman spectra**)
Doublet separation in NO, E. E. Witmer—629(L)
Of H_2S, P. C. Cross—536(L)
Vibrations of tetrahedral pentatomic molecules, J. E. Rosenthal—730
Multiplets (see also **Spectra, etc.**)
Relative transition probabilities from spectroscopic stability, C. W. Ufford, F. M. Miller—283

Neutrons
As combination of proton and electron, H. Margenau—107
Collisions, theory of, A. Nordsieck—234(L)
Energy spectra from the disintegration of F, B and Be, T. W. Bonner, L. M. Mott-Smith—258
Magnetic moment, I. I. Rabi, J. M. B. Kellogg, J. R. Zacharias—163
Mass of neutron, F. N. D. Kurie—324(A)
Removal of neutrons and α-particles from nuclei, E. D. Eastman—238(L)
Spontaneous disintegration of proton or neutron, H. C. Wolfe, G. E. Uhlenbeck—237(L)
Structure of, A. Landé—334(A)
Nuclear moments and spin (see also **Hyperfine structure**)
Of Cs, magnetic, L. P. Granath, R. K. Stranathan—317(L); V. W. Cohen—713; N. P. Heydenburg—802
Of Co, mechanical and magnetic, K. R. More—327(A); 470

Of Cb, magnetic from hyperfine structure, S. S. Ballard —233(L); 327(A); 806
Of H^2, G. M. Murphy, H. Johnston—95; I. I. Rabi, J. M. B. Kellogg, J. R. Zacharias—163
Interpretation of values of moments, G. Breit, I. I. Rabi—230(L)
Of La, magnetic, O. E. Anderson—473
Of neutron, magnetic, erratum, A. Landé, D. R. Inglis—76(L)
Of proton, magnetic, I. I. Rabi, J. M. B. Kellogg, J. R. Zacharias—157
Origin of magnetic moments, A. Landé—477
Of K^{39}, S. Millman, M. Fox, I. I. Rabi—320(L)
Of Na, magnetic, A. Ellett, N. P. Heydenburg—583; L. Larrick—581; I. I. Rabi, V. W. Cohen—707

Nucleus (see also **Disintegration of nucleus**)
Energy levels and a model, H. Margenau—613
Energy stability and composition of atomic nuclei, E. D. Eastman—1
Excited state in the α-particle, C. C. Lauritsen, H. R. Crane—537(L)
Genesis of the elements, G. N. Lewis—897
Heights of potential barriers, E. D. Eastman—744(L)
Mass of F^{19}, M. C. Henderson, M. S. Livingston, E. O. Lawrence—38
Negative protons in the nucleus, J. H. Bartlett, Jr.—435(L)
Nuclear stability and isotope shift, G. Breit—319(L)
Production of He^3, W. Bleakney, G. P. Harnwell, W. W. Lozier, P. T. Smith, H. D. Smyth—81(L)
Resonance levels and atomic number, H. Margenau, E. Pollard—228(L)

Optical constants and properties
Behavior of diffraction gratings coated by evaporation, J. Strong—326(A)
Of Be and Si, H. M. O'Bryan—336(A)
Refractivity of gas in magnetic field, O. Halpern, E. Wasser—177

Optical instruments (see **Methods and instruments**)

Paschen-Back effect
In Hg, J. B. Green, R. A. Loring—888; 335(A)

Photoelectric effect and properties; cells
Energy distribution of electrons from Na, L. A. DuBridge, A. G. Hill—339(A)
Energy distribution of electrons, thickness of film, J. J. Brady—768
For the *L*-shell, H. Hall, W. Rarita—143(L)
Work function of thoriated W, R. E. Smith, L. A. DuBridge—339(A)

Photometry
Photographic photometry of electric furnace spectra, R. B. King—327(A)

Photons
Collision of two light quanta, G. Breit, J. A. Wheeler—1087

Photovoltaic effect
Behavior of cells under x-radiation, M. F. Griffith, P. E. Boucher—341(A)

Piezoelectric effect
Decrement of quartz resonators, K. S. Van Dyke, J. P. Hagen—939(A)
Inverse effect in Rochelle salt, C. I. Vigness—255
X-ray study of a vibrating quartz crystal, M. Y. Colby, S. Harris—445

Plasmoidal discharges (see **Discharge of electricity in gases**)

Polarization of radiation
Fluorescence radiation, G. Breit, I. S. Lowen—590
Of Raman bands in CO_2, A. Langseth, J. R. Nielsen—1057
Of sky light during the total solar eclipses, W. M. Cohn—328(A)

Polymerization
Of heavy acetylene by α-rays, S. C. Lind, J. C. Jungers, C. H. Shiflett—825(L)

Potentials, critical (see also **Ionization potentials**)
Excitation of light by alkali ions, R. E. Holzer—280

Quenching of radiation
Of Hg by H_2, CO and N_2, O. S. Duffendack, J. S. Owens —417

Radioactivity (see also **Disintegration of nucleus**)
Absence of low energy radiations from K and Rb, W. F. Libby—745(L)
Chemistry of element 93, A. v. Grosse, M. Agruss—241(L)
Conversion of kinetic into γ-ray energy; disintegration by neutrons, W. D. Harkins, D. M. Gans—827(L)
Depositing Po on Ag, M. D. Whitaker, W. Bjorksted, A. C. G. Mitchell—629(L)
Determination of Rn and Ra in liquids, R. D. Evans—328(A)
Energy of a β-ray of Ra B, F. A. Scott—633
Induced by neutron bombardment, M. S. Livingston, M. C. Henderson, E. O. Lawrence—325(A)
Ionization by radon, Ra A and Ra C′ in cylindrical chambers, R. D. Evans—937(A)
Of Nd and Sm; tests of other elements, W. F. Libby—196
Radioactive O, M. S. Livingston, E. McMillan—437(L)
Removal of neutrons and α-particles from nuclei, E. D. Eastman—238(L)
Scattering of the Th C″ γ-rays, C. C. Lauritsen, J. R. Oppenheimer—80(L)
Of Na induced by deuton bombardment, E. O. Lawrence —746(L)
Spontaneous disintegration of proton or neutron, H. C. Wolfe, G. E. Uhlenbeck—237(L)

Raman spectra
Of acetylene, G. Glockler, C. Morrell—233(L)
In heavy acetylene (C_2D_2), G. Glockler, H. M. Davis—535(L)
Intensity measurements in CO_2, I. Hanson—122
Interpretation in benzene, E. B. Wilson, Jr.—146(L)
Polarization and intensity in Raman spectrum of CO_2, A. Langseth, J. R. Nielsen—1057

Rectifiers
Rectifying effect in chrome cast iron, I. G. Hall—1109(L)
Relativity
Velocity of light, anomalies, S. Freed—1025(L)
Resonance radiation
Escape from Hg vapor, D. W. Carpenter, W. M. Nielsen—608
Quenching of Hg radiation, O. S. Duffendack, J. S. Owens—417
Of Na, polarization, A. Ellett, N. P. Heydenburg—583; L. Larrick—581

Scattering of atoms and molecules (see **Atomic and molecular beams**)
Scattering of electrons and ions (see also **Electrons in gases; Electron diffraction**)
Elastic scattering of fast electrons in Hg, W. E. Stephens—935(L)
Elastic scattering in K, J. H. McMillen—983
In He, elastic and inelastic, A. L. Hughes, R. C. Hergenrother—180
Small-angle inelastic electron scattering in He, H_2 and Hg, S. N. Van Voorhis—480
Secondary electrons (see **Electrons, secondary**)
Solid state (see **Crystalline state**)
Spark discharge
Initial stages, H. J. White—99; 330(A)
Initiation in ion free gases, J. W. Flowers, J. W. Beams—338(A)
Potentials at low pressures, A. J. Dempster—728
Time lags; mechanism of discharge, A. Tilles—1015
Spectra, absorption (see also **Absorption of light**)
Of As_2, G. E. Gibson, A. Macfarlane—1059
Atmospheric bands of O, J. H. Van Vleck—334
Of formaldehyde and hydrogen cyanide in ultraviolet, W. C. Price—529(L)
Of formaldehyde, infrared, H. H. Nielsen—117
Of heavy water vapor, W. W. Sleator, E. F. Barker—336(A)
Infrared spectra of benzene, interpretation, E. B. Wilson, Jr.—146(L)
Of methyl chloride, 0.7μ to 7.0μ, A. H. Nielsen, E. F. Barker—970
Of mono-deutero acetylene, infrared, A. McKellar, C. A. Bradley, Jr.—236(L); 341(A); 664
Of the Sm ion in solids, F. H. Spedding, R. S. Bear—308; 975
Spectra, atomic
Of Cs III and Ba IV, M. A. Fitzgerald, R. A. Sawyer—576
C, N, O, calculation of energy levels by quantum mechanics, R. F. Bacher, S. Goudsmit—948
Of Cl IV, I. S. Bowen—377
Of Co V and Mo VI, M. W. Trawick—63
Configurations of the type $d^k ms$ and $d^k msns$, R. A. Merrill—487; 334(A)
d^3 configuration, Dirac vector model, M. Ostrofsky—604
Deepest terms of the isoelectronic sequences Ni I to Kr IX and Pd I, P. G. Kruger, W. E. Shoupp—124
Doubly-excited states in He, F. G. Fender, J. P. Vinti—77(L)
Of Eu I, H. N. Russell, A. S. King—1023
Fine structure of Balmer lines and Stark effect, N. P. Heydenburg—1069
General sum rule in intermediate coupling, G. H. Shortley—938(A)
Intensities in platinum-like spectra, A. T. Goble—334(A)
Isotope effect in Pb, B. H. Dickinson—598
Of Hg, high series terms, I. Walerstein—335(A); 874
Multiplet transition probabilities from spectroscopic stability, C. W. Ufford, F. M. Miller—283
Of Ne I, II, III and IV, J. C. Boyce—378
Of K IV, V, Ca V, VI, I. S. Bowen—791
Of K VI, VII, VIII, IX and Ca VII, VIII, A. E. Whitford—793
Of Ra; ionization potential, H. N. Russell—989
Second-order calculation of He I $2s2p\ ^{1,3}P$, W. M. Cady—439(L)
Of Se I, J. E. Ruedy, R. C. Gibbs—880
Series lines of Mg in solar spectrum, H. N. Russell, H. D. Babcock, C. E. Moore—826(L)
Spectra, continuous
In flames and arcs, W. Finkelnburg—330(A)
Of some incandescent lamps, W. E. Forsythe, B. T. Barnes—339(A)
Spectra, general
Abnormal rotation of molecules, O. Oldenberg—210
Afterglow in Hg, M. M. Mann, W. M. Nielsen—991
Spectra, molecular (see also **Molecular structure and constants**)
Abnormal rotation of molecules, O. Oldenberg—210
Of acetylene, G. Glockler, C. Morrell—233(L)
Of BaCl, A. E. Parker—301
Of BeCl, ultraviolet, W. R. Fredrickson, M. E. Hogan, Jr.—454
Of Cd_2, S. W. Cram—205
Of CaD, W. W. Watson—939(A)
Of CO, ultraviolet, D. N. Read—571
Of CS_2, F. W. Loomis, P. Kusch—292
Of the chlorine derivatives of ethylene, infrared, T.-Y. Wu—465
Of GaO, M. L. Guernsey—114
Of halogen molecules, energy states, J-J-like coupling, R. S. Mulliken—549
Of HF, E. O. Salant, D. E. Kirkpatrick—318(L)
Of H_2S, band at 10,100A, P. C. Cross—536(L)
Of LiH and LiD, F. H. Crawford, T. Jorgensen—746(L); 939(A)
Of HgH, anomalous rotation, F. F. Rieke—236(L)
Of N_2, J. Kaplan, L. D. Levanas—331(A)
Of N_2^+, F. H. Crawford, P. M. Tsai—935(L)
Of N_2 in ultraviolet, W. W. Watson, P. G. Koontz—32
Of N_2, ultraviolet, J. Kaplan—326(A); 534(L); 631(L)
Of O_4, W. Finkelnburg—326(A)
OH^+ bands, F. W. Loomis, W. H. Brandt—79(L)
Of PH, P. Nolan, F. A. Jenkins—327(A)
Pressure broadening of NO bands, O. R. Wulf—316(L)
Of NaK, F. W. Loomis, M. J. Arvin—286

Of S_2 in ultraviolet, R. M. Badger—1025(L)
Vibrational isotope effects, A. Adel—222
Of water vapor, vibrational, L. G. Bonner—458
Vibrations of tetrahedral pentatomic molecules, J. E. Rosenthal—730
Spectroscopy, technique
Simplified interval sorter, C. B. Ellis—341(A)
Wave numbers of infrared lines beyond λ10,000, H. D. Babcock—382
Stark effect
And fine structure of Balmer lines, N. P. Heydenburg—1069

Thermal conductivity
Of Bi single crystals in a magnetic field, M. T. Rodine—910
Of single crystal Zn; W-F ratio, C. A. Cinnamon—215
Thermal expansion
Of alloyed Bi crystals near eutectic melting point, A. Goetz, J. W. Buchta, T. L. Ho—538(L)
Of Bi single crystals near melting point, J. W. Buchta, A. Goetz—1092
Of Ni near Curie point, C. Williams—1011
Thermal radiation
Temperature scale for W, W. B. Nottingham—341(A)
Thermionic emission of electrons; Emitting surfaces (see also **Vacuum tubes**)
Emission from points, A. J. Dempster—165
Energy distribution of electrons under high fields, R. K. Dahlstrom, J. E. Henderson—323(A)
Reflection coefficient of electrons, M. J. Copley, T. E. Phipps—144(L)
From W as function of voltage, W. B. Nottingham—339(A)
Thermoelectric effects
In single crystals, H. P. Stabler—938(A)
Transmutation (see **Disintegration of nucleus**)

Vacuum tubes
Frequency variation of flicker effect, R. C. Meyer, E. A. Johnson—143(L)
Vapor pressure
Of Ca between 500 and 625°C, E. Rudberg—763; 937(A)

X-rays, absorption
Dependence of secondary structure on crystal form, V. P. Barton, G. A. Lindsay—362
L absorption in Bi, L. H. Carr—92
M-series of metallic bismuth, W. D. Phelps—357
Monochromatic rays of short wave-length, T. M. Hahn—149
Photoelectric effect for the *L*-shell, H. Hall, W. Rarita—143(L)
Secondary structure of edges from elements in certain cubic crystals, G. P. Brewington—861
Structure and width of *K* limits, W. H. Zinn—659
Structure and width of L_{III} limits of Ta, W and Au, H. Semat—688
Widths of the *L*-series lines, energy levels of Au(79), F. K. Richtmyer, S. W. Barnes, E. Ramberg—843
Of Xe, T. N. White—865
X-rays, diffraction, scattering, reflection, refraction and polarization
Calculation of mass scattering coefficients, L. M. Heil—58
Compton shift and velocity of electrons, G. E. M. Jauncey—667
Compton shift for 90°, effect of electron binding, P. A. Ross, P. Kirkpatrick—668
Diffraction patterns of a fluid at various densities, N. S. Gingrich, B. E. Warren—248
Diffuse scattering, Waller-Hartree theory, G. G. Harvey, P. S. Williams, G. E. M. Jauncey—365
Of ethyl ether in region of critical point, R. D. Spangler—698
Fourier integral analysis of powder patterns, B. E. Warren, N. S. Gingrich—368
Fourier series method for the determination of interatomic distances, A. L. Patterson—372
Of isopentane in region of critical point, C. A. Benz, G. W. Stewart—703
Lattice recovery of metals after cold working, J. E. Wilson, L. Thomassen—337(A)
Measuring index of refraction, H. C. Hoyt, G. A. Lindsay—337(A)
Pressure effect of x-rays scattered from N_2, G. G. Harvey—441
Refraction in quartz; absolute wave-lengths, J. A. Bearden, C. H. Shaw—759
Scattering monochromatic radiation from NaF, P. S. Williams—83
Scattering from sylvine, G. E. M. Jauncey, W. D. Claus—941
Scattering of the Th C″ γ-rays, C. C. Lauritsen, J. R. Oppenheimer—80(L)
Theory of broadening and position of Compton-line, F. Bloch—674
Variation of the *K* resonating strength, J. A. Wheeler, J. A. Bearden—755
X-rays, emission (see also **X-rays, spectra and spectroscopy, etc.**)
Depth of origin of characteristic rays, P. Kirkpatrick, D. G. Hare—831
Fluorescence yields from *K* shells, R. J. Stephenson—73(L); D. K. Berkey—74(L)
Intensities of satellites of $L\beta_2$, A. W. Pearsall—694
L-series and energy levels of Au, F. K. Richtmyer, S. W. Barnes, E. Ramberg—843
Line widths, correction for finite resolving power, L. G. Parratt—749
Origin of $K\alpha$-satellites, E. H. Kennard, E. Ramberg—1040
Probability of direct and fluorescent excitation of *K* level, K. B. Stoddard—837
Production of x-rays by swiftly moving Hg ions, W. M. Coates—542
Quadrupole lines in K-series of Ru, E. Wilhelmy—130

X-rays, emission (Continued)
Self-consistent fields and x-ray terms of Na, E. H. Kennard, E. Ramberg—1034
Widths of the *K*-series of W, F. K. Richtmyer, S. W. Barnes—352
X-rays, polarization
Of general X-radiation from thick targets, Y. F. Cheng—243
X-rays, spectra and spectroscopy, wave-length measurements (see also **X-rays, emission**)
Deviations in ionization measurements, R. C. Spencer—337(A)
Equation for crystal curves, R. C. Spencer—1108(L)
Grating and crystal wave-lengths, P. F. Gottling, J. A. Bearden—435(L)
High resolving power grating spectrometer, E. Dershem—337(A)
Line shapes by a double crystal spectrometer, L. P. Smith—343
Photo-densitometer charts of diffraction patterns, W. Soller—331(A)
Refraction in quartz; absolute wave-lengths, J. A. Bearden, C. H. Shaw—759
X-rays, tubes, apparatus
Curved crystal spectrograph, R. L. Doan—337(A)
Curved quartz crystal spectrograph, J. W. M. DuMond, B. B. Watson—316(L)
High voltage x-rays for medical uses, M. S. Livingston, M. A. Chaffee—330(A)
Intensities by use of G-M counter, G. L. Locher, D. P. LeGalley—1047

Zeeman effect
In As I, II and III, W. M. Barrows, J. B. Green—335(A)
In He, L. E. Kinsler, W. V. Houston—533(L)
In Ne, L. E. Kinsler—533(L)
Paschen-Back effect, *JJ*-coupling in Hg, J. B. Green, R. A. Loring—888; 335(A)

DEC 2 6

THE PHYSICAL REVIEW

VOLUME 46 *Second Series* NUMBER 12

DECEMBER 15, 1934

Published for the

AMERICAN PHYSICAL SOCIETY

by the

AMERICAN INSTITUTE OF PHYSICS
Incorporated

LANCASTER, PA., AND NEW YORK, N. Y.

CONTENTS

PHYS. REV. 46 (1934) DECEMBER 15

Counter Calibration and Cosmic-Ray Intensity . . . . . .
. . . . . J. C. STREET AND R. H. WOODWARD 1029

Self-Consistent Field and Some X-Ray Terms of the Sodium Atom . . . .
. . . . . E. H. KENNARD AND E. RAMBERG 1034

Origin of $K\alpha$-Satellites . . . . . E. H. KENNARD AND E. RAMBERG 1040

Measurement of Absolute X-Ray Intensities and Absolute Sensitivity of X-Ray Film with a Geiger-Müller Counter . . . . . .
. . . . . GORDON L. LOCHER AND DONALD P. LEGALLEY 1047

Contribution to the Theory of Barrier Layer Cells . . RUSSELL H. VARIAN 1051

Ionizing Potentials at Low Pressures . . . . . STEPHEN S. CERWIN 1054

Polarization and Intensity Measurements in the Raman Spectrum of Carbon Dioxide . . . . . A. LANGSETH AND J. RUD NIELSEN 1057

Absorption Spectrum of Arsenic . . G. E. GIBSON AND ANGUS MACFARLANE 1059

Influence of the Stark Effect on the Fine Structure of the Balmer Lines of Hydrogen . . . . . N. P. HEYDENBURG 1069

Production of Intense Beams of Positive Ions . . . . . .
. . . . . R. DUDLEY FOWLER AND G. E. GIBSON 1075

Emission of Two Light Quanta . . . . G. BREIT AND JOHN A. WHEELER 1087

Thermal Expansion of Bismuth Single Crystals Near the Melting Point . .
. . . . . J. W. BUCHTA AND A. GOETZ 1092

Magnetostriction of Pure and Alloyed Bi Single Crystals . . . . . .
. . . . . ALEXANDER WOLF AND ALEXANDER GOETZ 1095

Letters to the Editor:

Discontinuities of Magnetoresistance . . . . . C. W. HEAPS 1108
Equation for X-Ray Crystal Curves . . . . . ROY C. SPENCER 1108
Rectifying Effect in Chrome Cast Iron . . . . . LEO G. HALL 1109
Gamma-Rays from Boron Bombarded with Deutons . . . . . .
. . H. R. CRANE, L. A. DELSASSO, W. A. FOWLER AND C. C. LAURITSEN 1109
Capture of Charged Particles by Nuclei Due to Emission of Gamma-Radiation .
. . . . . G. BREIT AND F. L. YOST 1110
Criticism of Dr. L. G. H. Huxley's Theory of the Origin of Cosmic Rays . . .
. . . . . A. F. STEVENSON 1111

Author Index to Volume 46 1113

Analytic Subject Index to Volume 46 1122

LANCASTER PRESS, INC., LANCASTER, PA.